CHARACTERIZATION OF FATIGUE CRACKING AND HEALING OF ASPHALT MIXTURES

A Dissertation

by

XUE LUO

Submitted to the Office of Graduate Studies of
Texas A&M University
in partial fulfillment of the requirements for the degree of

DOCTOR OF PHILOSOPHY

May 2012

Major Subject: Civil Engineering

Characterization of Fatigue Cracking and Healing of Asphalt Mixtures

CHARACTERIZATION OF FATIGUE CRACKING AND HEALING OF ASPHALT MIXTURES

A Dissertation

by

XUE LUO

Submitted to the Office of Graduate Studies of
Texas A&M University
in partial fulfillment of the requirements for the degree of

DOCTOR OF PHILOSOPHY

Approved by:

Chair of Committee,	Robert L. Lytton
Committee Members,	Dallas N. Little
	Amy Epps Martin
	Karl T. Hartwig
	Rong Luo
Head of Department,	John Niedzwecki

May 2012

Major Subject: Civil Engineering

ABSTRACT

Characterization of Fatigue Cracking and Healing of Asphalt Mixtures. (May 2012)

Xue Luo, B.E., Zhejiang University; M.E., Texas A&M University

Chair of Advisory Committee: Dr. Robert Lytton

Fatigue cracking is one of the most common distresses of asphalt pavements, whereas healing is a counter process to cracking which alleviates cracking damage and extends fatigue life of asphalt pavements. Most of existing methods to characterize fatigue cracking and healing are generally empirical or phenomenological in nature, which does not satisfy the need to develop mechanistic-based pavement design methods. The objective of this study is to characterize fatigue cracking and healing of asphalt mixtures using an energy-based mechanistic approach.

A controlled-strain repeated direct tension (RDT) test is selected to generate both fatigue cracking and permanent deformation in an asphalt mixture specimen. Fatigue cracking is separated from permanent deformation from a mechanical viewpoint. The development of fatigue cracking is described by the evolution of the damage density and the increase of the average crack size with the increase of loading cycles.

A creep and step-loading recovery (CSR) test is designed to measure the internal stress in the recovery phase of an asphalt mixture specimen. The internal stress and the strain measured in the recovery phase are used to conduct the mechanistic analysis of

recovery and healing of the asphalt mixture specimen. Then healing is described using the decrease of the damage density and average crack size with time.

Different types of asphalt mixtures produce distinctly different fatigue cracking and healing characteristics. The effect of mixture composition, temperature, and aging are evaluated using the approach above. The entire series of tests for fatigue, permanent deformation and healing can be completed in one day, with the healing part requiring only a matter of minutes. The methods proposed in this study characterize fatigue cracking and healing of asphalt mixtures using its essential cause and effect relationship.

DEDICATION

To my parents

ACKNOWLEDGEMENTS

I would like to express my deepest appreciate to my committee chair, Dr. Robert L. Lytton, for his invaluable advice, guidance, and encouragement throughout my graduate studies at Texas A&M University. I have been fortunate to have an advisor who gives me the freedom to explore on my own, and at the same time the guidance and help when I meet obstacles. He is always patient and willing to listen to every problem. It has been a privilege and great pleasure to work with him. I also want to extend my gratitude to my committee members, Dr. Dallas Little, Dr. Amy Epps Martin, Dr. Karl T. Hartwig, and Dr. Rong Luo, for their guidance and support throughout the course of this research. I am sincerely grateful to Dr. Rong Luo, who motivates and selflessly helps me during these years. Many thanks go to all my friends and colleagues at Texas A&M University for their precious support and encouragement, which makes my time here a great experience. Last but not least, I would like to thank my parents, who receive my deepest gratitude and love for their dedication and these many years of support.

TABLE OF CONTENTS

Page

Page

LIST OF FIGURES

FIGURE Page

FIGURE Page

FIGURE Page

FIGURE Page

FIGURE Page

LIST OF TABLES

1. INTRODUCTION

1.1 Background of Fatigue Cracking and Healing

Fatigue cracking is one of the most common distresses in asphalt pavements. The asphalt layer of the pavement does not crack immediately after the pavement is opened to traffic, but after many load applications, cracks start to appear. As the loading application continues, the cracks develop and connect to form series of interconnected pieces, which is usually called "alligator cracking" that resembles the back of an alligator. In more serious cases, the alligator cracking will further deteriorate to potholes, allowing considerable moisture infiltration into the pavement and significantly reducing the strength and durability of the pavement. To avoid such serious problems, fatigue cracking must be reduced and controlled in asphalt pavements. As a result, asphalt mixtures should be designed with resistance to fatigue cracking. This leads to the need for characterization of fatigue cracking of asphalt mixtures, which includes both laboratory testing and modeling.

Healing is a counter process to cracking which can alleviate cracking damage. In asphalt pavements, healing of asphalt mixtures accompanies all kinds of cracking processes, such as fatigue cracking under repeated loading or creep crack growth under conditions of extensive creep deformation. It has been proven that healing of asphalt mixtures is a substantially important issue in the field of asphalt pavements, and its significance has been demonstrated in both the laboratory and field. Little et al. (2001)

This dissertation follows the style of *Journal of Transportation in Civil Engineering.*

used the flexural bending beam test to show that a rest period of 24 hours during which healing occurred can increase the fatigue life of a certain type of asphalt mixture by more than 100%. Maillard et al. (2004) measured healing by transmitting ultrasonic waves through an asphalt film after applying a cyclic tensile load. The result clearly suggested considerable healing occurred after each loading cycle in the asphalt film. Based on the data from four thick pavements, Nishizawa et al. (1997) concluded that at low loading levels minor fatigue cracks can heal completely. Williams et al. (2001) reported the most convincing field data regarding healing based on observations of four pavement sections. The result revealed that a greater amount of healing occurred in the pavement that had more fatigue damage. Since healing is found to be so significant in evaluating the performance of asphalt pavements, it is highly desired to quantify its effect and to incorporate its contribution into pavement design.

1.2 Problems in Characterization of Fatigue Cracking and Healing

In a visco-elasto-plastic material like an asphalt mixture, fatigue cracking is accompanied by a large amount of plastic deformation in localized regions around cracks or resulting from yielding of the bulk material. Accumulation of plastic strain in the asphalt mixture with the increase of loading cycles produces permanent deformation during the fatigue process. Fatigue cracking and permanent deformation always coexist with each other. However, current characterization methods only measure and model one aspect while ignoring the other one.

Common fatigue tests include the repeated flexural bending test (ASTM 2010),

indirect tension test (Roque et al. 1997; Kim et al. 2002) and uniaxial cyclic test (Si et al. 2002; Walubita 2006). These tests are usually conducted at room temperature in accordance with the understanding that fatigue cracking is predominant at moderate temperatures. Separate laboratory tests have also been developed to measure permanent deformation of asphalt mixtures, such as the creep test and repeated loading test in a temperature range from 40 to 70°C (Sousa et al. 1994) since yielding of the asphalt mixture and plastic deformation become vital at elevated temperatures. These laboratory tests are intended to separate fatigue cracking from permanent deformation by changing the testing temperature. However, the fact is that fatigue cracking and permanent deformation occur simultaneously as two indispensable components of damage in the fatigue process, and the development of one aspect affects the development of the other one. Elber (1971) used experiments and analytical techniques to prove that the existence of permanent deformation can lead to a considerable reduction of allowable load cycles to fatigue cracking failure. Consequently, it is better to treat the development of fatigue cracking and permanent deformation as one damaging process rather than treat them separately as two damaging processes using two tests.

Models for fatigue cracking used in asphalt pavement engineering generally can be divided into four categories: 1) the strain approach (Monismith et al. 1971; The Asphalt Institute 1981; Tayebali 1994); 2) the dissipated energy approach (Van Dijk et al. 1975; Tayebali et al. 1992; Ghuzlan and Carpenter 2000); 3) the fracture mechanics approach; and 4) the continuum damage mechanics approach. In the strain approach, the fatigue resistance is expressed as the number of load applications to failure, which is

related to the tensile strain by a regression function from the test data. In the dissipated energy approach, similarly, the fatigue resistance is represented by a regression function between the dissipated energy and the number of load applications to failure. There is a common feature for the first and second categories of models: the test data is analyzed using a statistical regression method so the regression coefficients depend on the experimental conditions, the materials used, and the geometry of the specimen, etc. This means that a different set of regression coefficients are required if any of these parameters changes. The empirical nature of this statistical analysis method and the resulting models limits their applications since it is not prudent to describe such phenomena outside the range of the original test data. In addition, these models are more dependent on experience rather than specifying the cause and effect of a particular phenomenon. In contrast, the mechanics-based approach and models do not have such problems. The need to develop mechanics-based pavement design and its benefits are now recognized by more and more people (NCHRP 1-37A, 2002). From this perspective, the third and fourth category, the fracture mechanics approach and continuum damage mechanics approach seem very attractive to model the fatigue cracking of asphalt mixtures.

Many approaches have been developed to quantify the effect of healing in a damaged asphalt mixture. Si et al. (2002) conducted cyclic load tests and added a series of rest periods to study the effect of healing. A healing index is defined as follows:

$$HI=\frac{\phi_{after}-\phi_{before}}{\phi_{before}} \tag{1.1}$$

where HI is the healing index; ϕ_{before} is the pseudo stiffness before a rest period; and ϕ_{after} is the pseudo stiffness after a rest period. Pseudo stiffness is the slope of the linear regression of the hysteresis loop of stress versus pseudo strain. It decreases with the accumulation of fatigue damage as the loading cycle increases, and increases in the rest period due to healing of the asphalt mixture. The extent of recovery of the pseudo stiffness in the rest period thus represents the effect of healing. Kim et al. (2003) investigated the effect of healing of fine asphalt mixtures (fine aggregate and asphalt binder) by applying two minute rest periods ten times in a cyclic loading test. Healing was measured by the recovery of dynamic modulus in the rest period. Carpenter and Shen (2006) described the effect of healing from the change of the fatigue resistance of an asphalt mixture. A constant rest period was inserted between every two adjacent loading cycles of a cyclic loading test to measure healing. They found a plateau region in the plot of the ratio of dissipated energy change versus the number of loading cycles, and defined the magnitude of the ratio of dissipated energy change in this region as the plateau value. The fatigue resistance of the asphalt mixture is quantified by the plateau value, and the change of the plateau value after the rest period represented the effect of healing. Kim and Roque (2006) conducted resilient modulus tests with a series of rest periods and used the recovered dissipated creep strain energy per unit time to quantify healing. The commonality of all these methods is that healing is quantified by its effect on some index, such as modulus or strain energy. This is a phenomenological method that relates empirical observations of a phenomenon (change of the index) to another phenomenon (healing). It is not based on the actual cause that drives the process of

healing, and it does not reflect the actual effect of healing in the material.

1.3 Research Objectives

The goal of this research is to address the shortcomings described previously pertaining to testing and modeling in the characterization of fatigue cracking and healing of asphalt mixtures. The research will focus on achieving the following objectives:

- Choose a test method suitable for characterizing fatigue cracking in an asphalt mixture with the presence of permanent deformation;
- Develop a pure mechanistic approach to separate fatigue cracking from permanent deformation using one asphalt mixture specimen and model the evolution of fatigue cracking;
- Develop a test method that can facilitate mechanistic analysis of healing; and
- Develop a pure mechanistic approach to model the healing process and to determine the healing rate.

1.4 Dissertation Outline

This dissertation is organized as follows:

Section 2 first identifies the problems in determination of material properties and strain energy under tensile loading for asphalt mixtures. Based on these problems, an appropriate testing method is proposed to characterize the tensile properties and fatigue damage in asphalt mixtures. In addition, an analysis method is developed to obtain complete material properties and accurate amounts of dissipation and storage of energy

of this test method as the foundation of damage characterization.

The testing method introduced in Section 2 is used to characterize fatigue cracking in asphalt mixtures, which always develops simultaneously with permanent deformation in an asphalt mixture under destructive loading. As a result, Section 3 develops an energy-based mechanistic approach to separate fatigue cracking from permanent deformation in terms of energy consumption.

After separating fatigue cracking from permanent deformation, Section 4 focuses on modeling fatigue crack growth in asphalt mixtures based on the energy-based mechanistic approach. The fatigue crack growth is characterized by its true driven force, and described by its direct effect: increase of the damage density in an asphalt mixture.

Sections 2 to 4 study the fatigue cracking in an asphalt mixture, its counter process, healing, is studied in Sections 5 and 6. Firstly, an innovative test is designed in Section 5 in order to measure the internal stress during the recovery phase of an asphalt mixture. Then the measured internal stress is used with the energy-based mechanistic approach in Section 6 to model the healing process by its direct effect: decrease of the damage density in the asphalt mixture.

In Section 7, the energy-based mechanistic approach developed in Sections 2 to 6 to characterize fatigue cracking and healing is applied to different types of asphalt mixtures to examine the effect of asphalt binder, air void content, temperature, and aging.

Section 8 summarizes the main findings of this work and the contributions of the developed testing and analysis methods. It also mentions a number of directions in which these methods could be further extended.

2. CHARACTERIZATION OF ASPHALT MIXTURES USING CONTROLLED-STRAIN REPEATED DIRECT TENSION TEST

2.1 Problems in Determination of Material Properties and Strain Energy under Tensile Loading

A controlled-strain repeated direct tension (RDT) test is a useful testing method in the material characterization of asphalt mixtures. The RDT test has been used primarily to evaluate tensile properties of asphalt mixtures and to assess the development of fatigue cracking in asphalt mixtures under repeated loading (Bolzan and Huber 1993). In a visco-elasto-plastic material like an asphalt mixture, fatigue cracking is accompanied by a large amount of plastic deformation in localized regions during the fatigue process. In order to simulate the presence of this significant localized plastic deformation, the RDT test is conducted not in the controlled-stress mode but in the controlled-strain mode, which is believed to better characterize the fatigue behavior (Stephens et al. 2001). In the controlled-strain RDT test, the strain is controlled in a standard haversine shape which has only the tensile portion. In order to impose the haversine shape on the strain, the stress curve always consists of a tensile portion and a compressive portion within each loading cycle. This phenomenon is described as process of residual compression stress building up due to the viscoelastic behavior of asphalt mixtures (Jacobs 1995). Three aspects of the controlled-strain RDT test are investigated in this study including: 1) the characteristics of the material responses, 2) the material properties obtained from the test, and 3) the storage and dissipation of energy in the test.

Since the asphalt mixture is a viscoelastic material in its undamaged state, its strain response in the nondestructive controlled-strain RDT test lags behind the stress, and the lag time is described using the phase angle φ. The modulus of the asphalt mixture is expressed in a complex form given as follows because of its viscoelastic nature (Findley et al. 1989):

$$E^* = E' + iE'' \tag{2.1}$$

where E^* is complex modulus; E' is the storage modulus; and E'' is the loss modulus. The magnitude of the complex modulus $\left|E^*\right|$ is defined as the dynamic modulus in the ASTM standard and is calculated as the ratio of σ_0 to ε_0 (ASTM 2003):

$$\left|E^*\right| = \sqrt{E'^2 + E''^2} = \frac{\sigma_0}{\varepsilon_0} \tag{2.2}$$

where σ_0 is the stress amplitude and ε_0 is the strain amplitude. The phase angle φ is calculated based on E' and E'':

$$\tan\varphi = \frac{E''}{E'} \tag{2.3}$$

Since the stress curve in a loading cycle of the controlled-strain RDT test consists of a tensile portion and a compressive portion, the dynamic modulus in the tensile stress portion may be different from that in the compressive stress portion. Khanal and Mamlouk (1995) reported that the dynamic modulus calculated from the tensile stress portion was different from that obtained from the compressive stress portion of the same loading cycle when applying a sinusoidal wave on an asphalt mixture. It has also been reported that the tension-induced damage has a significantly different nature from the

compression-induced damage in asphaltic materials (Erkens et al. 2003). Therefore, the modulus in the tensile stress portion should be differentiated from that in the compressive stress portion in the controlled-strain RDT test. Addressing the variation of the modulus of the asphalt mixture in different stress states leads to a more rational and realistic prediction of the fatigue and rutting lives of an asphalt pavement.

In addition to the moduli of the asphalt mixture in different stress states, the test data of the controlled-strain RDT test can also be used to investigate the storage and dissipation of energy in the asphalt mixture. The dissipated energy is defined as the dissipated strain energy (DSE), and the stored energy which can be recovered after removing the load is defined as the recoverable strain energy (RSE). The ratio of the DSE to the RSE indicates the damping ability of a viscoelastic material (Findley et al. 1989; Lakes 1999). The DSE and RSE can also be used to characterize the damage developed in asphalt mixtures. For example, the rate of change of the DSE was used to show the development of the fatigue damage (Ghuzlan and Carpenter 2006).

A prevalent method to determine the DSE and RSE in a loading cycle is to conduct the integration over every quarter of the period T of a loading cycle based on the basic equation that calculates the amount of the strain energy density (energy per unit volume) W in a loading period $[t_1, t_2]$:

$$W = \int_{t_1}^{t_2} \sigma(t) \frac{d\varepsilon(t)}{dt} dt \tag{2.4}$$

In a RDT test with a sinusoidal stress, the stress function is $\sigma = \sigma_0 \sin(\omega t)$ and the strain function is $\varepsilon = \varepsilon_0 \sin(\omega t - \varphi)$; then W in the first quarter of the first loading cycle

with $t_1 = 0$ and $t_2 = \pi/(2\omega)$ is calculated using Equation 2.5 (Lakes 1999):

$$W = \int_0^{\pi/2\omega} \sigma(t) \frac{d\varepsilon(t)}{dt} dt = \int_0^{\pi/2\omega} \left[\sigma_0 \varepsilon_0 \omega \sin(\omega t) \cos(\omega t - \varphi) \right] dt$$
$$= \sigma_0 \varepsilon_0 \frac{\pi \sin\varphi}{4} + \sigma_0 \varepsilon_0 \frac{\cos\varphi}{2} \tag{2.5}$$

where ω is the loading frequency in rad/sec and equals $2\pi / T$; and t is the loading time. In Equation 2.5, the term $\sigma_0 \varepsilon_0 \frac{\pi \sin\varphi}{4}$ is part of the DSE and it appears in the results of the integration over the next three quarters of the period T, while the term $\sigma_0 \varepsilon_0 \frac{\cos\varphi}{2}$ is part of the RSE and it appears in the integration result of the next quarter but with the opposite sign. Specifically, in the second quarter, W is calculated using Equation 2.6:

$$W = \int_{\pi/2\omega}^{\pi/\omega} \sigma(t) \frac{d\varepsilon(t)}{dt} dt = \sigma_0 \varepsilon_0 \frac{\pi \sin\varphi}{4} - \sigma_0 \varepsilon_0 \frac{\cos\varphi}{2} \tag{2.6}$$

The third quarter's W is the same as that of the first quarter, and the fourth quarter's W is the same as that of the second quarter. This traditional method considers that the RSE stored in the material in the first quarter is fully recovered in the second quarter and that the RSE stored in the third quarter is fully recovered in the fourth quarter. As a result, all RSE is recovered at the end of the cycle and the net RSE is zero. The total DSE is the sum of the DSE of every quarter of a loading cycle, which equals $\pi \sigma_0 \varepsilon_0 \sin\varphi$ ($4 \times \sigma_0 \varepsilon_0 \frac{\pi \sin\varphi}{4}$). This calculation of the total DSE using the traditional method is based on the assumption of no difference in material properties between the tensile stress portion and the compressive stress portion. This assumption may introduce non-

negligible errors in predicting the fatigue damage of asphalt mixtures. In addition, the RSE term $\sigma_0 \varepsilon_0 \frac{\cos\varphi}{2}$ is calculated mathematically without investigating the actual amount of energy recovered after unloading.

In order to address the material property variation in the controlled-strain RDT test and precisely determine the DSE and RSE in a loading cycle, this study investigates the material properties of an asphalt mixture specimen in the tensile stress portion and the compressive stress portion separately. The sign convention in this study is that tensile stresses and strains are considered positive and compressive stresses and strains are negative. The energy for heat generation is neglected in this study based on what is reported in the literature that the energy dissipated to generate heat in a fatigue test of asphalt mixtures is not significant (Kim et al. 2001).

2.2 Configurations and Procedure of Controlled-Strain RDT Test

The asphalt mixtures used are laboratory mixed and laboratory compacted using an unmodified asphalt binder and a common Texas limestone with a Type C dense aggregate gradation specified by the Texas Department of Transportation (TxDOT) (TxDOT 2004). The unmodified asphalt binder is labeled AAD in the Strategic Highway Research Program Materials Reference Library (Jones 1993). The limestone is shipped from a quarry in San Marcos, Texas. The optimum asphalt binder content is determined as 4.5% by weight of the mixture according to the TxDOT Tex-204-F test procedure (TxDOT 2005). The Superpave gyratory compactor is used to compact the asphalt mixture into cylindrical specimens 152 mm in diameter and 178 mm in height. In order

to obtain an approximately uniform air void distribution, the specimens produced by the Superpave gyratory compactor are cored and cut to 102 mm in diameter by 102 mm in height. The total air void content of the 102 mm by 102 mm specimens is controlled at 3.5 ± 0.5%.

The controlled-strain RDT test is conducted on the 102 mm by 102 mm specimens using the Material Test System (MTS) at a temperature of 20°C. Each test specimen is glued to a pair of end-caps and then set up in the environmental chamber of the MTS, as shown in Figure 2.1. Three axial linear variable differential transformers (LVDTs) and a bracelet LVDT are mounted on the middle part of the test specimen. The three axial LVDTs are placed at 120° apart from each other around the specimen surface to capture the axial deformation of the specimen. The bracelet LVDT is used to measure the radial deformation of the specimen.

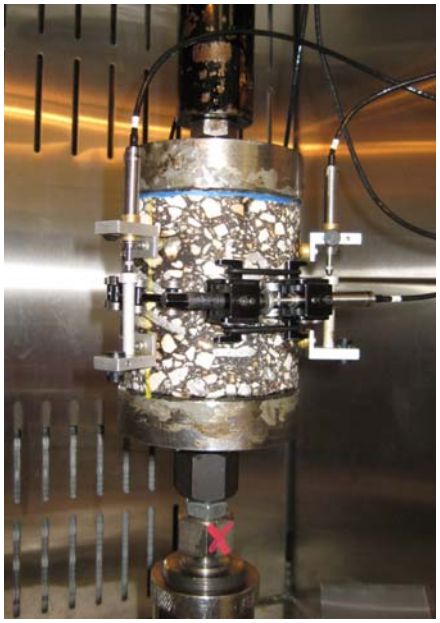

Figure 2.1 Configuration of Controlled-Strain RDT Test

Two consecutive controlled-strain RDT tests are performed on the same asphalt mixture specimen, including: 1) nondestructive RDT test with 200 cycles of load repetitions in which the maximum axial strain is approximately 40 με; and 2) destructive RDT test with 1,000 cycles of load repetitions in which the maximum axial strain is approximately 200 με. Two replicate specimens are tested following this same sequence. The loading frequency is 1 Hz in both the nondestructive and the destructive tests. The nondestructive RDT test is performed to obtain the properties of the undamaged specimen, which is the reference state from which the damage that is introduced into the asphalt mixture could be quantified. The reason for using the maximum strain level of 40 με in the nondestructive RDT test is that, in this small-strain condition, the asphalt mixture specimen exhibits linear viscoelastic properties and its deformation will fully recover after unloading (Carpenter et al. 2003; Gibson et al. 2003). After the nondestructive test is finished, the test specimen rests 10 min to recover its deformation before the destructive test starts. The destructive test uses a maximum axial strain of 200 με that is proven to be significant enough to introduce considerable damage to the asphalt mixture specimen.

In both nondestructive and destructive RDT tests, the axial strain is programmed to have a haversine shape, and it is found that the axial strain lags behind the axial stress because of the viscoelastic nature of the undamaged specimen. In order to control the axial strain in such a haversine profile, the applied axial stress has to consist of two parts, a tensile portion and a compressive portion, in a single loading cycle. Since the strain lags behind the stress, the strain is still positive at the point when the stress

changes from positive to zero. In order to make the strain zero, the stress must become negative. While the stress is negative, the specimen is still in tension because the strain is positive. This situation with a positive strain and a negative stress in the RDT tests is defined as "quasi-compression", and the corresponding material properties are defined with a prefix "quasi-" when the stress is compressive. Figure 2.2 shows the measured axial stress and axial strain curves in the destructive RDT test. As presented in Figure 2.2, a single loading cycle with a period of T from Point O to Point O' consists of two loading periods: T_t and T_c, where T_t refers to the period from Point O to Point N when the stress is tensile, and T_c refers to the period from Point N to Point O' when the stress is compressive. The time lag between the stress peak (Point L) and the strain peak (Point M') is the tensile phase angle φ_t; the time lag between the compressive stress peak (Point P) and the strain valley (Point Q') is the quasi-compressive phase angle φ_{qc}. Section 2.3 details the data filtering of the stress and strain signals, and the simulation of the filtered stress and strain curves.

2.3 Simulation of Stress Curve and Strain Curve

The accuracy of the magnitude and phase angle of the complex modulus depends on the accurate determination of the peak/valley of the stress and strain signals. The raw stress and strain signals provided by the MTS consist of a series of data points, from which the peak/valley are selected as the maximum/minimum value. Two factors influence the accuracy of the peak/valley from this selection. The first one is the time

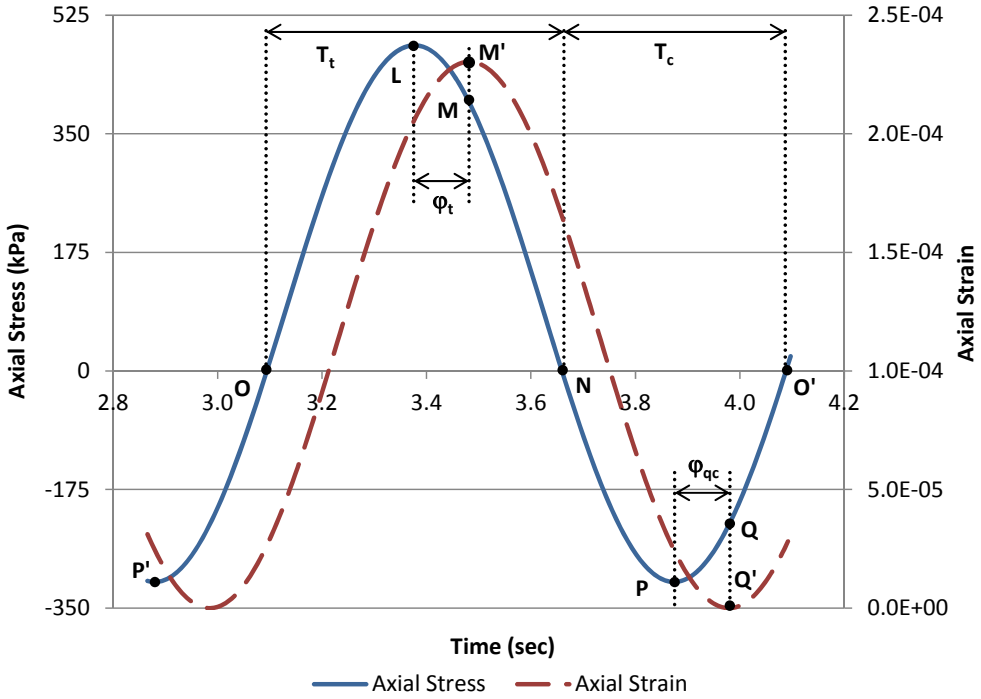

Figure 2.2 Measured Stress and Strain Data in a Destructive Controlled-Strain RDT Test

interval between two adjacent data points. If the time interval is too large, the maximum/minimum value determined from these data points are very likely not to be the true peak/valley values. It is desired to have a relatively small time interval in order to obtain more precise peak/valley values. However, a very small time interval makes the data processing time-consuming since a large amount of data points are acquired. In addition, even though the time interval can be set to be very small, it still cannot assure the accuracy because it is practically impossible to obtain a perfect haversine strain curve or a perfect shifted haversine stress curve due to the operational limitation of the MTS. The stress and strain curves are usually skewed and noisy to some extent. This operational limitation or precision of the MTS is the second factor that influences the

accuracy of data analysis. It is observed from the data analysis that the variation of the phase angle of the complex modulus among ten consecutive loading cycles can be as high as 10°. However, the actual increase of the phase angle of the complex modulus ranges from 5 to 10° due to 1,000 cycles of destructive loading. Therefore, the raw stress and strain signals from the MTS must be processed using a data filtering method.

Among the signal filtering methods that have been developed and documented in the literature, the Fourier Transform (FT) is found to successfully filter the stress and strain signals (Pellinen 2009). Consequently, the measured stress and strain signals are processed using the FT in the Matlab software. The transform of a single loading cycle is conducted on the tensile stress and compressive stress separately for the stress signal, and is also performed on the strain corresponding to the tensile stress and the strain corresponding to the compressive stress separately for the strain signal. The transformed data of the stress/strain in the tensile stress portion and the stress/strain in the compressive stress portion of a loading cycle are then composed to construct a new stress/strain curve for the entire loading cycle. The measured stress/strain signals and the stress/strain curves after the FT are presented in Figure 2.3, which demonstrates that the transformed stress/strain curves are significantly closer to perfect shifted-haversine/haversine curves. Since the skew and noise of the data are eliminated, the variation of the phase angle of the complex modulus among ten consecutive loading cycles is now within 2°. Using the FT to filter the stress/strain signals proves to successfully correct the operational errors attributed to the MTS apparatus, and significantly enhances the accuracy in determination of the magnitude and phase angle

of the complex modulus of asphalt mixtures.

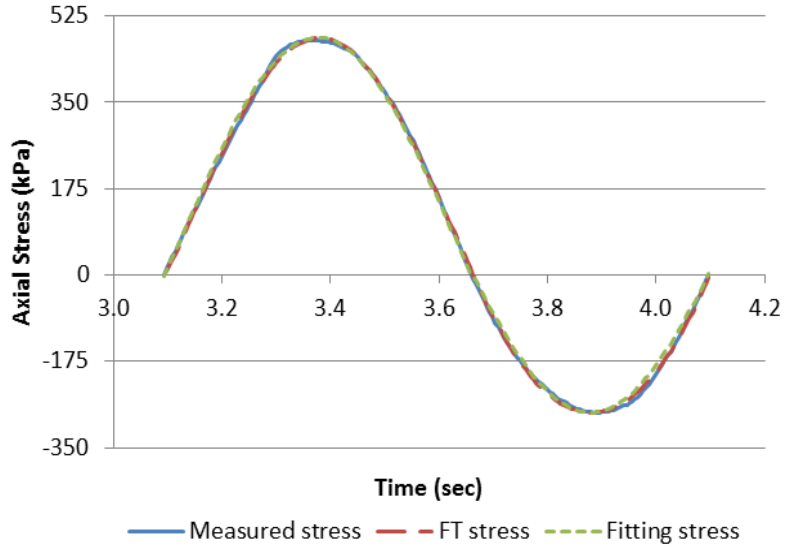

(a) Stress Curves

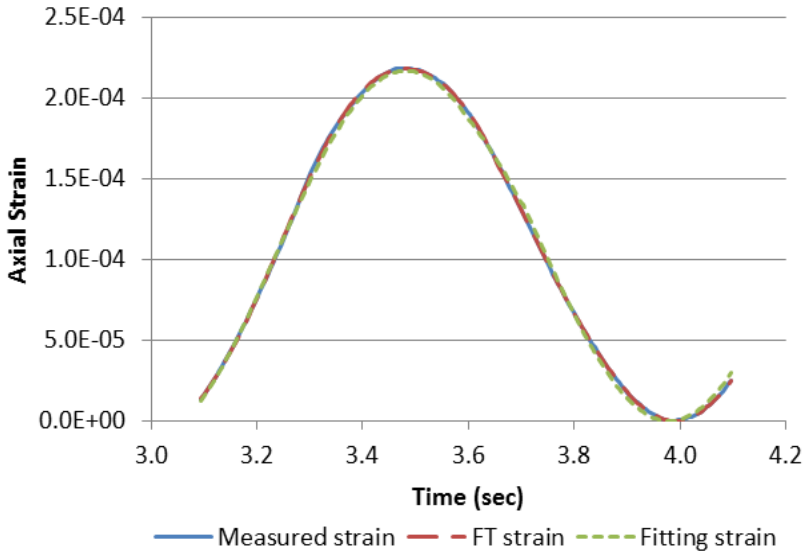

(b) Strain Curves

Figure 2.3 Stress and Strain Curves of the 1st Cycle in Destructive RDT Test

After filtering the stress/strain signals using the FT, the filtered stress and strain curves are simulated using mathematical models in order to determine the magnitude and phase angle of the complex modulus of the asphalt mixture specimen. During the simulation of the stress curve, the tensile stress and the compressive stress in a single loading cycle are simulated separately using the same functional form but with different parameters. Then the tensile stress curve and the compressive stress curve are superimposed to construct a smooth stress curve in the entire loading cycle, which simulates the filtered stress curve. Figure 2.4 illustrates how the tensile stress curve and compressive stress curve are simulated. The tensile stress curve is the solid curve from Point O to Point N in Figure 2.4(a); the time duration between the two points is T_t. The compressive stress curve is the solid curve from Point N to Point O' in Figure 2.4(b), and the time duration between the two points is T_c. The period of one complete loading cycle T is the sum of T_t and T_c. The tensile stress curve shown in Figure 2.4(a) is modeled by Equation 2.7:

$$\sigma_t = \sigma_{0t}\left[1-\cos\left(\omega t\right)\right]-\sigma_{st} \tag{2.7}$$

in which σ_{0t} is the tensile stress amplitude; and σ_{st} is the absolute value of the downward shift of a standard haversine wave as shown in Figure 2.4(a). If using σ_{tm} to denote the maximum tensile stress, the following relationship exists:

$$\sigma_{tm}+\sigma_{st}=2\sigma_{0t} \tag{2.8}$$

The difference between σ_{tm} and σ_{0t} is calculated as in Equation 2.9:

$$\sigma_{tm} - \sigma_{0t} = \sigma_{0t} \sin\left[\frac{2\pi}{T}\left(\frac{T_t}{2} - \frac{T}{4}\right)\right] \tag{2.9}$$

Solving Equation 2.9 for σ_{0t} gives:

$$\sigma_{0t} = \frac{\sigma_{tm}}{1 - \sin\left[\pi\left(\frac{1}{2} - \frac{T_t}{T}\right)\right]} \tag{2.10}$$

Substituting Equation 2.8 into Equation 2.10 gives:

$$\sigma_{st} = \sigma_{tm} \cdot \frac{1 + \sin\left[\pi\left(\frac{1}{2} - \frac{T_t}{T}\right)\right]}{1 - \sin\left[\pi\left(\frac{1}{2} - \frac{T_t}{T}\right)\right]} \tag{2.11}$$

Similarly, the compressive stress curve is modeled by Equation 2.12:

$$\sigma_c = \sigma_{0c}\left[1 - \cos\left(\omega t\right)\right] - \sigma_{cm} \tag{2.12}$$

and the compressive stress amplitude σ_{0c} is calculated as in Equation 2.13:

$$\sigma_{0c} - \sigma_{cm} = \sigma_{0c} \sin\left[\frac{2\pi}{T}\left(\frac{T}{4} - \frac{T_c}{2}\right)\right] \tag{2.13}$$

where σ_{cm} is the magnitude of the minimum stress as shown in Figure 2.4(b). Solving Equation 2.13 for σ_{0c} gives:

$$\sigma_{0c} = \frac{\sigma_{cm}}{1 - \sin\left[\pi\left(\frac{1}{2} - \frac{T_c}{T}\right)\right]} \tag{2.14}$$

Based on the calculated tensile stress amplitude and compressive stress amplitude, the filtered stress and strain curves are simulated using the following equations:

1. When the stress is tensile:

$$\sigma_t = \sigma_{0t}\left[1-\cos(\omega t)\right]-\sigma_{st} \tag{2.15}$$

$$\varepsilon = \varepsilon_0\left[1-\cos(\omega t-\varphi_t)\right] \tag{2.16}$$

2. When the stress is compressive:

$$\sigma_c = \sigma_{0c}\left[1-\cos(\omega t)\right]-\sigma_{cm} \tag{2.17}$$

$$\varepsilon = \varepsilon_0\left[1-\cos\left(\omega t-\varphi_{qc}\right)\right] \tag{2.18}$$

where ε_0 is the amplitude of the filtered strain curve. Accordingly, the magnitude of the tensile complex modulus $\left|E_t^*\right|$, and the magnitude of the quasi-compressive complex modulus $\left|E_{qc}^*\right|$, are defined by Equations 2.19 and 2.20, respectively:

$$\left|E_t^*\right| = \frac{\sigma_{0t}}{\varepsilon_0} \tag{2.19}$$

$$\left|E_{qc}^*\right| = \frac{\sigma_{0c}}{\varepsilon_0} \tag{2.20}$$

where E_t^* is the tensile complex modulus; and E_{qc}^* is the quasi-compressive complex modulus.

The simulation and calculation process detailed above is applied to every loading cycle of the 200 nondestructive loading cycles and the 1,000 destructive loading cycles. As a result, every loading cycle has a tensile phase angle φ_t, a quasi-compressive phase angle φ_{qc}, and a set of parameters of the stress and strain models, σ_{0t}, σ_{st}, σ_{0c}, σ_{cm}, and ε_0. These parameters are used to construct a fitting stress curve and a fitting strain curve in the corresponding loading cycle. The fitting stress curve of every loading cycle

is superimposed on the fitting stress curves of other loading cycles to construct a smooth fitting stress curve for all loading cycles in the nondestructive and destructive RDT tests. The same superimposition is conducted on the strain curves as well. Figure 2.3 illustrates the goodness of the curve fitting.

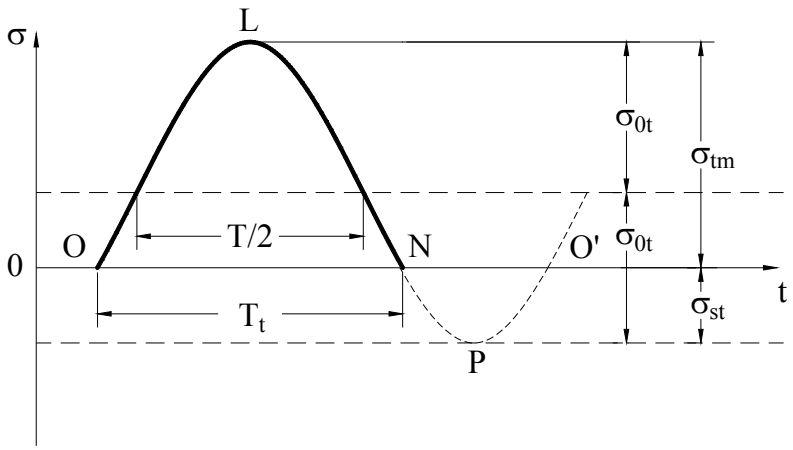

(a) Tensile Stress Curve

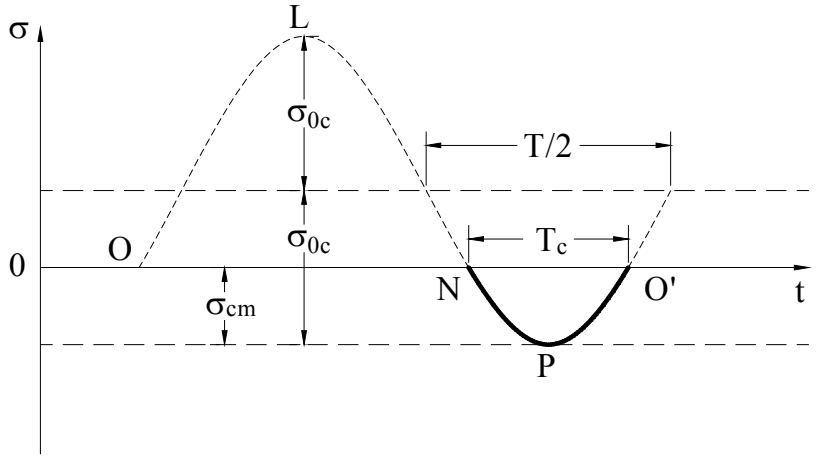

(b) Compressive Stress Curve

Figure 2.4 Simulation of Axial Stress Curve

The model parameters in each loading cycle are used to determine the magnitudes of the tensile complex modulus $\left|E_t^*\right|$ and the quasi-compressive complex modulus $\left|E_{qc}^*\right|$. To further reduce the operational error, the experimental data from ten consecutive loading cycles are averaged and this average value is designated to be the first loading cycle of the ten cycles. For example, the average value of $\left|E_t^*\right|$ of loading cycle No. 1, 2, 3, 4, 5, 6, 7, 8, 9, and 10 is regarded as $\left|E_t^*\right|$ of loading cycle No. 1; the average value of φ_t of loading cycle No. 50, 51, 52, 53, 54, 55, 56, 57, 58, and 59 is assigned to loading cycle No. 50. Section 2.4 will present the statistical analysis of the calculated magnitudes and phase angles of the complex moduli.

2.4 Statistical Analysis of Test Data

Statistical analysis is performed on the complex moduli calculated in Section 2.3 in order to investigate: a) whether there is a difference between the tensile complex modulus and the quasi-compressive modulus in every loading cycle of the nondestructive and destructive RDT tests; and b) whether the tensile complex modulus and the quasi-compressive modulus vary with the increase of the number of loading cycles in the nondestructive and destructive RDT tests. During the investigation, the magnitude and phase angle of the tensile and quasi-compressive complex moduli are firstly plotted against the number of loading cycles as shown in Figures 2.5 to 2.8, respectively. Two observations are made from Figures 2.5 to 2.8: a) both magnitude and phase angle of the tensile complex modulus are different from those of the quasi-

compressive complex modulus at every loading cycle of both nondestructive and destructive RDT tests; and b) the magnitude and phase angle of both tensile complex modulus and quasi-compressive complex modulus remain approximately constant with the increase of the number of loading cycles in the nondestructive RDT test, but they vary with the increase of the number of loading cycles in the destructive RDT test. These two observations are verified using the statistical hypothesis tests.

The first step of conducting a statistical hypothesis test is to state the null and alternative hypotheses for the population of interest. There are eight populations from the combination of four types of material properties and two types of controlled-strain RDT test: 1) $\left|E_t^*\right|$ in the nondestructive RDT test, denoted $\left|E_t^*\right|_N$; 2) φ_t in the nondestructive RDT test, denoted φ_{tN}; 3) $\left|E_{qc}^*\right|$ in the nondestructive RDT test, denoted $\left|E_{qc}^*\right|_N$; 4) φ_{qc} in the nondestructive RDT test, denoted φ_{qcN}; 5) $\left|E_t^*\right|$ in the destructive RDT test, denoted $\left|E_t^*\right|_D$; 6) φ_t in the destructive RDT test, denoted φ_{tD}; 7) $\left|E_{qc}^*\right|$ in the destructive RDT test, denoted $\left|E_{qc}^*\right|_D$; 8) φ_{qc} in the destructive RDT test, denoted φ_{qcD}. In order verify the two observations made from Figures 2.5 to 2.8, the null hypothesis H_0 and the alternative hypothesis H_a are constructed and presented in Table 2.1. Note the difference between the nondestructive and destructive RDT tests in the statement for H_0 and H_a. This is because Figures 2.5 to 2.8 seem to suggest that the material property in the nondestructive test has one value, but the material property in the destructive test has different values at different loading cycles.

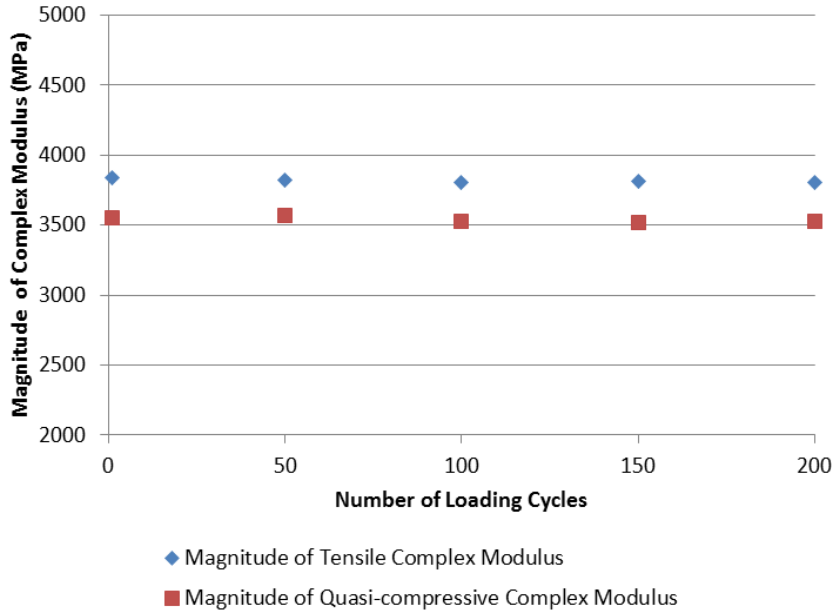

Figure 2.5 Magnitude of Complex Modulus at Various Numbers of Loading Cycles in Nondestructive RDT Test

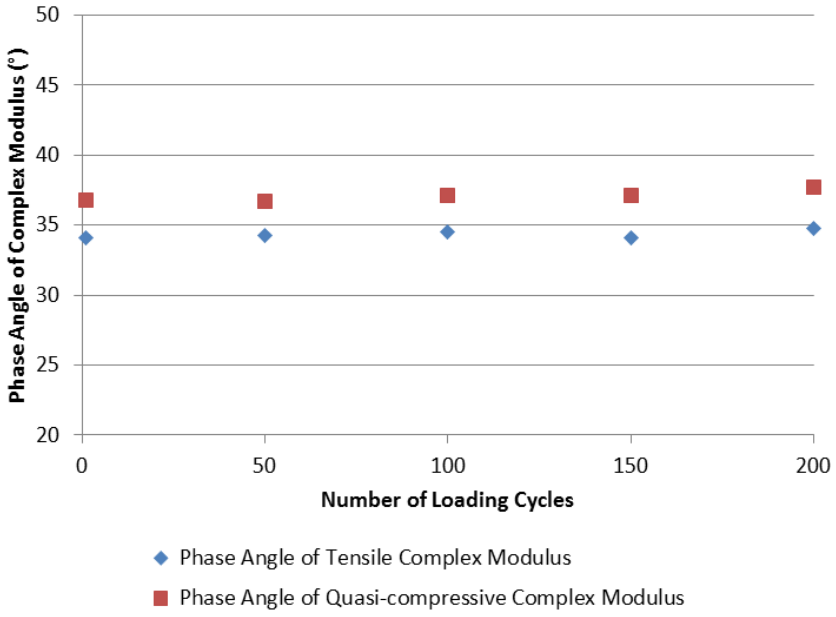

Figure 2.6 Phase Angle of Complex Modulus at Various Numbers of Loading Cycles in Nondestructive RDT Test

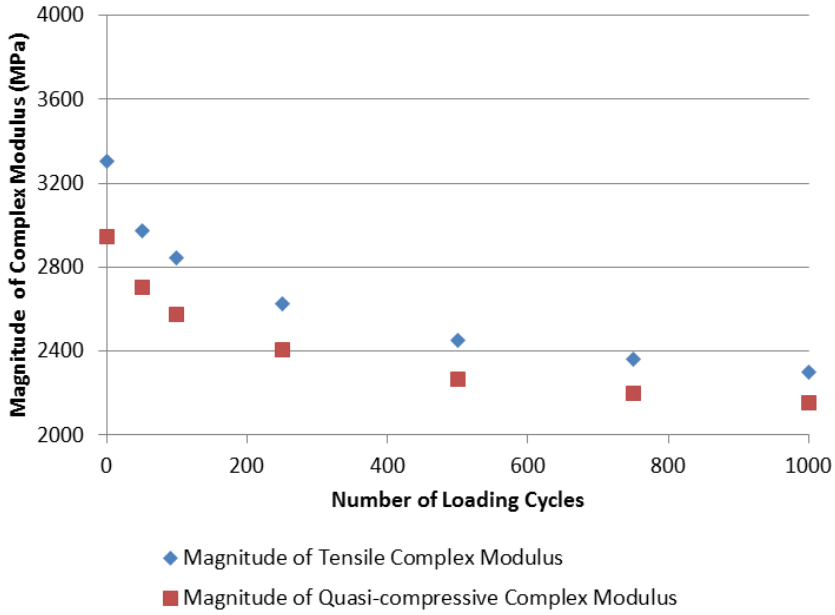

Figure 2.7 Magnitude of Complex Modulus at Various Numbers of Loading Cycles in Destructive RDT Test

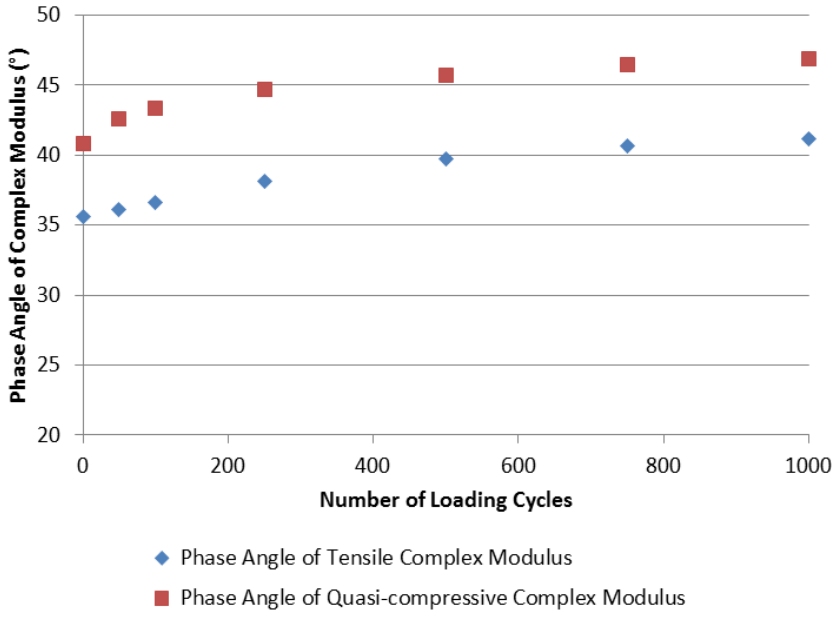

Figure 2.8 Phase Angle of Complex Modulus at Various Numbers of Loading Cycles in Destructive RDT Test

The second step is to select a subset representative of a population that is measured, i.e. sampling. The population size of 1), 2), 3) and 4) is 200, and the population size of 5), 6), 7), and 8) is 1,000. According to Bartlett et al. (2001), the minimum sample size for a population size of 200 at 95% confidence level is 75, and that for a population size of 1,000 at the same confidence level is 106. As a result, the sample size for 1) to 4) is selected as 80, which means that 80 loading cycles should be selected from the 200-cycles nondestructive RDT test. Specifically, 80 loading cycles are selected as 1^{st} - 10^{th}, 50^{th} - 59^{th}, 75^{th} - 84^{th}, 100^{th} - 109^{th}, 125^{th} - 134^{th}, 150^{th} - 159^{th}, 175^{th} - 184^{th}, and 190^{th} - 199^{th}. The sample size for 5) to 8) is selected as 110, indicating that 110 loading cycles is selected from the 1,000-cycles destructive RDT test. Specifically, 110 loading cycles are 1^{st} - 10^{th}, 50^{th} - 59^{th}, 100^{th} - 109^{th}, 175^{th} - 184^{th}, 250^{th} - 259^{th}, 375^{th} - 384^{th}, 500^{th} - 509^{th}, 625^{th} - 634^{th}, 750^{th} - 759^{th}, 875^{th} - 884^{th}, and 990^{th} - 999^{th}. Corresponding to the eight populations as described above, there are eight samples now, designated as S1, S2, S3, S4, S5, S6, S7, and S8, respectively.

After determining the sample for each population, the next step is to consider whether the statistical assumptions that are made about the sample are satisfied. There are two basic statistical assumptions: independence between variables and normality of data. The assumption of independence between variables is satisfied for Hypothesis I to XII shown in Table 2.1. This is because for each hypothesis none of the measurement of one variable is dependent on the measurement of others. The assumption of normality of data is assessed using the Q-Q plot (Ott and Longnecker 2001). The Q-Q plot for each sample (S1 to S8) is made using the software SPSS. The results suggest that the

normality condition appears to be satisfied for S1, S2, S3, and S4, but it is violated for S5, S6, S7, and S8. In other words, the data from S1, or S2, S3, S4, appear to have a normal distribution, while the data from S5, S6, S7, and S8 do not. Once the statistical assumptions are assessed, the statistical test that is appropriate for the hypotheses listed in Table 2.1 can be decided. The selected statistical tests for Hypothesis I to XII are presented in Table 2.2. A brief introduction about the purpose of each statistical test is given in Table 2.2 as well. Details of these statistical tests can be found in Ott and Longnecker (2001). All the statistical tests listed in Table 2.2 are conducted using SPSS and the results are shown in Appendix A.

Table 2.1 Null Hypothesis and Alternative Hypothesis for Statistical Testing

Hypothesis	**Null Hypothesis (H_0)**	**Alternative Hypothesis (H_a)**
I	$\left\|E_t^*\right\|_N - \left\|E_{qc}^*\right\|_N \le 0$	$\left\|E_t^*\right\|_N - \left\|E_{qc}^*\right\|_N > 0$
II	$\varphi_{tN} - \varphi_{qcN} \ge 0$	$\varphi_{tN} - \varphi_{qcN} < 0$
III	$\left\|E_t^*\right\|_D$ and $\left\|E_{qc}^*\right\|_D$ are identical	$\left\|E_t^*\right\|_D$ is shifted above $\left\|E_{qc}^*\right\|_D$
IV	φ_{tD} and φ_{qcD} are identical	φ_{tD} is shifted below φ_{qcD}
V*	$\overline{\left\|E_t^*\right\|}_{N1} = \overline{\left\|E_t^*\right\|}_{N2} = \overline{\left\|E_t^*\right\|}_{N3} = \cdots = \overline{\left\|E_t^*\right\|}_{Ni}$	At least one $\overline{\left\|E_t^*\right\|}_N$ differs from the rest
VI*	$\overline{\varphi}_{t\,N1} = \overline{\varphi}_{t\,N2} = \overline{\varphi}_{t\,N3} = \cdots = \overline{\varphi}_{t\,Ni}$	At least one $\overline{\varphi}_{t\,N}$ differs from the rest
VII*	$\overline{\left\|E_{qc}^*\right\|}_{N1} = \overline{\left\|E_{qc}^*\right\|}_{N2} = \overline{\left\|E_{qc}^*\right\|}_{N3} = \cdots = \overline{\left\|E_{qc}^*\right\|}_{Ni}$	At least one $\overline{\left\|E_{qc}^*\right\|}_N$ differs from the rest
VIII*	$\overline{\varphi}_{qc\,N1} = \overline{\varphi}_{qc\,N2} = \overline{\varphi}_{qc\,N3} = \cdots = \overline{\varphi}_{qc\,Ni}$	At least one $\overline{\varphi}_{qc\,N}$ differs from the rest

Table 2.1 Continued

Hypothesis	Null Hypothesis (H_0)	Alternative Hypothesis (H_a)
IX**	$\left\|E_t^*\right\|_{D1}, \left\|E_t^*\right\|_{D2}, \left\|E_t^*\right\|_{D3}, \cdots \left\|E_t^*\right\|_{Di}$ are identical	At least one $\left\|E_t^*\right\|_D$ differs from the rest
X**	$\varphi_{tD1}, \varphi_{tD2}, \varphi_{tD3}, \cdots \varphi_{tDi}$ are identical	At least one φ_{tD} differs from the rest
XI**	$\left\|E_{qc}^*\right\|_{D1}, \left\|E_{qc}^*\right\|_{D2}, \left\|E_{qc}^*\right\|_{D3}, \cdots \left\|E_{qc}^*\right\|_{Di}$ are identical	At least one $\left\|E_{qc}^*\right\|_D$ differs from the rest
XII**	$\varphi_{qcD1}, \varphi_{qcD2}, \varphi_{qcD3}, \cdots \varphi_{qcDi}$ are identical	At least one φ_{qcD} differs from the rest

*: $\overline{\left|E_t^*\right|}_{Ni}$, $\overline{\varphi}_{t\,Ni}$, $\overline{\left|E_{qc}^*\right|}_{Ni}$, $\overline{\varphi_{qc\,Ni}}$ are group means of a group of corresponding material property, and i is the number of groups.

**: $\left|E_t^*\right|_{Di}$, φ_{tDi}, $\left|E_{qc}^*\right|_{Di}$, φ_{qcDi} are a group of corresponding material property, and i is the number of groups.

Table 2.2 Statistical Tests for Statistical Hypothesis Testing

Hypothesis	Statistical Test	Purpose of Test
I	Independent t-test	Compare means between S1 and S3
II	Independent t-test	Compare means between S2 and S4
III	Wilcoxon Rank Sum test	Compare distributions between S5 and S7
IV	Wilcoxon Rank Sum test	Compare distributions between S6 and S8
V	One way ANOVA	Determine whether there are significant differences between the means of 8 groups (i = 8) of S1, 10 loading cycles in each group
VI	One way ANOVA	Determine whether there are significant differences between the means of 8 groups (i = 8) of S2, 10 loading cycles in each group
VII	One way ANOVA	Determine whether there are significant differences between the means of 8 groups (i = 8) of S3, 10 loading cycles in each group

Table 2.2 Continued

Hypothesis	Statistical Test	Purpose of Test
VIII	One way ANOVA	Determine whether there are significant differences between the means of 8 groups ($i = 8$) of S4, 10 loading cycles in each group
IX	Kruskal-Wallis test	Determine whether there are significant differences between the distributions of 11 groups ($i = 11$) of S5, 10 loading cycles in each group
X	Kruskal-Wallis test	Determine whether there are significant differences between the distributions of 11 groups ($i = 11$) of S6, 10 loading cycles in each group
XI	Kruskal-Wallis test	Determine whether there are significant differences between the distributions of 11 groups ($i = 11$) of S7, 10 loading cycles in each group
XII	Kruskal-Wallis test	Determine whether there are significant differences between the distributions of 11 groups ($i = 11$) of S8, 10 loading cycles in each group

For Hypotheses I, II, III, and IV, all the *p*-values, as circled, are almost zero. Since all $p\text{-values} < 0.05 = \alpha$, all the null hypotheses constructed for Hypotheses I, II, III, and IV shown in Table 2.1 are rejected. In other words, at the $\alpha = 0.05$ level of significance, there is enough evidence to conclude that there is a difference between the tensile complex modulus and the quasi-compressive complex modulus. Specifically , the magnitude of the tensile complex modulus is larger than that of the quasi-compressive complex modulus and that the phase angle of the tensile complex modulus is smaller than that of the quasi-compressive complex modulus.

The difference between the tensile complex modulus and the quasi-compressive complex modulus can be explained by the phenomenon of crack opening and closure in the test specimen during a single loading cycle. Figure 2.9 shows a schematic sketch of the opening and closure of a crack in the specimen at different stages of a complete loading cycle. The initial crack is an air void. When an increasing tensile load is applied to the specimen (from Point O to L in Figure 2.9), the deformation of the specimen is delayed due to the viscous effect, and the deformation in the vicinity of the air void is also delayed. Furthermore, the stress level has to be high enough to overcome the effect of interfacial forces of attraction (surface energy) and to generate new surfaces. Consequently, the initial crack (air void) may start to propagate at Point R as shown in Figure 2.9. The crack continues to grow while the strain increases to its peak value at Point S and decreases to reach Point T. The crack may have its largest size at Point T and starts to close. The viscosity and localized plastic deformation in damaged asphalt mixtures drive viscous fluid-induced closure and plasticity-induced closure, respectively, which are two of the five mechanisms for the crack closure identified by Suresh and Ritchie (1984). The closure of the crack continues until Point R', when the deformation in the vicinity of the air void completely recovers. Point R' is also the starting point of cracking opening for the next loading cycle.

When the crack is propagating, the material is losing cross-sectional area to take the tensile stress. Therefore, the larger the crack, the weaker the material behaves. The tensile properties are measured at Point S, where the crack is smaller than that at Point U at which the quasi-compressive properties are measured. As a result, the material

behaves stronger in the tensile stress portion than in the compressive stress portion. Specifically, $\left|E_t^*\right|$ is larger than $\left|E_{qc}^*\right|$, and φ_t is smaller than φ_{qc} in every loading cycle of the RDT test.

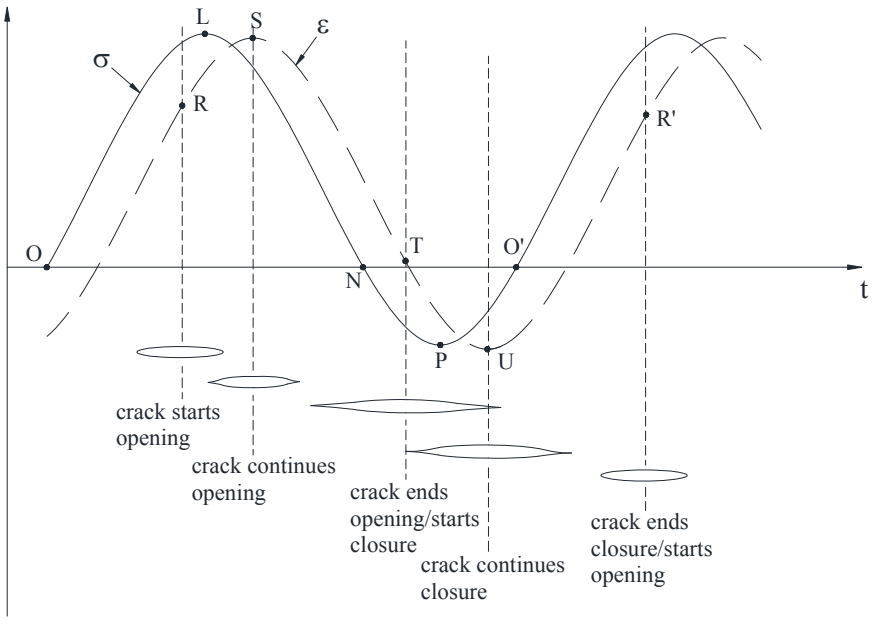

Figure 2.9 Schematic Plot of Crack Opening and Closure at Different Stages of a Complete Loading Cycle

For Hypotheses V, VI, VII, and VIII, all the *p*-values, as circled, are larger than α (0.05). Therefore, the results fail to reject each null hypothesis corresponding to Hypotheses V, VI, VII, and VIII in Table 2.1, respectively. This indicates that there is insufficient evidence to prove that $\left|E_t^*\right|_N$, φ_{tN}, $\left|E_{qc}^*\right|_N$ and φ_{qcN} vary with the increase of the number of loading cycles. In other words, it is proven that both the tensile and quasi-compressive complex moduli remain approximately the same in each loading cycle of

the nondestructive RDT test and that no damage is introduced to the specimen. The material properties obtained from the nondestructive RDT test are the properties of the undamaged asphalt mixture specimen and can serve as the reference state from which the damage grows in the destructive RDT test.

In the destructive RDT test, the results for Hypotheses IX, X, XI, and XII suggest that the corresponding null hypothesis is rejected at the $\alpha = 0.05$ level of significance, since the corresponding *p*-value is less than 0.05. This fact indicates that $\left|E_t^*\right|_D$, φ_{tD}, $\left|E_{qc}^*\right|_D$ and φ_{qcD} all vary with the increase of the number of loading cycles. Specifically, with the increase of the number of loading cycles in the destructive RDT test, $\left|E_t^*\right|_D$ and $\left|E_{qc}^*\right|_D$ decrease, and φ_{tD} and φ_{qcD} increase.

2.5 Calculation of Dissipated Strain Energy and Recoverable Strain Energy

Based on the measurement and analysis of the tensile and quasi-compressive properties of undamaged and damaged asphalt mixture specimens, Section 2.5 utilizes these material properties to determine the DSE and RSE. Firstly, the stress-strain diagram in the form of a hysteresis loop is plotted in Figure 2.10 based on the stress and strain data shown in Figure 2.2. Both Figures 2.2 and 2.10 show a full loading cycle from Point O through Points L, M, N, P, Q to Point O'. These points on a full loading cycle in Figures 2.2 and 2.10 correspond to each other. Point O and O' overlap each other in Figure 2.10. In the loading cycle from Point O to O', the tensile stress portion

T_t is from Point O through L to N, and the compressive stress portion T_c is from Point N through P to O'.

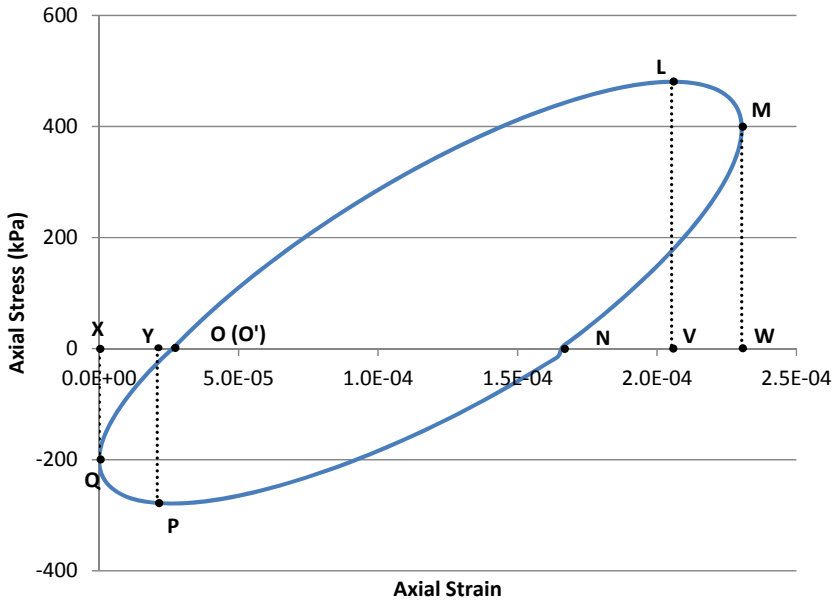

Figure 2.10. Hysteresis Loop of a Loading Cycle in Destructive RDT Test

As shown in Figure 2.10, the material is storing energy from Point O to L, and the amount of the stored energy during this period is the closed area OLV. From Point L to M, the material continues storing energy with an amount of the closed area $LMWV$. From Point M to N, the material is recovering energy, and the amount of the recovered energy is the area MWN. Therefore, the total amount of the stored energy in the period T_t is the area $OLMW$, and the recovered energy in T_t is the area MWN. Consequently, the amount of irrecoverable energy that dissipates to overcome the viscous resistance of the material and to develop damage is calculated by deducting the

recovered energy (area MWN) from the stored energy ($OLMW$) in this period. As a result, the total DSE in T_t is determined to be the area $OLMN$, and the RSE in T_t is the area MWN. Similar analysis is applied to the compressive stress portion T_c in Figure 2.10. During the period T_c, the stored energy is the area $NPQX$, and the recovered energy is the area QXO'. Therefore, the DSE in the period T_c is the area $NPQO'$, and the RSE is the area QXO'. Table 2.4 summarizes the stored energy, recovered energy, total DSE and RSE in T_t and T_c.

Table 2.4 Dissipated and Recoverable Strain Energy in a Loading Cycle

Loading Period			Energy Stored/Recovered	Amount of Energy
Stress State	**From Point**	**To Point**		
T_t	O	L	Stored	Area OLV
	L	M	Stored	Area $LMWV$
	M	N	Recovered	Area MWN
	Total DSE = Area $OLMN$; Total RSE = Area MWN			
T_c	N	P	Stored	Area NPY
	P	Q	Stored	Area $PQXY$
	Q	O'	Recovered	Area QXO'
	Total DSE = Area $NPQO'$; Total RSE = Area QXO'			

The DSE and RSE visualized in Figure 2.10 are further quantified using Equation 2.4. For loading period T_t, the stress and strain functions shown in Equations 2.15 and 2.16, respectively, are used in the integration. For loading period T_c, the stress and strain functions shown in Equations 2.17 and 2.18, respectively. For calculation convenience,

Point O in Figures 2.2 and 2.10 is supposed to correspond to $t=\frac{T_c}{2}$. Then Points L, M, N, P, Q and O' correspond to $t=\frac{\pi}{\omega},\frac{\pi}{\omega}+\frac{\varphi_t}{\omega},\frac{\pi}{\omega}+\frac{T_t}{2},\frac{2\pi}{\omega},\frac{2\pi}{\omega}+\frac{\varphi_{qc}}{\omega},\frac{2\pi}{\omega}+\frac{T_c}{2}$, respectively. Table 2.5 summarizes the lower limit and upper limit of each integration function to calculate the DSE or. All integrations are performed using Matlab and the determined DSE and RSE formulas are shown as follows:

$$\begin{aligned}\mathrm{DSE}=&\sigma_{0t}\varepsilon_0\left\{\frac{\sin\varphi_t\left[2\pi-\sin(T_c\omega)+\sin(T_t\omega)-T_c\omega+T_t\omega\right]}{4}-\frac{\cos\varphi_t\left[\cos(T_c\omega)-\cos(T_t\omega)\right]}{4}\right\}\\&+(\sigma_{0t}-\sigma_{st})\varepsilon_0\left\{\sin\varphi_t\left[\sin\left(\frac{T_t\omega}{2}\right)+\sin\left(\frac{T_c\omega}{2}\right)\right]+\cos\varphi_t\left[\cos\left(\frac{T_t\omega}{2}\right)+\cos\left(\frac{T_c\omega}{2}\right)\right]\right\}\\&+\sigma_{0c}\varepsilon_0\left\{\frac{\sin\varphi_{qc}\left[2\pi+\sin(T_c\omega)-\sin(T_t\omega)+T_c\omega-T_t\omega\right]}{4}+\frac{\cos\varphi_{qc}\left[\cos(T_c\omega)-\cos(T_t\omega)\right]}{4}\right\}\\&+(\sigma_{0c}-\sigma_{cm})\varepsilon_0\left\{-\sin\varphi_{qc}\left[\sin\left(\frac{T_t\omega}{2}\right)+\sin\left(\frac{T_c\omega}{2}\right)\right]-\cos\varphi_{qc}\left[\cos\left(\frac{T_t\omega}{2}\right)+\cos\left(\frac{T_c\omega}{2}\right)\right]\right\}\end{aligned}\tag{2.21}$$

$$\begin{aligned}\mathrm{RSE}=&\sigma_{0t}\varepsilon_0\left\{-\frac{\sin\varphi_t\left[2\varphi_t+\sin(2\varphi_t)-\sin(T_t\omega)-T_t\omega\right]}{4}-\frac{\cos\varphi_t\left[\cos^2\varphi_t-\cos^2\left(\frac{T_t\omega}{2}\right)\right]}{2}\right\}\\&+(\sigma_{0t}-\sigma_{st})\varepsilon_0\left\{\sin\varphi_t\left[\sin\left(\frac{T_t\omega}{2}\right)-\sin\varphi_t\right]+\cos\varphi_t\left[\cos\left(\frac{T_t\omega}{2}\right)-\cos\varphi_t\right]\right\}\\&+\sigma_{0c}\varepsilon_0\left\{-\frac{\sin\varphi_{qc}\left[2\varphi_{qc}+\sin(2\varphi_{qc})-\sin(T_c\omega)-T_c\omega\right]}{4}-\frac{\cos\varphi_{qc}\left[\cos^2\varphi_{qc}-\cos^2\left(\frac{T_c\omega}{2}\right)\right]}{2}\right\}\\&+(\sigma_{0c}-\sigma_{cm})\varepsilon_0\left\{-\sin\varphi_{qc}\left[\sin\left(\frac{T_c\omega}{2}\right)-\sin\varphi_{qc}\right]-\cos\varphi_{qc}\left[\cos\left(\frac{T_c\omega}{2}\right)-\cos\varphi_{qc}\right]\right\}\end{aligned}\tag{2.22}$$

Table 2.5 Integration Bands for the DSE and RSE in a Complete Loading Cycle

Energy	Stress Direction	Lower Limit t_1	Upper Limit t_2
DSE	Tensile	$\frac{T_c}{2}$	$\frac{\pi}{\omega}+\frac{T_t}{2}$
	Compressive	$\frac{\pi}{\omega}+\frac{T_t}{2}$	$\frac{2\pi}{\omega}+\frac{T_c}{2}$
RSE	Tensile	$\frac{\pi}{\omega}+\frac{\varphi_t}{\omega}$	$\frac{\pi}{\omega}+\frac{T_t}{2}$
	Compressive	$\frac{2\pi}{\omega}+\frac{\varphi_{qc}}{\omega}$	$\frac{2\pi}{\omega}+\frac{T_c}{2}$

The stress and strain data are then input to Equations 2.21 and 2.22 to calculate the DSE and RSE of every loading cycle. Figure 2.11 illustrates the calculated DSE and RSE of representative loading cycles of the destructive RDT test. It can be observed from Figure 2.11 that the DSE increases and the RSE decreases with the increase of the number of loading cycles. In order to verify the calculation results of the proposed method, a numerical method, the Double Meridian Distance (DMD) method, is used to calculate the DSE of each loading cycle. The DMD method is a surveying method used to numerically determine the actual area within a closed loop (Wolf and Ghilani 2005). Since the total DSE of a loading cycle is the area within the stress and strain hysteresis loop shown in Figure 2.10, the DMD method is able to successfully determine the DSE of a loading cycle by assessing the area of the stress-strain hysteresis loop. The calculation results of the DSE using the DMD method are also illustrated in Figure 2.11, in which the DSE calculated using the proposed method approximately overlays that

determined using the DMD method at each representative loading cycle. This fact clearly demonstrates the accuracy of the proposed method.

Furthermore, the traditional method, which does not address the difference between tensile properties and quasi-compressive properties, is also used to calculate the DSE and RSE in order to evaluate the assumption that material properties stay the same in the tensile state and quasi-compressive state. Since the tensile stress portion is not distinguished from the compressive stress portion in the traditional method, Equations 2.23 and 2.24 are the general stress and strain functions, respectively, in the integration of calculating the energy.

$$\sigma = \sigma_0 \left[1 - \cos(\omega t)\right] - \sigma_{cm} \tag{2.23}$$

$$\varepsilon = \varepsilon_0 \left[1 - \cos(\omega t - \varphi)\right] \tag{2.24}$$

in which $\sigma_0 = \frac{\sigma_{tm} + \sigma_{cm}}{2}$; and $\varphi = \varphi_t$ because the traditional tensile phase angle is measured from the tensile stress portion. The integration is conducted over a quarter of the period T of one loading cycle, and the integration result is multiplied by 4 to obtain the total DSE and RSE. Following the same procedure as stated in Section 2.1, the DSE and RSE as calculated based on Equations 2.23 and 2.24 are

$$\text{DSE} = \pi \sigma_0 \varepsilon_0 \sin\varphi_t \tag{2.25}$$

$$\text{RSE} = 2\left(\sigma_0 - \sigma_{cm}\right)\varepsilon_0 \cos\varphi_t \tag{2.26}$$

The DSE and RSE calculated using the traditional method are also shown in Figure 2.11 and are compared to the results of the other two methods. The DSE calculated using the traditional method is clearly smaller than that calculated using the proposed method or

the DMD method, indicating that assuming that the tensile properties are the same as the quasi-compressive properties underestimates the damage generated in the asphalt mixture. This underestimation is not conservative in pavement design. The RSE calculated using the traditional method is significantly smaller than that determined using the proposed method, suggesting that Equation 2.26 does not produce the actual amount of energy recovered after unloading. In fact, the term $\sigma_0\varepsilon_0\frac{\cos\varphi}{2}$ in Equation 2.5 for the sinusoidal loading wave and the term $2(\sigma_0-\sigma_{cm})\varepsilon_0\cos\varphi_t$ for the haversine loading wave are only mathematical terms in the integration results. The traditional method arbitrarily considers them as the RSE, which is not appropriate.

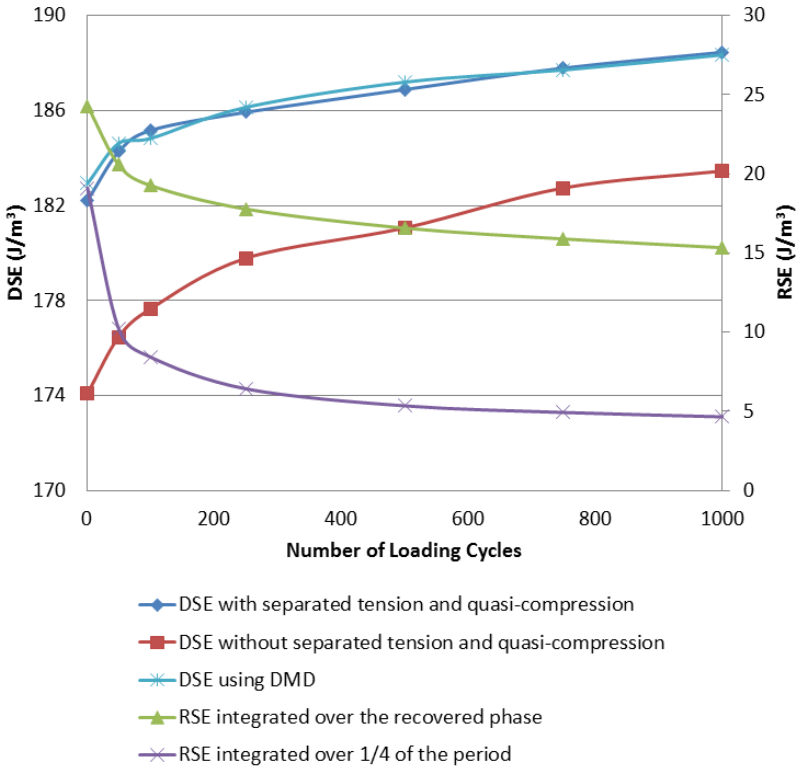

Figure 2.11. DSE and RSE in Destructive RDT Test

3. CHARACTERIZATION OF FATIGUE DAMAGE IN ASPHALT MIXTURES USING PSEUDO STRAIN ENERGY

3.1 Relationship between Fatigue Cracking and Permanent Deformation

Fatigue cracking and permanent deformation are prevalent distresses of asphalt pavements under repeated traffic loading. Fatigue cracking is induced by crack growth in a small increment in each loading cycle, while permanent deformation refers to an accumulation of plastic strain in the asphalt mixture with the increase of loading cycles. Both types of distress have been evaluated using laboratory experiments. Fatigue tests have been developed to evaluate the fatigue resistance of asphalt mixtures. Common fatigue tests include the repeated flexural bending test (ASTM 2010), indirect tension test (Roque et al. 1997; Kim et al. 2002) and uniaxial cyclic test (Si et al. 2002; Walubita 2006). These tests are usually conducted at room temperature in accordance with the understanding that fatigue cracking is predominant at moderate temperatures. Separate laboratory tests have also been developed to measure permanent deformation of asphalt mixtures, such as the creep test and repeated loading test in a temperature range from 40 to 70°C (Sousa et al. 1994) since yielding of the asphalt mixture and plastic deformation become vital at elevated temperatures. The results of the fatigue tests and permanent deformation tests are interpreted using models (most of which are empirical) to simulate the evolution of fatigue cracking and permanent deformation, respectively. For example, fatigue cracking is modeled using the Paris' law in terms of the crack growth rate per cycle as a function of material properties obtained from the fatigue tests (Kim 2008).

Models for permanent deformation are usually regression functions illustrating the relationship between the permanent strain and the number of loading cycles (Barksdale 1972; Monismith et al. 1975; Kenis 1977; NCHRP 1-37A 2002).

As a matter of fact, it is not appropriate to characterize the fatigue cracking and permanent deformation of asphalt mixtures separately because fatigue cracking and permanent deformation develop simultaneously as two companion components of the damage, regardless of the temperature. In other words, both cracking and permanent deformation develop simultaneously under destructive repeated loading at any temperature. Meanwhile, fatigue cracking and permanent deformation are closely related to each other. In a visco-elasto-plastic material like an asphalt mixture, cracking is accompanied by a large amount of plastic deformation in the localized regions around the cracks. The localized plastic deformation not only contributes to one part of the permanent deformation but also initiates the growth of fatigue cracking from air voids. The other part of the permanent deformation results from the yielding of the bulk intact material; when the yielding of the bulk intact material reaches a critical level, more cracks develop in the bulk intact material. Elber (1971) used experimental and analytical techniques to prove that the existence of permanent deformation led to a considerable reduction of allowable load cycles to fatigue cracking failure. Consequently, it is more realistic to treat the development of fatigue cracking and permanent deformation as one damaging process rather than treating them separately as two damaging processes using two separate tests. It is fairly easy to generate both fatigue cracking and permanent deformation in an asphalt mixture specimen using the destructive repeated loading test.

However, it has not been practical to simultaneously measure both fatigue cracking and permanent deformation generated in the same specimen.

An energy-based approach has been used to separate fatigue cracking from permanent deformation in terms of energy consumption. Specifically, separation of the two types of damage in an asphalt mixture specimen can be conducted by distinguishing the energy consumed for each damage type. The energy expended on fatigue cracking is then used in crack growth models to predict the development of fatigue cracking, and the remaining dissipated energy is used in plasticity models to predict the development of permanent deformation. The sum of these two parts of energy is the total energy dissipated for the total damage generated in the material, which is defined as the dissipated pseudo strain energy (DPSE). Although the DPSE has been used as an index to characterize the damage in asphalt mixtures for more than a decade (Little et al. 1998; Lytton 2000; Kim et al. 2002; Si et al. 2002; Arambula et al. 2007), it is still a challenge to properly separate the total DPSE into two parts: one for cracking and the other for permanent deformation. Masad et al. (2007) proposed to partition the DPSE into three components, including: 1) a component associated with the increase of the phase angle; 2) a component accounting for the change in the stiffness; and 3) a component related to permanent deformation. The first and second components are considered to be related to fatigue cracking since the increase of the phase angle and change in the stiffness are due to the crack growth in the material. The third component, which is calculated by subtracting the first and second components from the total DPSE, is thus associated with permanent deformation. However, this partition method is phenomenological rather than

mechanistic in nature and does not accurately describe the energy expended for each type of damage.

In order to address the aforementioned research gaps, Section 3 aims at characterizing the fatigue cracking and permanent deformation of asphalt mixtures by separating the DPSE for the fatigue cracking from the DPSE for the permanent deformation from a mechanistic perspective. Firstly, the material properties of a typical asphalt mixture under different stress levels are investigated to differentiate the linear viscoelastic, nonlinear viscoelastic and damaged regions on the stress-strain curve of the asphalt mixture. This investigation provides the theoretical foundation for the test protocol design.

3.2 Material Properties of Asphalt Mixtures under Different Stress Levels

Asphalt mixtures exhibit different properties at different levels of deformation. The stress-strain curve of a typical paving asphalt mixture consists of the undamaged region and the damaged region, as shown in Figure 3.1. These two regions are separated at the critical nonlinear viscoelastic point (Point E in Figure 3.1). The undamaged region includes the linear viscoelastic region and the nonlinear viscoelastic region, separated by Point B in Figure 3.1. The nonlinear viscoelastic behavior of an undamaged asphalt mixture is due to the rotation and translation of aggregates and localized high strains in the asphalt mastic (Kose et al. 2000). The different properties of the asphalt mixture in the three regions can be characterized using the controlled-strain RDT.

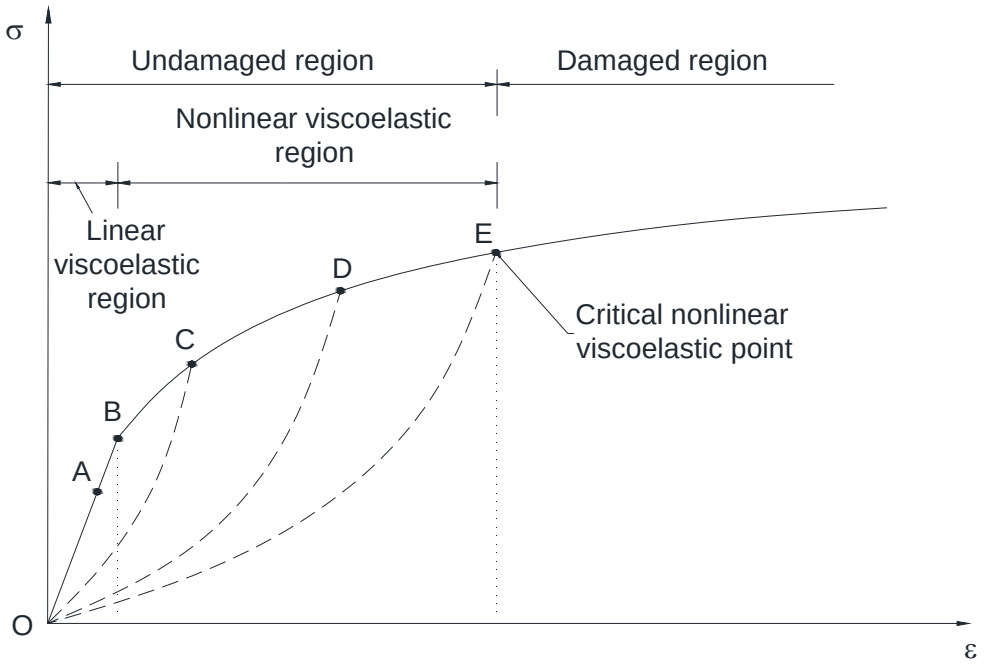

Figure 3.1 Stress-Strain Curve of Typical Asphalt Mixtures

When changing the stress amplitude in the controlled-strain RDT test, the deformation of the asphalt mixture may be in the linear viscoelastic region, nonlinear viscoelastic region or the damaged region. As a result, the measured E_t^* and E_{qc}^* may vary since the asphalt mixture behaves differently in the three regions.

- If the axial strain of the specimen is within the linear viscoelastic region (from Point O to Point B in Figure 3.1),
  - both E_t^* and E_{qc}^* remain the same with the increase of the number of loading cycles in the controlled-strain RDT test; and
  - neither E_t^* nor E_{qc}^* change when the loading level varies (as long as the loading level is low enough to produce only linear viscoelastic strain) in

the controlled-strain RDT test.

For example, if the loading curve is from Point O to A, $\left|E_t^*\right|$ and $\left|E_{qc}^*\right|$ stay constant since curve OB is a straight line and the slope of OA stays the same. In addition, the unloading curve AO is a straight line since it is within the linear viscoelastic region. Therefore, φ_t and φ_{qc} remain the same. If Point A moves to any other location on Line OB, the above statements remain correct because the slope of Line OB remains the same and the unloading curve BO overlies the loading curve OB.

- If the axial strain of the specimen is in the nonlinear viscoelastic region (from Point B to Point E in Figure 3.1),
  - both E_t^* and E_{qc}^* remain the same with the increase of the number of loading cycles in the controlled-strain RDT test, provided that the loading level stays constant; and
  - as long as the loading level changes to a higher level that produces a higher strain within the nonlinear viscoelastic region, both $\left|E_t^*\right|$ and $\left|E_{qc}^*\right|$ decrease, and both φ_t and φ_{qc} increase.

  For example, if the loading curve is OC (solid curve) in Figure 3.1 and the unloading curve is CO (dashed curve), both magnitude and phase angle of the complex moduli remain the same with the increase of the number of the loading cycles since the tangent to the stress-strain curve at Point C does not vary and the area within the loading and unloading loop does not change.

When strain level moves from Point C to Point D in Figure 3.1, the tangent to the stress-strain curve at Point D is smaller than that at Point C, and the area within the loading and unloading loop OD is larger than the area within the loading and unloading loop OC. Therefore, $\left|E_t^*\right|$ and $\left|E_{qc}^*\right|$ at Point D are smaller than those at Point C, and both φ_t and φ_{qc} at Point D are larger than those at Point C.

- If the axial strain of the specimen is in the damaged region (beyond Point E in Figure 3.1),
  - both $\left|E_t^*\right|$ and $\left|E_{qc}^*\right|$ decrease, and both φ_t and φ_{qc} increase, with the increase of the number of loading cycles in the controlled-strain RDT test; and
  - when the loading level changes to a higher level, both $\left|E_t^*\right|$ and $\left|E_{qc}^*\right|$ decrease, and both φ_t and φ_{qc} increase.

Based on the above investigation on the material properties of the asphalt mixture in different deformation regions, a comprehensive experimental plan is designed to measure the material properties of asphalt mixtures under different stress levels. An important objective of the experimental testing is to determine the strain level corresponding to Point E in Figure 3.1 in order to separate the undamaged region from the damaged region on the stress-strain curve of the asphalt mixture. The undamaged region must be separated from the damaged region in calculating the DPSE. The Section 3.3 details the laboratory tests conducted on selected asphalt mixture specimens.

3.3 Procedure of Laboratory Tests on Asphalt Mixtures

A series of consecutive controlled-strain RDT tests with different strain levels are performed on the same test specimen, as shown in Figure 3.2. All tests are conducted at a frequency of 1 Hz. There is a 15 min rest period between two consecutive RDT tests in order to completely recover any possible deformation.

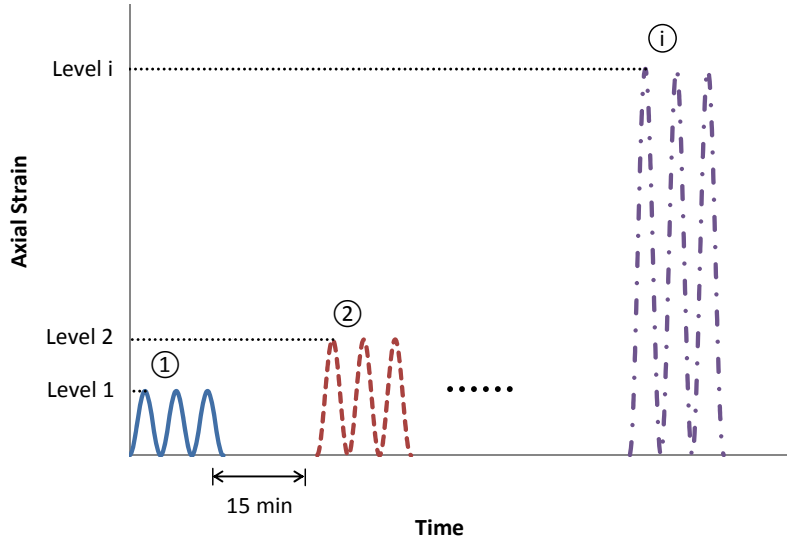

Figure 3.2 Sequence of Controlled-Strain RDT Tests

In the 1st controlled-strain RDT test, the maximum axial strain is controlled at 40 με to assure that the deformation of the asphalt mixture is within the linear viscoelastic region so that the deformation will fully recover after unloading (Carpenter et al. 2003; Gibson et al. 2003). The test data are used to calculate $\left|E_t^*\right|$, φ_t, $\left|E_{qc}^*\right|$ and φ_{qc} of the specimen for every loading cycle using Equations 1 through 6. Then the F-test is

performed on the calculated $\left|E_t^*\right|$, φ_t, $\left|E_{qc}^*\right|$ and φ_{qc} to determine whether they vary with the increase of the number of loading cycles. The null hypothesis H_0 and the alternative hypothesis H_a are constructed for $\left|E_t^*\right|$, φ_t, $\left|E_{qc}^*\right|$, and φ_{qc}, respectively, as listed in Table 3.1. The subscript of each notation in Table 3.1 has a number indicating the number of loading cycles. For example, $\left|E_{t1}^*\right|$ is the magnitude of the tensile complex modulus in loading cycle No. 1 in the corresponding RDT test. The values of F-statistic and critical F-statistic at a 95% confidence level are calculated using the software Excel and are presented in Table 3.2. For the 1st RDT test with a 40 με maximum axial strain, the F-statistic of each material property is smaller than the critical F-statistic. As a result, the F-test fails to reject the null hypotheses, and it is concluded that $\left|E_t^*\right|$, φ_t, $\left|E_{qc}^*\right|$, and φ_{qc} are approximately the same in each loading cycle. Therefore, the deformation of the test specimen is within the undamaged region during the 1st RDT test with a 40 με maximum axial strain. Subsequently, the average of $\left|E_{tN1}^*\right|$, $\left|E_{tN50}^*\right|$, $\left|E_{tN100}^*\right|$, $\left|E_{tN150}^*\right|$, and $\left|E_{tN200}^*\right|$ is computed to be the value of $\left|E_t^*\right|$. Similarly, the calculated values of each of the other three properties (φ_t, $\left|E_{qc}^*\right|$ and φ_{qc}) at loading cycle No. 1, 50, 100, 150 and 200 are averaged to be the value of the corresponding property. The calculated values of $\left|E_t^*\right|$, φ_t, $\left|E_{qc}^*\right|$ and φ_{qc} are listed in Table 3.3.

Since the deformation of the test specimen is proved to be in the undamaged region in the 1st RDT test, the maximum axial strain level is then increased from 40 με to

50 με by an increment of 10 με in order to search for the critical nonlinear viscoelastic point (Point E in Figure 3.1). As a result, the same test specimen is rested for 15 min and is then subjected to the 2nd RDT test with the maximum axial strain of 50 με. Then the same data analysis procedure for the 1st RDT test applies to the data of the 2nd RDT test:

1) Calculate $\left|E_t^*\right|$, φ_t, $\left|E_{qc}^*\right|$ and φ_{qc} of the specimen for every loading cycle; and
2) Perform the F-test on the calculated $\left|E_t^*\right|$, φ_t, $\left|E_{qc}^*\right|$ and φ_{qc} to determine whether they vary with the increase of the number of loading cycles.

The constructed null hypothesis H_0 and alternative hypothesis H_a for the F-test are shown in Table 3.1. The F-statistic of each material property is smaller than the critical F-statistic, as shown in Table 3.2. As a result, it is concluded that $\left|E_t^*\right|$, φ_t, $\left|E_{qc}^*\right|$, and φ_{qc} are approximately the same in each loading cycle of the 2nd RDT test with the maximum axial strain of 50 με. In other words, the deformation of the test specimen is within the undamaged region in the 2nd RDT test. The average values of $\left|E_t^*\right|$, φ_t, $\left|E_{qc}^*\right|$ and φ_{qc} at representative loading cycles are then computed to be the values of these properties, as listed in Table 3.3.

Because the deformation of the test specimen is still in the undamaged region in the 2nd RDT test, the maximum axial strain is once again increased by an increment of 10 με to the level of 60 με in the 3rd RDT test to continue searching for Point E in Figure 3.1. After performing the 3rd RDT test on the same test specimen, the same data analysis procedure applies to the test data of the 3rd RDT test, and the F-test hypotheses and statistics are listed in Tables 3.1 and 3.2. The statistical analysis proves that $\left|E_t^*\right|$, φ_t,

$\left|E_{qc}^{*}\right|$, and φ_{qc} are approximately the same in each loading cycle of the 3rd RDT test. Therefore, the deformation of the test specimen is still in the undamaged region in the 3rd RDT test. Then the average values of $\left|E_{t}^{*}\right|$, φ_{t}, $\left|E_{qc}^{*}\right|$ and φ_{qc} are calculated based on the corresponding values of representative loading cycles, and are listed in Table 3.3.

Table 3.1 Hypotheses in F-Test

Maximum Strain (με)	**Material Property**	**Null Hypothesis (H_0)**	**Alternative Hypothesis (H_a)**
40, 50, 60, 70	$\left\|E_{t}^{*}\right\|$	$\left\|E_{t1}^{*}\right\| = \left\|E_{t50}^{*}\right\| = \left\|E_{t100}^{*}\right\| = \left\|E_{t150}^{*}\right\| = \left\|E_{t200}^{*}\right\|$	At least one $\left\|E_{t}^{*}\right\|$ differs from the rest
	φ_{t}	$\varphi_{t1} = \varphi_{t50} = \varphi_{t100} = \varphi_{t150} = \varphi_{t200}$	At least one φ_{t} differs from the rest
	$\left\|E_{qc}^{*}\right\|$	$\left\|E_{qc1}^{*}\right\| = \left\|E_{qc50}^{*}\right\| = \left\|E_{qc100}^{*}\right\| = \left\|E_{qc150}^{*}\right\| = \left\|E_{qc200}^{*}\right\|$	At least one $\left\|E_{qc}^{*}\right\|$ differs from the rest
	φ_{qc}	$\varphi_{qc1} = \varphi_{qc50} = \varphi_{qc100} = \varphi_{qc150} = \varphi_{qc200}$	At least one φ_{qc} differs from the rest
200	$\left\|E_{t}^{*}\right\|$	$\left\|E_{t1}^{*}\right\| = \left\|E_{t50}^{*}\right\| = \left\|E_{t100}^{*}\right\| = \left\|E_{t250}^{*}\right\| = \left\|E_{t500}^{*}\right\| = \left\|E_{t750}^{*}\right\| = \left\|E_{t1000}^{*}\right\|$	At least one $\left\|E_{t}^{*}\right\|$ differs from the rest
	φ_{t}	$\varphi_{t1} = \varphi_{t50} = \varphi_{t100} = \varphi_{t250} = \varphi_{t500} = \varphi_{t750} = \varphi_{t1000}$	At least one φ_{t} differs from the rest
	$\left\|E_{qc}^{*}\right\|$	$\left\|E_{qc1}^{*}\right\| = \left\|E_{qc50}^{*}\right\| = \left\|E_{qc100}^{*}\right\| = \left\|E_{qc250}^{*}\right\| = \left\|E_{qc500}^{*}\right\| = \left\|E_{qc750}^{*}\right\| = \left\|E_{qc1000}^{*}\right\|$	At least one $\left\|E_{qc}^{*}\right\|$ differs from the rest
	φ_{qc}	$\varphi_{qc1} = \varphi_{qc50} = \varphi_{qc100} = \varphi_{qc250} = \varphi_{qc500} = \varphi_{qc750} = \varphi_{qc1000}$	At least one φ_{qc} differs from the rest

Table 3.2 Values of F-Statistic and Critical F-Statistic of F-Test

Material Property	F-Statistic				
	40 με	**50 με**	**60 με**	**70 με**	**200 με**
$\left\|E_t^*\right\|$	1.362	1.280	1.373	5.543	157.5
φ_t	1.740	1.181	0.208	4.080	16.15
$\left\|E_{qc}^*\right\|$	1.056	0.310	1.482	2.302	63.85
φ_{qc}	0.349	0.531	1.507	2.339	14.88
Critical F-Statistic (95% Confidence Level)	2.579				2.246

Table 3.3 Measured Material Properties in RDT Tests

Material Property	Strain Level		
	40 με	**50 με**	**60 με**
$\left\|E_t^*\right\|$ (MPa)	5027	4971	4953
φ_t (°)	26.28	26.87	27.59
$\left\|E_{qc}^*\right\|$ (MPa)	4412	4169	4076
φ_{qc} (°)	28.65	29.22	30.08

Although statistical analysis proves that the first three RDT tests are all nondestructive and that the material properties of the test specimen do not change with the increase of the number of loading cycles, Table 3.3 shows that the test specimen exhibits different properties when the maximum axial strain changes from one level to the next higher level. Specifically, as the maximum axial strain increases, the values of $\left|E_t^*\right|$ and $\left|E_{qc}^*\right|$ decreases, and the values of φ_t and φ_{qc} increases. These observations are verified using the t-test. The null hypothesis H_0 and the alternative hypothesis H_a are

constructed and presented in Table 3.4. The values of the t-statistic and critical t-statistic are calculated and listed in Table 3.5. The absolute values of the t-statistics of all four properties are larger than their corresponding critical t-statistics at a 95% confidence level. The results of the t-tests indicate that the constructed null hypotheses shown in Table 3.4 are rejected. In other words, the t-test results prove that, when the maximum axial strain increases, both $\left|E_t^*\right|$ and $\left|E_{qc}^*\right|$ decreases, and both φ_t and φ_{qc} increases. Based on Figure 3.1 and the analysis above, it can be inferred that the deformation of the test specimen must be within the nonlinear viscoelastic region in the 2nd and 3rd RDT test.

Table 3.4 Hypotheses in t-Test

Material Property	Null Hypothesis (H_0)	Alternative Hypothesis (H_a)
$\left\|E_t^*\right\|$	$\left\|\overline{E_t^*}\right\|_i - \left\|\overline{E_t^*}\right\|_{i+1} \le 0$	$\left\|\overline{E_t^*}\right\|_i - \left\|\overline{E_t^*}\right\|_{i+1} > 0$
φ_t	$\left(\overline{\varphi}_t\right)_i - \left(\overline{\varphi}_t\right)_{i+1} \ge 0$	$\left(\overline{\varphi}_t\right)_i - \left(\overline{\varphi}_t\right)_{i+1} < 0$
$\left\|E_{qc}^*\right\|$	$\left\|\overline{E}_{qc}^*\right\|_i - \left\|\overline{E}_{qc}^*\right\|_{i+1} \le 0$	$\left\|\overline{E}_{qc}^*\right\|_i - \left\|\overline{E}_{qc}^*\right\|_{i+1} > 0$
φ_{qc}	$\left(\overline{\varphi}_{qc}\right)_i - \left(\overline{\varphi}_{qc}\right)_{i+1} \ge 0$	$\left(\overline{\varphi}_{qc}\right)_i - \left(\overline{\varphi}_{qc}\right)_{i+1} < 0$

i = number of loading level, = 1, 2…

Table 3.5 Values of t-Statistic and Critical t-Statistic of t-Test

Material Property	t-Statistic (40 με vs. 50 με)	t-Statistic (50 με vs. 60 με)	Critical t-Statistic (95% Confidence Level)
$\left\|E_t^*\right\|$	5.339	4.944	2.132
φ_t	-3.313	-5.638	
$\left\|E_{qc}^*\right\|$	16.302	4.540	
φ_{qc}	-4.896	-3.283	

After the first three RDT tests, the test specimen is once again rested for 15 min and is subjected to the 4th RDT test with the maximum axial strain of 70 με. The F-test is performed on the test data; the hypotheses and statistics are listed in Tables 3.1 and 3.2. The F-statistics of $\left|E_t^*\right|$ and φ_t are larger than the critical F-statistic at the 95% confidence level, while the F-statistics of $\left|E_{qc}^*\right|$ and φ_{qc} are slightly smaller than the critical F-statistic at the 95% confidence level. This fact proves that at least $\left|E_t^*\right|$ and φ_t vary with the increase of the number of loading cycles, which suggests the occurrence of damage in the specimen. Consequently, the 4th RDT test is a destructive test that introduces damage to the test specimen, and the deformation of the specimen is within the damaged region in the 4th RDT test.

Based on the analysis on the test data of the four RDT tests, it can be concluded that the critical nonlinear viscoelastic point (Point E in Figure 3.1) corresponds to a strain level between 60 με and 70 με. For convenience, the strain level of 60 με is regarded as the critical nonlinear viscoelastic point (Point E in Figure 3.1), which is the threshold loading level between the nondestructive loading and the destructive loading. Therefore, the material properties at the strain level of 60 με are defined as critical nonlinear viscoelastic properties and will be used as reference properties in order to quantify the damage in the specimen. These critical nonlinear viscoelastic properties include the magnitudes and phase angles of the tensile and quasi-compressive complex moduli, which are denoted as $\left|E_{tNLVE}^*\right|$, φ_{tNLVE}, $\left|E_{qcNLVE}^*\right|$, and φ_{qcNLVE}, respectively.

Once the strain level corresponding to the critical nonlinear viscoelastic point is

determined, a destructive RDT test with 200 με is conducted on the same test specimen to introduce significant damage to the specimen. The test data are used to calculate the material properties, including $\left|E_t^*\right|$, φ_t, $\left|E_{qc}^*\right|$ and φ_{qc}, of the test specimen at every loading cycle.

After the properties of the test specimen at different stress levels are determined, the test data of the nondestructive and destructive RDT tests stated above are used to calculate the pseudo strain and pseudo strain energy of the specimen at different load levels. Section 3.4 details the calculation of the pseudo strain and pseudo strain energy.

3.4 Calculation of Pseudo Strain and Pseudo Strain Energy

3.4.1 Calculation of Pseudo Strain

Pseudo strain is an essential parameter for separating the viscoelastic effect from the damage that is generated in an asphalt mixture. It is defined based on Schapery's extended elastic-viscoelastic correspondence principle (Schapery 1984) as follows:

$$\varepsilon_R = \frac{1}{E_R}\int_0^t E(t-\tau)\frac{d\varepsilon(\tau)}{d\tau}d\tau = \frac{\sigma_{VE}(t)}{E_R} \tag{3.1}$$

where ε_R is the pseudo strain; t is the loading time; τ is any arbitrary time between 0 an t; $E(t)$ is the relaxation modulus of undamaged asphalt mixture; E_R is the reference modulus that is used to achieve a dimensionless variable for ε_R; and $\sigma_{VE}(t)$ is the viscoelastic stress corresponding to the strain history $\varepsilon(t)$.

In order to calculate ε_R in the controlled-strain RDT test, $\sigma_{VE}(t)$ should be determined first. As detailed in previous Section 2, a loading cycle in any controlled-strain RDT test has two stress portions, a tensile stress portion and a compressive stress portion, in order to maintain the strain curve with the haversine shape. When the stress is tensile in a loading cycle of the RDT test, the strain can be reformulated as:

$$\begin{aligned}\varepsilon &= \varepsilon_0\left[1-\cos\left(\omega t-\varphi_t\right)\right]\\ &= \varepsilon_0-\varepsilon_0\cos\left(\omega t-\varphi_t\right)\\ &= \varepsilon_1-\varepsilon_2\end{aligned} \tag{3.2}$$

where $\varepsilon_1=\varepsilon_0$, which is a constant strain history corresponding to the viscoelastic stress σ_{VE1}; and $\varepsilon_2=\varepsilon_0\cos\left(\omega t-\varphi_t\right)$, which is a sinusoidal strain history in response to the viscoelastic stress σ_{VE2}. The formulations of σ_{VE1} and σ_{VE2} are given in Equations 3.3 and 3.4, respectively (Wineman and Rajagopal 2000).

$$\sigma_{VE1}=\varepsilon_0 E(t) \tag{3.3}$$

$$\sigma_{VE2}=\varepsilon_0\left|E_{tu}^*\right|\cos\left(\omega t-\varphi_t+\varphi_{tu}\right) \tag{3.4}$$

where $\left|E_{tu}^*\right|$ and φ_{tu} are the magnitude and phase angle of the tensile complex modulus of the undamaged asphalt mixture, respectively, or the reference material properties of the undamaged asphalt mixture. Based on the identification of the threshold loading level between the nondestructive loading and the destructive loading in Section 3.3, the critical nonlinear viscoelastic properties at the critical nonlinear viscoelastic point (Point E in Figure 3.1) are used as the reference material properties in Equation 3.4, which then becomes:

$$\sigma_{VE2} = \varepsilon_0 \left| E^*_{tNLVE} \right| \cos\left(\omega t - \varphi_t + \varphi_{tNLVE}\right) \tag{3.5}$$

The viscoelastic stresses corresponding to ε_1 and ε_2 are superimposed to obtain the viscoelastic stress corresponding to ε, as shown in Equation 3.6.

$$\sigma_{VEt} = \varepsilon_0 E\left(t\right) - \varepsilon_0 \left| E^*_{tNLVE} \right| \cos\left(\omega t - \varphi_t + \varphi_{tNLVE}\right) \tag{3.6}$$

where σ_{VEt} is the viscoelastic stress in the tensile stress portion of a loading cycle of the RDT test. When the axial deformation of the asphalt mixture is at the critical nonlinear viscoelastic state, which is 60 με in the specific case stated in Section 3.3, σ_{VEt} is calculated by substituting $\varepsilon_0 = \varepsilon_{0,60}$ and $\varphi_t = \varphi_{NLVE}$ into Equation 3.6:

$$\sigma_{VEt,60} = \varepsilon_{0,60} E\left(t\right) - \varepsilon_{0,60} \left| E^*_{tNLVE} \right| \cos\left(\omega t - \varphi_{tNLVE} + \varphi_{tNLVE}\right) \tag{3.7}$$

where $\varepsilon_{0,60}$ is the strain amplitude in the RDT test with the maximum axial strain level of 60 με. The viscoelastic stress at this loading level is the same as the measured stress ($\sigma_{t,60}$) because there is no damage introduced to the specimen at this loading level and the measured stress corresponds to the viscoelastic strain. According to Equation 2.15, the measured stress can be formulated as:

$$\sigma_{t,60} = \sigma_{0t,60}\left[1 - \cos\left(\omega t\right)\right] - \sigma_{st,60} \tag{3.8}$$

Based on Equation 2.19, $\sigma_{0t,60} = \varepsilon_{0,60} \left| E^*_{tNLVE} \right|$, which is substituted into Equation 3.8 to obtain:

$$\sigma_{t,60} = \varepsilon_{0,60} \left| E^*_{tNLVE} \right| \left[1 - \cos\left(\omega t\right)\right] - \sigma_{st,60} \tag{3.9}$$

Since $\sigma_{t,60} = \sigma_{VEt,60}$, Equations 3.7 and 3.9 are utilized to solve for $E\left(t\right)$:

$$E(t) = \left|E^*_{tNLVE}\right| - \frac{\sigma_{st,60}}{\varepsilon_{0,60}} \tag{3.10}$$

As a result, instead of measuring the relaxation modulus ($E(t)$), $E(t)$ can be calculated using Equation 3.10 based on $\left|E^*_{tNLVE}\right|$, $\sigma_{st,60}$ and $\varepsilon_{0,60}$, all of which are obtained from the nondestructive RDT test with the maximum axial strain level of 60 με. Consequently, $E(t)$ is substituted into Equation 3.6 to obtain the final expression of σ_{VEt} for a controlled-strain RDT test at any loading level:

$$\sigma_{VEt} = \varepsilon_0 \left|E^*_{tNLVE}\right|\left[1 - \cos\left(\omega t - \varphi_t + \varphi_{tNLVE}\right)\right] - \frac{\varepsilon_0}{\varepsilon_{0,60}}\sigma_{st,60} \tag{3.11}$$

When the strain level is 60 με, $\sigma_{VEt,60}$ is given in Equation 3.11; when the strain level is 200 με, $\sigma_{VEt,200}$ is obtained using Equation 3.11:

$$\sigma_{VEt,200} = \varepsilon_{0,200} \left|E^*_{tNLVE}\right|\left[1 - \cos\left(\omega t - \varphi_{t,200} + \varphi_{tNLVE}\right)\right] - \frac{\varepsilon_{0,200}}{\varepsilon_{0,60}}\sigma_{st,60} \tag{3.12}$$

where $\sigma_{VEt,200}$ is the viscoelastic stress in the tensile stress portion of a loading cycle of the RDT test at the strain level of 200 με; $\varepsilon_{0,200}$ is the strain amplitude in the RDT test at 200 με; and $\varphi_{t,200}$ is the phase angle of the tensile complex modulus in the RDT test at 200 με.

Following the same procedure for the tensile stress portion of a loading cycle, the viscoelastic stress in the compressive stress portion of a loading cycle is also formulated as shown in Equation 3.13:

$$\sigma_{VEqc} = \varepsilon_0 \left|E^*_{qcNLVE}\right|\left[1-\cos\left(\omega t-\varphi_{qc}+\varphi_{qcNLVE}\right)\right]-\frac{\varepsilon_0}{\varepsilon_{0,60}}\sigma_{cm,60} \tag{3.13}$$

where σ_{VEqc} is the viscoelastic stress in the compressive stress portion of a loading cycle of the RDT test at any loading level.

Based on the determination of $\sigma_{VE}(t)$, Equation 3.1 is used to calculate the pseudo strain ε_R. The reference modulus E_R in Equation 3.1 is equal to $\left|E^*_{tNLVE}\right|$ when the stress is tensile, and is equal to $\left|E^*_{qcNLVE}\right|$ when the stress is compressive in a loading cycle. Consequently, the pseudo strain is calculated as follows:

1. When the stress is tensile:

$$\varepsilon_R = \frac{\sigma_{VE}(t)}{E_R} = \frac{\sigma_{VEt}}{\left|E^*_{tNLVE}\right|} = \varepsilon_0\left[1-\cos\left(\omega t-\varphi_t+\varphi_{tNLVE}\right)\right]-\frac{\varepsilon_0}{\varepsilon_{0,60}}\cdot\frac{\sigma_{st,60}}{\left|E^*_{tNLVE}\right|} \tag{3.14}$$

2. When the stress is compressive:

$$\varepsilon_R = \frac{\sigma_{VE}(t)}{E_R} = \frac{\sigma_{VEqc}}{\left|E^*_{qcNLVE}\right|} = \varepsilon_0\left[1-\cos\left(\omega t-\varphi_{qc}+\varphi_{qcNLVE}\right)\right]-\frac{\varepsilon_0}{\varepsilon_{0,60}}\cdot\frac{\sigma_{cm,60}}{\left|E^*_{qcNLVE}\right|} \tag{3.15}$$

Equations 3.14 and 3.15 are validated using the stress-strain and stress-pseudo strain diagrams, or hysteresis loops. The stress-strain hysteresis loops are produced based on Equations 2.15 through 2.18; the stress-pseudo strain hysteresis loops are generated based on Equations 2.15 and 3.14 for the tensile stress portion and based on Equations 2.17 and 3.15 for the compressive stress portion. The generated hysteresis loops are presented in Figures 3.3 and 3.4. The area of the stress-strain hysteresis loop represents the amount of the DSE in the corresponding loading cycle. When the test

specimen is at the critical nonlinear viscoelastic state, the entire amount of the DSE is expended on the viscoelastic effect of the asphalt mixture, which includes both linear and nonlinear viscoelastic effects.

In contrast, the stress-pseudo strain hysteresis loops become straight lines because the pseudo strain is in phase with the stress and all energy used for the viscoelastic effect of the material is removed from the stress-pseudo strain hysteresis loop. For example, for the first loading cycle of the nondestructive RDT test at 60 με, the stress-pseudo strain hysteresis loop becomes line OM for the tensile stress portion and line ON for the compressive stress portion, as shown in Figure 3.3. The slope of line OM is different from the slope of line ON because the tensile properties are different from the quasi-compressive properties of the asphalt mixture.

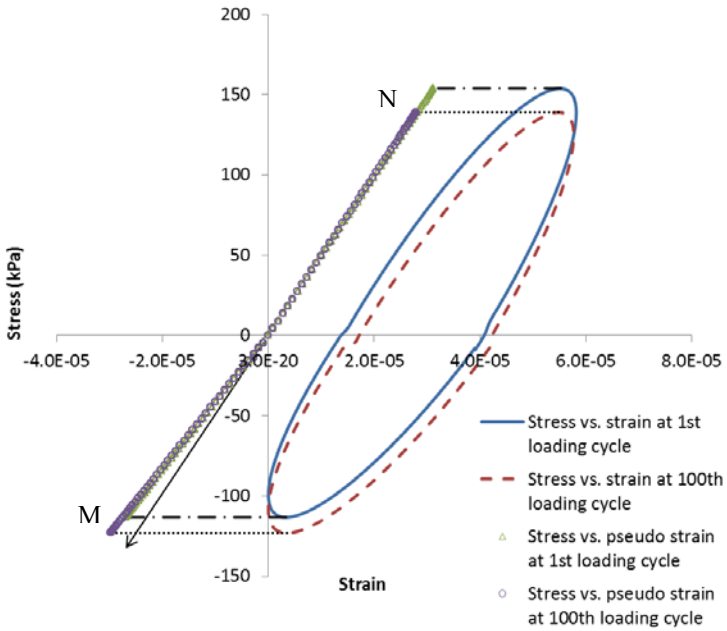

Figure 3.3 Hysteresis Loop of an Asphalt Mixture Specimen at the Critical Nonlinear Viscoelastic State in Nondestructive RDT Test

When the destructive RDT test is performed on the same specimen, the DSE is expended not only on the viscoelastic effect but also to drive the damage. As a result, the stress-pseudo strain hysteresis loops are no longer straight lines. Since the part of the DSE expended on the viscoelastic effect has been removed from the stress-pseudo strain hysteresis loop, the enclosed area of the stress-pseudo strain hysteresis loop represents the DPSE, which is the part of the DSE used to drive cracking and permanent deformation in the asphalt mixture, as shown in Figure 3.4.

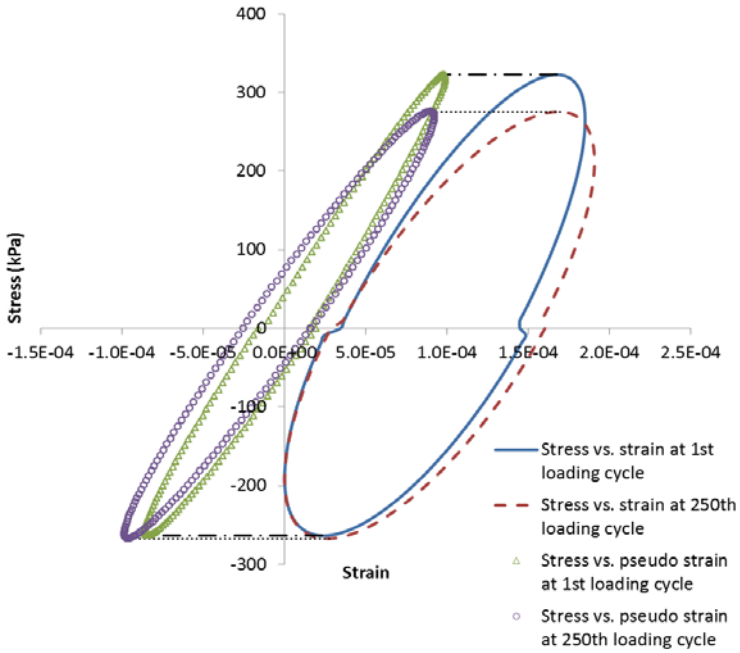

Figure 3.4 Hysteresis Loop of an Asphalt Mixture Specimen at the Damaged State in Destructive RDT Test

3.4.2 Calculation of Pseudo Strain Energy

Based on the pseudo strain formulated in Equations 3.14 and 3.15, the pseudo strain energy density (energy per unit volume) is calculated by integrating the stress and pseudo strain:

$$W_R = \int_{t_1}^{t_2} \sigma(t) \frac{d\varepsilon_R(t)}{dt} dt \tag{3.16}$$

where W_R is the pseudo strain energy density in a loading period $[t_1, t_2]$, which is equal to the strain energy density W minus the energy spent on the linear and nonlinear viscoelastic effects. There are two types of pseudo strain energy density, one of which is the energy dissipated to develop damage in the specimen, defined as the DPSE, the other of which is the recoverable pseudo strain energy (RPSE) that is stored and recovered corresponding to the purely elastic effect of the material. The DPSE and RPSE are both calculated using the same method and procedure as those for the DSE and RSE as described in Section 2. The final formulation of the DPSE and RPSE are presented in Equations 3.17 and 3.18.

Based on Equations 3.17 and 3.18, the DPSE and RPSE are calculated for every loading cycle of the destructive RDT test. Figure 3.5 shows the evolution of the DPSE and RPSE of a number of representative loading cycles. The DPSE increases with the increase of the number of loading cycles, indicating the damage accumulation in the asphalt mixture specimen. The rate of damage accumulation can be measured by the rate of the change of the DPSE with the increase of the number of loading cycles.

$$
\begin{aligned}
\mathrm{DPSE} = {} & \sigma_{0t}\varepsilon_0 \left\{ \begin{array}{l} \dfrac{\sin\left(\varphi_t - \varphi_{tNLVE}\right)\left[2\pi - \sin\left(T_c\omega\right) + \sin\left(T_t\omega\right) - T_c\omega + T_t\omega\right]}{4} \\ -\dfrac{\cos\left(\varphi_t - \varphi_{tNLVE}\right)\left[\cos\left(T_c\omega\right) - \cos\left(T_t\omega\right)\right]}{4} \end{array} \right\} \\
& + \left(\sigma_{0t} - \sigma_{st}\right)\varepsilon_0 \left\{ \begin{array}{l} \sin\left(\varphi_t - \varphi_{tNLVE}\right)\left[\sin\left(\dfrac{T_t\omega}{2}\right) + \sin\left(\dfrac{T_c\omega}{2}\right)\right] \\ +\cos\left(\varphi_t - \varphi_{tNLVE}\right)\left[\cos\left(\dfrac{T_t\omega}{2}\right) + \cos\left(\dfrac{T_c\omega}{2}\right)\right] \end{array} \right\} \\
& + \sigma_{0c}\varepsilon_0 \left\{ \begin{array}{l} \dfrac{\sin\left(\varphi_{qc} - \varphi_{qcNLVE}\right)\left[2\pi + \sin\left(T_c\omega\right) - \sin\left(T_t\omega\right) + T_c\omega - T_t\omega\right]}{4} \\ +\dfrac{\cos\left(\varphi_{qc} - \varphi_{qcNLVE}\right)\left[\cos\left(T_c\omega\right) - \cos\left(T_t\omega\right)\right]}{4} \end{array} \right\} \\
& + \left(\sigma_{0c} - \sigma_{cm}\right)\varepsilon_0 \left\{ \begin{array}{l} -\sin\left(\varphi_{qc} - \varphi_{qcNLVE}\right)\left[\sin\left(\dfrac{T_t\omega}{2}\right) + \sin\left(\dfrac{T_c\omega}{2}\right)\right] \\ -\cos\left(\varphi_{qc} - \varphi_{qcNLVE}\right)\left[\cos\left(\dfrac{T_t\omega}{2}\right) + \cos\left(\dfrac{T_c\omega}{2}\right)\right] \end{array} \right\}
\end{aligned} \tag{3.17}
$$

$$
\begin{aligned}
\mathrm{RPSE} = {} & \sigma_{0t}\varepsilon_0 \left\{ \begin{array}{l} -\dfrac{\sin\left(\varphi_t - \varphi_{tNLVE}\right)\left[2\left(\varphi_t - \varphi_{tNLVE}\right) + \sin\left(2\varphi_t - 2\varphi_{tNLVE}\right) - \sin\left(T_t\omega\right) - T_t\omega\right]}{4} \\ -\dfrac{\cos\left(\varphi_t - \varphi_{tNLVE}\right)\left[\cos^2\left(\varphi_t - \varphi_{tNLVE}\right) - \cos^2\left(\dfrac{T_t\omega}{2}\right)\right]}{2} \end{array} \right\} \\
& + \left(\sigma_{0t} - \sigma_{st}\right)\varepsilon_0 \left\{ \begin{array}{l} \sin\left(\varphi_t - \varphi_{tNLVE}\right)\left[\sin\left(\dfrac{T_t\omega}{2}\right) - \sin\left(\varphi_t - \varphi_{tNLVE}\right)\right] \\ +\cos\left(\varphi_t - \varphi_{tNLVE}\right)\left[\cos\left(\dfrac{T_t\omega}{2}\right) - \cos\left(\varphi_t - \varphi_{tNLVE}\right)\right] \end{array} \right\} \\
& + \sigma_{0c}\varepsilon_0 \left\{ \begin{array}{l} -\dfrac{\sin\left(\varphi_{qc} - \varphi_{qcNLVE}\right)\left[\begin{array}{l} 2\left(\varphi_{qc} - \varphi_{qcNLVE}\right) + \sin\left(2\varphi_{qc} - 2\varphi_{qcNLVE}\right) - \sin\left(T_c\omega\right) \\ -T_c\omega \end{array}\right]}{4} \\ -\dfrac{\cos\left(\varphi_{qc} - \varphi_{qcNLVE}\right)\left[\cos^2\left(\varphi_{qc} - \varphi_{qcNLVE}\right) - \cos^2\left(\dfrac{T_c\omega}{2}\right)\right]}{2} \end{array} \right\} \\
& + \left(\sigma_{0c} - \sigma_{cm}\right)\varepsilon_0 \left\{ \begin{array}{l} -\sin\left(\varphi_{qc} - \varphi_{qcNLVE}\right)\left[\sin\left(\dfrac{T_c\omega}{2}\right) - \sin\left(\varphi_{qc} - \varphi_{qcNLVE}\right)\right] \\ -\cos\left(\varphi_{qc} - \varphi_{qcNLVE}\right)\left[\cos\left(\dfrac{T_c\omega}{2}\right) - \cos\left(\varphi_{qc} - \varphi_{qcNLVE}\right)\right] \end{array} \right\}
\end{aligned} \tag{3.18}
$$

Specifically, an exponential function is fitted the DPSE curve using MATLAB:

$$\text{DPSE}=6.36N^{0.24}+7.19, \qquad R^2=0.998 \tag{3.19}$$

in which N is the number of loading cycles. The high R-squared value indicates the goodness of the model fit. The rate of the change of the DPSE is thus calculated as:

$$\frac{d\text{DPSE}}{dN}=1.53N^{-0.76} \tag{3.20}$$

Figure 3.5 also shows that the RPSE decreases with the increase of the number of loading cycles, implying that the specimen is losing the ability to store and recover energy, or the material is losing its integrity due to the damage accumulation.

The calculated DPSE will be further decomposed into two components: the DPSE for cracking and the DPSE for permanent deformation. The formulation of the two components of the DPSE will be detailed in Section 3.5.

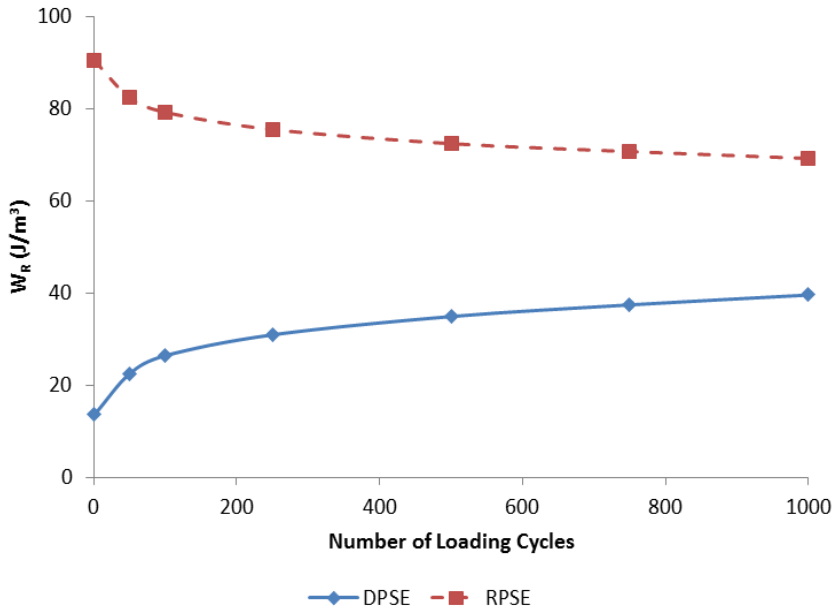

Figure 3.5 DPSE and RPSE in Destructive RDT Test

3.5 Balance of Pseudo Strain Energy

In order to separate the two components of the DPSE, Section 3.5 will firstly investigate the energy distribution around the cracks in the process of damage development at the microscopic level. At the microscopic level, the asphalt mixture specimen consists of intact material (asphalt binder and aggregates) and air voids, which act as the initial cracks in the specimen.

Figure 3.6(a) presents a schematic sketch of the micro-level view of an asphalt mixture subjected to a tensile stress σ_t, which is normally regarded to be uniformly distributed on the entire cross section of the specimen. This is an apparent description of the stress without considering any air voids or cracks in the material. As a matter of fact, due to the existence of air voids (initial cracks), the stress distribution is not uniform, which is represented using force lines (dashed curves) in Figure 3.6(a). Denser force lines at the crack tips indicate local stress concentration, and the curved force lines in the vicinity of the crack tips illustrate the nonlinear distribution of the stress. This localization of the stress (stress concentration and nonlinear distribution) results in a localization of strain in the corresponding regions surrounding the cracks. It has been reported that the average value of the localized strain can be from 4 to 100 times of the bulk strain in the asphalt mixture (Bahia et al. 1999; Kose et al. 2000; Masad and Somadevan 2002). It can be concluded that the presence of cracks significantly changes the stress and strain in the intact material at the microscopic level.

Because of the variation of the stress and strain distribution around the cracks, the energy is also redistributed around the cracks. Due to the visco-elasto-plastic nature

of the asphalt mixture, a large amount of energy is consumed as the plastic work to drive the advance of the fracture process zone, where material separation occurs which creates two new surfaces from the initial crack (Schapery 1984). Figure 3.6(b) illustrates the fracture process zone and the resulting enlargement of the initial crack, i.e., the propagation of the initial crack. Consequently, a plastic region develops surrounding the fracture process zone with large local plastic deformation. This plastic region is labeled "1" and is located approximately in the long-dashed and short-dashed circle in Figure 3.6(a). In addition to the localized plastic deformation, plastic deformation also develops in the area without any cracks due to yielding of the intact material, such as the region labeled "2" in Figure 3.6(a). These two parts of plastic deformation add up to the total plastic deformation, or the permanent deformation of the asphalt mixture specimen. The energy expended on the total plastic deformation is the DPSE for permanent deformation.

The propagation of the initial crack also results in the redistribution of the RPSE because of the relaxation of the intact material above and below the crack in the region enclosed in long-dashed and double short-dashed lines labeled "3" in Figure 3.6(a). The RPSE is released as the intact material in this region is unloaded due to crack propagation. Part of the released RPSE provides the surface energy that is required to separate the intact material to create new crack surfaces labeled "4" in Figure 3.6(a). This surface energy is absorbed by the newly created crack surfaces.

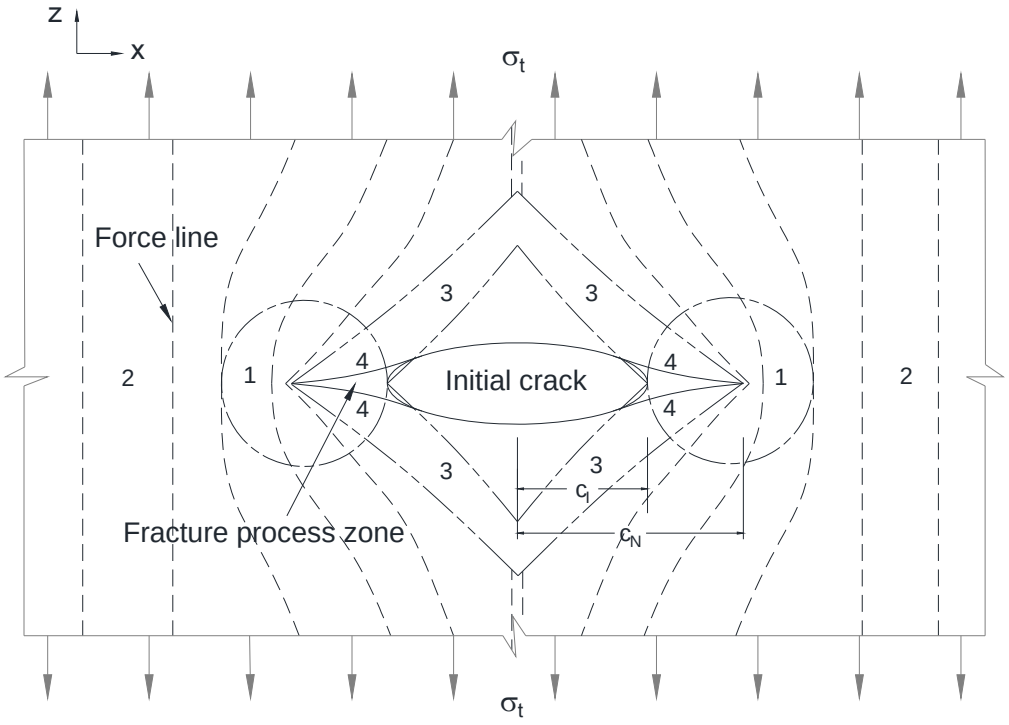

(a) Side View

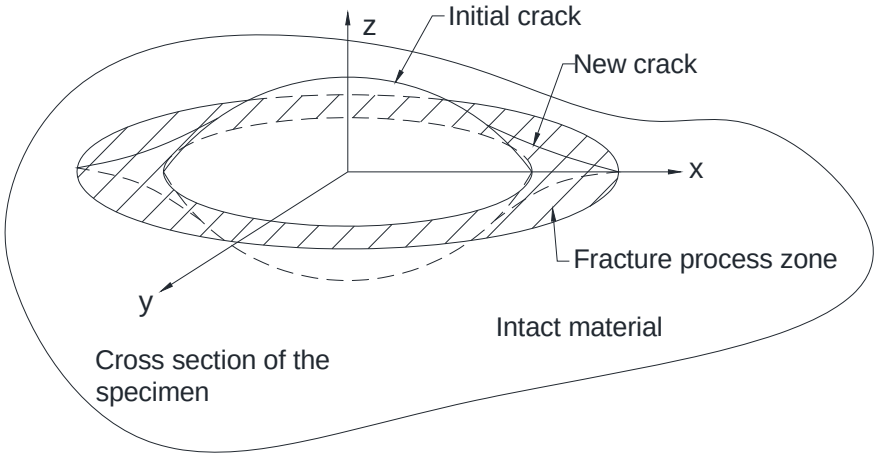

(b) Plan View

Figure 3.6. Micro-view of Cracked Asphalt Mixture Specimen in Destructive Test

Because of the presence of cracks in the asphalt mixture, the stress, strain and energy distribution in the intact material are certainly different from those in the bulk material. For example, the stress of the intact material should be equal to the applied load divided by the cross sectional area excluding the crack opening areas (instead of the entire cross section). This stress is defined as the "true stress" in this study. Similarly, the strain and energy in the intact material are defined as "true strain" and "true energy", respectively. In contrast, the stress in the bulk material is defined as the "apparent stress", which is equal to the applied load divided by the entire cross sectional area (including crack opening areas). The strain and energy of the bulk material are defined as "apparent strain" and "apparent energy". The RDT test provides measurements of the apparent stress, strain and energy, which are related to the true stress, strain and energy based on the principle of energy balance.

The principle of energy balance states that any kind of true energy within the intact material equals its counterpoint from the apparent measurement. This is because only the intact material can store, release and dissipate energy while cracks cannot. Consequently, the true energy within the intact material must equal the apparent energy within the entire specimen, including the intact material and cracks. According to this principle, energy balance equations, including strain energy balance equations and pseudo strain energy balance equations, are formulated between the true energy and the apparent energy.

First the strain energy balance equations are formulated for the DSE and RSE. The DSE balance equation states that the apparent DSE equals the true DSE:

$$\mathrm{DSE}^A = \mathrm{DSE}^T \tag{3.21}$$

in which the superscript "A" stands for "apparent" and "T" stands for "true". Similarly, the RSE balance equation states that the apparent RSE equals the true RSE:

$$\mathrm{RSE}^A = \mathrm{RSE}^T \tag{3.22}$$

Secondly the pseudo strain energy balance equations are constructed for damaged asphalt mixtures under destructive loading. The DPSE balance equation is formulated as follows:

$$\mathrm{DPSE}^A = \mathrm{DPSE}^T \tag{3.23}$$

in which DPSE^A is the DPSE calculated using Equation 3.17. The RPSE balance equation shown in Equation 3.24 is constructed on the basis that the apparent RPSE equals the true RPSE associated with the energy redistribution during crack propagation.

$$\mathrm{RPSE}^A V_m = \mathrm{RPSE}^T V_m - \left(\mathrm{RPSE}^T V_r - \gamma S\right) \tag{3.24}$$

in which:

- RPSE^A is the apparent RPSE calculated using Equation 3.18.
- V_m is the volume of the asphalt mastic in one layer of the asphalt mixture specimen, whose thickness equals the mean film thickness. The formulation of V_m is:

  $$V_m = A_m \bar{t} \tag{3.25}$$

  where A_m is the area of the asphalt mastic on a cross section of the specimen; and $\bar{t}$ is the mean film thickness, determined based on the aggregate surface area and the effective volume of the asphalt binder (Roberts et al. 1996):

$$\bar{t} = \frac{V_{asp}}{SA \times W} \tag{3.26}$$

where V_{asp} is the effective volume of the asphalt binder; SA is the surface area of the aggregate; and W is the weight of the aggregate.

- RPSE^T represents the true RPSE of the asphalt mastic before cracks propagate from the initial air voids.
- V_r is the volume of the asphalt mastic in region "3" in Figure 3.6(a), which is subjected to a relaxation process and releases the RPSE during the crack propagation. The crack is assumed to be penny-shaped (Lytton 2004), as shown in Figure 3.6(b). Therefore, V_r approximately equals the difference between the volume of the larger cone and the volume of the smaller cone above and the below the crack. If the radius of the initial crack is c_I and the radius of the new crack after crack propagation is c_N, the height of the smaller cone is πc_I and the height of the larger cone is πc_N (Roylance 2001). Thus V_r is calculated as follows:

$$V_r = 2 \cdot \left(\frac{1}{3} \pi {c_N}^2 \cdot \pi c_N \cdot M_N - \frac{1}{3} \pi {c_I}^2 \cdot \pi c_I \cdot M_I \right) \tag{3.27}$$

in which M_N is the number of new cracks within the volume V_m, and M_I is the number of initial cracks within the volume V_m.

- γ is the surface energy density (energy per unit area).

- S is the total area of the newly created crack surfaces corresponding to the region labeled "4" in Figure 3.6(a) and also the shadowed area in Figure 3.6(b). S is calculated as follows:

$$S = 2 \cdot \left(\pi {c_N}^2 \cdot M_N - \pi {c_I}^2 \cdot M_I \right) \tag{3.28}$$

γS is the amount of the energy absorbed from the released $\mathrm{RPSE}^T V_r$ and restored on the newly created crack surfaces.

Since $\mathrm{RPSE}^T V_r$ is the energy released around the crack during the crack propagation and γS is the surface energy absorbed from $\mathrm{RPSE}^T V_r$, the difference between $\mathrm{RPSE}^T V_r$ and γS is the energy dissipated due to crack growth, which is the DPSE for cracking as formulated in Equation 3.29:

$$\mathrm{DPSE_c} V = \mathrm{RPSE}^T V_r - \gamma S \tag{3.29}$$

where DPSE_c is the DPSE for cracking, and V is the volume of one layer of the asphalt mixture specimen, calculated by the entire cross sectional area multiplied by the mean film thickness. Then the DPSE for permanent deformation (DPSE_p) is calculated by subtracting DPSE_c from the total DPSE:

$$\mathrm{DPSE}_p = \mathrm{DPSE}^T - \mathrm{DPSE}_c \tag{3.30}$$

As a result, the DPSE expended on cracking and DPSE expended on permanent deformation are completely formulated, respectively. The next step is to calculate the amount of DPSE_c and DPSE_p based on the test data using the above formulation, which is presented in Section 4.

4. MODEL FATIGUE CRACK GROWTH IN ASPHALT MIXTURES USING PSEUDO STRAIN ENERGY BALANCE

4.1 Current Models for Fatigue Cracking

Models for fatigue cracking used in asphalt pavement engineering generally can be divided into four categories: 1) the strain approach (Monismith et al. 1971; The Asphalt Institute 1981; Tayebali 1994); 2) the dissipated energy approach (Van Dijk et al. 1975; Tayebali et al. 1992; Ghuzlan and Carpenter 2000); 3) the fracture mechanics approach; and 4) the continuum damage mechanics approach. In the strain approach, the fatigue resistance is expressed as the number of load applications to failure, which is related to the tensile strain by a regression function from the test data. In the dissipated energy approach, similarly, the fatigue resistance is represented by a regression function between the dissipated energy and the number of load applications to failure. There is a common feature for the first and second categories of models: the test data is analyzed using a statistical regression method so the regression coefficients depend on the experimental conditions, the materials used, and the geometry of the specimen, etc. This means that a different set of regression coefficients are required if any of these parameters changes. The empirical nature of this statistical analysis method and the resulting models limits their applications since it is not prudent to describe such phenomena outside the range of the original test data. In addition, these models are more dependent on experience rather than specifying the cause and effect of a particular phenomenon. In contrast, the mechanics-based approach and models do not have such

problems. The need to develop mechanics-based pavement design and its benefits are now recognized by more and more people (NCHRP 1-37A, 2002). From this perspective, the third and fourth category, the fracture mechanics approach and continuum damage mechanics approach seem very attractive to model the fatigue cracking of asphalt mixtures.

In fracture mechanics, the most widely used model for fatigue cracking is a power function in the form of Paris' Law (Paris and Erdogan 1963), which relates the crack growth per cycle to the stress intensity factor or the *J* integral by two coefficients A and n.

$$\frac{dc}{dN} = AK^n \quad \text{or} \quad \frac{dc}{dN} = AJ^n \tag{4.1}$$

where dc/dN is the crack growth per cycle; K is the stress intensity factor; J is the *J* integral; and A and n are fracture coefficients determined from experiments. Schapery (1975, 1978) studied the crack growth in viscoelastic materials and derived A and n as a function of fundamental material properties. Based on Schapery's work, more modifications have been made for A and n so that the fatigue crack growth of asphalt mixtures can be predicted from a series of simple tests such as the creep test, the tensile strength test, and surface energy measurement instead of extensive fatigue tests (Little et al. 1997 and 2001; Walubita et al. 2006; Masad et al. 2007). The major problem of these Paris' Law based models is that they are derived from the analysis of growth of one crack, which is not suitable to simulate the situation of numerous cracks growing in the asphalt mixture specimen under repeated loading.

Another important mechanics approach that studies cracking damage is continuum damage mechanics. Compared to fracture mechanics, it has the advantage of considering all cracks as damage and measures the damage by the effect that all cracks exert on the macro response of the material (nonlinear stress-strain behavior and degradation of material stiffness). Kachanov (1958) pioneered this area by differentiating the initial area of an undamaged section of the material and the actual area of this section after a certain part of the section is "lost" as a result of crack growth. He defined a damage parameter as follows:

$$\omega = \frac{A - \overline{A}}{A} \tag{4.2}$$

where ω is the damage parameter; A is the initial area of the undamaged section; and $\overline{A}$ is the actual area of the damaged section. The value $A - \overline{A}$ represents the lost area which is the total area of all cracks. Then through the force equilibrium $\sigma A = \overline{\sigma}\,\overline{A}$, the damage parameter can be expressed by the stress ratio as follows:

$$\omega = 1 - \frac{\sigma}{\overline{\sigma}} \tag{4.3}$$

where σ is nominal stress on the initial area of the undamaged section; and $\overline{\sigma}$ is effective stress on the actual area of the damaged section. In this way, the damage parameter can be formulated in constitutive equations, and further in the damage evolution law to analytically describe the effect of crack growth. Application of continuum damage mechanics to fatigue yields many different models (Hashin and Rotem 1978; Lemaitre and Chaboche 1978; Ostergren and Krempl 1979; Hashin and

Laird 1980; Altus 1991; Suresh 1991; Lemaitre 1992). In these models, the incremental damage per loading cycle is postulated to be a function of stress, plastic strain, and already accumulated damage, and the damage evolution law is usually manipulated into the form of well-established empirical rules so as to provide legitimacy to the model. Most of these models require adjustable parameters to fit the test data. As a result, these models are still phenomenological in nature (Krajcinovic 1996).

In order to address the shortcomings associated with the aforementioned methods, Section 4 aims at using the energy-based mechanistic approach developed in Section 3 to model the fatigue crack growth in asphalt mixtures. The first step of using this approach is to determine the true stress, true strain, and true pseudo strain in order to calculate all types of true energy.

4.2 Simulation of True Stress, True Strain, and True Pseudo Strain

In a typical controlled-strain RDT test, the stress/strain/pseudo strain in the intact material, or the true stress/true strain/true pseudo strain, should have the same pattern as those in the bulk specimen. In other words, the true stress has the same formulation as the apparent stress shown in Equation 2.15 or 2.17; the true strain has the same formulation as the apparent strain shown in Equation 2.16 or 2.18; the true pseudo strain has the same formulation as the apparent pseudo strain shown in Equation 3.14 or 3.15. However, the apparent stress/strain/pseudo strain which have tension and quasi-compression due to crack opening and closure are different from the true stress/true strain/true pseudo strain which do not need to distinguish the tension and quasi-

compression since the cracks are excluded from the intact material. As a result, the true stress/true strain/true pseudo strain can be expressed by Equation 4.4, 4.5, and 4.6, respectively.

$$\sigma^T = \sigma_0^T \left[1 - \cos\left(\omega t\right)\right] - \sigma_{cm}^T \tag{4.4}$$

$$\varepsilon^T = \varepsilon_0^T \left[1 - \cos\left(\omega t - \varphi^T\right)\right] \tag{4.5}$$

$$\varepsilon_R^T = \varepsilon_0^T \left[1 - \cos\left(\omega t - \varphi^T + \varphi_{NLVE}^T\right)\right] - \frac{\varepsilon_0^T}{\varepsilon_{0,NLVE}^T} \cdot \frac{\sigma_{cm,NLVE}^T}{\left|E_{NLVE}^{*T}\right|} \tag{4.6}$$

where σ^T is the true stress; σ_0^T is the true stress amplitude; σ_{cm}^T is the magnitude of the true minimum stress; ε^T is the true strain; ε_0^T is the true strain amplitude, which is related to σ_0^T by the magnitude of true complex modulus $\left|E^{*T}\right|$ as follows:

$$\varepsilon_0^T = \frac{\sigma_0^T}{\left|E^{*T}\right|} \tag{4.7}$$

φ^T is the phase angle of the true complex modulus; ε_R^T is the true pseudo strain; φ_{NLVE}^T is the phase angle of the true complex modulus at the critical nonlinear viscoelastic state; $\left|E_{NLVE}^{*T}\right|$ is the magnitude of the true complex modulus at the critical nonlinear viscoelastic state; $\varepsilon_{0,NLVE}^T$ is the true strain amplitude in the RDT test at the threshold loading level; and $\sigma_{cm,NLVE}^T$ is the magnitude of the true minimum stress at the threshold loading level. The simulation parameters, such as σ_0^T, σ_{cm}^T, and ε_0^T, and the true material properties ($\left|E^{*T}\right|$ and φ^T) are not directly obtainable since it is impossible to

extract the intact material from the bulk specimen and test it separately. Instead, they must be obtained using the apparent measurements provided by the controlled-strain RDT test. The method of determining the simulation parameters and the true material properties are introduced as follows.

4.2.1 Determination of Simulation Parameters in Undamaged Asphalt Mixtures

There are five simulation parameters in Equations 4.4 to 4.7: σ_0^T, σ_{cm}^T, ε_0^T, $\varepsilon_{0,NLVE}^T$, and $\sigma_{cm,NLVE}^T$. As a matter of fact, there are only two independent simulation parameters: σ_0^T and σ_{cm}^T, since ε_0^T is related to σ_0^T by Equation 4.7 and $\varepsilon_{0,NLVE}^T$, and $\sigma_{cm,NLVE}^T$ are ε_0^T, and σ_{cm}^T in a RDT test at the threshold loading level. These two independent simulation parameters are determined using the principle of force equilibrium.

The principle of force equilibrium states that the true force carried by the intact material equals the apparent force assumed to be carried by the entire cross section of the specimen. According to this principle, a force equilibrium equation can be constructed between the true stress and the apparent stress. Specifically, for a complete loading cycle of the RDT test, a force equilibrium equation is constructed between σ_t and σ^T for the tensile stress portion as shown in Equation 4.8, and a force equilibrium equation between σ_c and σ^T for the compressive stress portion as shown in Equation 4.9:

$$A\left\{\sigma_{0t}\left[1-\cos(\omega t)\right]-\sigma_{st}\right\}=\left(A-S_{ct}\right)\left\{\sigma_0^T\left[1-\cos(\omega t)\right]-\sigma_{cm}^T\right\} \tag{4.8}$$

$$A\left\{\sigma_{0c}\left[1-\cos(\omega t)\right]-\sigma_{cm}\right\}=\left(A-S_{cc}\right)\left\{\sigma_0^T\left[1-\cos(\omega t)\right]-\sigma_{cm}^T\right\} \tag{4.9}$$

where A is the entire cross sectional area of the asphalt mixture specimen; S_{ct} is the area of the cracks on a cross section in the tensile stress portion. The value of $A-S_{ct}$ represents the area of the intact material on a cross section in the tensile stress portion; S_{cc} is the area of the cracks on a cross section in the compressive stress portion, which is different from S_{ct} because the extent of the crack opening and closure is different. The value of $A-S_{cc}$ represents the area of the intact material on a cross section in the compressive stress portion.

Arranging Equation 4.8 can yield the following two equations:

$$A\sigma_{0t}=\left(A-S_{ct}\right)\sigma_0^T \tag{4.10}$$

$$A\sigma_{st}=\left(A-S_{ct}\right)\sigma_{cm}^T \tag{4.11}$$

Similarly, Equation 4.9 yields two equations as follows:

$$A\sigma_{0c}=\left(A-S_{cc}\right)\sigma_0^T \tag{4.12}$$

$$A\sigma_{cm}=\left(A-S_{cc}\right)\sigma_{cm}^T \tag{4.13}$$

Combine Equations 4.10 and 4.12 by adding the left side of the equation and the right side of the equation, respectively:

$$A\left(\sigma_{0t}+\sigma_{0c}\right)=\left(A-S_{ct}+A-S_{cc}\right)\sigma_0^T \tag{4.14}$$

Combine Equations 4.11 and 4.13 in the same way:

$$A\left(\sigma_{st}+\sigma_{cm}\right)=\left(A-S_{ct}+A-S_{cc}\right)\sigma_{cm}^T \tag{4.15}$$

Define the average of S_{ct} and S_{cc} as the average area of the cracks on a cross section in a loading cycle of the RDT test, denoted S_c

$$\frac{S_{ct} + S_{cc}}{2} = S_c \tag{4.16}$$

Substituting Equation 4.16 into Equations 4.14 and 4.15, gives:

$$A\left(\sigma_{0t} + \sigma_{0c}\right) = 2\left(A - S_c\right)\sigma_0^T \tag{4.17}$$

$$A\left(\sigma_{st} + \sigma_{cm}\right) = 2\left(A - S_c\right)\sigma_{cm}^T \tag{4.18}$$

Solve for σ_0^T by Equation 4.17 and for σ_{cm}^T by Equation 4.18:

$$\sigma_0^T = \frac{\left(\sigma_{0t} + \sigma_{0c}\right)/2}{1 - S_c/A} \tag{4.19}$$

$$\sigma_{cm}^T = \frac{\left(\sigma_{st} + \sigma_{cm}\right)/2}{1 - S_c/A} \tag{4.20}$$

Equations 4.19 and 4.20 are the expressions of the simulation parameters for the true stress calculated using the apparent measurements extracted from the RDT test. They are applicable to both an undamaged asphalt mixture in a nondestructive RDT test and a damaged specimen in a destructive test. In the nondestructive test, the value of S_c/A equals the air void content since the air voids are the initial cracks and the area of the air voids does not change in the nondestructive test. However, in the destructive test, S_c, is a unknown variable and changes with the increase of the number of loading cycles as the cracks grow. Consequently, Equations 4.19 and 4.20 are used to determine the true stress in an undamaged asphalt mixture. The method to determine the true stress in a damaged asphalt mixture will be introduced later. After determining the true stress, the true strain and true pseudo strain can be obtained once the true material properties are determined, which is presented as follows.

4.2.2 Determination of True Material Properties in both Undamaged and Damaged Asphalt Mixtures

The true material properties are the material properties of the intact material in an asphalt mixture specimen. In a controlled-strain RDT test, the true complex modulus E^{*T} ($\left|E^{*T}\right|$ and φ^T) has the following characteristics:

- Both $\left|E^{*T}\right|$ and φ^T remain the same with the increase of the number of loading cycles in a RDT test at any loading level. This is because the air voids and cracks are excluded from the intact material, so the crack growth within a RDT test does not influence the behavior of the intact material.
- Both $\left|E^{*T}\right|$ and φ^T change ($\left|E^{*T}\right|$ decrease and φ^T increase) from one loading level to a higher loading level if the asphalt mixture specimen is within the nonlinear viscoelastic region or the damaged region. This is because of the nonlinear viscoelastic nature of the intact material when an asphalt mixture specimen is under a high loading level.

According to these characteristics, the true material properties are classified into two categories:

1) The true material properties of an undamaged asphalt mixture, which are defined as nondestructive true material properties; and
2) The true material properties of a damaged asphalt mixture, which are defined as destructive true material properties.

The nondestructive true material properties at the threshold loading between the

nondestructive and destructive loading are the true critical nonlinear viscoelastic properties ($\left|E^{*T}_{NLVE}\right|$ and φ^{T}_{NLVE}). The nondestructive true material properties are obtained from the nondestructive RDT tests; the destructive true material properties are obtained from the destructive RDT test. However, they cannot be measured directly. Instead, the true material properties are determined using the DSE and RSE balance equations.

In order to use the DSE balance equation (Equation 3.21) and the RSE balance equation (Equation 3.22), DSE^T and RSE^T must be determined first. They are calculated by integrating σ^T (Equation 4.4) and ε^T (Equation 4.5) using the same method and procedure as those for the DSE^A and RSE^A. The formulation of the DSE^T and RSE^T are:

$$DSE^T = \pi\sigma_0^T\varepsilon_0^T \sin\varphi^T \tag{4.21}$$

$$\begin{aligned} RSE^T = {} & \sigma_0^T\varepsilon_0^T \cdot \frac{\sin\varphi^T\left(\pi - 2\varphi^T\right) + \cos\varphi^T\left[\cos\left(T_t\omega\right) - 1\right]}{2} \\ & + 2\left(\sigma_0^T - \sigma_{cm}^T\right)\varepsilon_0^T \cos\varphi^T \cos\left(\frac{T_t\omega}{2}\right) \end{aligned} \tag{4.22}$$

where T_t is the period corresponding to the tensile stress portion. Substituting Equations 4.21 and 4.22 into Equations 3.21 and 3.22, respectively, gives:

$$DSE^A = \pi\sigma_0^T\varepsilon_0^T \sin\varphi^T \tag{4.23}$$

$$\begin{aligned} RSE^A = {} & \sigma_0^T\varepsilon_0^T \cdot \frac{\sin\varphi^T\left(\pi - 2\varphi^T\right) + \cos\varphi^T\left[\cos\left(T_t\omega\right) - 1\right]}{2} \\ & + 2\left(\sigma_0^T - \sigma_{cm}^T\right)\varepsilon_0^T \cos\varphi^T \cos\left(\frac{T_t\omega}{2}\right) \end{aligned} \tag{4.24}$$

Combining Equations 4.23 and 4.24 by dividing the left side and right side of two equations, respectively, gives:

$$\frac{\mathrm{DSE}^A}{\mathrm{RSE}^A}=\frac{\pi\sigma_0^T\sin\varphi^T}{\left\{\begin{array}{l}\sigma_0^T\cdot\dfrac{\sin\varphi^T\left(\pi-2\varphi^T\right)+\cos\varphi^T\left[\cos\left(T_t\omega\right)-1\right]}{2}\\ +2\left(\sigma_0^T-\sigma_{cm}^T\right)\cos\varphi^T\cos\left(\dfrac{T_t\omega}{2}\right)\end{array}\right\}} \tag{4.25}$$

Equation 4.25 has the simulation parameters σ_0^T and σ_{cm}^T, so substitute Equations 4.19 and 4.20 into Equation 4.25:

$$\frac{\mathrm{DSE}^A}{\mathrm{RSE}^A}=\frac{\pi\left(\sigma_{0t}+\sigma_{0c}\right)\sin\varphi^T}{\left\{\begin{array}{l}\left(\sigma_{0t}+\sigma_{0c}\right)\cdot\dfrac{\sin\varphi^T\left(\pi-2\varphi^T\right)+\cos\varphi^T\left[\cos\left(T_t\omega\right)-1\right]}{2}\\ +2\left(\sigma_{0t}+\sigma_{0c}-\sigma_{st}-\sigma_{cm}\right)\cos\varphi^T\cos\left(\dfrac{T_t\omega}{2}\right)\end{array}\right\}} \tag{4.26}$$

In Equation 4.26, DSE^A, RSE^A, σ_{0t}, σ_{0c}, σ_{st}, σ_{cm}, and T_t are all apparent measurements from the RDT test, so φ^T is the only unknown variable in this equation. The Solver function in Excel is used to solve for φ^T by Equation 4.26.

After determining φ^T, Equation 4.27 is used to determine $\left|E^{*T}\right|$. Based on Equation 4.7, $\varepsilon_0^T=\sigma_0^T/\left|E^{*T}\right|$, which is substituted into Equation 4.23 to obtain:

$$\mathrm{DSE}^A=\pi\sigma_0^T\frac{\sigma_0^T}{\left|E^{*T}\right|}\sin\varphi^T \tag{4.27}$$

Solving for $\left|E^{*T}\right|$ from Equation 4.27 gives:

$$\left|E^{*T}\right|=\frac{\pi\left(\sigma_0^T\right)^2\sin\varphi^T}{\mathrm{DSE}^A} \tag{4.28}$$

In Equation 4.28, σ_0^T is calculated by Equation 4.19 and φ^T is provided by Equation

4.26. Equations 4.26 and 4.28 are applied to the nondestructive RDT test at the threshold loading and destructive RDT test to determine the true critical nonlinear viscoelastic properties and destructive true material properties, respectively.

The true critical nonlinear viscoelastic properties, $\left|E^{*T}_{NLVE}\right|$ and φ^{T}_{NLVE}, are determined using the test data from the controlled-strain RDT test at 60 με. The procedure is as follows:

1) Calculate φ^{T}_{NLVE} of the test specimen using Equation 4.26;
2) Calculate σ^{T}_{0} using Equation 4.19, in which S_c/A equals the air void content;
3) Calculate $\left|E^{*T}_{NLVE}\right|$ using Equation 4.28 with determined φ^{T}_{NLVE} and σ^{T}_{0}.

The calculated values of φ^{T}_{NLVE} and $\left|E^{*T}_{NLVE}\right|$ are presented in Table 4.1. The apparent critical nonlinear viscoelastic properties are also given in Table 4.1. It shows that the true material properties are different from the apparent properties.

Table 4.1 Material Properties in Nondestructive and Destructive RDT Tests

Nondestructive Test at Threshold Loading				**Destructive Test**			
True		**Apparent**		**True**		**Apparent (1st loading cycle)**	
φ^{T}_{NLVE} (°)	28.06	φ_{tNLVE}(°)	27.59	φ^{T} (°)	38.47	φ_t(°)	37.24
		$\left\|E^{*}_{tNLVE}\right\|$(MPa)	4912			$\left\|E^{*}_{t}\right\|$(MPa)	3161
$\left\|E^{*T}_{NLVE}\right\|$ (MPa)	5315	φ_{qcNLVE}(°)	30.08	$\left\|E^{*T}\right\|$ (MPa)	3634	φ_{qc}(°)	42.47
		$\left\|E^{*}_{qcNLVE}\right\|$(MPa)	4076			$\left\|E^{*}_{qc}\right\|$(MPa)	3025

The same procedure is applied to the controlled-strain RDT test at 200 με to determine the destructive true material properties. However, the determination of σ_0^T is different since S_c is unknown in the destructive test. The above procedure of calculating σ_0^T is modified in the following way:

- Calculate the simulation parameters for the apparent stress as shown in Equations 2.15 and 2.17 for every loading cycles, which are σ_{0t} and σ_{0c};
- Plot σ_{0t} and σ_{0c} versus the number of loading cycles through the entire destructive test, respectively. Fit the plotted curve using a best-fit function; then extrapolate the fitted curve to intersect with the vertical axis to determine the value when the number of loading cycle is zero. Such values are defined as the simulation parameters for the apparent stress at the beginning of the test, denoted σ_{0t}^0 and σ_{0c}^0. An example of σ_{0t} in the destructive test is shown in Figure 4.1. A power function is fitted to the curve of σ_{0t} versus the number of loading cycles N using the software MATLAB:

  $$\sigma_{0t} = -8.988N^{0.244} + 304.6, \qquad R^2 = 0.9945 \tag{4.29}$$

  If the fitted curve is extrapolated as shown by the dotted curve, it will intersect with the vertical axis at σ_{0t}^0, which is 304.6 kPa.
- Substitute σ_{0t}^0 and σ_{0c}^0 into Equation 4.19 to calculate σ_0^T at the beginning of the test. Since σ_{0t}^0 and σ_{0c}^0 are determined at the beginning of the test, the specimen is not damaged so the value of S_c/A still equals the air void content.

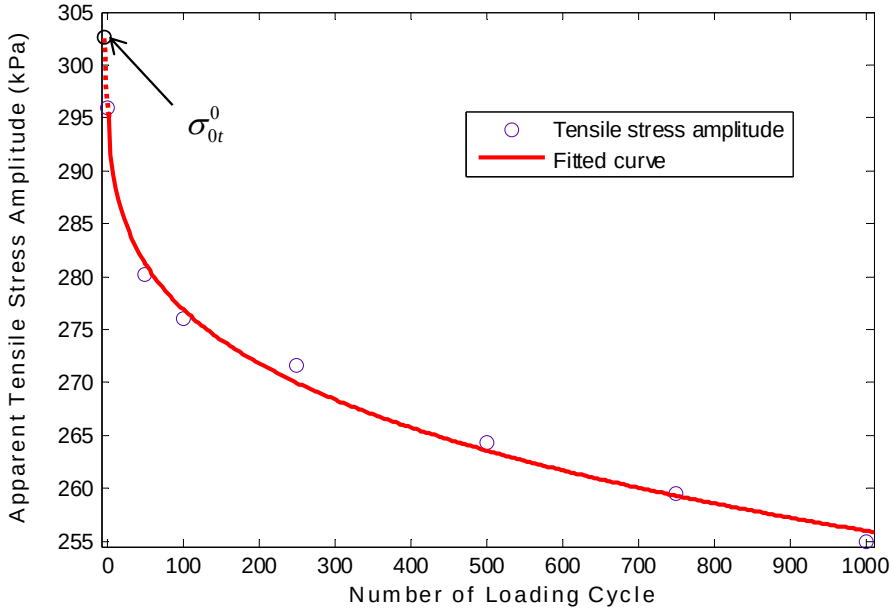

Figure 4.1 Apparent Tensile Stress Amplitude in Destructive RDT Test

The calculated values of φ^T and $\left|E^{*T}\right|$ in the destructive test are presented in Table 4.1, and the apparent material properties at the 1st loading cycle of the destructive are shown as well for comparison. The true destructive material properties are also different from the true nondestructive material properties.

Based on the determined simulation parameters for the apparent stress in the nondestructive test and the determined true nondestructive material properties, the hysteresis loops can be produced to illustrate the difference between the true stress/strain and the apparent stress/strain, as shown in Figure 4.2. The true stress-true strain hysteresis loop is slightly larger than the apparent stress-strain hysteresis loop. As the loading cycle increases (e.g. 1st to 100th), the shape and area of both loops do not change.

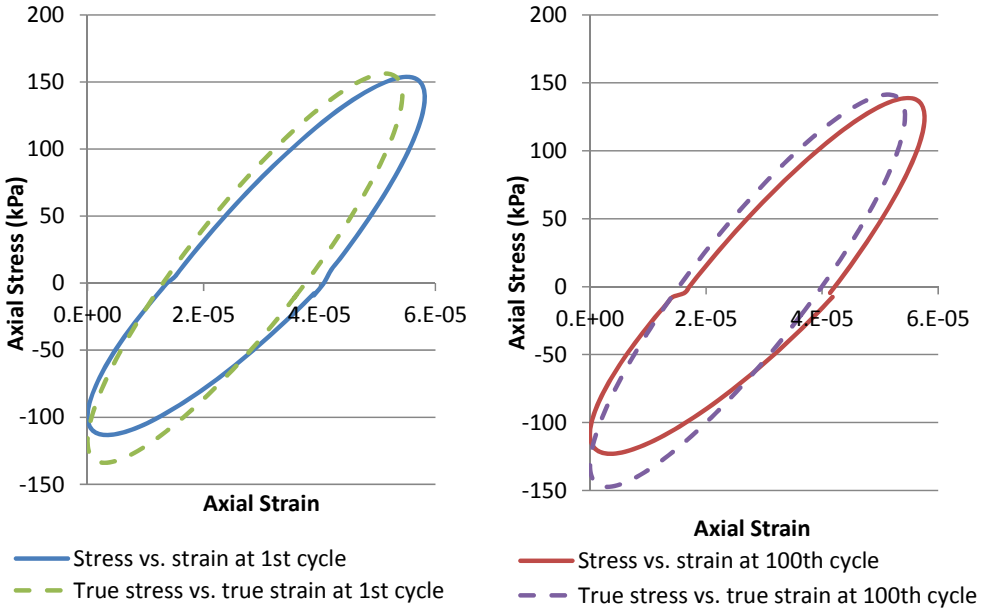

(a) 1st Loading Cycle **(b) 100th Loading Cycle**

Figure 4.2 Apparent and True Hysteresis Loop in Nondestructive RDT Test

4.2.3 Determination of Simulation Parameters in Damaged Asphalt Mixtures

After determining the true stress/strain in nondestructive tests and the true material properties in nondestructive/destructive tests, this subsection further determines the true stress/true strain in a damaged asphalt mixture specimen in destructive tests. The DPSE balance equation (Equation 3.23) is proposed to solve for the true stress in the destructive RDT test. Firstly, the DPSE^{T} is calculated by integrating σ^T and ε_R^T as:

$$\text{DPSE}^T = \pi\sigma_0^T\varepsilon_0^T \sin\left(\varphi^T - \varphi_{NLVE}^T\right) \tag{4.30}$$

Substitute for ε_0^T by Equation 4.7 to obtain:

$$\text{DPSE}^T = \pi\frac{\left(\sigma_0^T\right)^2}{\left|E^{*T}\right|}\sin\left(\varphi^T - \varphi_{NLVE}^T\right) \tag{4.31}$$

in which φ_{NLVE}^{T} and $\left|E_{NLVE}^{*T}\right|$ are the nondestructive true material properties determined above in Table 4.1; φ^{T} and $\left|E^{*T}\right|$ are the destructive true material properties determined above in Table 4.1. Substituting Equation 4.31 into Equation 3.23, gives:

$$\mathrm{DPSE}^{A} = \pi \frac{\left(\sigma_0^T\right)^2}{\left|E^{*T}\right|} \sin\left(\varphi^T - \varphi_{NLVE}^T\right) \tag{4.32}$$

Solving for σ_0^T from Equation 4.32 gives:

$$\sigma_0^T = \sqrt{\frac{\mathrm{DPSE}^{A}\left|E^{*T}\right|}{\pi \sin\left(\varphi^T - \varphi_{NLVE}^T\right)}} \tag{4.33}$$

The other simulation parameter, σ_{cm}^T, is determined from the ratio of σ_{cm}^T to σ_0^T, which is calculated by combining Equations 4.19 and 4.20 in the following way:

$$\frac{\sigma_{cm}^T}{\sigma_0^T} = \frac{\sigma_{st} + \sigma_{cm}}{\sigma_{0t} + \sigma_{0c}} \tag{4.34}$$

Based on the determined σ_0^T and σ_{cm}^T for the true stress and the destructive true material properties, the hysteresis loops in the destructive test can be produced as shown in Figure 4.3. The true stress-true strain hysteresis loop is larger than the stress-strain hysteresis loop; this difference becomes much more distinct as the loading cycles increase to 250. Furthermore, the stress-strain hysteresis loop becomes smaller from 1st to 250th cycle; however, the true stress-true strain hysteresis loop becomes larger. To better explain this phenomenon, the true and apparent stress amplitudes are plotted versus the number of loading cycles for the destructive test, which is shown in Figure 4.4.

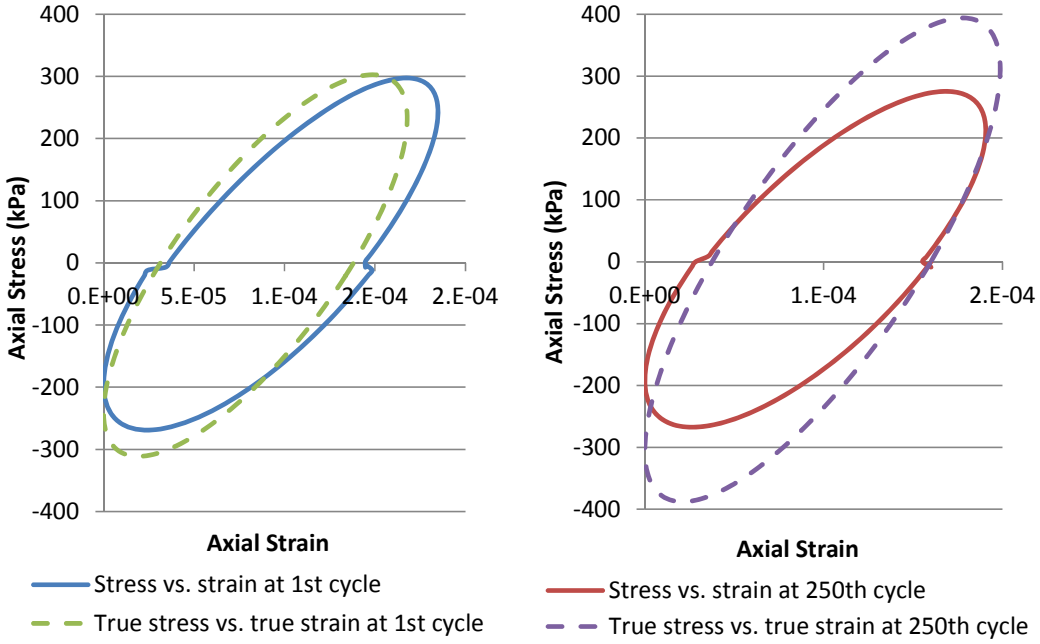

(a) 1st Loading Cycle **(b) 250th Loading Cycle**

Figure 4.3 Apparent and True Hysteresis Loop in Destructive RDT Test

Two observations are made from Figure 4.4:

1) σ_0^T is larger than σ_{0t} and σ_{0c} at the same loading cycle; and

2) σ_0^T increases whereas σ_{0t} and σ_{0c} decrease with the increase of loading cycles.

The first observation is explained by the fact that the area of the intact material sustaining the true stress is smaller than the entire cross sectional area that is used to calculate the apparent stress. To satisfy the force equilibrium, the true stress must be larger than the apparent stress. In the second observation, the decrease of σ_{0t} and σ_{0c} represents the reduction of the modulus in the controlled-strain RDT test. This conforms to the common explanation for the effect of cracking damage: the degradation of material stiffness. However, the stiffness is a material property, which should not change

as loading cycles increase. That is the reason for introducing the true measure of cracking damage: the cracks, which affect the true stress/strain; and the intact material, whose material properties (destructive true material properties) do not change through a destructive test.

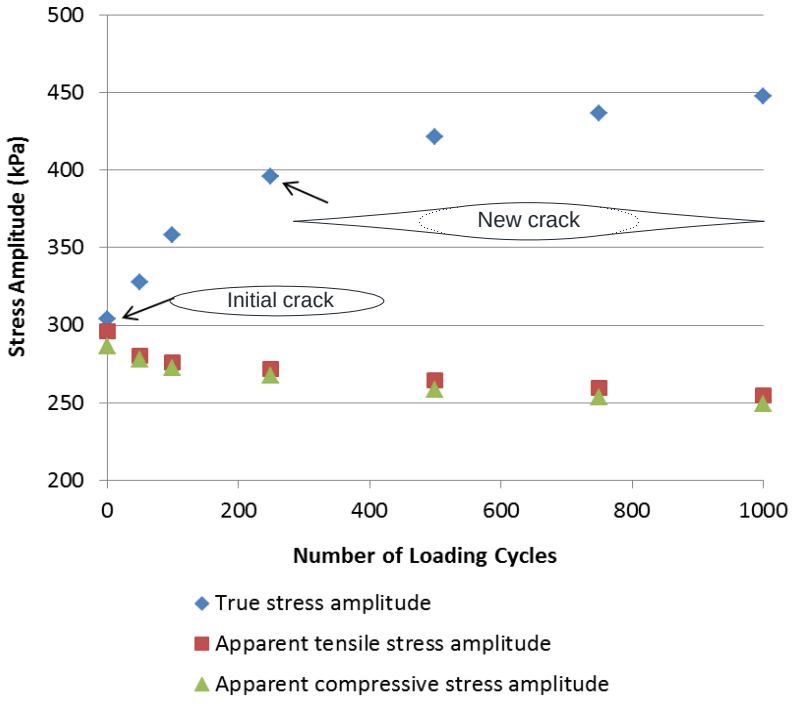

Figure 4.4 Stress Amplitudes in Destructive RDT Test

The influence of the crack damaging on the true stress/true strain is explained by the fact of the change of geometry of the cracks, which is schematically shown in Figure 4.4. The initial cracks, or the air voids in the asphalt mixture specimen are approximately elliptical holes with shorter minor axis relative to the major axis. As the air voids grow to the 250th cycle, the major axis increases greatly to form the "new crack", when the air

voids begin to take on the appearance of a real crack: two surfaces meeting at a very sharp edge at the crack tip. During the process of crack growth, the stress concentration in the intact material is aggravated significantly at the crack tip due to the change of geometry of the crack according to Inglis' stress concentration analysis (Inglis 1913). Since the material properties of the intact material do not change as cracks grow, the strain in the intact material increases correspondingly. As a result, the actual effect of crack damaging is the aggravation of the true stress/true strain localization.

On the other hand, the aggravation of true stress localization promotes the crack growth in asphalt mixtures. Paris and Sih (1965) pointed out that the stress concentration near the tip of a crack most likely initiated the growth of the crack. Other researchers also proved that the high local stress and strain concentration would dominate the fatigue failure process (Li and Metcalf 2004; Wang et al. 2007). Therefore, the complete description of the relationship between the crack growth and the true stress/true strain is: the true stress/true strain localization is the cause for the crack growth; then the growth of cracks further enhances the severity of the true stress/true strain localization. Compared to a phenomenological description by the apparent stress/apparent strain, the true stress/true strain reveals the essence of crack growth and should be used to model the crack growth in an asphalt mixture, which is described in Section 4.3.

4.3 Determination of Damage Density and Average Crack Size

4.3.1 Determination of Damage Density

Damage density is an index that describes the extent of cracking damage in an

asphalt mixture specimen. Since the cracks grow on a basis of the air voids in the asphalt mixture specimen, the damage density can be expressed in the following way:

$$\phi = \phi_0 + \phi_\Delta \tag{4.35}$$

where ϕ is the damage density; ϕ_0 is the initial damage density, which equals the air void content; and ϕ_Δ is the increase of the damage density due to the crack growth, which is calculated in the following way:

$$\phi_\Delta = \frac{D\% \cdot A_m}{A} = D\% \cdot \frac{V_m}{V} = D\% \cdot V_m\% \tag{4.36}$$

in which $D\%$ is the percentage of cracking damage on a cross section of the asphalt mixture specimen; A_m is the area of the asphalt mastic on the cross section of the specimen. The value of $D\% \cdot A_m$ represents the increased area of the cracks on the cross section due to the crack growth in the asphalt mastic. V_m and V is the volume of the asphalt mastic and asphalt specimen, respectively; and $V_m\%$ is the volumetric percentage of the asphalt mastic that is determined from the volumetric analysis and aggregate gradation of the mixture design.

The cracking damage on a cross section of the specimen cannot be measured directly; instead, it is inferred from the force equilibrium equation by solving S_c/A from Equation 4.19:

$$D\% = \frac{S_c}{A} = 1 - \frac{(\sigma_{0t} + \sigma_{0c})/2}{\sigma_0^T} \tag{4.37}$$

Substitute Equations 4.36 and 4.37 into 4.35 to obtain the damage density as follows:

$$\phi = \phi_0 + \left[1 - \frac{(\sigma_{0t} + \sigma_{0c})/2}{\sigma_0^T}\right] V_m\% \tag{4.38}$$

Figure 4.5 shows the damage density of a number of representative loading cycles calculated by Equation 4.38 in the destructive test. At the end of the 1,000 cycles, ϕ_Δ is about 4.4%; the total damage density is 8.2% by adding ϕ_Δ to ϕ_0 (3.8%). There is a rapid increase of the damage density at the beginning of the test; then the rate of the change of the damage density decreases as the loading cycles increase. The evolution of the damage density with the increase of the number of loading cycle N is modeled by a power function using MATLAB:

$$\phi = 0.536N^{0.310} + 3.790, \qquad R^2 = 0.989 \tag{4.39}$$

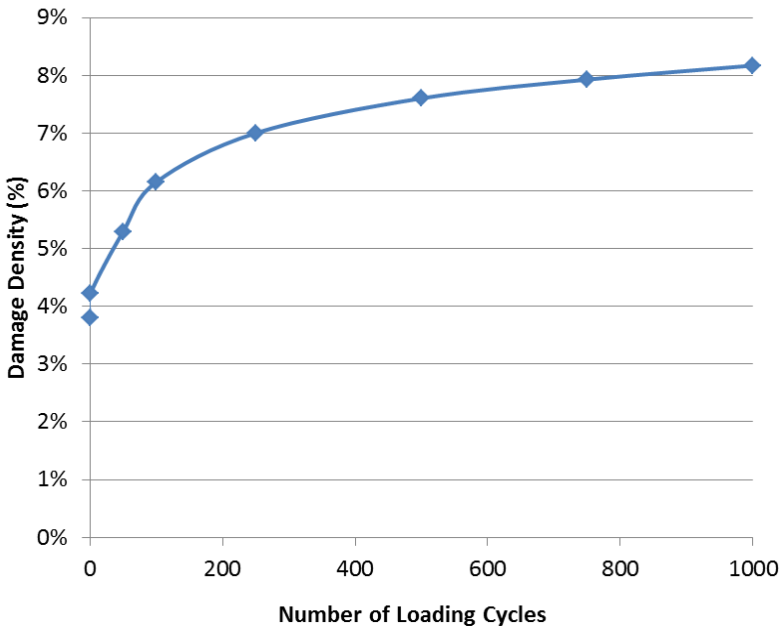

Figure 4.5 Damage Density in Destructive RDT Test

4.3.2 Determination of Fracture Coefficients

Application of the damage density into the Paris' Law can address its shortcoming that only describes the growth of one crack. The Paris' Law is thus modified in the following way:

$$\frac{d\phi}{dN} = A'\left(J_R\right)^{n'} \tag{4.40}$$

where $d\phi/dN$ represents the evolution of the damage density of an asphalt mixture specimen per cycle; A' and n' are fracture coefficients associated with the evolution of the damage density; and J_R is the pseudo *J* integral that is calculated based on the pseudo strain energy and used to model crack growth in asphalt mixtures (Masad et al. 2007; Si et al. 2002; Walubita et al. 2006).

In contrast to the traditional experimental methods of measuring the fracture coefficients, A' and n' can be determined using the damage density calculated above. Firstly, calculate J_R using the DPSE as shown in Equation 4.41:

$$J_R = \frac{\partial \text{DPSE}}{\partial(\text{crack surface area})} = \frac{\dfrac{\partial \text{DPSE}}{\partial N}}{\dfrac{\partial(\text{crack surface area})}{\partial N}} \tag{4.41}$$

"Crack surface area" refers to the area of the crack surfaces on a cross section of the specimen, so it is calculated using the damage density multiplied by the cross sectional area A:

$$\text{crack surface area} = 2\phi A \tag{4.42}$$

in which the factor "2" is needed since each crack has two surfaces. $\partial \text{DPSE}/\partial N$

represents the rate of change of the DPSE as the loading cycles increase, which is obtained by simulating the curve of the DPSE versus the number of loading cycles as:

$$\text{DPSE} = cN^{d} \tag{4.43}$$

where c and d are regression coefficients for the DPSE. Substitute Equations 4.41, 4.42 and 4.43 into Equation 4.40 to obtain:

$$\frac{d\phi}{dN} = A'\left(\frac{cdN^{d-1}}{2A\dfrac{d\phi}{dN}}\right)^{n'} \tag{4.44}$$

Arrange Equation 4.44 in the following way:

$$d\phi = A'^{\frac{1}{n'+1}}\left(\frac{cd}{2A}\right)^{\frac{n'}{n'+1}} N^{\frac{n'(d-1)}{n'+1}}\, dN \tag{4.45}$$

Integrate Equation 4.45 on the both sides: the left side from ϕ_0 to ϕ; the right side from the corresponding cycle zero to cycle N as:

$$\int_{\phi_0}^{\phi} d\phi = \int_0^N A'^{\frac{1}{n'+1}}\left(\frac{cd}{2A}\right)^{\frac{n'}{n'+1}} N^{\frac{n'(d-1)}{n'+1}}\, dN \tag{4.46}$$

Integration of Equation 4.46 yields the following expression for ϕ:

$$\phi = A'^{\frac{1}{n'+1}}\left(\frac{cd}{2A}\right)^{\frac{n'}{n'+1}}\left(\frac{n'+1}{dn'+1}\right)N^{\frac{dn'+1}{n'+1}} + \phi_0 \tag{4.47}$$

On the other hand, the damage density is calculated from the destructive RDT test as shown in Equation 4.39. A general form of Equation 4.39 is defined as:

$$\phi = aN^{b} + c \tag{4.48}$$

where a, b, and c are regression coefficients for the damage density. Comparing

Equation 4.47 with 4.48, gives:

$$a = A'^{\frac{1}{n'+1}} \left(\frac{cd}{2A} \right)^{\frac{n'}{n'+1}} \left(\frac{n'+1}{dn'+1} \right) \tag{4.49}$$

$$b = \frac{dn'+1}{n'+1} \tag{4.50}$$

$$c = \phi_0 \tag{4.51}$$

As a result, n' is solved from Equation 4.50 and A' is solved from Equation 4.49 as:

$$n' = \frac{1-b}{b-d} \tag{4.52}$$

$$A' = a^{n'+1} \left(\frac{2A}{cd} \right)^{n'} \left(\frac{dn'+1}{n'+1} \right)^{n'+1} = (ab)^{\frac{1-d}{b-d}} \left(\frac{2A}{cd} \right)^{\frac{1-b}{b-d}} \tag{4.53}$$

Using the damage density plotted in Figure 4.5 and the regression values in Equation 4.39, the fracture coefficients associated with the damage density are:

$n' = 4.46$; $A' = 2.27 \times 10^{-14}$.

4.3.3 Determination of Average Crack Size and Number of Cracks

The damage density and fracture coefficients determined above describe the cracking damage of an asphalt mixture on a macro scale. This subsection continues to solve for the average crack size and number of cracks in a damaged asphalt mixture specimen. "Average" means that the crack size calculated here is the mean value of the size of all cracks on a cross section of the specimen. The crack size follows a Weibull distribution. The ability to measure this distribution is important for modeling aging and moisture damage in asphalt mixtures (Luo and Lytton 2011). In order to determine the parameters of the Weibull distribution model, the average crack size must be obtained first.

The average crack size is determined using the RPSE balance equation based on the destructive RDT test data. The RPSE balance equation (Equation 3.24) is applied to every loading cycle of the RDT test: c_I is the average crack size at the current loading cycle: c_N is the average crack size at the next loading cycle. The crack growth from the current cycle to the next cycle is an increment $c_N - c_I$. Denote the number of loading cycle i ($i = 1, 2, ...1000$) and Equation 14 can be rewritten as:

$$\mathrm{RPSE}_i^A V_m = \mathrm{RPSE}_i^T V_m - \mathrm{RPSE}_i^T \left(\frac{2}{3} M_i \pi^2 {c_i}^3 - \frac{2}{3} M_{i-1} \pi^2 {c_{i-1}}^3 \right) + 2\gamma \left(M_i \pi {c_i}^2 - M_{i-1} \pi {c_{i-1}}^2 \right) \tag{4.54}$$

in which RPSE_i^T is calculated by integrating σ^T and ε_R^T and the result is as follows:

$$\mathrm{RPSE}^T = \sigma_0^T \varepsilon_0^T \cdot \left\{ \frac{\sin\left(\varphi^T - \varphi_{NLVE}^T\right)\left[\pi - 2\left(\varphi^T - \varphi_{NLVE}^T\right)\right] + \cos\left(\varphi^T - \varphi_{NLVE}^T\right)\left[\cos\left(T_t \omega\right) - 1\right]}{2} \right\} + 2\left(\sigma_0^T - \sigma_{cm}^T\right) \varepsilon_0^T \cos\left(\varphi^T - \varphi_{NLVE}^T\right) \cos\left(\frac{T_t \omega}{2}\right) \tag{4.55}$$

The number of cracks at the i^{th} cycle M_i and the number of cracks at $(i\text{-}1)^{\text{th}}$ cycle M_{i-1} has the following relationship with c_i and c_{i-1}, respectively:

$$M_i \pi {c_i}^2 = \phi_i A \tag{4.56}$$

$$M_{i-1} \pi {c_{i-1}}^2 = \phi_{i-1} A \tag{4.57}$$

in which ϕ_i and ϕ_{i-1} are the damage density at i^{th} and $(i\text{-}1)^{\text{th}}$ cycle, respectively. As a result, the only independent variables in Equation 4.54 are c_i and c_{i-1}. The procedures

of solving for c_i and c_{i-1} are detailed as follows.

1) Derive the cumulative RPSE balance equation to estimate c_i

The cumulative RPSE balance equation is derived by summing up Equation 4.54 from $i = 1$ to $i = N$ as follows:

$$\begin{aligned}\sum_{i=1}^{N} \mathrm{RPSE}_i^A V_m = \sum_{i=1}^{N} \mathrm{RPSE}_i^T V_m \\ -\begin{pmatrix} \frac{2}{3}\mathrm{RPSE}_1^T M_1 \pi^2 {c_1}^3 - \frac{2}{3}\mathrm{RPSE}_1^T M_0 \pi^2 {c_0}^3 \\ +\frac{2}{3}\mathrm{RPSE}_2^T M_2 \pi^2 {c_2}^3 - \frac{2}{3}\mathrm{RPSE}_2^T M_1 \pi^2 {c_1}^3 \\ +\frac{2}{3}\mathrm{RPSE}_3^T M_3 \pi^2 {c_3}^3 - \frac{2}{3}\mathrm{RPSE}_3^T M_2 \pi^2 {c_2}^3 \\ +\cdots+\frac{2}{3}\mathrm{RPSE}_{N-1}^T M_{N-1} \pi^2 {c_{N-1}}^3 - \frac{2}{3}\mathrm{RPSE}_{N-1}^T M_{N-2} \pi^2 {c_{N-2}}^3 \\ +\frac{2}{3}\mathrm{RPSE}_N^T M_N \pi^2 {c_N}^3 - \frac{2}{3}\mathrm{RPSE}_N^T M_{N-1} \pi^2 {c_{N-1}}^3 \end{pmatrix} \\ +2\gamma\begin{pmatrix} M_1 \pi {c_1}^2 - M_0 \pi {c_0}^2 + M_2 \pi {c_2}^2 - M_1 \pi {c_1}^2 + M_3 \pi {c_3}^2 - M_2 \pi {c_2}^2 \\ +\cdots+ M_{N-1} \pi {c_{N-1}}^2 - M_{N-2} \pi {c_{N-2}}^2 + M_N \pi {c_N}^2 - M_{N-1} \pi {c_{N-1}}^2 \end{pmatrix}\end{aligned} \tag{4.58}$$

in which c_0 is the initial average crack size, or average air void size. Assume RPSE_i^T in two adjacent cycles are the same, i.e. $\mathrm{RPSE}_i^T = \mathrm{RPSE}_{i-1}^T$. Then Equation 4.58 reduces to:

$$\begin{aligned}\sum_{i=1}^{N} \mathrm{RPSE}_i^A V_m = \sum_{i=1}^{N} \mathrm{RPSE}_i^T V_m \\ -\left(\frac{2}{3}\mathrm{RPSE}_N^T M_N \pi^2 {c_N}^3 - \frac{2}{3}\mathrm{RPSE}_1^T M_0 \pi^2 {c_0}^3\right) \\ +2\gamma\left(M_N \pi {c_N}^2 - M_0 \pi {c_0}^2\right)\end{aligned} \tag{4.59}$$

In this step temporarily assume c_0 to be zero so Equation 4.59 further reduces to:

$$\sum_{i=1}^{N} \mathrm{RPSE}_i^A V_m = \sum_{i=1}^{N} \mathrm{RPSE}_i^T V_m - \frac{2\pi}{3}\mathrm{RPSE}_N^T M_N \pi {c_N}^2 c_N + 2\gamma M_N \pi {c_N}^2 \tag{4.60}$$

Since $M_N \pi c_N{}^2 = \phi_N A$, Equation 4.60 becomes:

$$\sum_{i=1}^{\mathrm{N}} \mathrm{RPSE}_i^A V_m = \sum_{i=1}^{\mathrm{N}} \mathrm{RPSE}_i^T V_m - \frac{2\pi}{3} \mathrm{RPSE}_N^T \phi_N A c_N + 2\gamma \phi_N A \tag{4.61}$$

Substitute Equation 4.38 into Equation 4.61 to obtain:

$$\begin{aligned} \sum_{i=1}^{\mathrm{N}} \mathrm{RPSE}_i^A V_m = & \sum_{i=1}^{\mathrm{N}} \mathrm{RPSE}_i^T V_m \\ & - \frac{2\pi}{3} \mathrm{RPSE}_N^T \left\{ A \left[\phi_0 + \left(1 - \frac{\left(\sigma_{0t,N} + \sigma_{0c,N} \right)/2}{\sigma_{0,N}^T} \right) V_m \% \right] \right\} c_N \\ & + 2\gamma A \left[\phi_0 + \left(1 - \frac{\left(\sigma_{0t,N} + \sigma_{0c,N} \right)/2}{\sigma_{0,N}^T} \right) V_m \% \right] \end{aligned} \tag{4.62}$$

Furthermore, substitute Equation 3.25, $V_m = A_m \bar{t}$, into Equation 4.62 and divide A_m over both sides of the equation, yielding:

$$\begin{aligned} \sum_{i=1}^{\mathrm{N}} \mathrm{RPSE}_i^A \bar{t} = & \sum_{i=1}^{\mathrm{N}} \mathrm{RPSE}_i^T \bar{t} \\ & - \frac{2\pi}{3} \mathrm{RPSE}_N^T \left\{ \frac{A}{A_m} \left[\phi_0 + \left(1 - \frac{\left(\sigma_{0t,N} + \sigma_{0c,N} \right)/2}{\sigma_{0,N}^T} \right) V_m \% \right] \right\} c_N \\ & + 2\gamma \frac{A}{A_m} \left[\phi_0 + \left(1 - \frac{\left(\sigma_{0t,N} + \sigma_{0c,N} \right)/2}{\sigma_{0,N}^T} \right) V_m \% \right] \end{aligned} \tag{4.63}$$

Since $A_m = V_m \% A$, Equation 4.63 is simplified to:

$$\begin{aligned} \sum_{i=1}^{\mathrm{N}} \mathrm{RPSE}_i^A \bar{t} = & \sum_{i=1}^{\mathrm{N}} \mathrm{RPSE}_i^T \bar{t} \\ & - \frac{2\pi}{3} \mathrm{RPSE}_N^T \left[\frac{\phi_0}{V_m \%} + 1 - \frac{\left(\sigma_{0t,N} + \sigma_{0c,N} \right)/2}{\sigma_{0,N}^T} \right] c_N \\ & + 2\gamma \left[\frac{\phi_0}{V_m \%} + 1 - \frac{\left(\sigma_{0t,N} + \sigma_{0c,N} \right)/2}{\sigma_{0,N}^T} \right] \end{aligned} \tag{4.64}$$

Solve for c_N from Equation 4.64 to obtain:

$$c_N = \frac{\sum_{i=1}^{N} \mathrm{RPSE}_i^T \bar{t} + 2\gamma \left[\frac{\phi_0}{V_m\%} + 1 - \frac{\left(\sigma_{0t,N} + \sigma_{0c,N}\right)/2}{\sigma_{0,N}^T} \right] - \sum_{i=1}^{N} \mathrm{RPSE}_i^A \bar{t}}{\frac{2\pi}{3} \mathrm{RPSE}_N^T \left[\frac{\phi_0}{V_m\%} + 1 - \frac{\left(\sigma_{0t,N} + \sigma_{0c,N}\right)/2}{\sigma_{0,N}^T} \right]} \tag{4.65}$$

Based on Equation 4.65, c_N is calculated for a number of loading cycles in the destructive RDT test, which is shown in Figure 6 and labeled by "first estimation". For example, c_1 is calculated to be 0.270 mm. It is called "first estimation" because c_N calculated in this step is based on two simplifications: $\mathrm{RPSE}_i^T = \mathrm{RPSE}_{i-1}^T$ and $c_0 = 0$.

2) Calculate c_0 based on the first estimation of c_N

A best-fit function is fitted to the curve of c_N versus N in Figure 4.6, as shown in Equation 4.66:

$$c_N = 0.0032N + 0.2048, \qquad R^2 = 0.9992 \tag{4.66}$$

If the best-fit function is extrapolated, it will intersect with the vertical axis at c_0, which is 0.205 mm. The values of c_0 and c_1 calculated above will be used as feed values in the next step.

3) Determine accurate value of c_N using the RPSE balance equation

The RPSE balance equation stated in Equation 4.54 is modified using the same substitutions for Equations 4.61 to 4.64, which yields a balance equation with only two unknown variables c_i and c_{i-1} as shown in Equation 4.67:

$$\mathrm{RPSE}_i^{A}\bar{t} = \mathrm{RPSE}_i^{T}\bar{t} - \mathrm{RPSE}_i^{T}\frac{2\pi}{3}\left\{\begin{array}{l}\left[\dfrac{\phi_0}{V_m\%}+\left(1-\dfrac{\left(\sigma_{0t,i}+\sigma_{0c,i}\right)/2}{\sigma_{0,i}^{T}}\right)\right]c_i \\ -\left[\dfrac{\phi_0}{V_m\%}+\left(1-\dfrac{\left(\sigma_{0t,i-1}+\sigma_{0c,i-1}\right)/2}{\sigma_{0,i-1}^{T}}\right)\right]c_{i-1}\end{array}\right\} + 2\gamma\left\{\begin{array}{l}\left[\dfrac{\phi_0}{V_m\%}+\left(1-\dfrac{\left(\sigma_{0t,i}+\sigma_{0c,i}\right)/2}{\sigma_{0,i}^{T}}\right)\right] \\ -\left[\dfrac{\phi_0}{V_m\%}+\left(1-\dfrac{\left(\sigma_{0t,i-1}+\sigma_{0c,i-1}\right)/2}{\sigma_{0,i-1}^{T}}\right)\right]\end{array}\right\} \quad (4.67)$$

Equation 4.67 is solved for every loading cycle of the destructive test to obtain c_i, from *i* = 1 to 1,000. The procedure is as follows:

- For the 1st loading cycle, c_0 and c_1 based on the first estimation ($c_0 = 0.205$ mm, $c_1 = 0.270$ mm), are fed into Equation 4.67. The Solver function in Excel is then used to solve for the new values of c_0 and c_1, so the left side and right side of the equation can be balanced. The new values are: $c_0 = 0.226$ mm, and $c_1 = 0.241$ mm. The feed values of c_0 and c_1 are required in order to get the accurate solution for them through Equation 4.67.
- The determined c_1 is fed into Equation 4.67 for the 2nd loading cycle. Now c_2 is the only unknown variable, which is obtained by solving Equation 4.67.
- The determined c_2 is fed into Equation 4.67 for 3rd loading cycle to solve for c_3.

This calculation is repeated for every loading cycle till the last cycle of the RDT test. It is conducted automatically by the Macro program that is designed and embedded in the

Excel. The result is shown in Figure 4.6, labeled "second estimation". There are no assumptions or simplifications for the second estimation, so it is the final result for the average crack size.

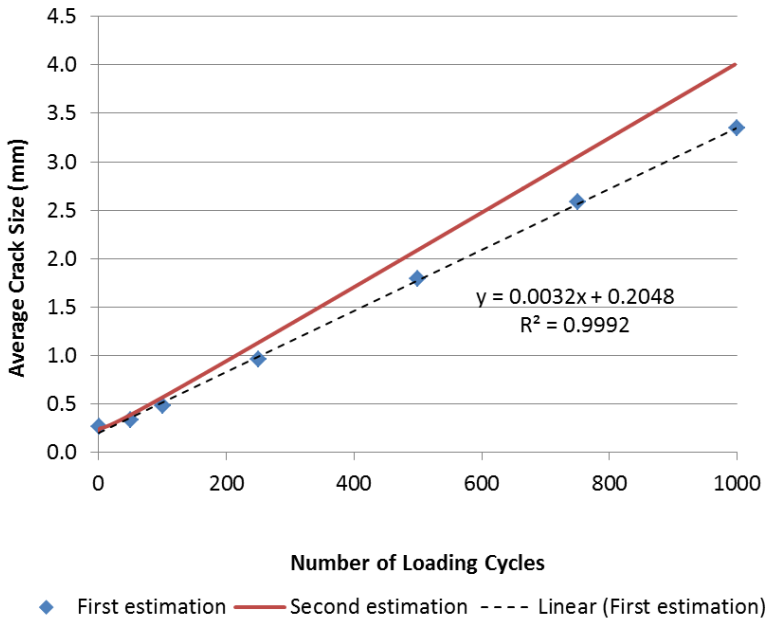

Figure 4.6 Average Crack Size in Destructive RDT Test

4) Calculate the number of cracks based on the determined average crack size

Once the average crack size in i^{th} loading cycle, c_i, is determined, the number of cracks in the corresponding cycle, M_i, can be calculated by solving M_i from Equation 4.68 as:

$$M_i = \frac{\phi_i A}{\pi c_i^2} \tag{4.68}$$

For example, substitute $\phi_0 = 3.8\%$ (air void content) and $c_0 = 0.226$ mm into Equation 4.68 to obtain $M_0 = 1916$, which is the number of air voids in the asphalt mixture

specimen before it is damaged. A plot of M_i versus the number of loading cycles is shown in Figure 4.7. The result suggests that the number of cracks starts from the number of air voids, gains a rapid increase and reaches its peak value in the early stage of the test. After that the number of cracks decreases quickly until only 10 to 20 remain at the end of the test. This indicates a process of creating more and more hair-like cracks in the early stage of loading. As the loading cycle increases, these hair-like cracks grow and their size increases. When the size increases to a certain value, the hair-like cracks start to merge with each other. In other words, coalescence of adjacent cracks occurs, so the number of cracks starts to decrease. As the cracks continue to grow and coalesce with the increase of loading cycles, the number of cracks continues to decrease.

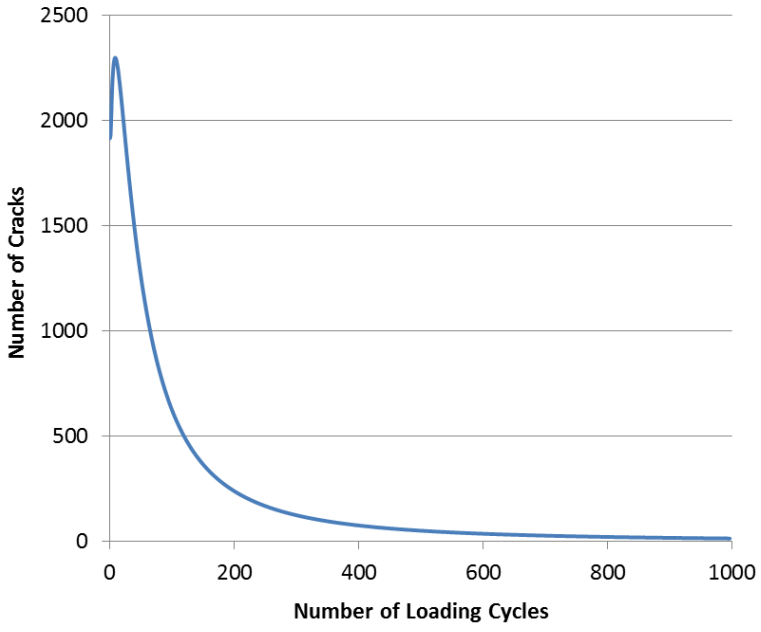

Figure 4.7 Number of Cracks in Destructive RDT Test

5) Compare the calculated average crack size and number of cracks to those measured by the X-ray Computed Tomography (X-ray CT)

In order to justify the average crack size and number of cracks calculated above, they are compared to those measured by the X-ray CT system. The X-ray CT system has been used to measure the air void size and the internal structure of an asphalt mixture (Arambula et al. 2007; Masad et al. 1999). The same asphalt mixture specimen is subjected to the X-ray CT measurement before the nondestructive and destructive RDT tests. Details of the test procedure and analysis method of the X-ray CT system can be found in the relevant literature (Arambula et al. 2007). The result of the X-ray CT analysis is: $c_0 = 0.428$ mm and $M_0 = 535$.

Compared to the values calculated above, which are $c_0 = 0.226$ mm and $M_0 = 1916$, the average air void size derived from the X-ray CT is much larger and the number of cracks is much smaller. This is because the results from the X-ray CT are flawed by two critical parameters: the image resolution and the threshold gray intensity. The image resolution determines the minimum crack size that can be detected by the X-ray CT system. It is usually around 0.2 mm/pixel. Therefore, the cracks whose size is smaller than 0.2 mm can not be detected by the X-ray CT system, which eliminates a lot of small cracks in the X-ray CT images. In addition to the measurement error, the analysis of the X-ray CT images also introduces errors due to the selection of the threshold gray intensity. The threshold gray intensity is used to differentiate the cracks from the asphalt binder and aggregates. Its selection usually depends on experience, which causes errors in identifying the percentage of cracks in the X-ray CT images.

These limits associated with the X-ray CT system lead to a considerable underestimation of the number of air voids and an overestimation of the average air void size for an undamaged asphalt mixture specimen. Furthermore, another critical problem associated with the X-ray CT system is its limitation in damage detection for asphalt mixtures. The X-ray CT measurement takes about 3 to 4 hours for a specimen 150 mm high and 100 mm in diameter. During this period, considerable healing (crack closure) occurs in the damaged asphalt mixture specimen, so the cracks measured by the X-ray CT system are far less than the damage originally generated in the specimen. Consequently, the X-ray CT is not capable of measuring the crack growth of asphalt mixtures under destructive loading. In this aspect, the approach proposed above has the advantage of determining the average crack size for every loading cycle of the destructive test.

4.4 Separation of DPSE for Fatigue Cracking and DPSE for Permanent Deformation

After solving the RPSE balance equation, the DPSE for fatigue cracking and DPSE for permanent deformation can be determined as formulated in Equations 3.29 and 3.30. The result of $DPSE_c$ and $DPSE_p$ is shown in Figure 4.8. The DPSE for fatigue cracking starts from zero and increases with the development of fatigue cracking as the loading cycle increases. The DPSE for permanent deformation is larger than the DPSE for fatigue cracking, and it does not start from zero. This is because fatigue cracking in the asphalt mixture specimen is initiated by the localized plastic deformation

surrounding the cracks. A large amount of energy must be expended first as the plastic work so that the material separation can occur and the fracture process zone can advance to form new cracks.

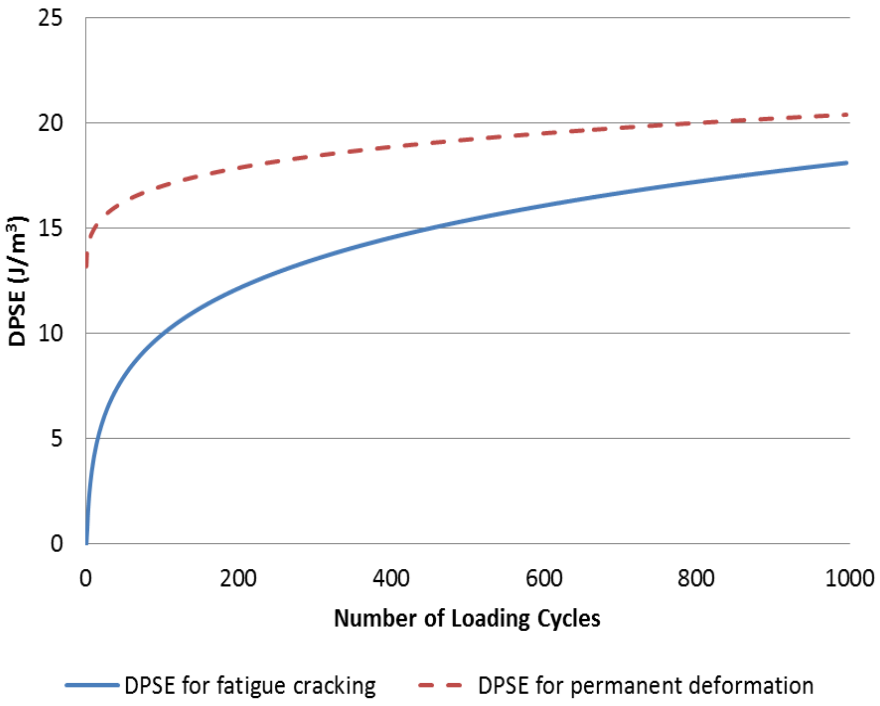

Figure 4.8 DPSE for Fatigue Cracking and DPSE for Permanent Deformation in Destructive RDT Test

5. CHARACTERIZATION OF RECOVERY PROPERTIES OF ASPHALT MIXTURES

5.1 Background of Characterization of Recovery Properties

Recovery of an asphalt mixture refers to the behavior of a deformed material after the load is removed. Before removing the load, the asphalt mixture undergoes a deforming process, in which cracking and permanent deformation are generated in the material if the load is destructive. Development of cracks produces alligator cracking and accumulation of permanent deformation results in rutting, which are two major distresses in asphalt pavements. Most existing researches studying damage characterization and prediction in asphalt pavements focus on how to reduce cracking and permanent deformation during the loading phase, while much less attention is paid to the unloading phase. As a matter of fact, the recovery of asphalt mixtures contributes to the damage characterization and prediction as well. During the recovery phase, the cracks generated during the loading phase start to heal. As a counter effect to cracking, healing alleviates cracking damage, so it affects the accuracy in predicting the remaining cracks in asphalt mixtures. On the other hand, an asphalt pavement that has better recovery ability leaves less deformation in the asphalt layer, so the occurrence of excessive deformation which produces permanent deformation less under repetitive traffic loading. Rutting is thus reduced, especially for asphalt pavements under high frequency traffic. A number of State Departments of Transportation have adopted this idea, and used the elastic recovery test as complement to examine the rutting resistance

of asphalt materials (Shenoy 2007). In addition to the elastic recovery test, the creep recovery test has also been used to evaluate the rutting resistance of non-modified and modified bitumen (Manuel 2010).

The elastic recovery test characterizes the recovery of asphalt materials. It examines the ability of an asphalt material to recover by a ductilometer following the procedure as documented in American Association of State Highway and Transportation Officials (AASHTO) T301-99 (AASHTO 2003) or American Society of Testing Materials (ASTM) D6084 (ASTM 2005). In this test, a briquet specimen is pulled apart till it reaches a specified elongation of 20 cm (AASHTO 2003) or 10 cm (ASTM 2005). The specimen is then severed at the center and allowed to recover without disturbance for an hour. At the end of one hour, rejoin the two halves and measure the elongation of recovered specimen. The ability of the material to recovery is described as the percentage of recovered length to the specified 20 cm or 10 cm. The elastic recovery test appears to be simple, but it actually requires elaboration on sample preparation and testing. Moreover, the result is not very accurate and often fails to discriminate the behaviors between different asphalt binders (Shenoy 2007). To fulfill the objective of the elastic recovery test and avoid the associated problems, Shenoy (2007) proposed a dynamic test using the dynamic shear rheometer (DSR). In a dynamic oscillatory test, the modulus is a complex number, defined as the complex modulus, including two components: the storage modulus and the loss modulus. The proportion of the storage modulus to the complex modulus is used as a measure of the recovery ability of the asphalt material. However, the storage modulus does not represent the total recovery of

an asphalt mixture. An asphalt mixture has an elastic response that instantaneously recovers upon load removal. It also exhibits considerable delayed elastic response (viscoelastic response), which non-instantaneously recovers (time-dependent) and is completely recoverable given sufficient time. The elastic and viscoelastic responses constitute the total recovery response of the asphalt mixture. From the viewpoint of the complex modulus, the elastic response and a portion of the viscoelastic response are contained in the storage modulus; the other portion of the viscoelastic response is contained in the loss modulus (Anderson et al. 1994). Therefore, measuring the storage modulus with a dynamic oscillatory apparatus is not an appropriate method to characterize the recovery of asphalt mixtures.

The creep recovery test is another method to characterize the recovery of viscoelastic materials. The recovery behavior of the viscoelastic material is recorded in the recovery phase of the test. Creep recovery compliance is defined as a measure of such behavior (Mezger 2006).

$$J_r(t) = \frac{\varepsilon_r(t)}{\sigma_0} \tag{5.1}$$

where $J_r(t)$ is the creep recovery compliance; $\varepsilon_r(t)$ is the recovered strain in the recovery phase, which is the difference between the maximum strain at the end of the creep phase and the remaining deformation in the recovery phase; and σ_0 is the applied stress in the creep phase. Defined using σ_0, $J_r(t)$ can only act as a material parameter that quantitatively describes how the material behaves after removing the load; it is not a material property because the recovery response is not stimulated by σ_0. The actual

driven force for the recovery response should be the force existing in the recovery phase. Since no external load remains, this driven force is provided by the material itself, which is defined as internal force or internal stress. As a result, in order to obtain the material properties in the recovery phase, the internal stress must be determined first during the recovery of asphalt mixtures.

The internal stress has been studied by many researchers for metals and polymers using the creep recovery test (Ahlquist and Nix 1971; Mindel and Brown 1973; Pahutova et al. 1979; Kubat et al. 1975; Fotheringham and Cherry 1978; Teoh et al. 1987; Raghavan and Meshii 1994). In the loading phase of the creep recovery test on a metal or polymer, the creep strain is partitioned into two parts: recoverable part (including elastic component and time-dependent component) and plastic part. Accordingly, the applied creep stress is decomposed to two components, as shown in Equation 5.2:

$$\sigma = \sigma_i + \sigma_e \tag{5.2}$$

where σ is the applied creep stress; σ_i is the internal stress, or the recovery stress, responsible for the recoverable strain that restores the deformed material into its original state; and σ_e is the effective stress, responsible for the plastic strain that results in the activated rate process of plastic deformation. According to this partition and definition, the positive creep strain rate is explained as being caused by a positive σ_e since σ is much larger than σ_i in the loading phase. When σ becomes zero in the recovery phase, the rate of recovery is only governed by σ_i, which is proportional to the unrecovered

strain (Mindel and Brown 1973, 1974). These studies define and measure the internal stress in the loading phase of the creep recovery test, aiming at explaining the deformation mechanism of a metal or polymer under the load. In order study the recovery behavior of an asphalt mixture when it is unloaded, the internal stress of the asphalt mixture in the recovery phase must be measured.

The objective of Section 5 is to design a test to measure the internal stress of an asphalt mixture in the recovery phase and uses the internal stress to characterize the recovery properties of the asphalt mixture. The principle of measurement of the internal stress is first introduced as follows.

5.2 Principle of Measurement of Internal Stress

In the current literature, there are three common techniques to measure the internal stress as summarized by Teoh (1987), including: 1) the strain transient dip test used in the creep test (Ahlquist and Nix 1971; Pahutova et al. 1979; Raghavan and Meshii 1994; Teoh et al. 1987); 2) the stress transient dip test used in constant strain rate test (Fotheringham and Cherry 1978); and 3) stress relaxation methods used in the relaxation test (Kubat et al. 1975). The strain transient dip test is relevant to this study, so it is described in detail here.

5.2.1 Strain Transient Dip Test

The strain transient dip test is designed based on the creep test to measure the internal stress in the loading phase. A schematic sketch of the strain transient dip test is shown in Figure 5.1. The creep load is interrupted by a continuous step-load reduction,

which is indicated by $\Delta\sigma_1$, $\Delta\sigma_2$, and $\Delta\sigma_3$, respectively. Change of the creep load results in the change of the effective stress in the material, which further causes the change of the creep strain rate. To demonstrate this change, the effective stress in the strain transient dip test is calculated by modifying Equation 5.2 as follows:

$$\sigma_e = (\sigma - \Delta\sigma_k) - \sigma_i \quad (k = 1,2,3) \tag{5.3}$$

where $\Delta\sigma_k$ is the magnitude of the load reduction, $k = 1,2,3$. After a load reduction, one of the three conditions may happen:

- $(\sigma - \Delta\sigma_1) > \sigma_i$ so $\sigma_e > 0$: the material continues to deform in the same direction as the creep strain ε, as indicated by $\dot{\varepsilon} > 0$ in Figure 5.1;
- $(\sigma - \Delta\sigma_2) = \sigma_i$ so $\sigma_e = 0$: no further deformation occurs and ε remains constant, as indicated by $\dot{\varepsilon} = 0$;
- $(\sigma - \Delta\sigma_3) < \sigma_i$ so $\sigma_e < 0$: the material deforms in the opposite direction, as indicated by $\dot{\varepsilon} < 0$.

The second condition where $\dot{\varepsilon} = 0$ enables the internal stress to be measured as $\sigma_i = \sigma - \Delta\sigma_2$. In general, the load reduction that produces a zero creep strain rate condition gives the internal stress in the loading phase. Following this idea, the internal stress in the recovery phase can be obtained by modifying the creep recovery test, which is introduced as follows.

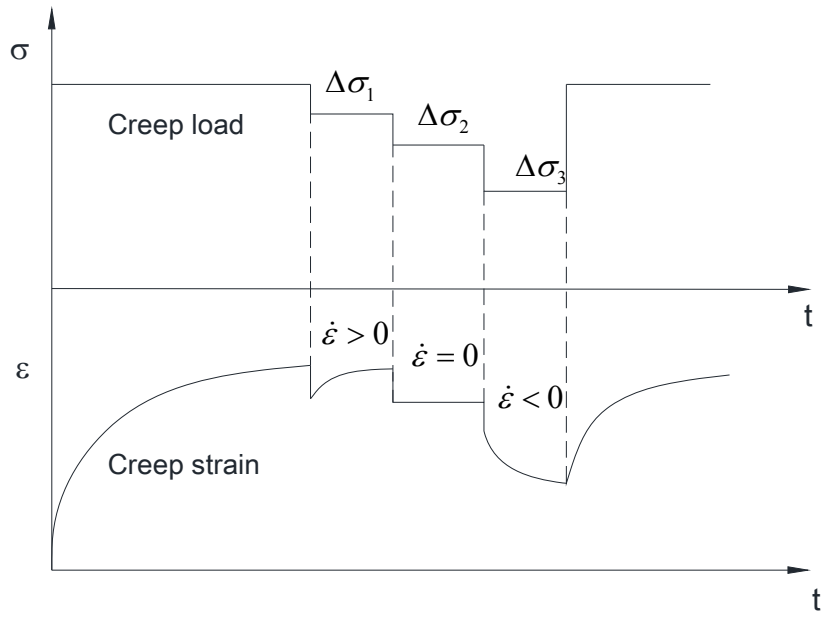

Figure 5.1 Schematic of Strain Transient Dip Test

5.2.2 Creep and Step-Loading Recovery Test

An asphalt mixture specimen in the creep recovery test is shown in Figure 5.2. Under the creep load, the creep strain is induced and the asphalt mixture specimen is stretched as shown from point A to point B. When the creep load is removed at t_0, the asphalt mixture specimen starts to recover. The recovered deformation is defined as recovery strain; the remaining deformation is defined as residual strain. The recovery process is driven by the internal stress, which is represented by a group of arrows as shown at points C, D, and E. According to the principle of measurement of the internal stress described above, the condition of zero residual strain rate is required to measure the internal stress. Since the internal stress is the only force in the recovery phase, an external load must be added in the opposite direction to achieve this condition,

as illustrated by an arrow at point D. Once the zero residual strain rate is produced, the added external load is equal to the internal stress of the asphalt mixture.

The external load is added by three steps in an increased order as shown in Figure 5.2, indicated by σ_1, σ_2, and σ_3, respectively. The corresponding change of the residual strain is measured in order to search for the point with zero residual strain rate. The rate of the residual strain is originally less than zero with only the presence of the internal stress. After adding the three step-loading at t_1, one of the three conditions may happen:

- $\dot{\varepsilon} < 0$ at σ_1: $\sigma_1 < \sigma_i$;
- $\dot{\varepsilon} = 0$ at σ_2: $\sigma_2 = \sigma_i$;
- $\dot{\varepsilon} > 0$ at σ_3: $\sigma_3 > \sigma_i$.

As a result, the internal stress at t_1 equals σ_2. Similarly, the internal stress at other times can be obtained by adding another step-load at the corresponding point. Such creep recovery test incorporated with several step-loads in the recovery phase is termed creep and step-loading recovery (CSR) test in this study. Section 5.3 presents an elaborate description pertaining to the design of this test in order to measure the internal stress at different time points to characterize the recovery properties of asphalt mixtures.

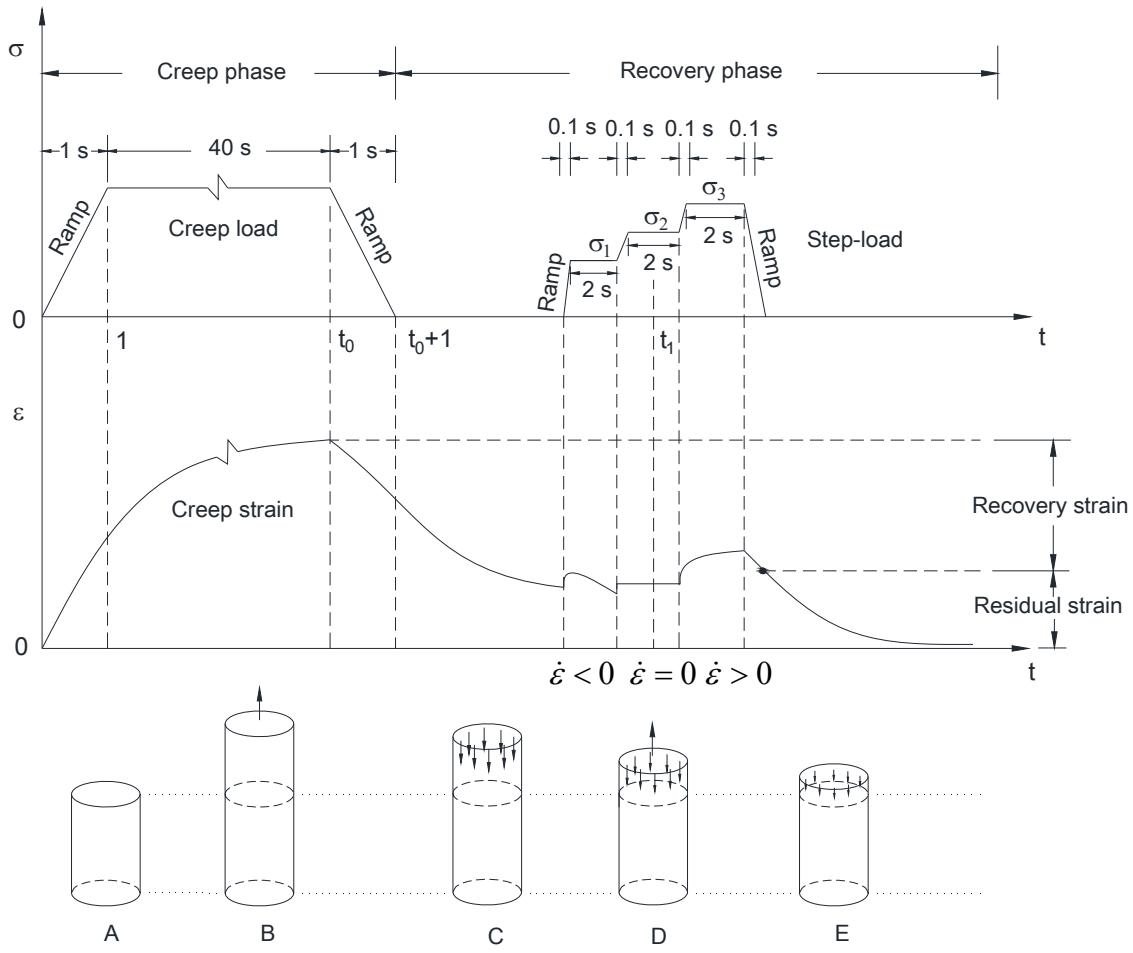

Figure 5.2 Schematic of Creep and Step-Loading Recovery Test

5.3 Configurations and Procedures of Creep and Step-Loading Recovery Test

Section 5.3 first discusses the principles in designing a CSR test in order to measure the internal stress at different time points. Then the materials and test procedures are presented to acquire adequate data to verify the accuracy of the test and determine the recovery properties.

5.3.1 Principles of Test Design

Design of a CSR test should consider several aspects, including: 1) the loading

duration and loading rate of the creep load in the creep phase and those of the step-load in the recovery phase; 2) the number of step-loads in the recovery phase and the number of steps in each step-load; 3) the position of each step-load in the recovery phase; and 4) the value of each step of every step-load in the recovery phase. They are discussed in sequence as follows.

1) Loading duration and loading rate of creep load and step-load

Selecting the loading duration for the creep load in the creep phase is simple, which only needs to satisfy the condition of enough data to determine the creep compliance. In this study, the loading duration for the creep load is chosen to be 40 sec. Selecting the loading duration for the step-load in the recovery phase is more complex: it should ensure less distrubance to the recovery of the asphalt mixture specimen, which requires smaller time duration; meantime, the loading duration of the step-load needs to be long enough in order to accurately determine the residual strain rate corresponding to the step-load. To satisfy the both conditions, the time duration of the step-load is selected to be 2 sec.

The loading duration reflects the length of holding the creep load or step-load at the given level. However, the load cannot instantaneously reach the given level; instead, it must be applied through a ramp as shown in Figure 5.3. The time required to increase the load from zero to the given level, or from the given level back to zero, is referred to the loading rate. To reduce the error caused by the ramp in analyzing the creep and recovery data, the loading duration should be as least ten times larger than the loading rate (Turner 1973). Therefore, it is better to choose smaller loading rate, but it should

also consider the feasibility of the testing machine. In this study, the loading time of the creep load ramp is selected to be 1 sec, and the loading time of the step-load ramp in the recovery phase is 0.1 sec, as shown in Figure 5.3.

2) Number of step-loads and number of steps in each step-load

The number of step-loads in the recovery phase decides the number of points at which the internal stress is measured. Selection of this number depends on three considerations. Firstly, the time duration of the recovery phase of the asphalt mixture specimen influences the number of step-loads that can be added to the recovery phase. In the nondestructive tests, which are conducted at low loading levels, instinctively, the internal stress in the undamaged asphalt mixture specimen is also low and diminishes very quickly. The time duration of the nondestructive test is thus short. In contrast, the time duration of the destructive test is relatively much longer, which allows more step-loads to be added in the recovery phase. The second consideration arises from the need of adequate data to simulate an accurate continuous curve of the internal stress versus time. To satisfy this need, more measured points for the internal stress should be added to the recovery phase. However, excessive measured points will lead to intense interruption to the recovery of the specimen. Based on these considerations, it has been tested and proven that five step-loads are suitable for the nondestructive test; seven step-loads are appropriate for the destructive test, as shown in Figure 5.3.

After selecting the number of step-loads for both nondestructive and destructive tests, the number of steps in each step-load is considered to further reduce the interruption to the specimen by adding step-loads. The number of steps in each step-load

indicates the time duration for measuring the internal stress at one measurement point. For example, there are three steps in the step-load shown in Figure 5.3 at t_1, so the time needed to measure the internal stress at t_1 is 6 sec. Usually, three steps in a step-load is best for searching for the zero strain rate, so there are three steps in each step-load in the destructive test, as shown in Figure 5.3(b). However, considering the short time duration of the recovery phase in the nondestructive test, a two-step loading is employed in the nondestructive test, which is shown in Figure 5.3(a). Therefore, the time required for measuring the internal stress is 4 sec at one measurement point for an undamaged asphalt mixture specimen.

3) Position of each step-load in the recovery phase

Determination of the position of each step-load in the recovery phase depends on the characteristic of the internal stress associated with the residual strain, which is inferred from the stress-strain relationship of an undamaged asphalt mixture, as expressed in Equation 4 (Findley et al. 1989):

$$\sigma_u(t) = \int_0^t E(t-\tau)\, d\varepsilon(\tau) \tag{5.4}$$

where $\sigma_u(t)$ is the stress in an undamaged asphalt mixture; t is the loading time; τ is any arbitrary time between 0 an t; $E(t)$ is the relaxation modulus of undamaged asphalt mixtures; and $\varepsilon(t)$ is any strain history. Equation 4 indicates that a greater residual strain rate corresponds to a larger internal stress in the asphalt mixture. The residual strain rate is much larger at the beginning of the recovery phase, and decreases with time as the recovery of the specimen continues, as indicated by Figure 5.2.

Consequently, the internal stress is very large immediately after unloading, and diminishes as the residual strain rate decreases with time. For example, the internal stress at point C is larger than that at point D in Figure 5.2, and the internal stress at point E becomes even smaller. The internal stress will vanish eventually if the asphalt mixture specimen fully recovers its deformation.

According to the characteristic of the internal stress, the position of each step-load, i.e. where to measure the internal stress, is determined as follows. The first step-load is set to be 1 sec after the end of the creep phase because the internal stress changes quickly at the beginning of the recovery phase, indicating considerable recovery of the asphalt mixture specimen. Therefore, it is crucial to measure the internal stress at this time so that the initial recovery behavior can be captured. After setting the first step-load, the criterion to place sequential step-loads is the rate of the change of the internal stress. This rate decreases with time, indicating that more change of the internal stress occurs in the short term of the recovery phase, whereas the internal stress changes less in the long term of the recovery phase. As a result, more step-loads should be placed in the short term than in the long term. In other words, the interval between the two step-loads should be smaller in the short term. Consequently, as shown in Figure 5.3, the interval between two adjacent step-loads is designed as 5 sec, 5 sec, 10 sec, and 15 sec, respectively, for the nondestructive test, and 6 sec, 6 sec, 10 sec, 10 sec, 15 sec, and 15 sec, respectively, for the destructive test. The duration of the recovery phase in both nondestructive and destructive tests is 150 sec.

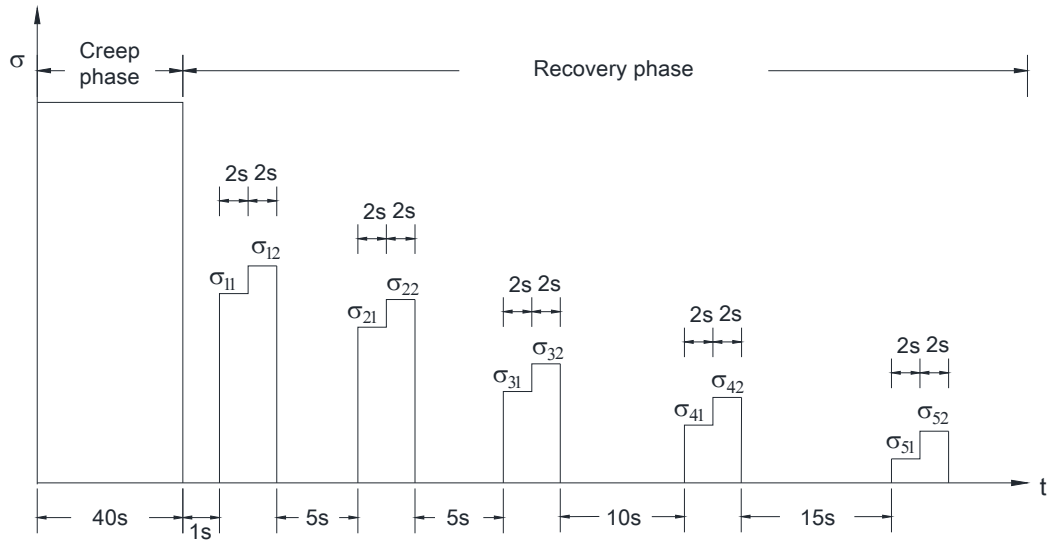

(a) Nondestructive Test

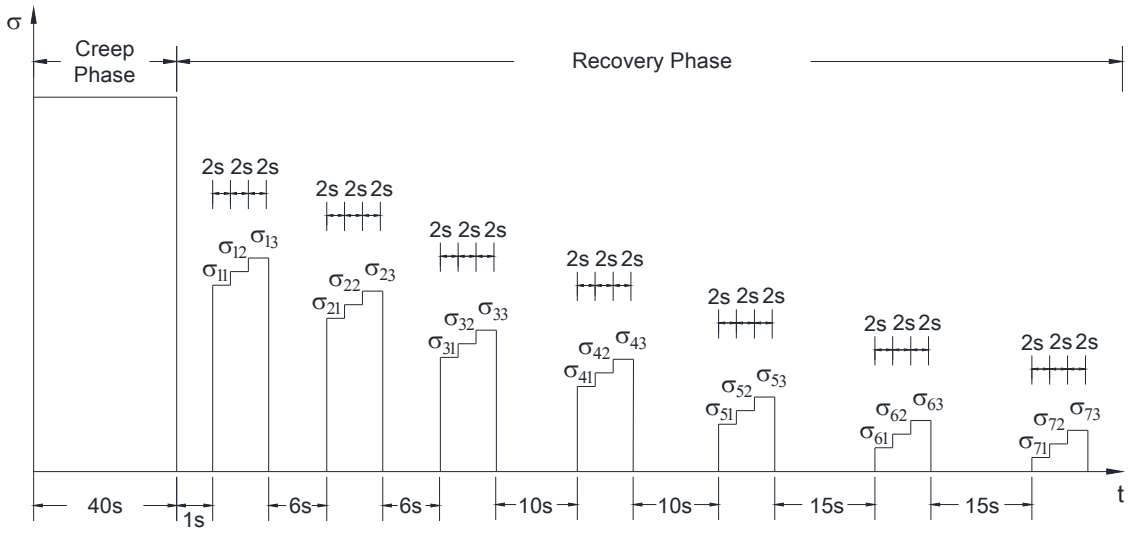

(b) Destructive Test

Figure 5.3 Loading Configuration of the Creep and Step-loading Recovery Test

4) Value of each step of every step-load

The last step of designing a CSR test is to determine the value of each step of every step-load so as to produce zero residual strain rate in the corresponding residual strain. The ideal outcome of a step-load is: for example, $\dot{\varepsilon} < 0$ for σ_{11} and $\dot{\varepsilon} = 0$ for σ_{12}, or $\dot{\varepsilon} = 0$ for σ_{11} and $\dot{\varepsilon} > 0$ for σ_{12} for the first step-load in Figure 5.3(a); $\dot{\varepsilon} < 0$ for σ_{11}, $\dot{\varepsilon} = 0$ for σ_{12}, and $\dot{\varepsilon} > 0$ for σ_{13} for the first step-load in Figure 5.3(b). This outcome is achieved by trial and error.

According to the testing experience, the trial value of each step is given in Table 5.1 and can be used as guidance for the first trial on any kind of asphalt mixture specimen. The symbol "σ" in Table 5.1 indicates the load of one step in a step-load; the number in the second row represents one of the five step-loads in the nondestructive test; the number in the sixth row represents one of the seven step-loads in the destructive test; and the number in the first column represents one of the steps in a step-load. The load "σ" is combined with the number in the second (or sixth) row and the number in the first column to produce a step in a step-load. For example, σ with "2" from second row and "1" from first column corresponds to the first step of the second step-load in the nondestructive test, the value of which is 20% of the creep load.

After the first trial, the residual strain rate measured from test is examined to determine whether it conforms to the ideal outcome mentioned above. If it is not, the value of the step-load is adjusted, which will be used in the next trial. After examining all the step-loads, all the changes required for the next trial are decided, and then the test is conducted again with adjusted values. This process is repeated till the result is close to

the ideal outcome. For example, if $\dot{\varepsilon} < 0$ for σ_{21} and $\dot{\varepsilon} > 0$ for σ_{22} in a nondestructive test, the value of σ_{22} needs to be lower for the next trial. Normally, two or three trials are enough to produce good outcomes and obtain accurate values of the internal stress at all measure points.

Table 5.1 Trial Values for the Step-load in the First Trial

σ	**Nondestructive Test (Creep Load: P_1)**				
	1	2	3	4	5
1	25% P_1	20% P_1	12.5% P_1	7% P_1	3% P_1
2	50% P_1	35% P_1	25% P_1	15% P_1	6% P_1

σ	**Destructive Test (Creep Load: P_2)**						
	1	2	3	4	5	6	7
1	15% P_2	10% P_2	7% P_2	5% P_2	2.5% P_2	1.5% P_2	1% P_2
2	25% P_2	15% P_2	12.5% P_2	8% P_2	7% P_2	3% P_2	2% P_2
3	35% P_2	20% P_2	15% P_2	12.5% P_2	10% P_2	6% P_2	4% P_2

After three trials, if the outcome is still not good enough, a regression method used by Teoh (1987) can be applied to avoid more trails. Specifically, for the step-load that does not produce a good outcome in the last trial, the corresponding residual strain rate is plotted against the value of each step, as shown in Figure 5.4. Then a regression model is fitted to the measured data: a linear regression model for two data points in the nondestructive test; a best-fit function for three data points in the destructive test. The intercept at which the strain rate is zero is taken to be the value of the internal stress.

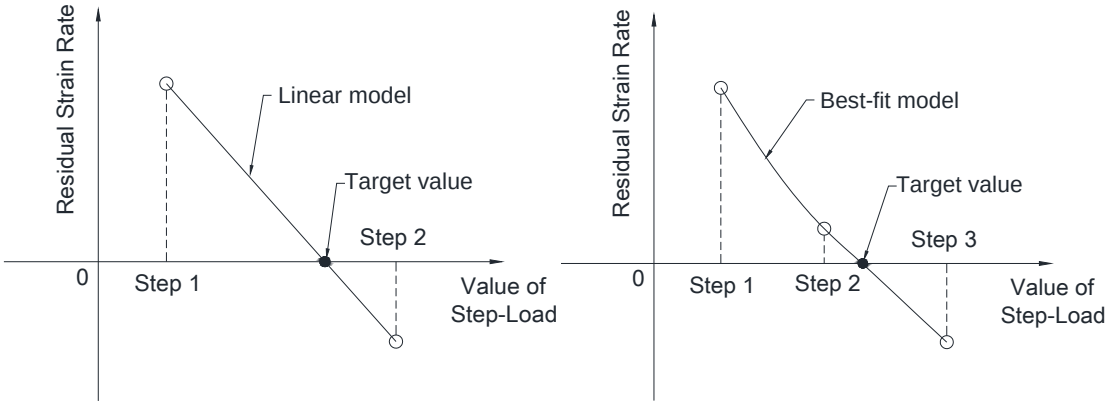

(a) Nondestructive Test **(b) Destructive Test**

Figure 5.4 Regression Method to Determine Internal Stress

5.3.2 Materials and Procedures

The CSR test designed above is applied to two types of laboratory mixed and laboratory compacted asphalt mixtures in this study. The two kinds of asphalt mixtures have the same aggregate and mixture design, but different types of asphalt binder. The two asphalt binders are from the Strategic Highway Research Program Materials Reference Library (Jones 1993), labeled AAD and AAM, respectively. The aggregate is a common Texas limestone shipped from a quarry in San Marcos, Texas. The optimum asphalt binder content is determined as 4.5% by weight of the mixture according to the Department of Transportation (TxDOT) Tex-204-F test procedure (TxDOT 2005). The aggregate gradation is a Type C gradation specified by TxDOT (TxDOT 2004). The Superpave gyratory compactor is used to compact asphalt mixtures into cylindrical specimens with 152 mm diameter and 178 mm height. Then specimens are cored and cut to a dimension of 102 mm in diameter by 150 mm in height recommended by the

Superpave models Team (1999). The target air void content of the trimmed 102 mm by 150 mm specimen is 4.0 with a tolerance of ±0.5%.

The CSR test is conducted using the Material Test System (MTS) at a temperature of 20°C. A series of consecutive creep recovery tests and CSR tests are performed on the same asphalt mixture specimen:

1) A nondestructive creep recovery test and a nondestructive CSR test at the same loading level 1;
2) A nondestructive creep recovery test and a nondestructive CSR test at the same loading level 2;
3) A nondestructive creep recovery test and a nondestructive CSR test at the same loading level 3 (loading levels 1, 2, and 3 are in an increased order);
4) A destructive CSR test under a constant destructive load.

There is a 15 min rest period between two consecutive tests in order to recover any possible deformation in an undamaged asphalt mixture specimen. The nondestructive creep recovery test is performed before each nondestructive CSR test to examine the effect of interruption by the step-loads on the recovery of the specimen. The creep recovery test has the same loading duration (40 sec) and recovery time (150 sec) as the CSR test. The nondestructive CSR tests are performed to obtain the creep and recovery properties of undamaged asphalt mixtures. They are conducted at different loading levels to examine whether the recovery properties of an undamaged asphalt mixture are dependent on the loading level. The recovery properties of a damaged asphalt mixture are measured by the destructive test, which are compared to those measured by the

nondestructive tests to investigate if any change occurs and identify the reason for the change.

To ensure that the test is nondestructive, the maximum strain at the end of the creep phase is controlled below 80 με. The first nondestructive test is conducted at very low loading level to avoid excessive deformation. Then the loading level is adjusted and increased by a small amount for the subsequent tests. For asphalt mixtures with the binder AAD, the loading level identified for the three nondestructive test is 89N (20 lbf), 133 N (30 lbf) and 178 N (40 lbf), respectively. For asphalt mixtures with AAM, the load of three nondestructive test is 267 N (60 lbf), 356 N (80 lbf), and 534 N (120 lbf), respectively. In the destructive test, the maximum strain at the end of the creep phase of the destructive test is controlled above 200 με to introduce significant damage to the test specimen. The identified destructive load for both the AAD and AAM mixtures is 890 N (200 lbf) and 1780 N (400 lbf), respectively.

To further prove the selected nondestructive loading levels are truly nondestructive, the creep compliance measured at each loading level for each asphalt mixture specimen is assessed, which is calculated by:

$$D(t) = \frac{\varepsilon_c(t)}{\sigma_0} \tag{5.5}$$

where $D(t)$ is the creep compliance; $\varepsilon_c(t)$ is the creep strain in the creep phase; and σ_0 is the creep stress. A plot of $D(t)$ versus time at three nondestructive loading levels is shown in Figure 5.5. For both AAD and AAM asphalt mixtures, the creep compliance

does not change as the loading level changes, so the nondestructive tests are truly nondestructive and the measured material properties are those of an undamaged asphalt mixture specimen.

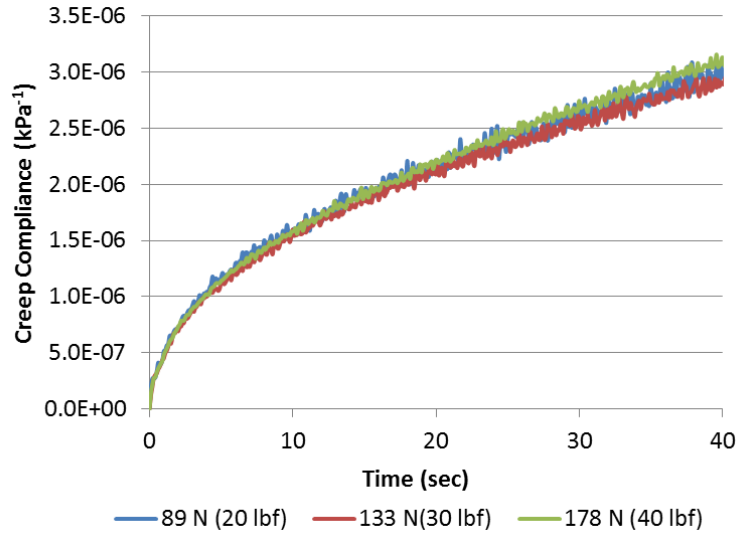

(a) AAD

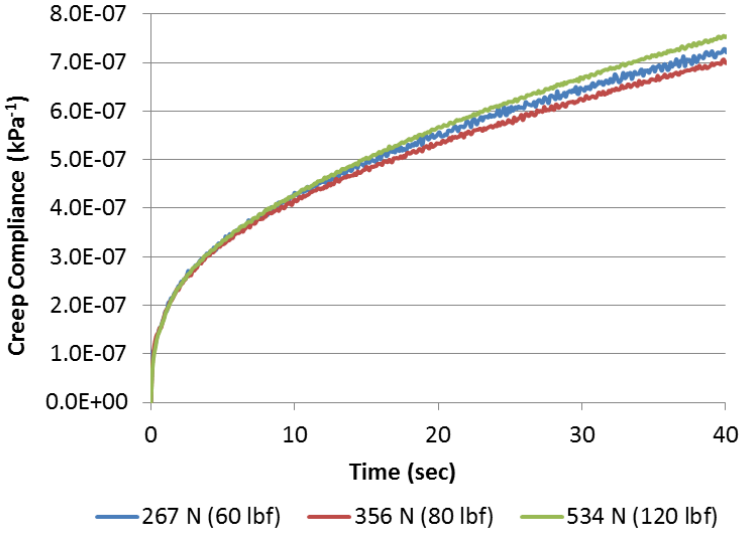

(b) AAM

Figure 5.5 Measured Creep Compliance in Nondestructive CSR Tests

A typical measurement by the nondestructive and destructive CSR tests is shown in Figures 5.6 and 5.7, respectively. Since this testing method to measure the internal stress is innovative for asphalt materials, accuracy of the test results needs to be verified, which is discussed in the next section.

5.4 Verification of Creep and Step-Loading Recovery Test

The CSR test is verified in two aspects: the effect of disturbance by the step-loads on the recovery of the asphalt mixture specimen; and the accuracy of the internal stress measured from the test.

5.4.1 Effect of Disturbance by Step-Loads

In the CSR test, incorporation of step-loads into the recovery phase causes interruption to the recovery of the asphalt mixture specimen. The effect of this disturbance should be examined to ensure that the influence is acceptable. Specifically, after introducing several step-loads, the material response of the specimen can still reflect the actual recovery of the specimen before adding the step-loads. This examination is conducted by comparing the axial strain measured from a CSR test to that measured from a creep recovery test at the same loading level shown in Figure 5.8. The result demonstrates that the axial strain from the CSR test matches well with that from the creep recovery test in the creep phase and in the recovery phase after five step-loads. Even under the step-loads, the difference between two strain curves is not significant. As a result, the effect of disturbance caused by adding step-loads is acceptable, and the material response provided by this test can be used to characterize the recovery property.

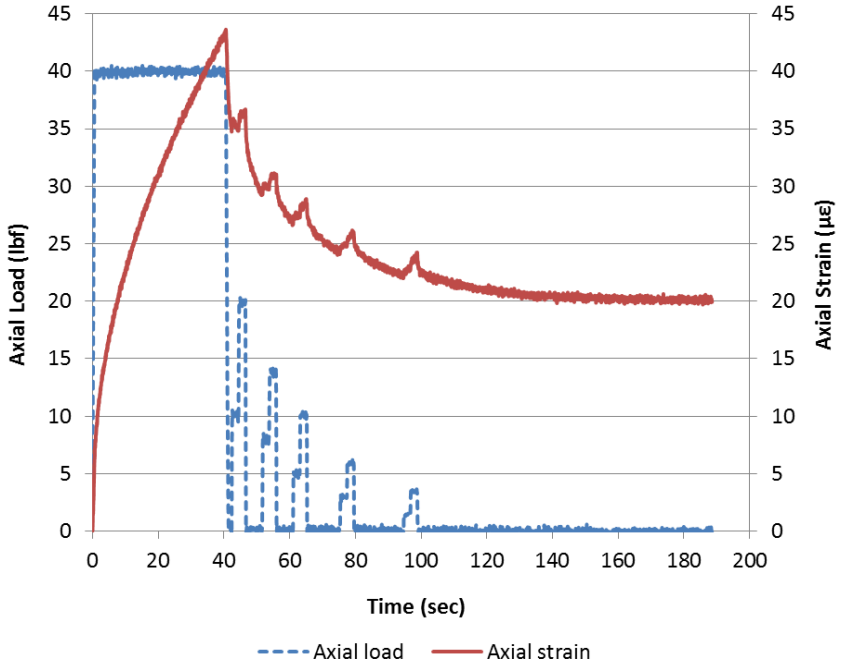

Figure 5.6 Axial Load and Axial Stain versus Time in Nondestructive CSR Test

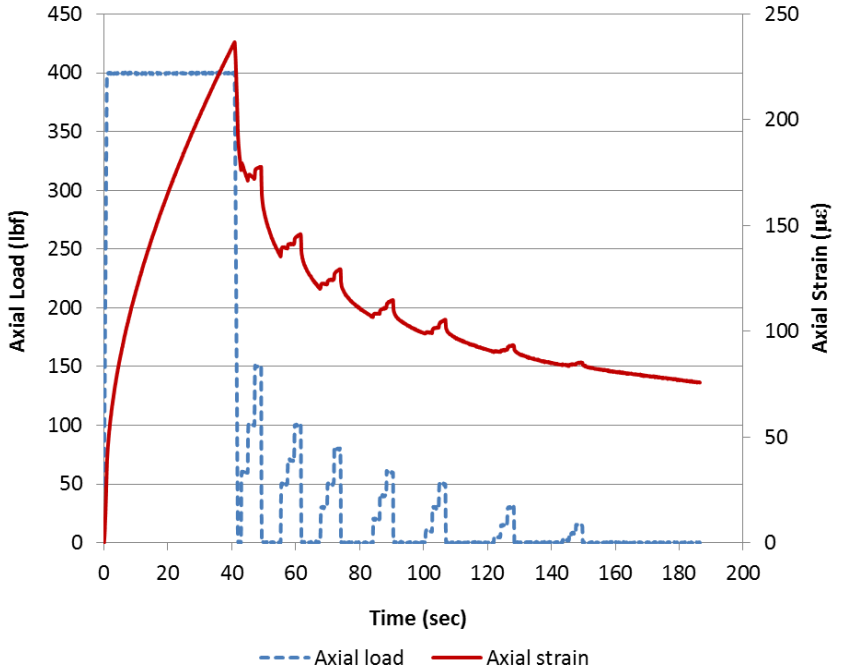

Figure 5.7 Axial Load and Axial Stain versus Time in Destructive CSR Test

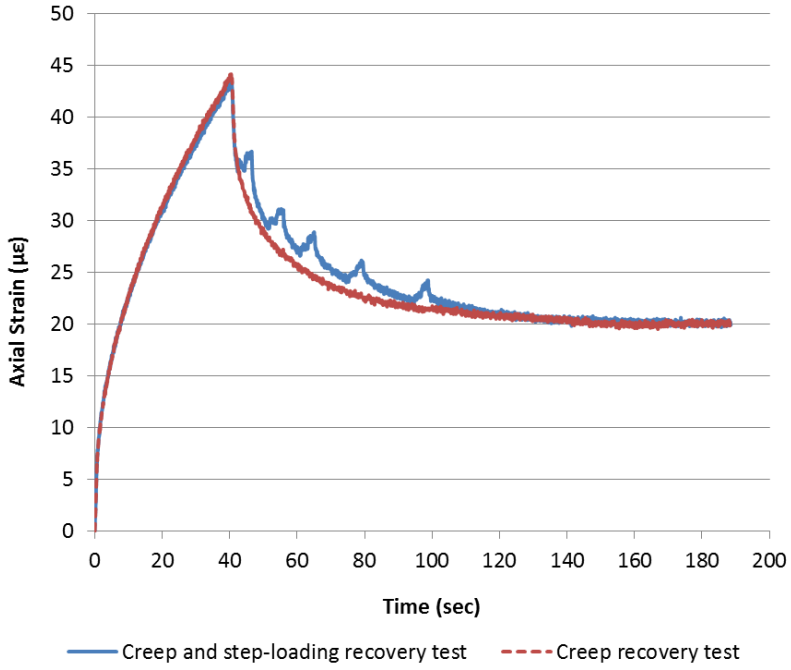

Figure 5.8 Measured Axial Strain from Creep Recovery Test and CSR Test

5.4.2 Accuracy of Measured Internal Stress

The accuracy of the internal stress obtained from the CSR test should be examined to prove the validity the test. The verification is conducted by comparing the measured internal stresses to those calculated by the theory of viscoelasticity for undamaged asphalt mixtures (defined as theoretical internal stress). The calculation of theoretical internal stress is first introduced as follows.

Figure 5.9 illustrates a nondestructive CSR test that is used to calculate the theoretical internal stress. The one step of loading between $[t_1, t_2]$ produces zero residual strain rate, which is used to represent any step in a step-load that gives the internal stress at that measured point. For example, if σ_{21} in the second step-load and σ_{42} in the fourth

step-load in Figure 5.3(a) are equal to the corresponding internal stress, σ_k in Figure 5.9 can represent either σ_{21} or σ_{42}. In order to calculate σ_k, the expression of the residual strain needs to be determined first.

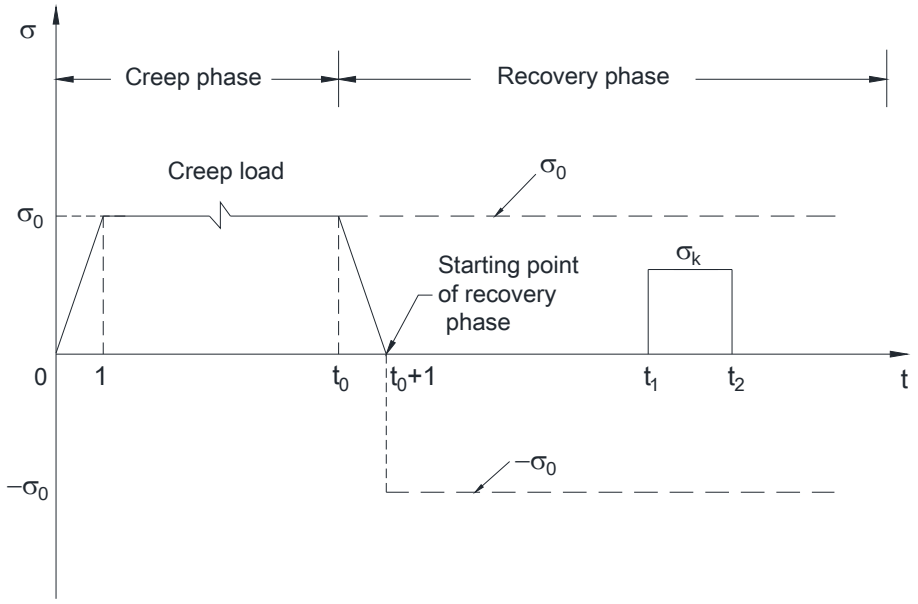

Figure 5.9 Calculation of Theoretical Internal Stress in Nondestructive CSR Test

According to the Boltzmann superposition principle (Findley et al. 1989), the residual strain between $[t_1, t_2]$ can be considered as the output due to the combination of three different stresses: a positive stress σ_0 (creep stress), a negative stress $-\sigma_0$, and a positive stress σ_k, as shown in Figure 5.9. Each stress produces one strain component for the residual strain. Therefore, the residual strain between $[t_1, t_2]$ can be expressed in the following way:

$$\varepsilon_r = \varepsilon_{r1} + \varepsilon_{r2} + \varepsilon_{r3} \tag{5.6}$$

where ε_r is the residual strain; ε_{r1} is the residual strain component corresponding to σ_0; ε_{r2} is the residual strain component corresponding to $-\sigma_0$; and ε_{r3} is the residual strain component corresponding to σ_k. These three residual strain components are calculated based on the stress-strain relationship in the theory of viscoelasticity, which is given in Equation 5.7:

$$\varepsilon(t) = \int_0^t D(t-\xi)\frac{d\sigma(\xi)}{d\xi}d\xi \tag{5.7}$$

where $\sigma(t)$ is an arbitrary stress history; $\varepsilon(t)$ is the strain corresponding to this stress; ξ is any arbitrary time between 0 and t; and $D(t)$ is the creep compliance of an undamaged asphalt mixture. Substitute $\sigma(t) = \sigma_0$ into Equation 5.7 and integrate it from 0 to t, giving:

$$\varepsilon_{r1} = \sigma_0 D(t) \tag{5.8}$$

Substitute $\sigma(t) = -\sigma_0$ into Equation 5.7 and integrate it from $t_0 + 1$ to t to obtain:

$$\varepsilon_{r2} = -\sigma_0 D\left[t - (t_0 + 1)\right] \tag{5.9}$$

Substitute $\sigma(t) = \sigma_k$ into Equation 5.7 and integrate it from t_1 to t to obtain the expression of ε_{r3} as:

$$\varepsilon_{r3} = \sigma_k D(t - t_1) \tag{5.10}$$

Therefore, ε_r in the period of $[t_1, t_2]$ is calculated by substituting Equations 5.8, 5.9, and 5.10 into Equation 5.6:

$$\varepsilon_r = \sigma_0 D(t) - \sigma_0 D\left[t - (t_0 + 1)\right] + \sigma_k D(t - t_1) \tag{5.11}$$

Then the residual strain rate is obtained by Equation 5.11 as:

$$\dot{\varepsilon}_r = \sigma_0 \dot{D}(t) - \sigma_0 \dot{D}\left[t - (t_0 + 1)\right] + \sigma_k \dot{D}(t - t_1) \tag{5.12}$$

Let $\dot{\varepsilon}_r = 0$, and then solve for σ_k from Equation 5.12, which gives:

$$\sigma_k = \frac{\sigma_0 \dot{D}\left[t - (t_0 + 1)\right] - \sigma_0 \dot{D}(t)}{\dot{D}(t - t_1)} \tag{5.13}$$

Given σ_0, $D(t)$, t_0, and t_1, the value of σ_k can be obtained by Equation 5.13. This value is the theoretical internal stress that is calculated for an undamaged asphalt mixture. Equation 5.13 is only applicable for undamaged asphalt mixtures due to the availability of $D(t)$. To calculate σ_k by Equation 5.13, $D(t)$ must be determined for the period of $[t_0 + 1, t_2]$ in Figure 5.9. However, the creep compliance calculated by Equation 5.5 is limited for $t \in [0, t_0 + 1]$. To obtain $D(t)$ in the recovery phase, it must use an appropriate model to simulate $D(t)$ and extrapolate it beyond the measurement.

In general, there are two types of model available to simulate the creep compliance for an asphalt mixture. One is an exponential function that is based on the mechanical analog for a viscoelastic material. The mechanical response of a viscoelastic material can be interpreted according to a mechanical analog, which is composed of springs (representing perfectly elastic solids) and dashpot (representing perfectly viscous fluid). Based on this analog, an exponential function can be formulated as follows:

$$D(t) = D_0 + D_1\left(1 - e^{-\frac{t}{\tau}}\right) \tag{5.14}$$

where D_0 is instantaneous creep compliance; D_1 is creep compliance coefficient; and τ is retardation time. The other model is based on the shape of the curve $D(t)$ versus time shown in Figure 5, which is a power function as follows:

$$D(t) = at^b + c \tag{5.15}$$

where a, b, and c are fitting coefficients. The creep compliance of an undamaged asphalt mixture modeled by Equations 5.14 and 5.15 is plotted in Figure 5.10, as well as the measured creep compliance. Both functions show goodness of fitting, but the power function fits better than the exponential function at the beginning of the creep phase (about first 5 sec). The initial goodness of fitting is important for calculating σ_k by Equation 5.13, so the power function is used to calculate the internal stress. Substitute Equation 5.15 into Equation 5.13, which gives

$$\sigma_k = \frac{\sigma_0\left[t - (t_0 + 1)\right]^{b-1} - \sigma_0 t^{b-1}}{(t - t_1)^{b-1}} \tag{5.16}$$

Based on Equation 5.16, the theoretical internal stress of an undamaged asphalt mixture is calculated from the measurement by a nondestructive CSR test. Figures 5.11 and 5.12 present both the measured and theoretical internal stresses at five measurement points in the nondestructive CSR test for AAD and AAM asphalt mixture specimens, respectively. The measured values match well with the theoretical values, which indicates the accuracy of the internal stress obtained from the CSR test and thus prove

the validity of this test. Note that this verification method is only suitable for a nondestructive CSR test because only the creep compliance of undamaged asphalt mixtures can be extrapolated beyond the measurement using a mathematical model. The creep compliance of a damaged asphalt mixture is not obtainable beyond the creep phase, i.e. $[t_0+1, t_2]$ in Figure 5.9. Consequently, a destructive CSR test is essential to measure the internal stress for damaged asphalt mixtures. Simulation of the measured internal stress and determination of the recovery properties for both undamaged and damaged asphalt mixtures are discussed in the next section.

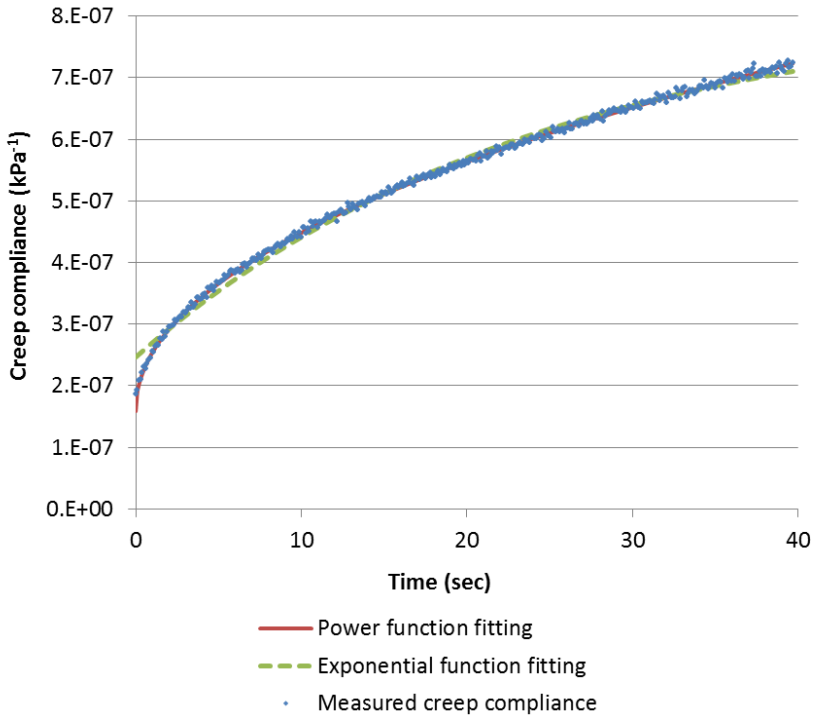

Figure 5.10 Simulation of Creep Compliance for Undamaged Asphalt Mixtures

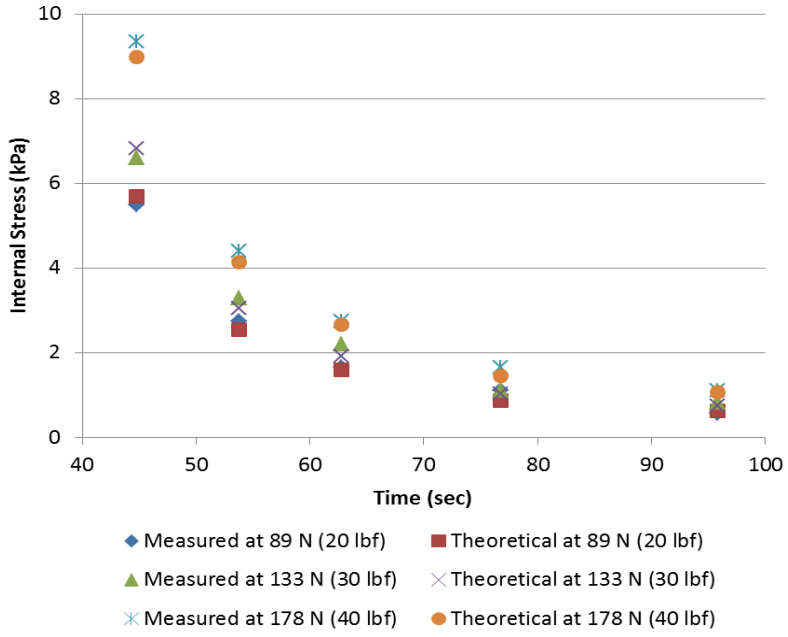

Figure 5.11 Measured and Theoretical Internal stresses of AAD Asphalt Mixtures in Nondestructive CSR Test

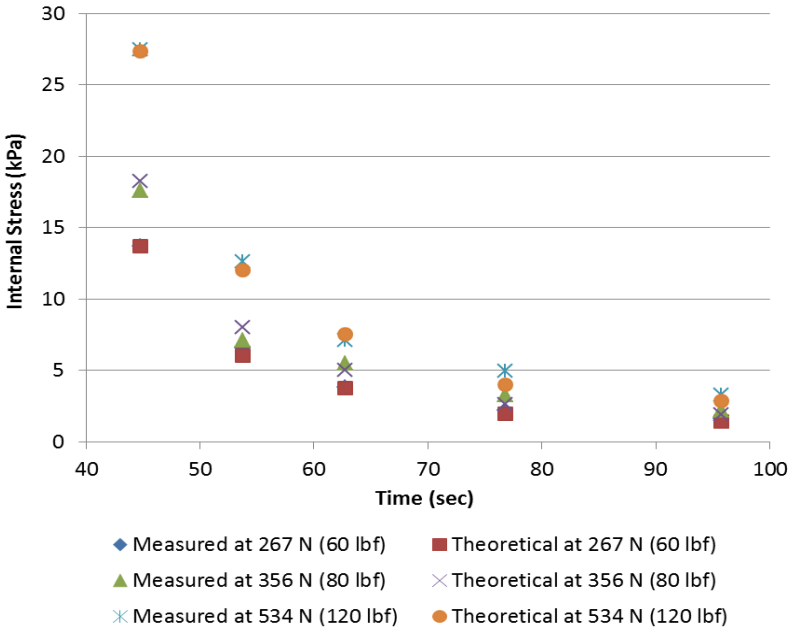

Figure 5.12 Measured and Theoretical Internal stresses of AAM Asphalt Mixtures in Nondestructive CSR Test

5.5 Simulation of Internal Stress and Determination of Recovery Properties

Section 5.4 first discusses the rationale of selecting an appropriate model to simulate the internal stress; then the simulated internal stress is used to determine the recovery properties of asphalt mixtures.

5.5.1 Simulation of Internal Stress

The internal stress measured from the nondestructive and destructive CSR tests are a series of points in the recovery phase, for example as shown in Figures 5.11 and 5.12. To obtain a continuous curve of the internal stress versus time, an appropriate model is required to fit these discrete points. Selecting such a model is conducted using the software MATLAB by trying different mathematical functions incorporated in the MATLAB. It is found that two kinds of functions show high goodness of fitting. One is an exponential function as shown in Equation 5.17:

$$\sigma_i(t) = \sigma_a e^{-\frac{t}{\eta_1}} + \sigma_b e^{-\frac{t}{\eta_2}} \tag{5.17}$$

where $\sigma_i(t)$ is the internal stress; t is the recovery time, $t \in [t_0 + 1, \infty]$; σ_a, σ_b, η_1, and η_2 are fitting parameters. The other function is in the form of power law:

$$\sigma_i(t) = dt^f + g \tag{5.18}$$

where d, f, and g are fitting parameters; and $t \in [t_0 + 1, \infty]$. The R squared statistic of both functions is above 0.99, which indicates that these two models are suitable to simulate the internal stress within the measure range. Beyond the measure range, the suitability of the model also needs to be assessed so that it can be used to predict the internal stress in a wider range.

The suitability of the two models beyond the measured range is examined by comparing the fitted value to the theoretical value that is calculated by Equation 5.16. A plot of measured internal stress, the fitted internal stress by Equation 5.17, the fitted internal stress by Equation 5.18, and the theoretical internal stress in the nondestructive CSR test is shown in Figures 5.13 and 5.14 for AAD and AAM asphalt mixture specimens, respectively. Four kinds of internal stress match well with each other within the measure range, from 40 sec to approximately 100 sec, as mentioned above. However, the curve simulated by Equation 5.18 starts to deviate from the other two curves after 100 sec, while the curve simulated by Equation 5.17 still conforms to the theoretical value. After 120 sec, the curve simulated by Equation 5.17 is almost flat, while the other two curves remain decreasing. The tendency of continuous reduction of the internal stress reflects the actual recovery behavior of an undamaged asphalt mixture. The residual strain of the undamaged asphalt mixture specimen decreases with time and can completely recover given sufficient time. Therefore, the corresponding internal stress should continue diminishing and vanish eventually, as indicated by the curve simulated by Equation 5.17 and the theoretical value.

Based on the investigation both within and beyond the measured range, the exponential function shown in Equation 5.17 is the best model to simulate the internal stress. The modeled internal stresses for damaged asphalt mixtures in destructive CSR tests are plotted in Figure 5.15.

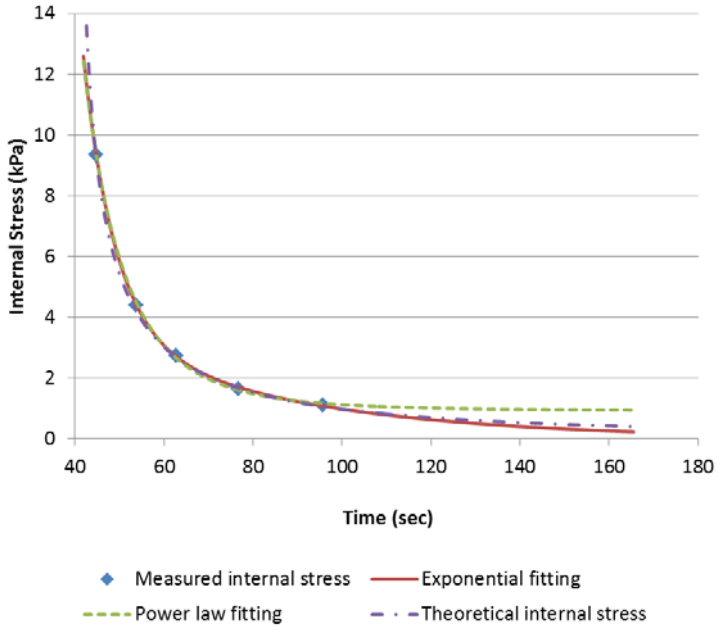

Figure 5.13 Simulation of Internal Stress of AAD Asphalt Mixtures in Nondestructive CSR Test

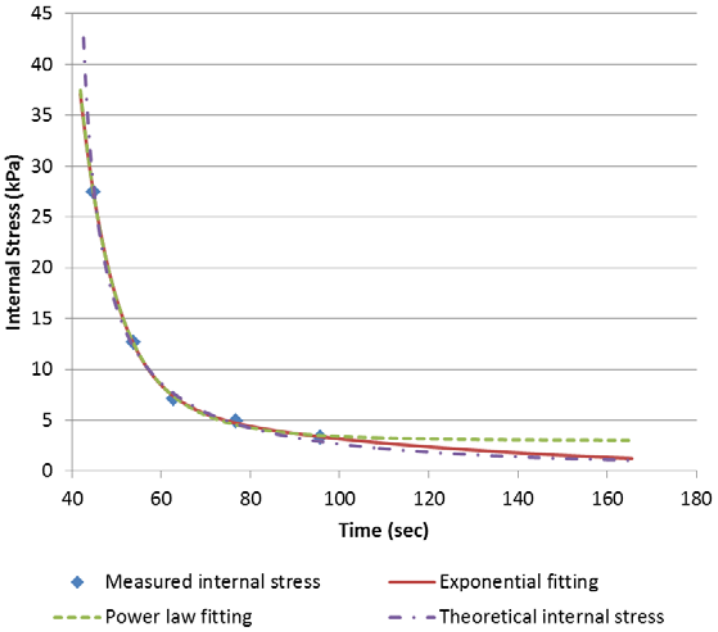

Figure 5.14 Simulation of Internal Stress of AAM Asphalt Mixtures in Nondestructive CSR Test

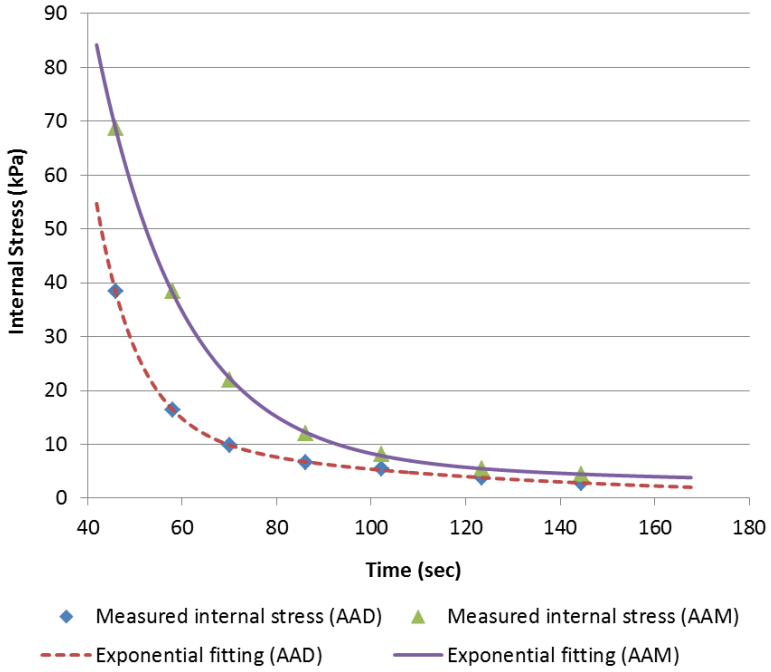

Figure 5.15 Simulation of Internal Stress of Damaged Asphalt Mixtures in Destructive CSR Test

5.5.2 Determination of Recovery Properties

Since the internal stress is obtained as the driven force in the recovery phase, it is used with the residual strain to define a new type of modulus: recovery modulus, which is a material property that describes the recovery behavior of asphalt mixtures. The recovery modulus is defined as the ratio of the internal stress to the residual strain as follows:

$$R(t) = \frac{\sigma_i(t)}{\varepsilon_r(t)} \tag{5.19}$$

in which $\sigma_i(t)$ is the internal stress calculated by Equation 5.17; and $\varepsilon_r(t)$ is the residual strain in the recovery phase, which is simulated by the following function:

$$\varepsilon_t(t) = \varepsilon_{0,r} + \varepsilon_{1,r} e^{-\frac{t}{\gamma_r}} \tag{5.20}$$

in which $t \in [t_0 + 1, \infty]$; $\varepsilon_{0,r}$, $\varepsilon_{1,r}$, and γ_r are fitting parameters for the residual strain. The recovery modulus is calculated for all three nondestructive CSR tests and one destructive CSR test, which are shown in Figure 5.16 for the AAD mixtures and in Figure 5.17 for AAM mixtures. Both figures suggest that the recovery modulus in the nondestructive test does not change as the loading levels increase. This fact indicates that the recovery of undamaged asphalt mixtures only depends on the material itself. Another observation from these two figures is that the recovery modulus in the nondestructive test is different from that in the destructive test. This fact is explained by the occurrence of healing of the damaged asphalt mixture specimen in the recovery phase of the destructive CSR test. Furthermore, it can be seen that the shape of the recovery modulus curve under the destructive loading level in Figure 5.16 is different from that in Figure 5.17. This phenomenon is probably due to the different healing ability of AAD and AAM asphalt binders.

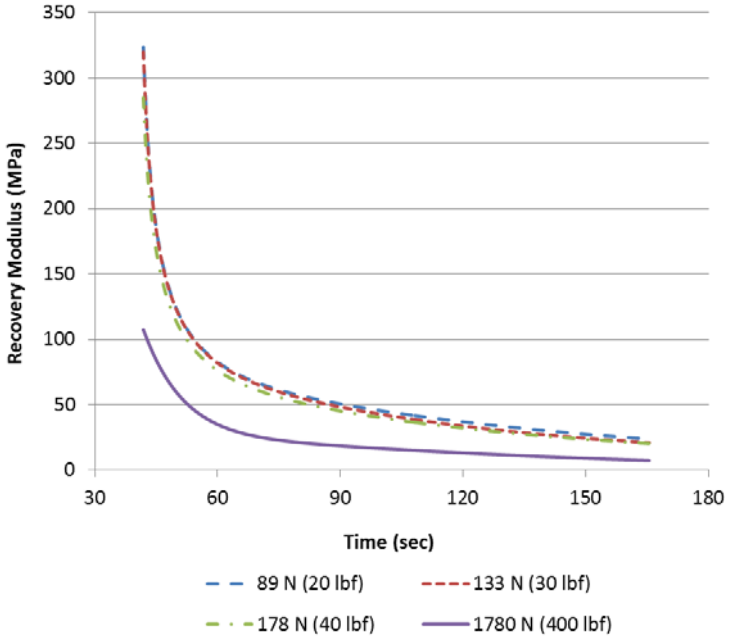

Figure 5.16 Recovery Modulus of AAD Asphalt Mixtures in Nondestructive and Destructive CSR Test

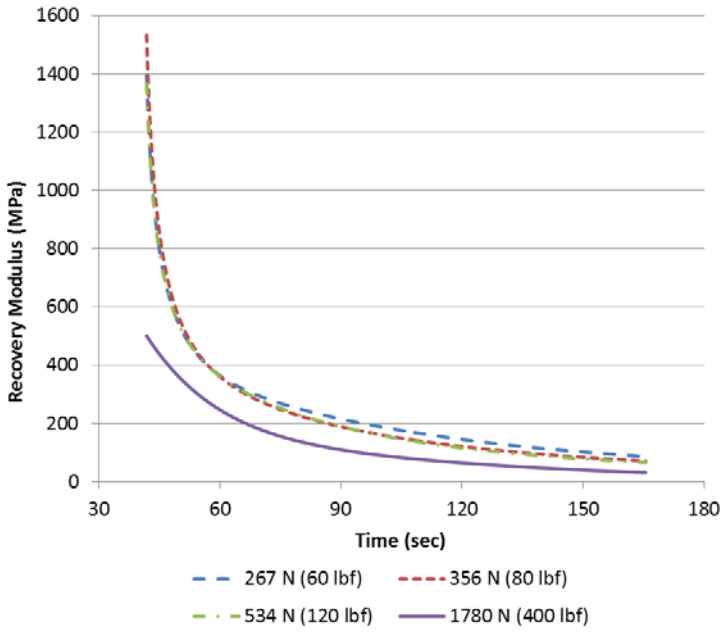

Figure 5.17 Recovery Modulus of AAM Asphalt Mixtures in Nondestructive and Destructive CSR Test

6. CHARACTERIZATION OF HEALING OF ASPHALT MIXTURES

6.1 Theoretical Background of Healing

In Section 6, a comprehensive literature review on the mechanism of healing is first presented; then a new perspective to study the healing in asphalt mixtures is proposed from a mechanistic viewpoint.

6.1.1 Literature Review on Mechanism of Healing

Extensive studies of healing have been carried out in the field of polymer science. A comprehensive review on this subject is given in Kausch et al. (1987) with eighty references. One of these theories that is applied to asphalt materials is Wool and O'Connor's theory (Wool and O'Connor 1981), which states that healing is combination of two processes: wetting of two crack surfaces ("wetting") and an increase of the joint strength of the two crack surfaces. "Wetting" is a process in which contact and adhesion are established between two crack surfaces. Increase of the joint strength of the two crack surfaces that are in complete contact is a process in which strength is developed through molecular interchange across the interface and random entanglement formation. It is a diffusion process characterized by molecular motion. Wool and O'Connor proposed a convolution integral function to describe the healing process:

$$R = \int_{\tau=-\infty}^{\tau=t} R_h\left(t-\tau\right)\frac{d\phi\left(\tau, X\right)}{d\tau}d\tau \tag{6.1}$$

where R is the healing that contains both the wetting and the joint-strength processes; $\phi\left(\tau, X\right)$ is the wetting distribution function controlled by the wetting process; and

$R_h\left(t-\tau\right)$ is the intrinsic healing function that defines the rate of the joint-strength process. Bhasin et al. (2008) employed Equation 6.1 to model the healing of asphalt materials. The wetting process of asphalt materials is represented by $\phi(\tau, X)$, of which the formulation is based on Schapery's crack closing and bonding theory (Schapery 1989). The joint-strength process is represented by $R_h(t-\tau)$, which has a similar formulation suggested by Wool and O'Connor (1981). The value of $R_h\left(t-\tau\right)$ is determined by testing asphalt binders using the dynamic shear rheometer (DSR).

Studies pertaining to the wetting process in damaged materials can be traced to the work of so-called autohesion in the 1960s (Anand and Karam 1969; Anand and Balwinski 1969; Anand and Dipzinski 1970; Anand 1969, 1970). Autohesion refers to self-adhesion of two surfaces of the same material: the two surfaces are gradually closed and the contact area between them increases correspondingly. The growth of the contact area of two surfaces is predicted by applying an external compressive force. However, there should be no external load during the closure of the two surfaces, of which the driven force is provided by the material itself. Schapery (1989) introduced the concept of the interfacial force of attraction, which acts on the adjacent separated crack surfaces and tends to draw the surfaces together until complete contact exists. He conducted rigorous mechanistic analysis of the wetting process of one crack using the interfacial force of attraction for viscoelastic materials. The stress calculated by the interfacial force of attraction is defined as the bonding stress. The two separated crack surfaces gradually close by the action of the bonding stress to produce surface-to-surface contact. The

length of the crack surfaces over which contact occurs is defined as the bonding zone length. The rate of the growth of the contact area is defined as the bonding speed. The bonding zone length and bonding speed are predicted from the analysis of the bonding stress and the resulting movement of the surfaces during the wetting process. The expressions of the bonding zone length and bonding speed are derived for a linear viscoelastic material. This result is extended by Baney and Hui (1999) for a standard linear solid. Although Schapery's analysis gives a theoretical solution for the closure of two crack surfaces, it is not suitable for the wetting process of a damaged asphalt mixture. There are numerous cracks closing in the wetting of the asphalt mixture, whereas Schapery's analysis only focuses on the closure of one crack. In addition to the interfacial force of attraction which draws the two surfaces together, as is considered in Schapery's theory, the two crack surfaces are also driven together by the internal stress.

Once the crack surfaces are brought into contact in the wetting process, an immediate adhesion arises from the effect of the change of the surface work due to the action of the bonding stress. If the bonding stress is the only stress that drives the closure of a crack, the strength achieved by the wetting process is of the order of the surface energy, which is very low and not the full strength of the material. Some of the literature also claim low strength achievement in the wetting process; the full strength is gained in the joint-strength process following the wetting process, which controls the buildup of mechanical strength and mechanical properties of the material (Jut et al. 1981; Wool and O'Connor 1981). However, according to the principle of fracture mechanics, the surface energy alone does not constitute the strength of the material, which, in fact, varies as the

square root of the product of the modulus and the surface energy and is much larger than the surface energy. In other words, the immediate attainment of strength by the wetting process is underestimated by stating that the strength achieved in the process is of the order of the surface energy. A solid laboratory evidence to prove the high strength attainment in the wetting process is provided in Section 1. In a nondestructive controlled-strain RDT test, the material properties variation in a loading cycle is due to the crack opening (crack growth) and crack closure ("wetting") in this loading cycle. However, the material properties do not change from the first loading cycle to subsequent cycles. This fact indicates that strength change due to the crack growth in a loading cycle is completely offset by the "wetting" of cracks in the same cycle. The attainment of strength in the wetting process is thus the full strength of the mixture.

Review of the literature above demonstrates the importance of the wetting process: its contribution to the healing of an asphalt mixture is significant and needs to be accurately characterized. Since the wetting process can produce the full strength of the asphalt mixture, there should be other forces that drive this process besides the bonding stress for the closure of the crack. To address these problems, the wetting process of a damaged asphalt mixture is studied as follows.

6.1.2 Healing and Recovery of Asphalt Mixtures

Healing occurs after removing the external load on a damaged asphalt mixture so it always accompanies the recovery of the material. Recovery of asphalt mixtures occurs at any loading level after removing the load, but healing only occurs after cracking damage is generated in the material. More specifically, when the asphalt mixture is not

damaged, there is only a recovery process in which the material recovers its deformation. When the asphalt mixture is damaged, there are a recovery process and a healing process in the material. “Healing” here refers to the wetting process.

Recovery of both undamaged and damaged asphalt mixtures has been studied using a creep and step-loading recovery (CSR) test in Section 5. The recovery process is driven by the internal stress in the asphalt mixture, which is measured in the recovery phase of a CSR test. The relationship between the internal stress and the corresponding strain in the recovery process is described by the recovery modulus (Equation 5.19). It is proven that the recovery modulus does not change in undamaged asphalt mixtures at different loading levels as long as the load is nondestructive. This fact is explained as the recovery is due to rearrangement of molecules so it only depends on the intact material in an asphalt mixture specimen. However, the recovery modulus becomes different when the asphalt mixture is damaged. This difference is caused by the healing of the cracks. At this time, there are two processes in the recovery of the bulk asphalt mixture specimen: the recovery of the intact material and healing (or closure) of the cracks.

Recovery of the bulk specimen under a destructive loading is what is observed in a destructive CSR test. It is an apparent description of what actually happens inside the specimen, which is defined as apparent recovery. The measured internal stress is thus defined as apparent internal stress. The apparent internal stress is assumed to be uniformly on the entire cross section of the specimen. However, the internal stress can only act on the intact material to drive the recovery of the intact material. Therefore, the internal stress carried by the intact material is defined as the true internal stress, and the

recovery of the intact material is defined as the true recovery. An illustration of the apparent and true internal stresses is given in Figure 6.1. The apparent internal stress, denoted σ_i^{A+} and σ_i^{A-}, is uniformly distributed over the Plane A, while the true internal stress, denoted σ_i^{T+} and σ_i^{T-}, is distributed on Plane B excluding the cracked area.

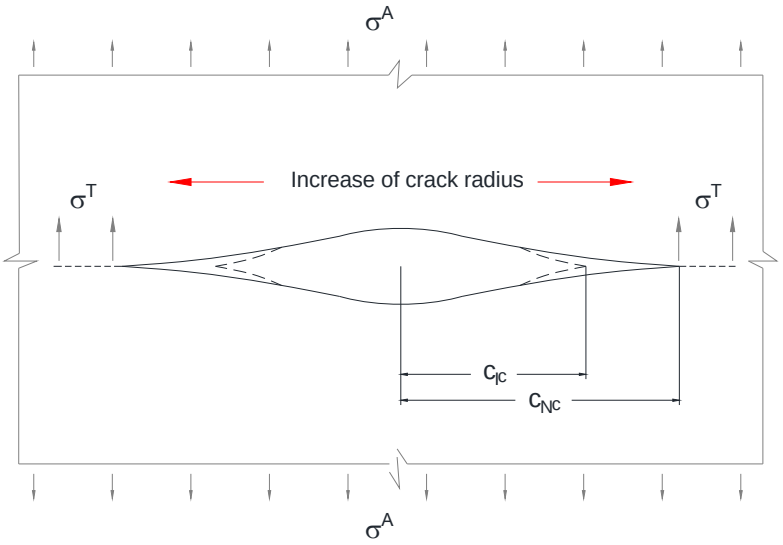

(a) Crack growth

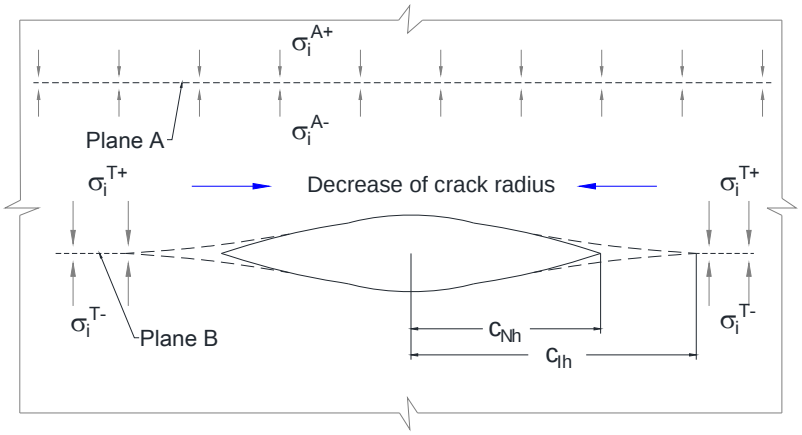

(b) Crack Closure

Figure 6.1 Illustration of Apparent Stress and True Stress for Damaged Asphalt Mixtures

The true internal stress is the driving force for the true recovery of the asphalt mixture. The driving forces for the healing of the cracks, as mentioned above, include the bonding stress obtained from the interfacial force of attraction. Other forces driving the healing process are examined by the energy redistribution around the crack caused by the action of the forces associated with this process. Since healing is a process counter to cracking, the energy redistribution in the healing process is counter to that in the cracking process. The energy redistribution in the cracking process of an asphalt mixture is elaborated in Section 5. In brief, the energy redistribution around the crack as a result of crack propagation involves the recoverable pseudo strain energy (RPSE) released in the intact material above and below the crack in the region labeled "3" in Figure 6.2, and the RPSE restored as surface energy on the newly created crack surfaces labeled "4" in Figure 6.2. Therefore, the RPSE redistributed around the crack as a result of healing should be the RPSE restored in the intact material above and below the crack and the RPSE released from the closure of the crack surfaces. The RPSE released from closure of crack surfaces equals the surface energy, which is the work done by the interfacial force of attraction. The RPSE restored in the intact material above and below the crack is the work done by the true internal stress in the intact material. There are in fact two forces involved in the healing process: the interfacial force of attraction and the true internal stress, which are shown in Figure 6.3. Both of them contribute to the energy interchange and drive the growth of the contact area of the crack surfaces.

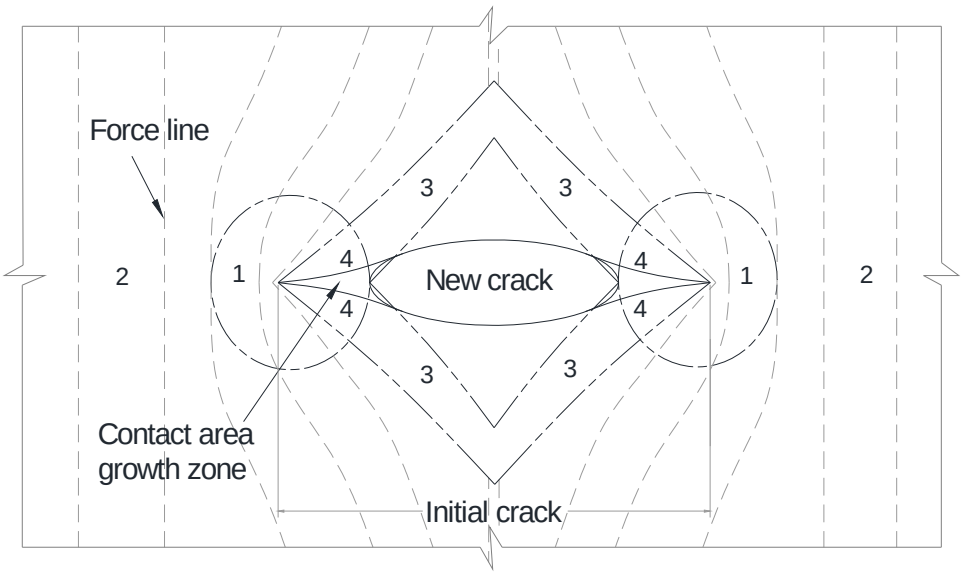

Figure 6.2 Energy Redistribution during Healing of Damaged Asphalt Mixtures

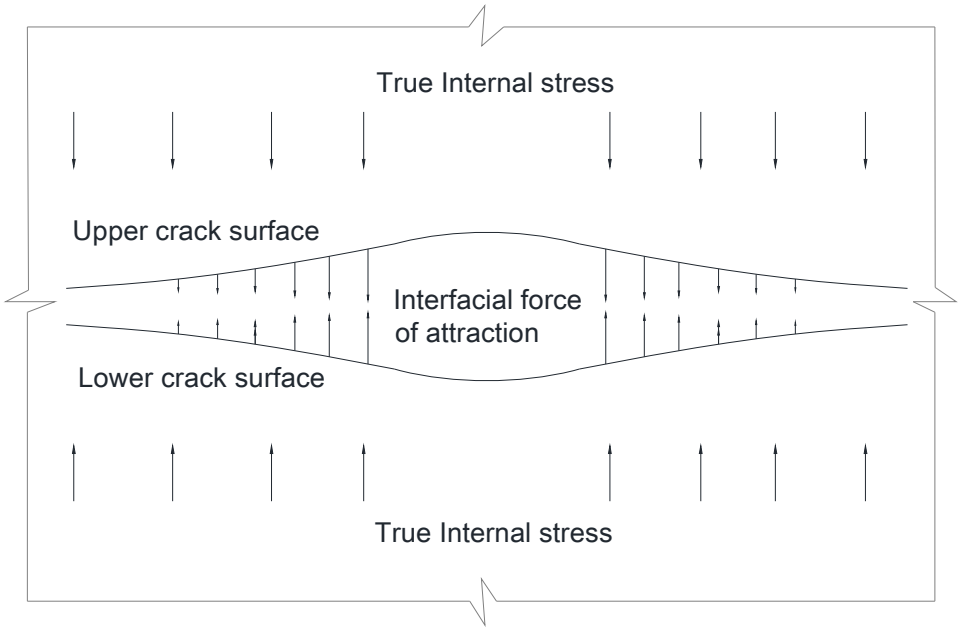

Figure 6.3 Driven Forces for Healing of Damaged Asphalt Mixtures

6.2 Laboratory Testing and Analysis Method

After determining the driven forces (causes) for the healing process, the next step is to determine the effect of these causes, which is the decrease of the average crack radius as a result of the growth of the contact area of the crack surfaces. In this way, healing is characterized by an essential cause and effect relationship. Decrease of the average crack radius is determined by measuring the apparent recovery of a damaged asphalt mixture specimen from a destructive CSR test and using an energy-based mechanistic approach to solve the true recovery and the healing of cracks. The configuration and procedure of the CSR tests was elaborated in Section 5. In order to characterize healing properties based on the measurements of these CSR tests, the test data is analyzed using an energy-based mechanistic approach.

The energy-based mechanistic approach is developed to characterize the fatigue damage and model crack growth in Sections 2 and 3. It is based on the difference between the apparent measurement from the test and the true circumstance inside the test specimen. The true stress/energy is related to the apparent stress/energy based on the principle of force equilibrium and the principle of energy balance, respectively.

The principle of force equilibrium states that the true force carried by the intact material equals the apparent force assumed to be carried by the entire cross section of the specimen. According to this principle, force equilibrium equations are constructed between the true stress and the apparent stress.

The principle of energy balance states that any kind of true energy within the intact material equals its counterpart from the apparent measurement. This is because

only the intact material can store, release and dissipate energy while cracks cannot. Consequently, the true energy within the intact material must equal the apparent energy within the entire specimen, including the intact material and cracks. According to this principle, energy balance equations are formulated between the true energy and the apparent energy.

These two principles are also suitable for the creep phase of the destructive CSR test, in which there is creep crack growth as shown in Figure 6.1(a). The asphalt mixture specimen is subjected to a tensile loading, represented by σ^A. After crack propagation, the crack radius increases from the initial crack size c_{Ic} to the new crack size c_{Nc}. During this process, energy is dissipated due to the viscoelastic effect of the asphalt mixture and the damage generated in the material (DSE). If replacing strain with pseudo strain to eliminate the viscoelastic effect from the DSE, the remaining energy represents the energy expended for the damage generated in the asphalt mixture (DPSE). The force equilibrium equation and the energy balance equations are presented as follows:

- Force equilibrium:

$$\sigma^A A = \sigma^T \left(A - S_c \right) \tag{6.2}$$

where σ^A is the apparent stress, which is calculated by the creep load in the CSR test divided by the cross sectional area; A is the cross sectional area; σ^T is the true stress, which is the stress in the intact material and equal to the creep load divided by the cross sectional area excluding the crack opening area; and S_c is the average area of all the cracks on the cross section.

- Energy balance:

$$\mathrm{DSE}^A = \mathrm{DSE}^T \tag{6.3}$$

$$\mathrm{DPSE}^A = \mathrm{DPSE}^T \tag{6.4}$$

where DSE^A and DSE^T are the apparent DSE and true DSE, respectively; DPSE^A and DPSE^T are the apparent DPSE and true DPSE, respectively.

When applying the principle of force equilibrium to the recovery phase of the destructive CSR test, the force equilibrium equations are slightly different. The apparent internal stress and true internal stress are self-balanced as shown in Figure 6.1(b). The superscripts "+" and "-" denote the stress above a plane and below a plane, respectively. The force equilibrium equations are expressed as:

$$\sigma_i^{A+} + \sigma_i^{A-} = 0 \tag{6.5}$$

$$\sigma_i^{T+} + \sigma_i^{T-} = 0 \tag{6.6}$$

The principle of energy balance is still applicable to the recovery phase of the destructive CSR test. During the recovery of the asphalt mixture specimen, the strain energy originally stored in the material recovers with time. This part of strain energy is RSE. The apparent RSE recovered by the bulk specimen is equal to the true RSE of the intact material, which is expressed as:

$$\mathrm{RSE}^A = \mathrm{RSE}^T \tag{6.7}$$

where RSE^A and RSE^T are the apparent RSE and true RSE, respectively. After removing the viscoelastic effect from the RSE using the pseudo strain, the remaining energy, or the RPSE, is the stored and recovered energy corresponding to the elastic

effect of the material. The apparent RPSE associated with the apparent recovery of the bulk specimen equals the true RPSE associated with the true recovery of the intact material and healing of the cracks, which has the energy redistribution as described above. It is expressed in the following equation:

$$\mathrm{RPSE}^{A}V_m = \mathrm{RPSE}^{T}V_m + \mathrm{RPSE}^{T}\left(\frac{2M_{Ih}\pi^2 {c_{Ih}}^3}{3} - \frac{2M_{Nh}\pi^2 {c_{Nh}}^3}{3}\right) - \gamma\left(2M_{Ih}\pi {c_{Ih}}^2 - 2M_{Nh}\pi {c_{Nh}}^2\right) \tag{6.8}$$

in which:

- RPSE^{A} is the apparent RPSE;
- V_m is the volume of the asphalt mastic in one layer of the asphalt mixture specimen;
- $+\mathrm{RPSE}^{T}\left(\frac{2M_{Ih}\pi^2 {c_{Ih}}^3}{3} - \frac{2M_{Nh}\pi^2 {c_{Nh}}^3}{3}\right)$ represents the energy restored in the intact material above and below the crack in the region labeled "3" in Figure 6.2; RPSE^{T} is the true RPSE; M_{Ih} is the number of initial cracks before healing; c_{Ih} is the average crack size of the initial crack before healing; M_{IhN} is the number of new cracks after healing; c_{Nh} is the average crack size of the new crack after healing;
- $-\gamma\left(2M_{Ih}\pi {c_{Ih}}^2 - 2M_{Nh}\pi {c_{Nh}}^2\right)$ represents the energy released from closure of crack surfaces labeled "4" in Figure 6.2; γ is the surface energy density (energy per unit of surface area).

The RPSE balance equation shown in Equation 6.8 quantifies healing in the damaged asphalt mixture using the recovery properties measured from the destructive CSR test. The initial damage at the beginning of the recovery phase when healing starts is represented by M_{Ih} and c_{Ih}, which is also the final damage at the end of the creep phase when cracking stops. The damage at any time during the recovery phase is represented by M_{Nh} and c_{Nh}. The change from the initial damage at the beginning of the recovery phase to the damage at any time during the recovery phase thus represents the extent of healing that occurs during that period. As a result, in order to obtain the extent of healing, the initial damage in the healing process must be determined first since it is the starting point based on which the change can be quantified. The initial damage in the healing process, or the final damage at the end of the creep phase, is obtained by determining the crack growth in the creep phase, which is presented in Section 6.3.

6.3 Determination of Crack Growth in the Creep Phase

The crack growth in the creep phase of a destructive CSR test is determined based on basic mechanistic equations as shown in Equations 6.2 to 6.4. To solve these equations and quantify the crack growth in the damaged asphalt mixture specimen, the mechanistic analysis is conducted on the data of both the nondestructive and destructive CSR tests. A detailed step by step procedure is given as follows.

Step 1. Determination of Apparent Creep Material Properties of Undamaged Asphalt Mixtures

The apparent creep material properties of undamaged asphalt mixtures are

obtained from the creep phase of the nondestructive CSR tests, which include apparent creep compliance and apparent relaxation modulus. The apparent creep compliance of the undamaged asphalt mixture is calculated as follows:

$$D(t) = \frac{\varepsilon_{cN}(t)}{\sigma_{cN}} \tag{6.9}$$

Where $D(t)$ is the apparent creep compliance of undamaged asphalt mixtures; t is the time in the creep phase, $t \in [0, t_0]$ as shown in Figure 6.4; $\varepsilon_{cN}(t)$ is the creep strain in the nondestructive test, the subscript "c" indicating "creep" and "N" indicating "nondestructive"; and σ_{cN} is the creep stress in the nondestructive test.

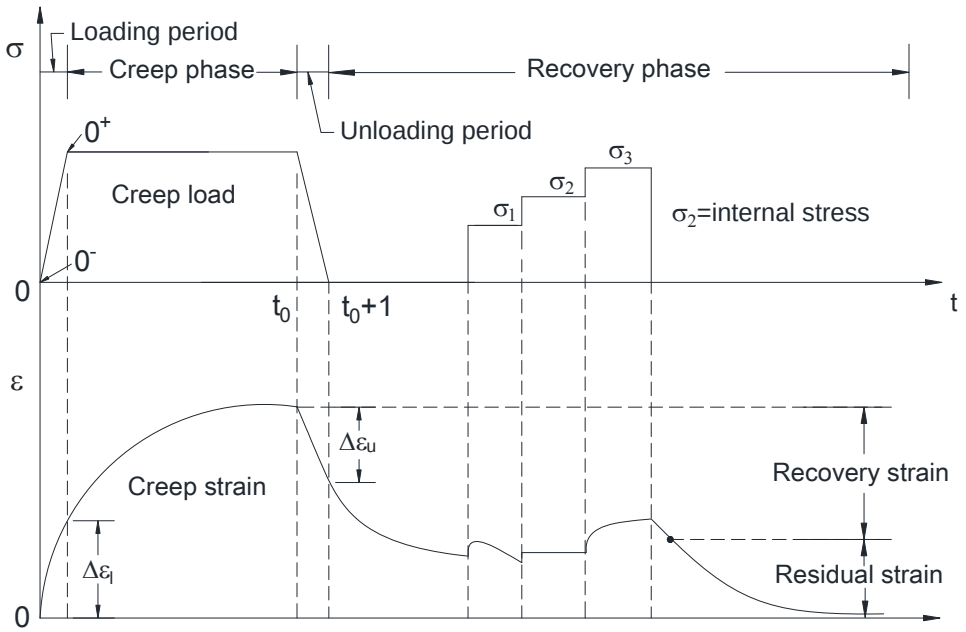

Figure 6.4 Schematic of Stress and Strain in the CSR Test

The apparent relaxation modulus is obtained by the Laplace transform of the apparent creep compliance. To facilitate the process of the Laplace transform, $D(t)$ calculated by Equation 6.9 is simulated using the following function:

$$D(t) = D_0 + D_1\left(1 - e^{-\frac{t}{\tau}}\right) \tag{6.10}$$

where D_0 is the instantaneous creep compliance; D_1 is the creep compliance coefficient; and τ is the retardation time. Apply the Laplace transform to $D(t)$ in Equation 6.10, which gives:

$$\mathcal{L}\{D(t)\} = \hat{D}(s) = \frac{D_0}{s} + D_1\frac{1/\tau}{s(s+1/\tau)} = \frac{D_0}{s} + \frac{D_1}{s(s\tau+1)} \tag{6.11}$$

where $\mathcal{L}\{D(t)\}$ or $\hat{D}(s)$ is the Laplace transform of $D(t)$; and s is the transformed variable. For undamaged asphalt mixtures, $\hat{D}(s)$ has the following relationship with the Laplace transform of the relaxation modulus (Findley et al. 1989):

$$\hat{D}(s)\hat{E}(s) = \frac{1}{s^2} \tag{6.12}$$

where $\hat{E}(s)$ is the Laplace transform of the relaxation modulus. Substitute Equation 6.11 into 6.12 and solve for $\hat{E}(s)$ to obtain

$$\hat{E}(s) = \frac{1}{s^2\left[\frac{D_0}{s} + \frac{D_1}{s(s\tau+1)}\right]} \tag{6.13}$$

Apply the inverse Laplace transform for $\hat{E}(s)$ in Equation 6.13 to obtain the expression

for the relaxation modulus:

$$E(t) = \mathcal{L}^{-1}\left\{\hat{E}(s)\right\} = \frac{1}{D_0 + D_1} + \frac{D_1}{D_0\left(D_0 + D_1\right)} e^{-\frac{D_0 + D_1}{D_0 \tau} t} \tag{6.14}$$

where $E(t)$ is the relaxation modulus of the undamaged asphalt mixtures; $\mathcal{L}^{-1}\left\{\hat{E}(s)\right\}$ is the inverse Laplace transform of $\hat{E}(s)$. Define $E(t)$ in the following way:

$$E(t) = E_\infty + E_1 e^{-\frac{t}{\kappa}} \tag{6.15}$$

in which E_∞ is the long term relaxation modulus; E_1 is the relaxation modulus coefficient; and κ is the relaxation time. Comparing Equations 6.14 and 6.15 gives:

$$E_\infty = \frac{1}{D_0 + D_1} \tag{6.16}$$

$$E_1 = \frac{D_1}{D_0\left(D_0 + D_1\right)} \tag{6.17}$$

$$\kappa = \frac{D_0 \tau}{D_0 + D_1} \tag{6.18}$$

Step 2. Determination of True Creep Material Properties of Undamaged Asphalt Mixtures

The true creep material properties are the creep material properties of the intact material, including the true creep compliance and true relaxation modulus. The true creep compliance is calculated by the true creep stress and true creep strain; the true relaxation modulus is obtained by applying the Laplace transform to the true creep compliance.

The true creep stress is inferred from the apparent creep stress by the force equilibrium equation (Equation 6.2).

$$\sigma_{cN} A = \sigma_{cN}^{T} \left(A - S_c \right) \tag{6.19}$$

where σ_{cN}^{T} is the true creep stress in the nondestructive test. In undamaged asphalt mixtures, the value of S_c / A equals the air void content since the air voids are the initial cracks and the area of the air voids does not change in the nondestructive test. Consequently, σ_{cN}^{T} can be solved from Equation 6.19 as follows:

$$\sigma_{cN}^{T} = \frac{\sigma_{cN}}{1 - AV\%} \tag{6.20}$$

where $AV\%$ is the air void content.

The true creep strain is inferred from the apparent creep stress and apparent creep strain by the DSE balance equation (Equation 6.3), in which DSE^{A} is calculated by integrating σ_{cN} and ε_{cN}:

$$\mathrm{DSE}^{A} = \int_0^t \sigma_{cN} d\varepsilon_{cN} \tag{6.21}$$

Since σ_{cN} is constant in the creep phase, Equation 6.21 reduces to

$$\mathrm{DSE}^{A} = \sigma_{cN} \left[\varepsilon_{cN}(t) - \varepsilon_{cN}(0) \right] \tag{6.22}$$

Similarly, DSE^{T} is calculated by integrating σ_{cN}^{T} and the true creep strain ε_{cN}^{T}, and the result is:

$$\mathrm{DSE}^{T} = \sigma_{cN}^{T} \left[\varepsilon_{cN}^{T}(t) - \varepsilon_{cN}^{T}(0) \right] \tag{6.23}$$

Substitute Equations 6.22 and 6.23 into Equation 6.3, yielding:

$$\sigma_{cN}\left[\varepsilon_{cN}\left(t\right)-\varepsilon_{cN}\left(0\right)\right]=\sigma_{cN}^{T}\left[\varepsilon_{cN}^{T}\left(t\right)-\varepsilon_{cN}^{T}\left(0\right)\right] \tag{6.24}$$

Equation 6.24 can be rewritten in the following form:

$$\sigma_{cN}\varepsilon_{cN}\left(t\right)=\sigma_{cN}^{T}\varepsilon_{cN}^{T}\left(t\right) \tag{6.25}$$

Solve $\varepsilon_{cN}^{T}\left(t\right)$ from Equation 6.25 as:

$$\varepsilon_{cN}^{T}\left(t\right)=\frac{\sigma_{cN}}{\sigma_{cN}^{T}}\varepsilon_{cN}\left(t\right) \tag{6.26}$$

Using the true creep stress and true creep strain determined above, the true creep compliance is calculated as:

$$D^{T}\left(t\right)=\frac{\varepsilon_{cN}^{T}\left(t\right)}{\sigma_{cN}^{T}} \tag{6.27}$$

where $D^{T}\left(t\right)$ is the true creep compliance. The true relaxation modulus is obtained following the same procedure to calculate $E\left(t\right)$ as shown in Equations 6.10 through 6.18. Similarly, the true relaxation modulus has the formulation as follows:

$$E^{T}\left(t\right)=E_{\infty}^{T}+E_{1}^{T}e^{-\frac{t}{\kappa^{T}}} \tag{6.28}$$

in which E_{∞}^{T} is the true long term relaxation modulus; E_{1}^{T} is the true relaxation modulus coefficient; and κ^{T} is the true relaxation time. A plot of the apparent creep compliance, apparent relaxation modulus, true creep compliance, and true relaxation modulus of undamaged asphalt mixtures is given in Figure 6.5. The determined apparent and true creep material properties are used to calculate the apparent pseudo strain and true pseudo strain in the CSR test, respectively, which is discussed as follows.

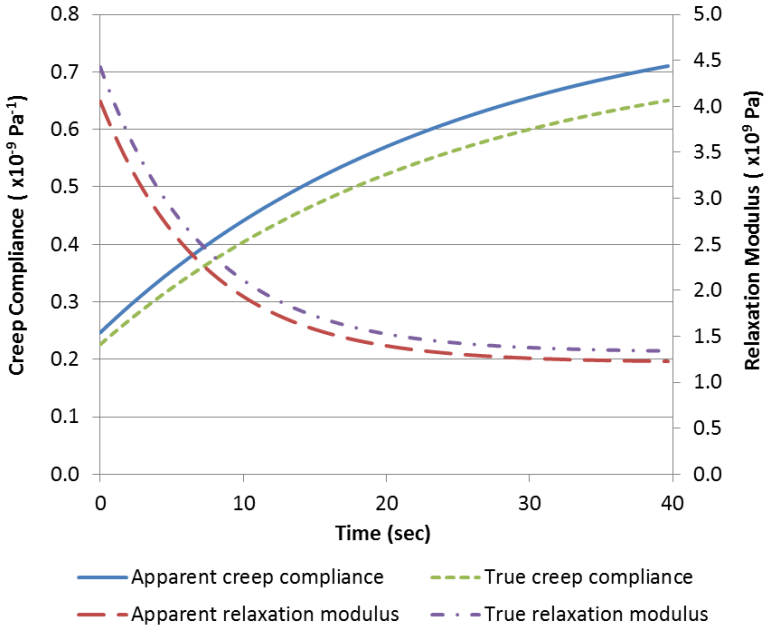

Figure 6.5 Apparent and True Creep Properties of Undamaged Asphalt Mixtures

Step 3. Calculation of Pseudo Strain Using Determined Creep Material Properties

Pseudo strain is calculated as follows:

$$\varepsilon_R = \frac{1}{E_R}\int_0^t E(t-\xi)\frac{d\varepsilon(\xi)}{d\xi}d\xi = \frac{\sigma_{VE}(t)}{E_R} \tag{6.29}$$

where ε_R is the pseudo strain; ξ is any arbitrary time between 0 an t; the lower integration limit "0" is 0^- to allow for a discontinuous change in stress at $t=0$, which is shown in Figure 6.4; $E(t)$ is the relaxation modulus of undamaged asphalt mixtures; E_R is the reference modulus that is used to achieve a dimensionless variable for ε_R; and $\sigma_{VE}(t)$ is the viscoelastic stress corresponding to the strain history $\varepsilon(t)$.

Apply Equation 6.29 to the creep phase of the destructive CSR test to calculate

the apparent pseudo strain for $t \in [0, t_0]$ in Figure 6.4. There is a jump discontinuity of the creep stress at $t = 0$, so Equation 6.29 can be written in the form (Wineman and Rajagopal 2000):

$$\varepsilon_{RcD} = \frac{1}{E_R}\left[\varepsilon_{cD}(0)E(t) + \int_0^t E(t-\xi)\frac{d\varepsilon_{cD}(\xi)}{d\xi}d\xi\right] \tag{6.30}$$

in which ε_{RcD} is the apparent pseudo strain in the creep phase of the destructive test, the subscript "D" indicating "destructive"; ε_{cD} is the creep strain in the destructive test; the lower integration limit 0 now implies 0^+ in Figure 6.4; and $E(t)$ is calculated above by Equation 6.15. Model ε_{cD} using the following function:

$$\varepsilon_{cD}(t) = \varepsilon_{0,cD} + \varepsilon_{1,cD}\left(1 - e^{-\frac{t}{\gamma_{cD}}}\right) \tag{6.31}$$

where $\varepsilon_{0,cD}$, $\varepsilon_{1,cD}$, and γ_{cD} are fitting parameters for ε_{cD}. Substitute Equations 6.15 and 6.31 into Equation 6.30 to calculate ε_{RD}:

$$\begin{aligned}\varepsilon_{RcD} &= \frac{1}{E_R}\left\{\varepsilon_{cD}(0)E(t) + \int_0^t\left(E_\infty + E_1 e^{-\frac{t-\xi}{\kappa}}\right)\frac{d\left[\varepsilon_{0,cD} + \varepsilon_{1,cD}\left(1 - e^{-\frac{\xi}{\gamma_{cD}}}\right)\right]}{d\xi}d\xi\right\} \\ &= \frac{1}{E_R}\left\{\varepsilon_{0,cD}E(t) + E_\infty\varepsilon_{1,cD}\left(1 - e^{-\frac{t}{\gamma_{cD}}}\right) + \frac{E_1\varepsilon_{1,cD}\kappa}{\gamma_{cD} - \kappa}\left(e^{-\frac{t}{\gamma_{cD}}} - e^{-\frac{t}{\kappa}}\right)\right\}\end{aligned} \tag{6.32}$$

The reference modulus E_R is selected to be the magnitude of the complex modulus to make ε_{RcD} comparable to ε_{cD}. The complex modulus is calculated by its

relationship with the relaxation modulus of the undamaged asphalt mixtures as follows (Findley et al. 1989):

$$E^*(\omega) = i\omega \mathcal{L}\{E(t)\}_{s=i\omega} \tag{6.33}$$

where $E^*(\omega)$ is the complex modulus of undamaged asphalt mixtures; and ω is the frequency. Substituting Equation 6.15 into 6.33 gives:

$$E^*(\omega) = E_\infty + \frac{E_1 \omega \kappa^2}{\omega \kappa^2 + 1} + \frac{E_1 \omega \kappa}{\omega \kappa^2 + 1} i \tag{6.34}$$

The magnitude of $E^*(\omega)$ is calculated as follows, the value of which is assigned to E_R.

$$\left|E^*(\omega)\right| = \sqrt{\left(E_\infty + \frac{E_1 \omega \kappa^2}{\omega \kappa^2 + 1}\right)^2 + \left(\frac{E_1 \omega \kappa}{\omega \kappa^2 + 1}\right)^2} = E_R \tag{6.35}$$

where $\left|E^*(\omega)\right|$ is the magnitude of the complex modulus. Substitute Equation 6.35 into 6.32, which gives the expression for ε_{RD}:

$$\varepsilon_{RcD} = \frac{\varepsilon_{0,cD} E(t) + E_\infty \varepsilon_{1,cD}\left(1 - e^{-\frac{t}{\gamma_{cD}}}\right) + \frac{E_1 \varepsilon_{1,cD} \kappa}{\gamma_{cD} - \kappa}\left(e^{-\frac{t}{\gamma_{cD}}} - e^{-\frac{t}{\kappa}}\right)}{\sqrt{\left(E_\infty + \frac{E_1 \omega \kappa^2}{\omega \kappa^2 + 1}\right)^2 + \left(\frac{E_1 \omega \kappa}{\omega \kappa^2 + 1}\right)^2}} \qquad \left(t \in [0, t_0]\right) \tag{6.36}$$

The true pseudo strain in the creep phase of the destructive CSR test is calculated following the same procedure as that for ε_{RD} by Equation 6.37:

$$\varepsilon_{RcD}^T = \frac{1}{E_R^T}\left[\varepsilon_{cD}^T(0) E^T(t) + \int_0^t E^T(t - \xi) \frac{d\varepsilon_{cD}^T(\xi)}{d\xi} d\xi\right] \tag{6.37}$$

where ε_{RcD}^{T} is the true pseudo strain in the creep phase; ε_{cD}^{T} is the true creep strain in the destructive test; $E^{T}(t)$ is calculated above by Equation 6.18; and E_{R}^{T} is the true reference modulus. First, simulate ε_{cD}^{T} using the same formulation as that in Equation 6.31:

$$\varepsilon_{cD}^{T}(t)=\varepsilon_{0,cD}^{T}+\varepsilon_{1,cD}^{T}\left(1-e^{-\frac{t}{\gamma_{cD}^{T}}}\right) \tag{6.38}$$

where $\varepsilon_{0,cD}^{T}$, $\varepsilon_{1,cD}^{T}$, and γ_{cD}^{T} are fitting parameters for ε_{cD}^{T}. Then E_{R}^{T} is calculated by analogy with E_{R}, which has the following formulation:

$$E_{R}^{T}=\sqrt{\left(E_{\infty}^{T}+\frac{E_{1}^{T}\omega\left(\kappa^{T}\right)^{2}}{\omega\left(\kappa^{T}\right)^{2}+1}\right)^{2}+\left(\frac{E_{1}^{T}\omega\kappa^{T}}{\omega\left(\kappa^{T}\right)^{2}+1}\right)^{2}} \tag{6.39}$$

Substitute Equations 6.38 and 6.39 into Equation 6.37 and integrate it to obtain the expression of ε_{RD}^{T}:

$$\varepsilon_{RcD}^{T}=\frac{\varepsilon_{0,cD}^{T}E^{T}(t)+E_{\infty}^{T}\varepsilon_{1,cD}^{T}\left(1-e^{-\frac{t}{\gamma_{cD}^{T}}}\right)+\frac{E_{1}^{T}\varepsilon_{1,cD}^{T}\kappa^{T}}{\gamma_{cD}^{T}-\kappa^{T}}\left(e^{-\frac{t}{\gamma_{cD}^{T}}}-e^{-\frac{t}{\kappa^{T}}}\right)}{\sqrt{\left(E_{\infty}^{T}+\frac{E_{1}^{T}\omega\left(\kappa^{T}\right)^{2}}{\omega\left(\kappa^{T}\right)^{2}+1}\right)^{2}+\left(\frac{E_{1}^{T}\omega\kappa^{T}}{\omega\left(\kappa^{T}\right)^{2}+1}\right)^{2}}}\quad\left(t\in[0,t_{0}]\right) \tag{6.40}$$

Step 4. Calculation of DPSE Using Pseudo Strain for Damaged Asphalt Mixtures

The apparent pseudo strain and true pseudo strain determined above are used to calculate the apparent DPSE and true DPSE in the creep phase of the destructive CSR

test, respectively. The apparent DPSE is calculated by integrating the apparent creep stress and the apparent pseudo strain for $t \in [0, t_0]$ as follows:

$$\text{DPSE}^A = \int_0^t \sigma_{cD} d\varepsilon_{RcD} = \sigma_{cD} \left[\varepsilon_{RcD}(t) - \varepsilon_{RcD}(0) \right] \tag{6.41}$$

where σ_{cD} is the creep stress in the destructive test; and ε_{RcD} is the apparent pseudo strain calculated above by Equation 6.36. The true DPSE is calculated by integrating the true creep stress and the true pseudo strain as follows:

$$\text{DPSE}^T = \int_0^t \sigma_{cD}^T d\varepsilon_{RcD}^T \tag{6.42}$$

where $\sigma_{cD}^T(t)$ is the true creep stress in the destructive test; and ε_{RcD}^T is the true pseudo strain calculated above by Equation 6.40. The true creep stress always has the following relationship with the true creep strain because it is the viscoelastic stress of the intact material corresponding to the true creep strain.

$$\begin{aligned} \sigma_{cD}^T(t) = \sigma_{VE}^T(t) &= \int_0^t E^T(t-\xi) \frac{d\varepsilon_{cD}^T(\xi)}{d\xi} d\xi \\ &= \varepsilon_{cD}^T(0) E^T(t) + \int_0^t E^T(t-\xi) \frac{d\varepsilon_{cD}^T(\xi)}{d\xi} d\xi \\ &= \varepsilon_{0,cD}^T E^T(t) + E_\infty^T \varepsilon_{1,cD}^T \left(1 - e^{-\frac{t}{\gamma_{cD}^T}} \right) + \frac{E_1^T \varepsilon_{1,cD}^T \kappa^T}{\gamma_{cD}^T - \kappa^T} \left(e^{-\frac{t}{\gamma_{cD}^T}} - e^{-\frac{t}{\kappa^T}} \right) \end{aligned} \tag{6.43}$$

where σ_{VE}^T is the true viscoelastic stress, or the viscoelastic stress of the intact material. Comparing Equations 6.43 with Equation 6.37, σ_{cD}^T and ε_{RD} has the following relationship:

$$\sigma_{cD}^T(t) = E_R^T \varepsilon_{RcD}^T \tag{6.44}$$

Substituting Equation 6.44 into 6.42, gives:

$$\text{DPSE}^T = \int_0^t E_R^T \varepsilon_{RcD}^T d\varepsilon_{RcD}^T = \frac{E_R^T}{2}\left[\varepsilon_{RcD}^T(t)^2 - \varepsilon_{RcD}^T(0)^2\right] \tag{6.45}$$

Step 5. Solve for True Creep Strain of Damaged Asphalt Mixtures by DPSE Balance Equation

The apparent DPSE and true DPSE calculated above are substituted into the DPSE balance equation (Equation 6.4), which gives the following equation:

$$\sigma_{cD}\left[\varepsilon_{RcD}(t) - \varepsilon_{RcD}(0)\right] = \frac{E_R^T}{2}\left[\varepsilon_{RcD}^T(t)^2 - \varepsilon_{RcD}^T(0)^2\right] \tag{6.46}$$

The left side of Equation 6.46 is provided by the measurements of the destructive CSR test. Substituting for ε_{RcD}^T using Equation 6.40 into Equation 6.46, the resulting DPSE balance equation have three unknown variables: $\varepsilon_{0,cD}^T$, $\varepsilon_{1,cD}^T$, and γ_{cD}^T, which are three fitting parameters for ε_{cD}^T. As a result, Equation 6.46 can be used to solve for ε_{cD}^T, of which the procedure is as follows:

- Solve for $\varepsilon_{0,cD}^T$ by the stress-strain relationship at $t = 0$:

  $$\varepsilon_{0,cD}^T = \varepsilon_{cD}^T(0) = D^T(0)\sigma_{cD}^T(0) \tag{6.47}$$

  where $D^T(0)$ is calculated by Equation 6. 30; $\sigma_{cD}^T(0)$ is the true creep stress at $t = 0$,

  which is related to σ_{cD} by the force equilibrium equation:

  $$\sigma_{cD}(0)A = \sigma_{cN}^T(0)(A - S_c) \tag{6.48}$$

in which $\sigma_{cD}(0)$ is the apparent creep stress at $t = 0$; and the value of S_c/A equals the air void content at $t = 0$. Consequently, $\sigma_{cD}^{T}(0)$ is solved from Equation 6.48 as:

$$\sigma_{cD}^{T}(0) = \frac{\sigma_{cN}(0)}{1 - AV\%} \tag{6.49}$$

- Solve for $\varepsilon_{1,cD}^{T}$ and γ_{cD}^{T} by Equation 6.46 using the "Solver" function in Excel. Before using "Solver", assign $\varepsilon_{1,cD}^{T}$ and γ_{cD}^{T} initial feed values as shown in Equation 6.40:

$$\varepsilon_{1,cD}^{T} = \varepsilon_{1,cD}, \text{ and } \quad \gamma_{1,cD}^{T} = \gamma_{1,cD} \tag{6.50}$$

in which $\varepsilon_{1,cD}$ and γ_{cD} are fitting parameters for ε_{cD} in Equation 6.31. These initial feed values ensure that the "Solver" function provides the correct values for $\varepsilon_{1,cD}^{T}$ and γ_{cD}^{T}.

Step 5. Determination of True Creep Stress and Damage Density for Damaged Asphalt Mixtures

After obtaining the true creep strain in the destructive CSR test, the true creep stress is also determined by Equation 6.43. A plot of the apparent creep stress, apparent creep strain, true creep stress, and true creep strain in the destructive CSR test is presented in Figure 6.6. When the apparent creep stress is controlled constant in the creep phase, the true creep stress in the damaged asphalt mixture specimen is much larger than the apparent creep stress, and it increases with time as the cracking damage accumulates in the specimen.

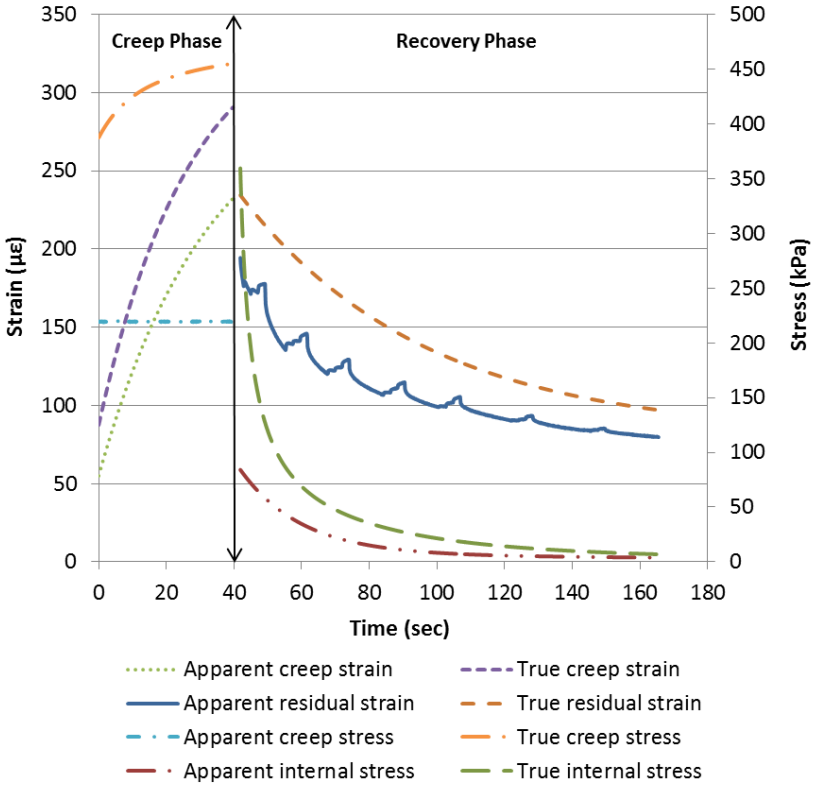

Figure 6.6 Apparent Stress/Strain and True Stress/Strain in Destructive CSR Test

With determined true creep stress, the damage density in the damaged asphalt mixture can be calculated by the following function:

$$\phi = \phi_0 + \left(1 - \frac{\sigma_{cD}}{\sigma_{cD}^{T}}\right) V_m\% \tag{6.51}$$

where ϕ is the damage density; ϕ_0 is the initial damage density in the creep phase, which equals the air void content; and $V_m\%$ is the volumetric percentage of the asphalt mastic that is determined from the volumetric analysis and aggregate gradation of the mixture design. A plot of the damaged density versus time of both the AAD and AAM mixtures is given in Figure 6.7. At the end of the creep phase, the damage density of the

AAD and AAM mixtures is 5.28% and 5.13%, respectively. These values are the final damage density in the creep phase, and also are the initial damage density from which the healing starts in the recovery phase. The change between the initial damage density and the damage density at any time during the recovery phase represents the extent of healing that occurs during this period. Therefore, the next step of quantifying healing is to determine the damage density at any time during the recovery phase, which is studied in Section 6.4.

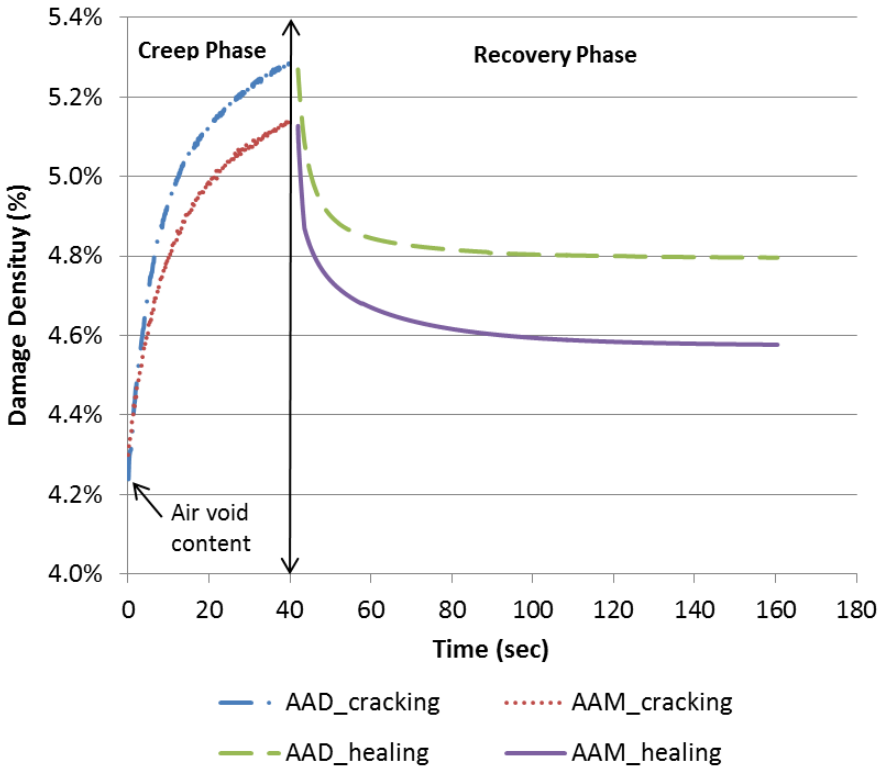

Figure 6.7 Damage Density versus Time in the Destructive CSR Test

6.4 Determination of Healing in the Recovery Phase

The procedure of determining the damage density in the recovery phase involves 5 steps, which are presented as follows in sequence.

Step 1. Calculation of Pseudo Strain in the Recovery Phase of Destructive CSR Test

The apparent pseudo strain and true pseudo strain in the recovery phase of the destructive CSR test must be determined first in order to calculate the apparent RPSE and true RPSE, respectively, in the damaged asphalt mixture. To calculate the apparent pseudo strain when $t \in [t_0, \infty]$, the strain history of the destructive CSR test is modeled using the following three functions:

$$\varepsilon(t) = \begin{cases} \varepsilon_{cD}(t) = \varepsilon_{0,cD} + \varepsilon_{1,cD}\left(1 - e^{-\frac{t}{\gamma_{cD}}}\right) & t \in [0, t_0] \\ \varepsilon_u(t) = mt + n & t \in [t_0, t_0 + 1] \\ \varepsilon_{rD}(t) = \varepsilon_{0,rD} + \varepsilon_{1,rD} e^{-\frac{t}{\gamma_{rD}}} & t \in [t_0 + 1, \infty] \end{cases} \quad (6.52)$$

where ε_{cD} is the creep strain of the destructive test as in Equation 6.31; ε_u is the strain in the unloading period as shown in Figure 6.4, during which the creep load is reduced to zero within 1 sec; m and n are fitting parameters for ε_u; ε_{rD} is the residual strain in the recovery phase of the destructive test; $\varepsilon_{0,rD}$, $\varepsilon_{1,rD}$, and γ_{rD} are fitting parameters for ε_{rD}. Substitute Equation 6.52 in to Equation 6.29 to calculate the apparent pseudo strain:

$$\varepsilon_{RrD}=\frac{\varepsilon_{cD}(0)E(t)+\int_0^{t_0}E(t-\xi)\frac{d\varepsilon_{cD}(\xi)}{d\xi}d\xi+\int_{t_0}^{t_0+1}E(t-\xi)\frac{d\varepsilon_u(\xi)}{d\xi}d\xi}{E_R}$$

$$+\frac{\int_{t_0+1}^{t}E(t-\xi)\frac{d\varepsilon_{rD}(\xi)}{d\xi}d\xi}{E_R}$$

$$=\frac{\varepsilon_{cD}(0)E(t)+\int_0^{t_0}\left(E_\infty+E_1e^{-\frac{t-\xi}{\kappa}}\right)\frac{d\left[\varepsilon_{0,cD}+\varepsilon_{1,cD}\left(1-e^{-\frac{\xi}{\gamma_{cD}}}\right)\right]}{d\xi}d\xi}{E_R}$$

$$+\frac{\int_{t_0}^{t_0+1}\left(E_\infty+E_1e^{-\frac{t-\xi}{\kappa}}\right)\frac{d(m\xi+n)}{d\xi}d\xi}{E_R}+\frac{\int_{t_0+1}^{t}\left(E_\infty+E_1e^{-\frac{t-\xi}{\kappa}}\right)\frac{d\left(\varepsilon_{0,rD}+\varepsilon_{1,rD}e^{-\frac{\xi}{\gamma_{rD}}}\right)}{d\xi}d\xi}{E_R}$$

$$=\frac{\varepsilon_{0,cD}E(t)+E_\infty\varepsilon_{1,cD}\left(1-e^{-\frac{t_0}{\gamma_{cD}}}\right)+\frac{E_1\varepsilon_{1,cD}\kappa}{\gamma_{cD}-\kappa}\left(e^{\left(\frac{1}{\kappa}-\frac{1}{\gamma_{cD}}\right)t_0-\frac{t}{\kappa}}-e^{-\frac{t}{\kappa}}\right)}{E_R}$$

$$+\frac{E_\infty m+E_1m\kappa\left(e^{\frac{t_0+1}{\kappa}-\frac{t}{\kappa}}-e^{\frac{t_0}{\kappa}-\frac{t}{\kappa}}\right)}{E_R}+\frac{E_\infty\varepsilon_{1,rD}\left(e^{-\frac{t}{r_{rD}}}-e^{-\frac{t_0}{\gamma_{rD}}}\right)-\frac{E_1\varepsilon_{1,rD}\kappa}{\gamma_{rD}-\kappa}\left(e^{-\frac{t}{r_{rD}}}-e^{\left(\frac{1}{\kappa}-\frac{1}{r_{rD}}\right)t_0-\frac{t}{\kappa}}\right)}{E_R} \tag{6.53}$$

where ε_{RrD} is the apparent pseudo strain in the recovery phase of the destructive test; and E_R is calculated above by Equation 6.35.

The true pseudo strain is calculated using the same procedure for ε_{RrD}. First, the true strain history of the destructive CSR test when $t\in[t_0,\infty]$ is formulated as follows:

$$\varepsilon^T(t)=\begin{cases}\varepsilon_{cD}^T(t)=\varepsilon_{0,cD}^T+\varepsilon_{1,cD}^T\left(1-e^{-\frac{t}{\gamma_{cD}^T}}\right) & t\in[0,t_0]\\ \varepsilon_u^T(t)=m^Tt+n^T & t\in[t_0,t_0+1]\\ \varepsilon_{rD}^T(t)=\varepsilon_{0,rD}^T+\varepsilon_{1,rD}^Te^{-\frac{t}{\gamma_{rD}^T}} & t\in[t_0+1,\infty]\end{cases} \tag{6.54}$$

where ε_{cD}^T is the true creep strain as in Equation 41; ε_u^T is the true strain in the unloading period; m^T and n^T are fitting parameters for ε_u^T; ε_{rD}^T is the true residual strain in the recovery phase of the destructive test; $\varepsilon_{0,rD}^T$, $\varepsilon_{1,rD}^T$, and γ_{rD}^T are fitting parameters for ε_{rD}^T. Substitute Equation 6.54 in to Equation 6.29 to calculate the true pseudo strain:

$$\begin{aligned}\varepsilon_{RrD}^T&=\frac{\varepsilon_{cD}^T(0)E^T(t)+\int_0^{t_0}E^T(t-\xi)\frac{d\varepsilon_{cD}^T(\xi)}{d\xi}d\xi+\int_{t_0}^{t_0+1}E^T(t-\xi)\frac{d\varepsilon_u^T(\xi)}{d\xi}d\xi}{E_R^T}\\&+\frac{\int_{t_0+1}^{t}E^T(t-\xi)\frac{d\varepsilon_{rD}^T(\xi)}{d\xi}d\xi}{E_R^T}\\&=\frac{\varepsilon_{0,cD}^TE^T(t)+E_\infty^T\varepsilon_{1,cD}^T\left(1-e^{-\frac{t_0}{\gamma_{cD}^T}}\right)+\frac{E_1^T\varepsilon_{1,cD}^T\kappa^T}{\gamma_{cD}^T-\kappa^T}\left(e^{\left(\frac{1}{\kappa^T}-\frac{1}{\gamma_{cD}^T}\right)t_0-\frac{t}{\kappa^T}}-e^{-\frac{t}{\kappa^T}}\right)}{E_R^T}\\&+\frac{E_\infty^Tm^T+E_1^Tm^T\kappa^T\left(e^{\frac{t_0+1}{\kappa^T}-\frac{t}{\kappa^T}}-e^{\frac{t_0}{\kappa^T}-\frac{t}{\kappa^T}}\right)}{E_R^T}\\&+\frac{E_\infty^T\varepsilon_{1,rD}^T\left(e^{-\frac{t}{r_{rD}^T}}-e^{-\frac{t_0}{\gamma_{rD}^T}}\right)-\frac{E_1^T\varepsilon_{1,rD}^T\kappa^T}{\gamma_{rD}^T-\kappa^T}\left(e^{-\frac{t}{r_{rD}^T}}-e^{\left(\frac{1}{\kappa^T}-\frac{1}{r_{rD}^T}\right)t_0-\frac{t}{\kappa^T}}\right)}{E_R^T}\end{aligned} \tag{6.55}$$

where ε_{RrD}^T is the true pseudo strain in the recovery phase of the destructive test; and E_R^T

is calculated above by Equation 6.39. To calculate the value of ε_{RrD}^{T}, ε_{u}^{T} and ε_{rD}^{T} must be determined first, as introduced in the next step.

Step 2. Determination of True Strain in the Recovery Phase for Damaged Asphalt Mixtures

The strain in the loading and unloading periods in Figure 6.4 is considered to be the elastic response to the stress in that period. Therefore, the change of the strain in the unloading period, $\Delta\varepsilon_u$, is equal to the change of the strain in the loading period, $\Delta\varepsilon_l$, as shown in Figure 6.4. The change of the true creep strain in the loading period is obtained by the true creep strain at $t=0$, which is $\varepsilon_{0,cD}^{T}$ calculated by Equation 6.47. The change of the true strain in the unloading phase $\Delta\varepsilon_u^T$ is thus calculated by:

$$\Delta\varepsilon_u^T = \varepsilon_{0,cD}^T \tag{6.56}$$

In addition, the true strain at t_0 is already obtained above in the creep phase as $\varepsilon_{cD}^{T}\left(t=t_0\right)$. Based on $\Delta\varepsilon_u^T$ and $\varepsilon_{cD}^{T}\left(t=t_0\right)$, a linear function can be fitted for ε_u^T with the determined values of m^T and n^T.

The true residual strain ε_{rD}^{T} is determined using the RSE balance equation (Equation 6.7) from the apparent measurements provided by the destructive CSR test. The apparent RSE is calculated integrating the apparent internal stress and apparent residual strain for $t\in\left[t_0+1,\infty\right]$:

$$\mathrm{RSE}^{A} = \int_{t_0+1}^{t} \sigma_{iD}\left(t\right) d\varepsilon_{rD} \tag{6.57}$$

where $\sigma_{iD}(t)$ is the apparent internal stress measured in the destructive CSR test, which is simulated by an exponential function:

$$\sigma_{iD}(t) = \sigma_a e^{-\frac{t}{\eta_1}} + \sigma_b e^{-\frac{t}{\eta_2}} \tag{6.58}$$

in which σ_a, σ_b, η_1, and η_2 are fitting parameters for σ_{iD}. The true RSE is calculated by integrating the true internal stress and true residual strain as follows:

$$\mathrm{RSE}^T = \int_{t_0+1}^{t} \sigma_{iD}^T(t)\, d\varepsilon_{rD}^T \tag{6.59}$$

where σ_{iD}^T is the true internal stress in the destructive CSR test, which is calculated based on the recovery modulus:

$$\sigma_{iD}^T(t) = R_N(t)\,\varepsilon_{rD}^T(t) \tag{6.60}$$

in which $R_N(t)$ is the recovery modulus of undamaged asphalt mixtures measured from the nondestructive CSR test. Substituting Equation 6.60 into 6.59, gives:

$$\mathrm{RSE}^T = \int_{t_0+1}^{t} R_N(t)\,\varepsilon_{rD}^T(t)\, d\varepsilon_{rD}^T = \frac{R_N(t)}{2}\left[\varepsilon_{rD}^T(t)^2 - \varepsilon_{rD}^T(t_0+1)^2\right] \tag{6.61}$$

in which:

$$\varepsilon_{rD}^T(t_0+1) = \varepsilon_u^T(t_0+1) \tag{6.62}$$

Substitute Equations 6.57, 6.61, and 6.62 into the RPSE balance equation, which gives:

$$\int_{t_0+1}^{t} \sigma_{iD}(t)\, d\varepsilon_{rD} = \frac{R_N(t)}{2}\left[\varepsilon_{rD}^T(t)^2 - \varepsilon_u^T(t_0+1)^2\right] \tag{6.63}$$

Substitute the expression of $\varepsilon_{rD}^T(t)$ in Equation 6.54 into Equation 6.63, which gives:

$$\int_{t_0+1}^{t} \sigma_{iD}(t)\, d\varepsilon_{rD} = \frac{R_N(t)}{2}\left[\left(\varepsilon_{0,rD}^{T} + \varepsilon_{1,rD}^{T} e^{-\frac{t}{\gamma_{rD}^{T}}}\right)^2 - \varepsilon_u^T (t_0+1)^2\right] \tag{6.64}$$

in which $\varepsilon_{0,rD}^{T}$ is solved from the following relationship:

$$\varepsilon_{rD}^{T}(t_0+1) = \varepsilon_{0,rD}^{T} + \varepsilon_{1,rD}^{T} e^{-\frac{t_0+1}{\gamma_{rD}^{T}}} = \varepsilon_u^T (t_0+1) \tag{6.65}$$

Solve for $\varepsilon_{1,rD}^{T}$ and γ_{rD}^{T} by Equation 6.64 using the "Solver" function in Excel. A plot of the apparent internal stress, true internal stress, apparent residual strain, and true residual strain of the destructive CSR test is given in Figure 6.6.

Step 3. Calculation of RPSE Using Pseudo Strain for Damaged Asphalt Mixtures

The apparent pseudo strain and true pseudo strain in the recovery phase determined above are used to calculate the apparent RPSE and true RPSE in the recovery phase of the destructive CSR test, respectively. The apparent RPSE is calculated by integrating the apparent internal stress and the apparent pseudo strain in the recovery phase for $t \in [t_0+1, \infty]$:

$$\text{RPSE}^{A} = \int_{t_0+1}^{t} \sigma_{iD}(t)\, d\varepsilon_{RrD} \tag{6.66}$$

where ε_{RrD} is calculated above in Equation 6.53. The true RPSE is calculated by integrating the true internal stress and true pseudo strain in the recovery phase as follows:

$$\text{RPSE}^{T} = \int_{t_0+1}^{t} \sigma_{iD}^{T}(t)\, d\varepsilon_{RrD}^{T} \tag{6.67}$$

where ε_{RrD}^{T} is calculated above in Equation 6.67 based on the determined true strain in the last step.

Step 4. Solve for Damage Density in the Recovery Phase Using RPSE Balance Equation

The calculated apparent RPSE and true RPSE are substituted into the RPSE balance equation (Equation 6.8) to solve for the change of the damage density with time in the recovery phase. The time duration of the recovery phase is 2 min and the time interval between data acquisitions is 0.1 sec, so there are 1200 data points for which the RPSE balance equation is solved. Rewritten Equation 6.8 in the following form for each data point:

$$\mathrm{RPSE}^{A}V_m = \mathrm{RPSE}^{T}V_m + \mathrm{RPSE}^{T}\left(\frac{2M_{i-1}\pi^2 {c_{i-1}}^3}{3} - \frac{2M_i\pi^2 {c_i}^3}{3}\right) - \gamma\left(2M_{i-1}\pi {c_{i-1}}^2 - 2M_i\pi {c_i}^2\right) \tag{6.68}$$

in which i is the number of data point in the recovery phase, $i = 1, 2, \cdots, 1200$.

For the 1st data point ($i = 1$), M_0 and c_0 are the initial number of cracks and initial average crack size in the recovery phase, respectively; M_1 and c_1 are the number of cracks and average crack size at the 1st data point, respectively. The number of cracks does not change in the recovery phase since healing (or crack closure) of the asphalt mixture specimen only results in the decrease of the average crack size. As a result, there are three independent unknown variables in Equation 6.68: M_0, c_0, and c_1, which are solved as follows:

- The initial number of cracks and initial average crack size in the recovery phase are also the final number of cracks and final average crack size in the creep

phase, so M_0 and c_0 are related to the final damage density in the creep phase as follows:

$$M_0 \pi c_0^{\,2} = \phi_{fc} A \tag{6.69}$$

where ϕ_{fc} is the final damage density at the end of the creep phase, which is calculated by Equation 6.51; and A is the cross sectional area. Assume the number of cracks does not change in the creep phase since the loading time is very short; then M_0 is equal to the initial number of cracks in the creep phase. Determination of the initial number of cracks before loading can be found in Section 4. After obtaining M_0, c_0 can be calculated by Equation 6.69.

- After obtaining M_0 and c_0, c_1 is the only unknown variable in Equation 6.68. The "Solver" function in Excel is used to solve for the value of c_1, so the left side and right side of the equation can be balanced.

The determined c_1 is fed into Equation 6.68 for $i = 2$, in which c_2 is the only unknown variable. The "Solver" function is used again to solve for the value of c_2. Then c_2 is fed into Equation 6.68 for $i = 3$ to solve for c_3. This process is repeated until $i = 1200$, which is conducted automatically by the Macro program that is designed and embedded in the Excel.

Using the determined c_i for the 1200 data points in the recovery phase, the damage density for each data point ϕ_i is then calculated as:

$$\phi_i = \frac{M_0 \pi c_i^{\,2}}{A} \tag{6.70}$$

The plot of ϕ_i versus time of both AAD and AAM mixtures are shown in Figure 6.7 as the two curves in the recovery phase. The decrease of the damage density with the increase of time demonstrates that healing occurs in the asphalt mixture specimen.

Step 5. Determination of Healing Rates from the Healing Curve

Based on the determined damage density at every data point in the recovery phase, the extent of healing is thus quantified as the difference between the damage density at any data point (ϕ_i) and the initial damage density before healing starts, which is determined above as the final damage density at the end of the creep phase (ϕ_{fc}). To make it a normalized value, the extent of healing is defined in the following way:

$$h = \frac{\phi_{fc} - \phi_i}{\phi_{fc} - \phi_0}, \qquad h \in [0,1] \tag{6.71}$$

where h is the normalized healing measured from the CSR test, or the measured healing; $\phi_{fc} - \phi_i$ represents the extent of healing that occurs from the beginning of the recovery phase to the data point i; ϕ_0 is the initial damage density defined in Equation 6.51, which equals the air void content; $\phi_{fc} - \phi_0$ is thus the maximum increase of damage density due to the crack growth in the creep phase, representing the maximum extent of healing that can occur in the damaged asphalt mixture specimen. A plot of h versus the rest time is presented in Figure 6.8. The rest time refers to the length of the time during which healing occurs. It has the following relationship with t in Figure 6.4:

$$\Delta t = t - (t_0 + 1), \qquad t \in [t_0 + 1, \infty] \tag{6.72}$$

where Δt is the rest time. The point of $h = 0$ corresponds to $\phi_{fc} = \phi_i$, indicating no healing occurs when $\Delta t = 0$; the point of $h = 1$ corresponds to $\phi_i = \phi_0$, indicating all the cracking damage generated in the material is healed, i.e. complete healing. This curve showing the healing rate at different rest times is defined as the healing curve.

It is observed from Figure 6.8 that there is a rapid increase of the measured healing in the approximately first 5 sec. In other words, the healing rate is very large during this period. After that, the healing rate gradually decreases and the change of the measured healing is less with the increase of the rest time. To demonstrate such characteristics of the healing of asphalt mixtures, Lytton (2004) used an equation to model the healing curve in the form of the Ramberg-Osgood equation (Ramberg and Osgood 1943):

$$\hat{h} = \dot{h}_2 \Delta t + \frac{\left(\dot{h}_1 - \dot{h}_2\right)\Delta t}{1 + \frac{\left(\dot{h}_1 - \dot{h}_2\right)\Delta t}{h_\beta}} \tag{6.73}$$

where $\hat{h}$ is the calculated healing based on three parameters: $\dot{h}_1$, $\dot{h}_2$, and h_β; $\dot{h}_1$ is the short-term healing rate, representing the healing speed of the material at the beginning of unloading; $\dot{h}_2$ is the long-term healing rate, indicating the healing speed of the material after a long time; and h_β is the healing rate scale, reflecting the overall ability of the material to heal. These three parameters are illustrated in Figure 6.8. The advantage of using this healing model is that the healing ability of the asphalt mixture can be readily described by these three parameters, so it is convenient to compare and select a type of

asphalt mixture with good healing ability.

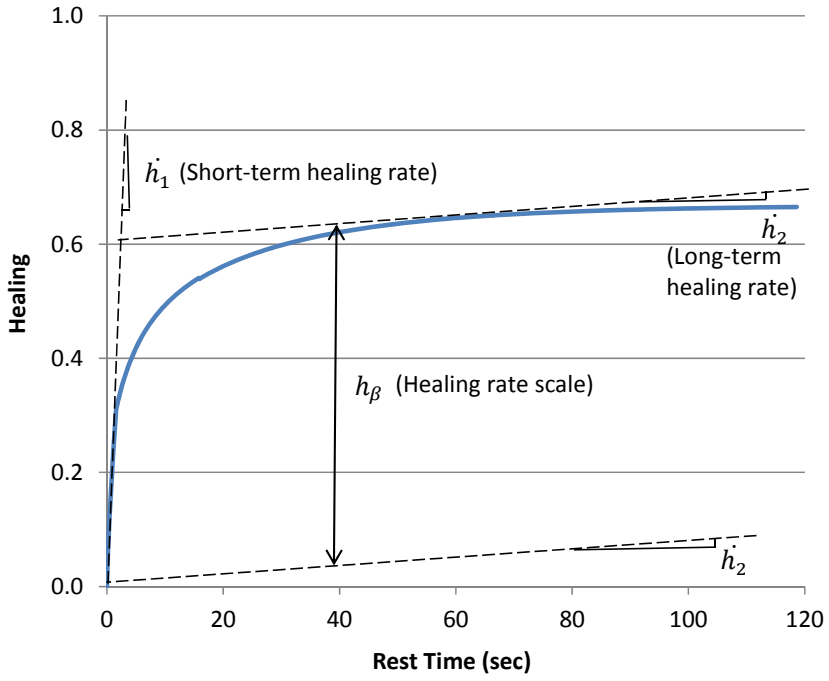

Figure 6.8 Healing Curve with Short-Term and Long-Term Healing Rates

A plot of the measured healing by Equation 6.71 and the calculated healing by Equation 6.73 are shown in Figure 6.9 for both AAD and AAM mixtures. The calculated healing matches well with the measured healing for both mixtures. Figure 6.9 suggests that the shape of the healing curve of the AAD mixtures is different from that of the AAM mixtures. More precise description of this difference is given by the healing parameters as shown in Table 6.1. The AAM mixtures have a larger short-term healing rate, larger long-term healing rate, and larger healing rate scale. Therefore, the AAM mixtures have better healing ability than the AAD mixtures. This conclusion conforms to

the finding in other research (Si et al. 2002).

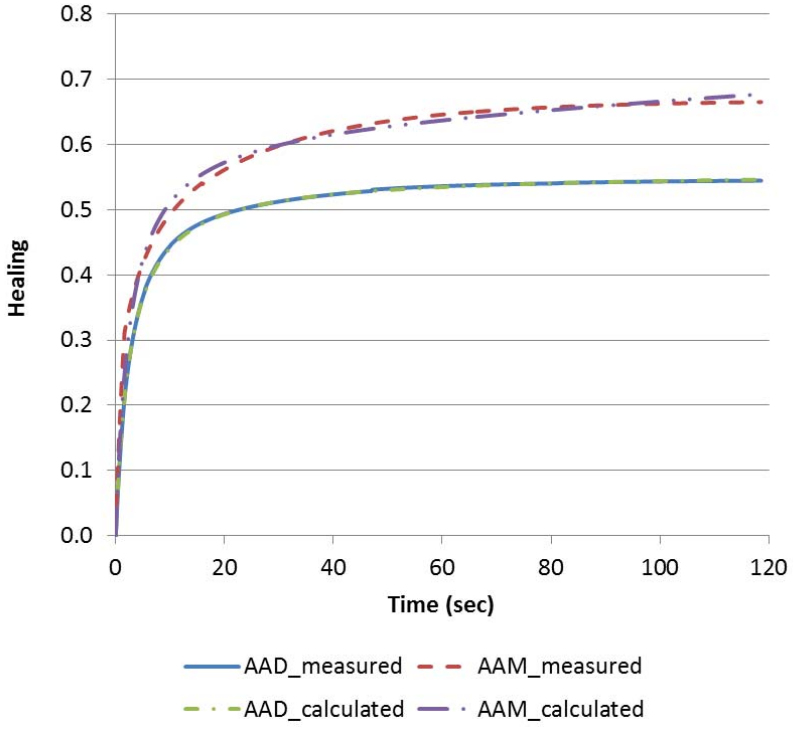

Figure 6.9 Measured and Calculated Healing for Damaged Asphalt Mixtures

Table 6.1 Values of Healing Rates from the Healing Curve

Type of Asphalt Mixtures	$\dot{h}_1$	$\dot{h}_2$	$\dot{h}_\beta$
AAD	0.2106	7.643×10^{-7}	0.5583
AAM	0.2515	4.761×10^{-4}	0.6341

7. APPLICATION OF THE ENERGY-BASED MECHANISTIC APPROACH TO DIFFERENT TYPES OF ASPHALT MIXTURES

The objective of Section 7 is to examine the application of the energy-based mechanistic approach that is developed in the previous sections for characterization of fatigue cracking and healing of asphalt mixtures. Because of the mechanistic nature of this approach, it is believed the approach can be applied to all kinds of asphalt mixtures, and even materials other than asphalt mixtures. As examples, this approach will be employed to evaluate the fatigue resistance and healing ability of twenty different types of asphalt mixtures.

7.1 Materials and Experiments

The asphalt mixtures used are laboratory mixed and laboratory compacted hot asphalt mixtures. There are four types of asphalt binders: the binder AAD and binder AAM from the Strategic Highway Research Program Materials Reference Library (Jones 1993); the binder designated "NuStar" that is supplied by the NuStar Energy, Paulsboro, New Jersey; and the binder designated "Valero" that is supplied by the Valero Refining, Benicia, California. There are two types of aggregate: Texas limestone as mentioned in the previous sections and Hanson limestone, New Braunfels, Texas. There are two kinds of air void content: 4% and 7%., and three different aging periods: 0, 3, and 6 months. Combination of all these variables yields twenty types of asphalt mixtures, as shown in Table 7.1. In the first column of Table 7.1, for example, "M1" is

one type of asphalt mixture using AAD and Texas limestone with 4% air voids and is aged for zero month. The mixture design, process of fabrication of cylindrical specimens, test machine, and the test set up are the same as those in the previous sections, which are not repeated here.

Table 7.1 Material Information of Tested Asphalt Mixtures

Type of Asphalt Mixture	Design Variables			
	Asphalt Binder	Aggregate	Air Void Content	Aging Period
M1	AAD	Texas limestone	4%	0
M2				6
M3			7%	0
M4				6
M5	AAM		4%	0
M6				6
M7			7%	0
M8				6
M9	NuStar	Hanson limestone	4%	0
M10				3
M11				6
M12			7%	0
M13				3
M14				6
M15	Valero		4%	0
M16				3
M17				6
M18			7%	0
M19				3
M20				6

The twenty different types of asphalt mixtures are subjected to a series of laboratory tests in order to characterize the fatigue and healing properties. The controlled-strain RDT test that is described in Sections 2, 3, and 4 is used to obtain the fatigue properties, and the CSR test that is developed in Section 5 and 6 is used to obtain the healing properties, as shown in Table 7.2. Detailed test configuration, test process, measured properties, and analysis method have already been presented in the previous sections. In the following of this section, the test results are given to verify the findings that are presented in the previous sections; in addition, to evaluate the change of the fatigue resistance and healing by changing the design variable of asphalt mixtures.

Table 7.2 Testing Procedure of Laboratory Experiments

	Testing Procedure	Temperature	Asphalt Mixtures
Fatigue cracking	1. X-ray CT Test 2. Nondestructive controlled-strain RDT test 3. Destructive controlled-strain RDT test	20°C	M1, M2, M3, M4, M5, M6, M7, M8, M9, M10, M11, M12, M13, M14, M15, M16, M17, M18, M19, M20
Healing	1. Normal creep recovery test 2. Nondestructive CSR test at loading level 1 3. Nondestructive CSR test at loading level 2 4. Nondestructive CSR test at loading level 3 5. Destructive CSR test	20°C	M1, M2, M3, M4, M5, M6, M7, M8
	1. Normal creep recovery test 2. Nondestructive CSR test 3. Destructive CSR test	10°C 20°C 30°C	M9, M10, M11, M12, M13, M14, M15, M16, M17, M18, M19, M20

7.2 Variation of Material Properties in Controlled-Strain RDT Test

In Section 2, it is found that the tensile material properties which are measured in the tensile stress portion are different from the quasi-compressive material properties that are measured in the compressive stress portion in one loading cycle of the controlled-strain RDT test. This difference is due to the crack opening (crack growth) and crack closure (healing) in this loading cycle. Both of the material properties do not change in the nondestructive RDT tests, but change in the destructive RDT tests. These findings are verified for all asphalt mixtures, regardless of the type of asphalt binder, aggregate, air void content, and the aging period. As an example, the tensile and quasi-compressive complex moduli of the AAD mixtures are given in Figures 7.1 to 7.4. In the legend of all the figures in this section, the number "4%" or "7%" represents the air void content; the number "0", "3", or "6" represents the aging period. For example, "4%, 3" indicates that the air void content is 4% and the specimen is aged for 3 month.

7.3 Average Air Void Size and Number of Air Voids

In Section 4, the initial average crack size, or average air void size, and number of air voids calculated using the energy-based mechanistic approach are compared to those measured by the X-ray CT. The calculated average air void size is smaller than that measured by the X-ray CT since the measurement of the X-ray CT is flawed by its own limitations. This fact is also found for all the twenty types of asphalt mixtures. Comparison of the calculated and measured values is presented in Figures 7.5 and 7.6.

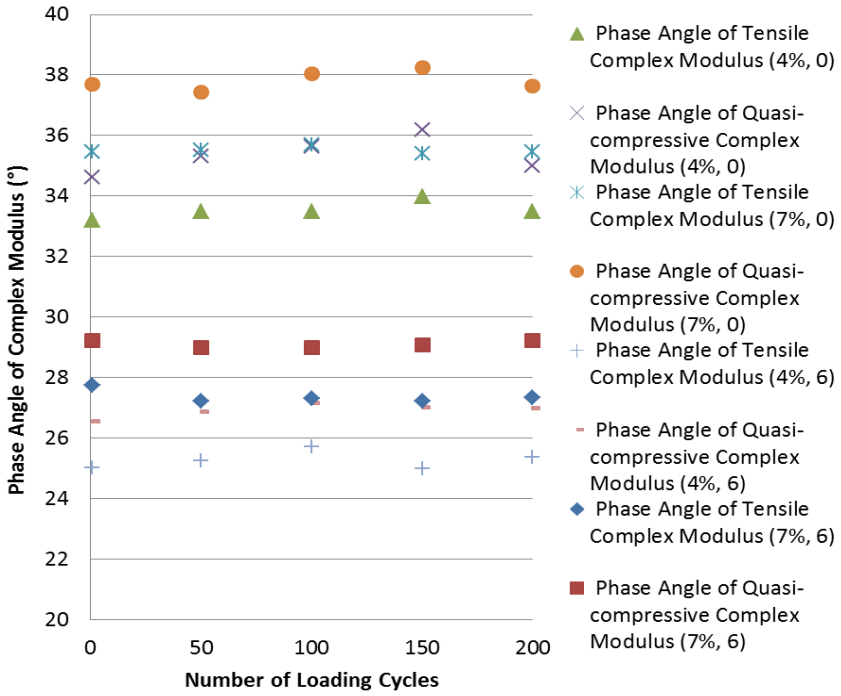

Figure 7.1 Phase Angle of Complex Modulus in Nondestrucitve RDT Test

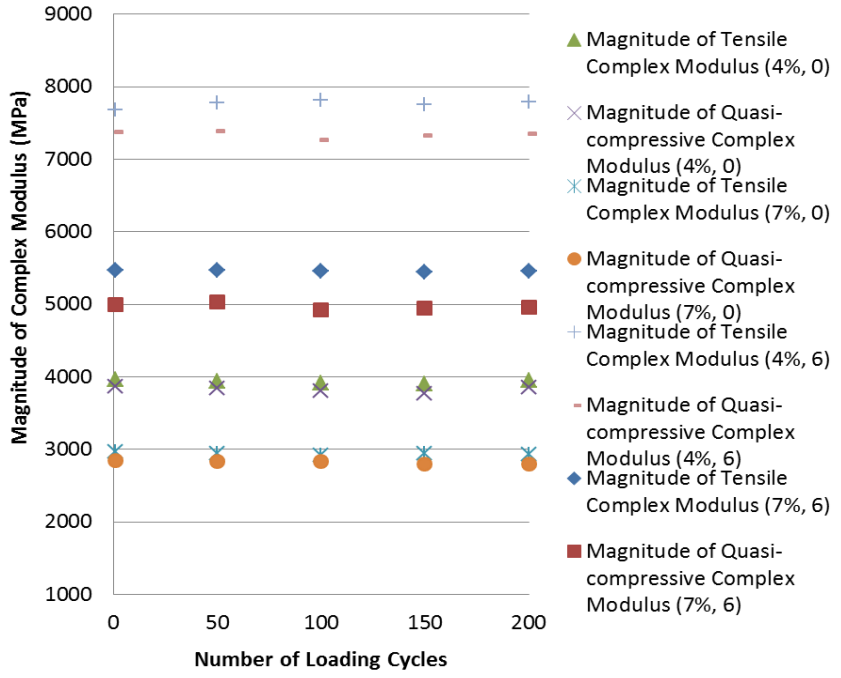

Figure 7.2 Magnitude of Complex Modulus in Nondestructive RDT Test

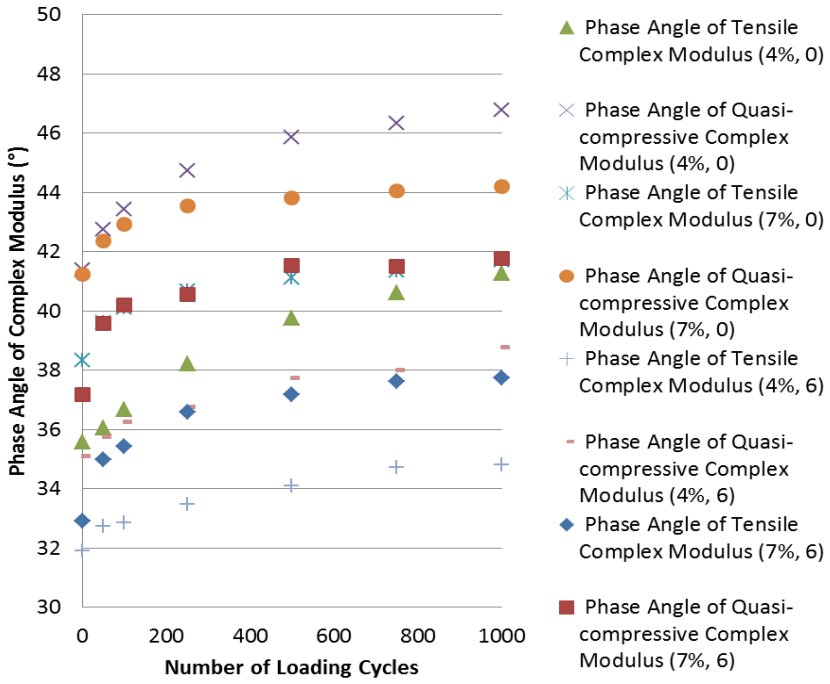

Figure 7.3 Phase Angle of Complex Modulus in Destrucitve RDT Test

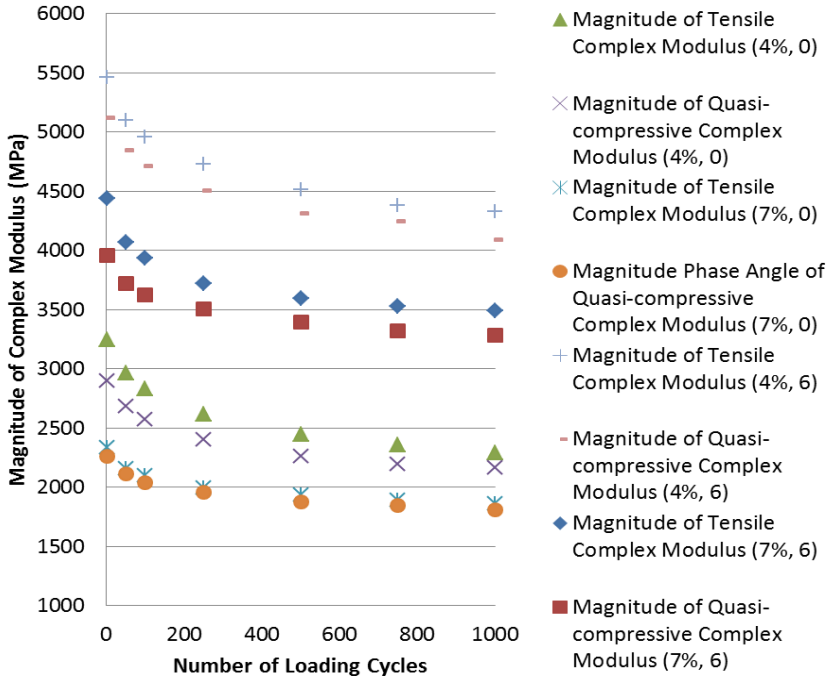

Figure 7.4 Magnitude of Complex Modulus in Destrucitve RDT Test

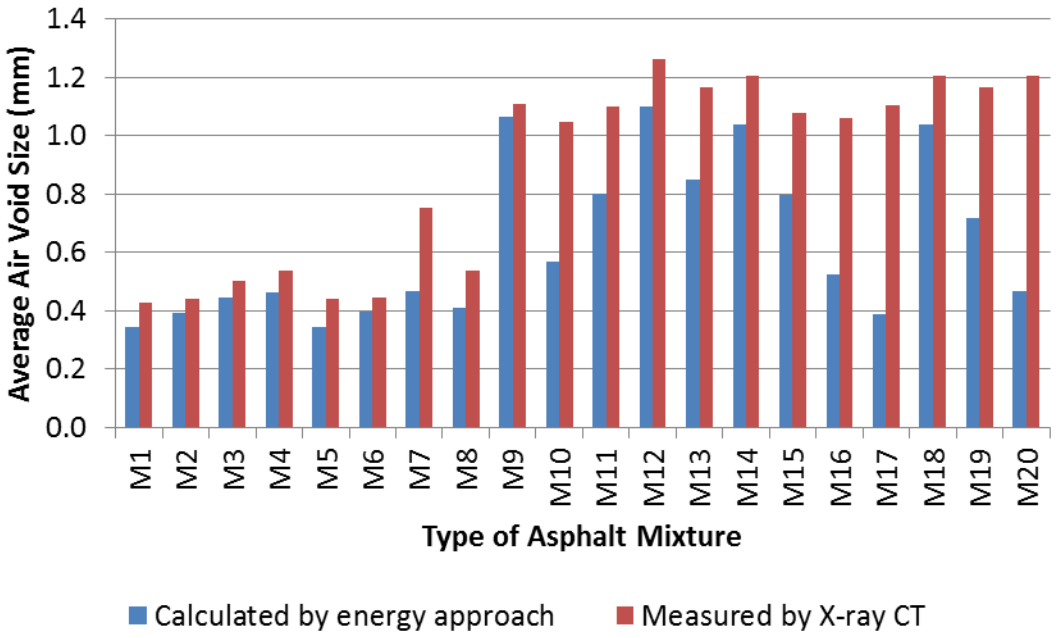

Figure 7.5 Calculated and Measured Average Air Void Size

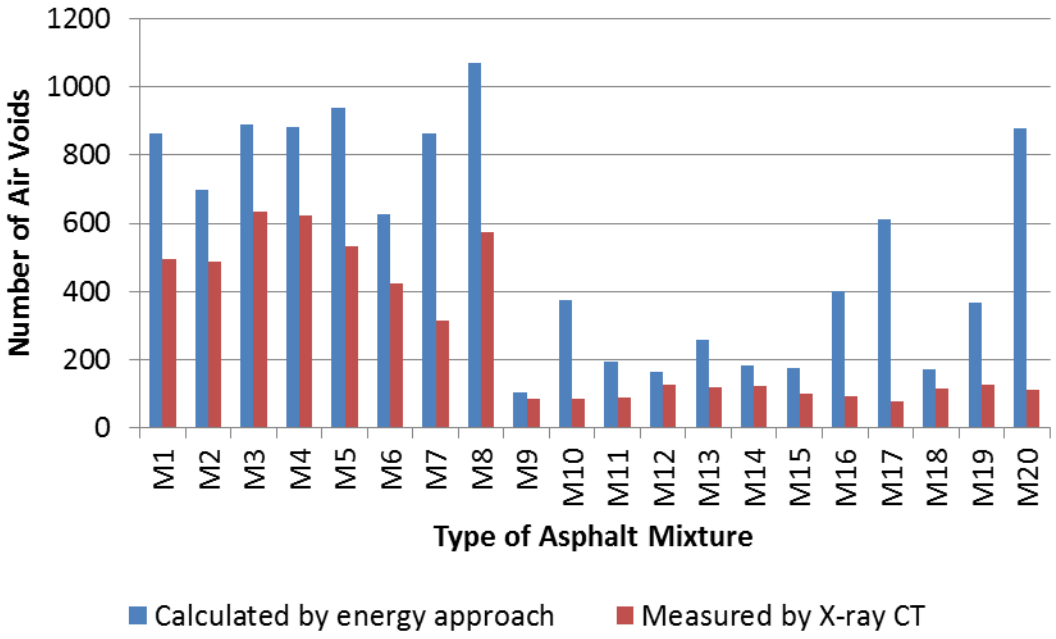

Figure 7.6 Calculated and Measured Number of Air Voids

7.4 Fatigue Resistance of Different Asphalt Mixtures

In Section 4, the development of fatigue cracking in an asphalt mixture specimen is described by the evolution of the damage density and the fracture coefficients associated with the evolution of the damage density, A' and n'. Plots of damage density versus the number of loading cycles are given in Figures 7.7 to 7.10 for AAD mixtures (M1, M2, M3, and M4), AAM mixtures (M5, M6, M7, and M8), NuStar mixtures (M9, M10, M11, M12, M13, and M14), and Valero mixtures (M15, M16, M17, M18, M19, and M20), respectively. The value of A' and n' of these twenty types of asphalt mixtures is given in Table 7.3. The value of n' represents the fatigue resistance of the asphalt mixture, which is used as index to evaluate the effect of asphalt binder, effect of air void content, and the effect of aging on different types of asphalt mixtures.

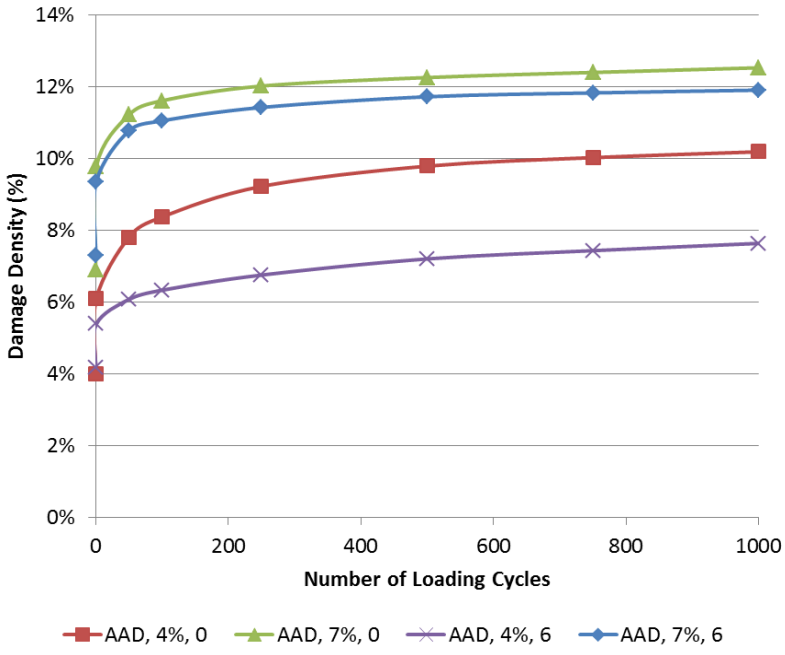

Figure 7.7 Evolution of Damage Density of AAD Asphalt Mixutres

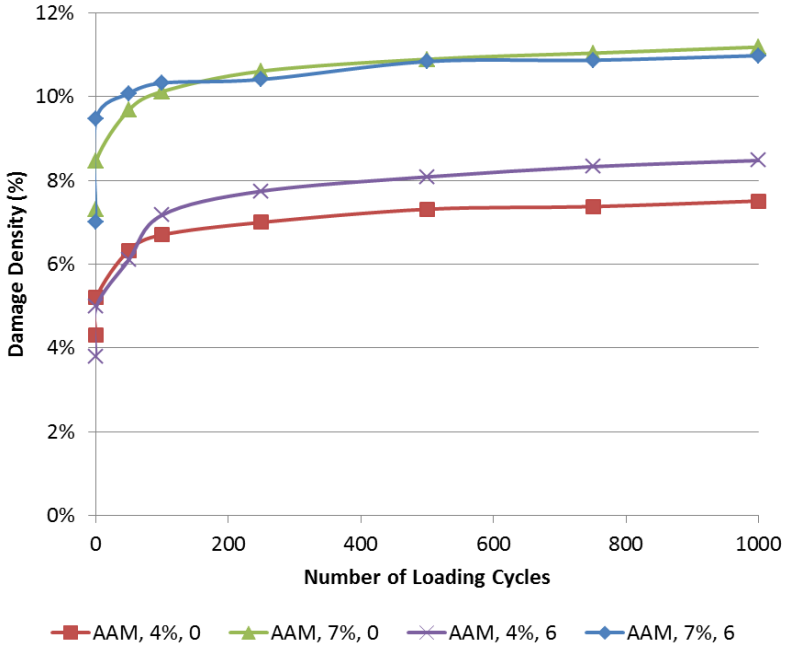

Figure 7.8 Evolution of Damage Density of AAM Asphalt Mixtures

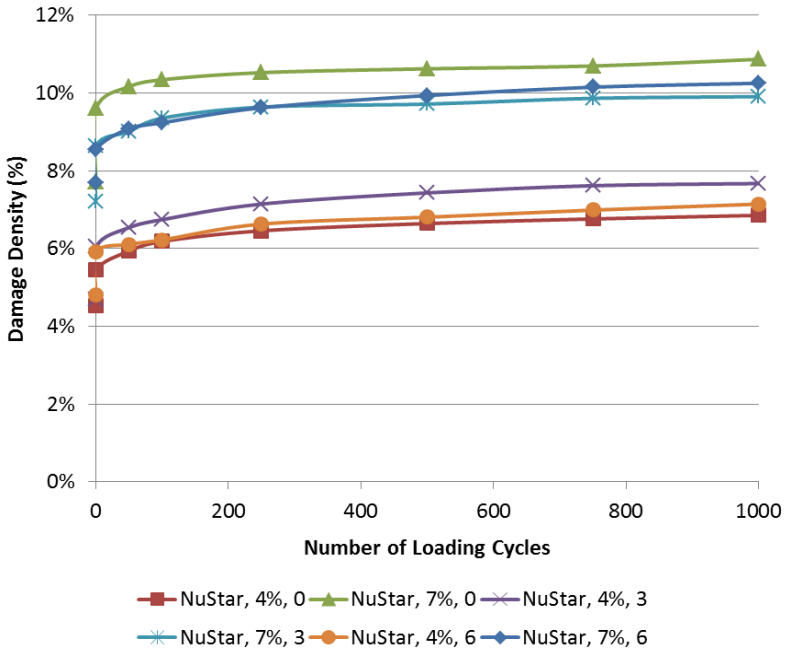

Figure 7.9 Evolution of Damage Density of NuStar Asphalt Mixtures

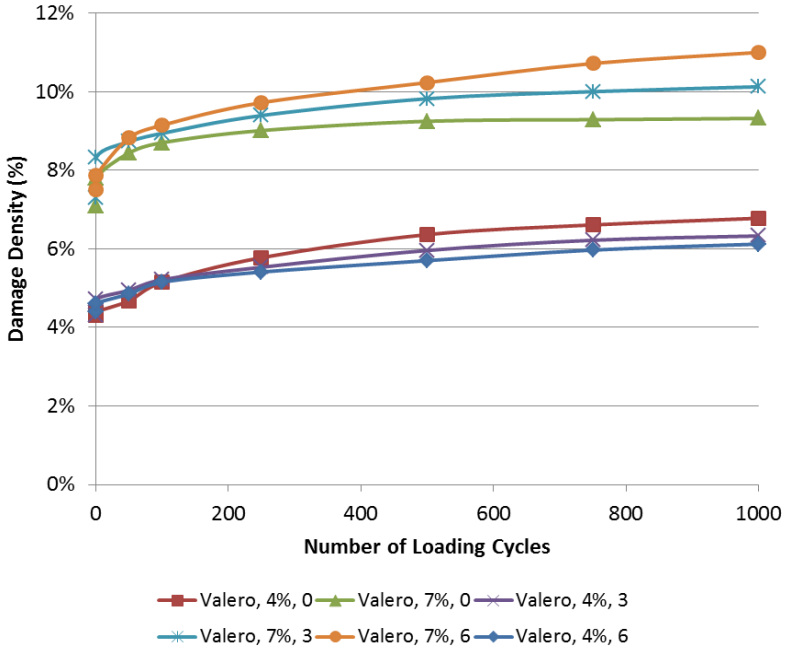

Figure 7.10 Evolution of Damage Density of Valero Asphalt Mixtures

Table 7.3 Fracture Coefficients for the Evolution of Damage Density

Type of Asphalt Mixture	A'	n'
M1	3.24×10^{-13}	4.86
M2	4.07×10^{-20}	7.34
M3	7.82×10^{-15}	6.84
M4	2.72×10^{-24}	9.43
M5	2.64×10^{-14}	5.98
M6	1.47×10^{-27}	10.34
M7	2.53×10^{-20}	7.84
M8	7.57×10^{-31}	14.57
M9	3.01×10^{-16}	6.48
M10	3.06×10^{-26}	9.12
M11	9.08×10^{-36}	13.27
M12	1.74×10^{-25}	11.52

Table 7.3 Continued

Type of Asphalt Mixture	A'	n'
M13	2.78×10^{-34}	13.52
M14	3.61×10^{-40}	14.37
M15	7.39×10^{-6}	1.11
M16	7.97×10^{-10}	2.35
M17	6.54×10^{-14}	4.01
M18	3.17×10^{-15}	5.77
M19	3.18×10^{-17}	6.29
M20	2.98×10^{-22}	7.48

7.4.1 Effect of Asphalt Binder on Fatigue Resistance

Variation of the fatigue resistance of the asphalt mixtures that is caused by different types of asphalt binder is studied here. Comparison of the fatigue resistance of the AAD mixtures and AAM mixtures is presented in Figure 7.11, which have the same aggregate, Texas limestone. The same comparison of the NuStar mixtures and Valero mixtures is presented in Figure 7.12, which have the same aggregate, Hanson limestone. These two figures indicate that the AAD mixtures have better resistance to fatigue cracking than the AAM mixtures; the Valero mixtures have much better resistance to fatigue cracking than the NuStar mixtures in all the unaged and aged conditions.

7.4.2 Effect of Air Void Content on Fatigue Resistance

Change of the fatigue resistance of the asphalt mixtures due to the change of the air void content is investigated here. Comparison of the fatigue resistance of all twenty types of asphalt mixtures is given in Figure 7.13. It shows that the asphalt mixtures with

7% air void content are always more susceptible to crack than those with 4% air void content under repeated loading.

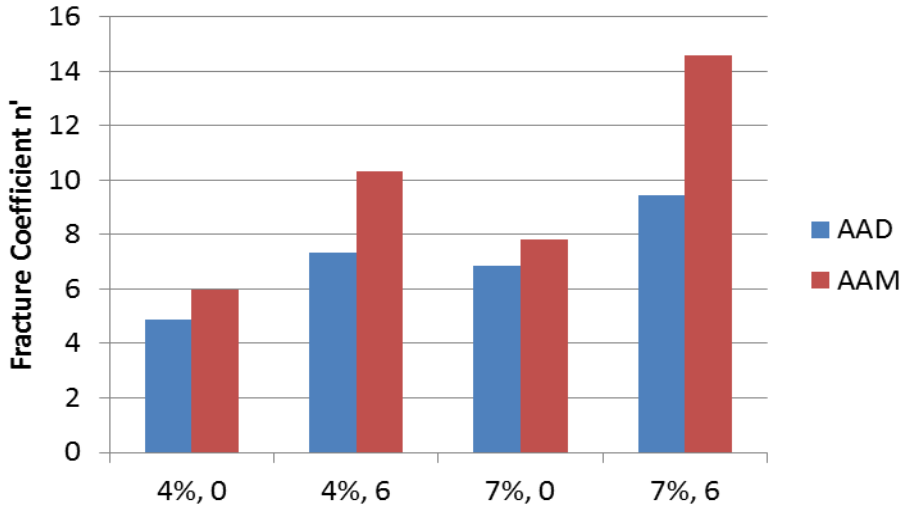

Figure 7.11 Comparison of Fatigue Resistance due to Asphalt Binder for AAD and AAM Asphlat Mixtures

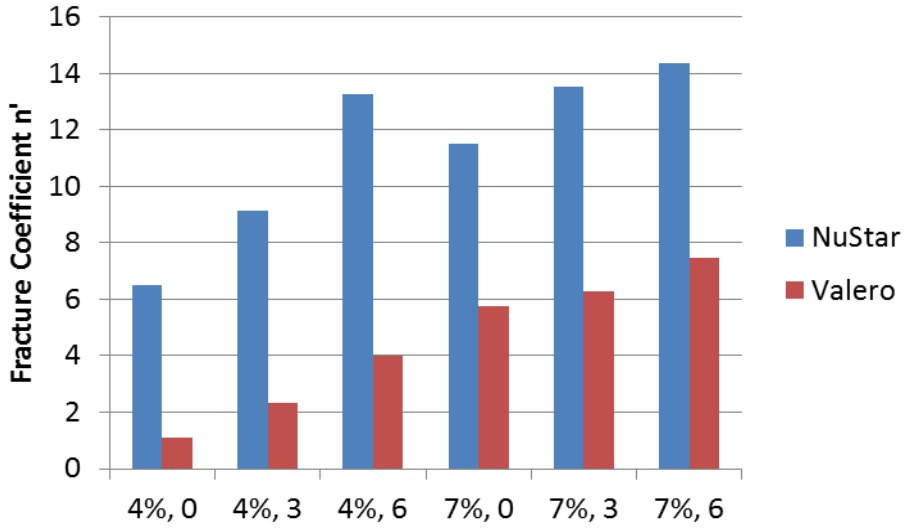

Figure 7.12 Comparison of Fatiuge Resistance due to Asphalt Binder for NuStar and Valero Asphalt Mixtures

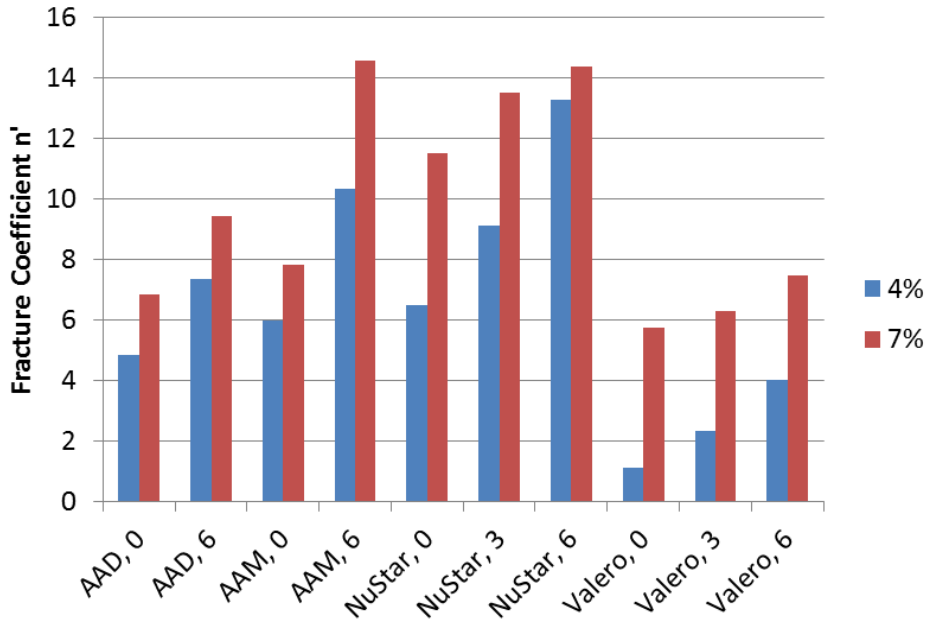

Figure 7.13 Comparison of Fatigue Resistance due to Air Void Content

7.4.3 Effect of Aging on Fatigue Resistance

The effect of aging on the fatigue resistance of the asphalt mixtures is investigated here and the results are presented in Figures 7.14 (AAD and AAM mixtures) and 7.15 (NuStar and Valero mixtures). It can be seen that the aged asphalt mixtures are more susceptible to fatigue cracking than unaged mixtures. The fatigue resistance of asphalt mixtures decreases with an increase of the aging period.

7.4.4 Relationship between A' and n'

A plot of $-\log(A')$ versus n' of all the twenty types of asphalt mixtures is shown in Figure 7.16, which demonstrates the high correlation between these two fracture coefficients. Furthermore, the twenty types of asphalt mixtures are divided to three categories according to the aging periods, and then in each category $-\log(A')$ is plotted

versus n'. A linear regression model is fitted to the dots of $-\log(A')$ versus n' for each category, which produced even higher R-square statistic as shown in Figure 7.17.

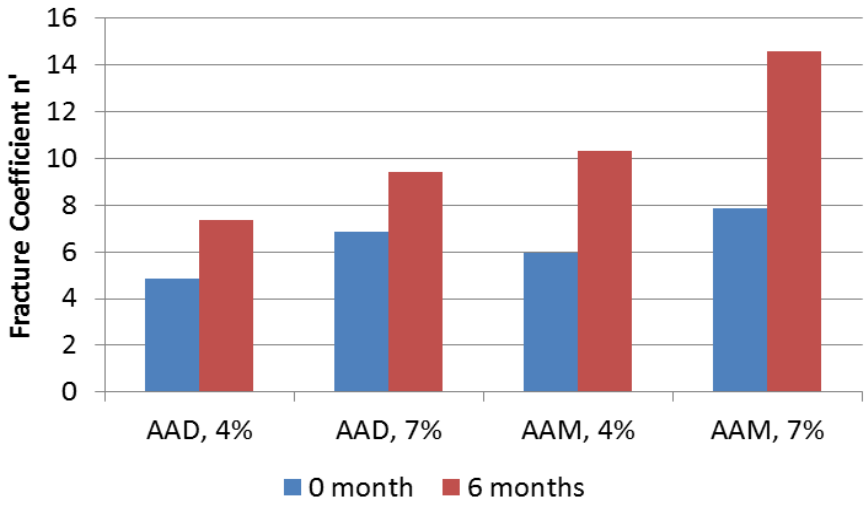

Figure 7.14 Comparison of Fatigue Resistance due to Aging for AAD and AAM Asphalt Mixtures

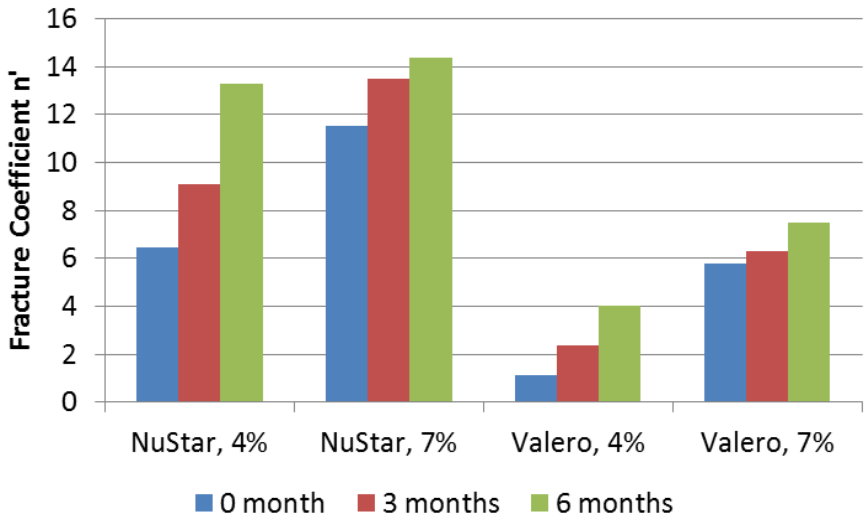

Figure 7.15 Comparison of Fatigue Resistance due to Aging for NuStar and Valero Asphalt Mixtures

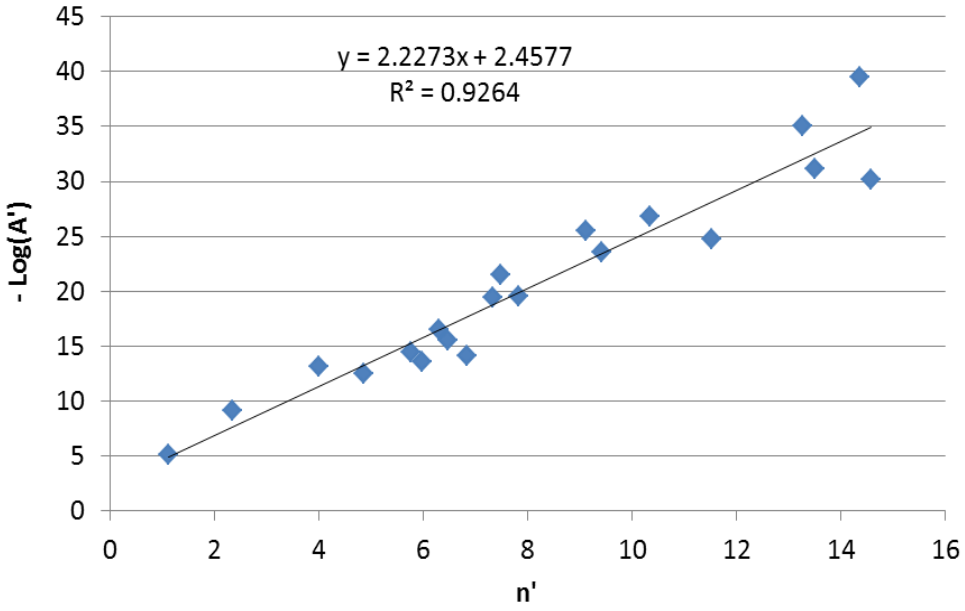

Figure 7.16 Correlation between A' and n'

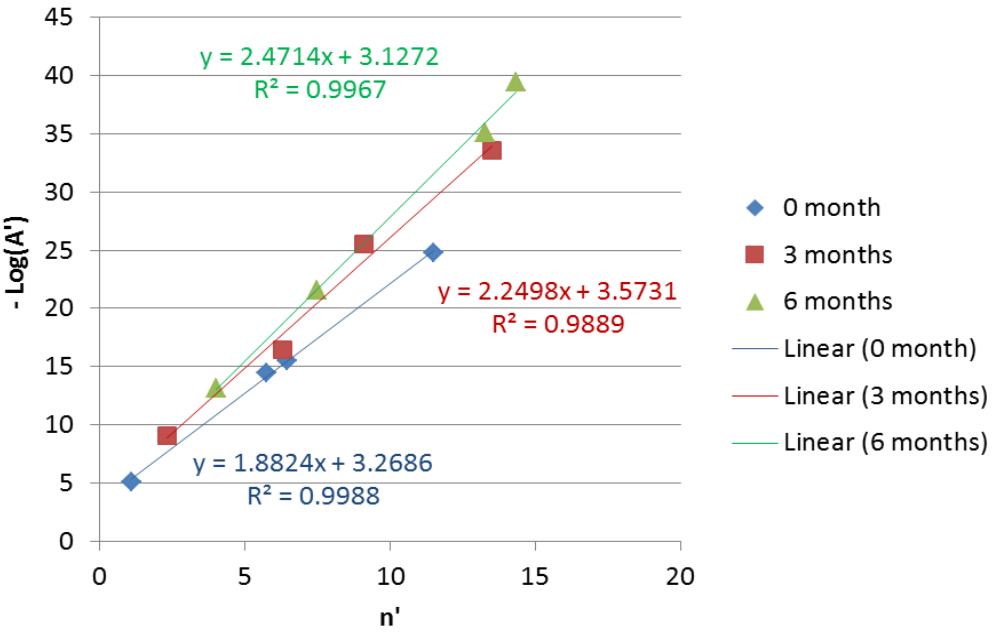

Figure 7.17 Relationship between A' and n' at Different Aging Periods

7.5 Recovery Modulus of Different Asphalt Mixtures

In Section 5, the recovery modulus is defined to describe the recovery behavior of the asphalt mixture in the unloading phase. The effect of loading level, the effect of temperature, and the effect of aging on the recovery modulus of the asphalt mixture are studied here.

7.5.1 Effect of Loading Level on Recovery Modulus

It has been proven in Section 5 that the recovery modulus of two types of asphalt mixtures (M1 and M5 in Table 7.1) does not change in the nondestructive CSR test, but it becomes different in the destructive CSR test. In this section, this phenomenon is examined and proven to be true for all other types of mixtures in Table 7.1. As an example, the recovery modulus of M6 mixtures (AAM, 4%, 6) is given in Figure 7.18.

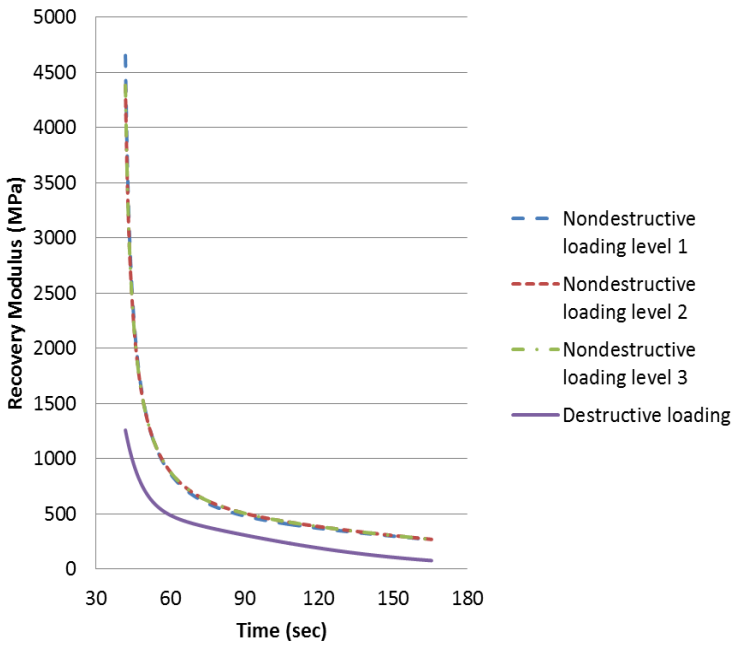

Figure 7.18 Recovery Modulus at Different Loading Levels

7.5.2 Effect of Air Void Content on Recovery Modulus

In general, an increase of the air void content results in the reduction in the modulus of asphalt mixtures. After examining all of the twenty types of asphalt mixtures in Table 7.1 at different temperatures and different aging periods, this statement is also applicable to the recovery modulus that is calculated by the internal stress. An example is presented in Figure 7.19. In the legend of Figure 7.15, "20C" is the temperature. For example, "NuStar, 4%, 0, 20C" means that this asphalt mixture specimen has Nustar binder and 4% air void content; it is unaged (0 month); and this test is conducted at 20°C.

7.5.3 Effect of Temperature on Recovery Modulus

The change of the recovery modulus of the asphalt mixture that is caused by the change of the temperature is investigated here. For all the twenty types of asphalt mixtures in Table 7.1, the recovery modulus at 10°C is the largest and the recovery modulus at 30°C is the smallest. This finding suggests that the recovery modulus calculated by the internal stress has the same feature as other moduli calculated by the external forces: it is temperature dependent and increases as the temperature decreases. Two examples are given in Figures 7.20 and 7.21.

7.5.4 Effect of Aging on Recovery Modulus

The effect of aging on the recovery modulus of the asphalt mixtures is studied here. It is found that the recovery modulus of all the twenty types of asphalt mixtures in Table 7.1 becomes larger as the aging period increases. This feature is also the same as the modulus calculated by the external force, such as the relaxation modulus. Two examples are given in Figures 7.22 and 7.23.

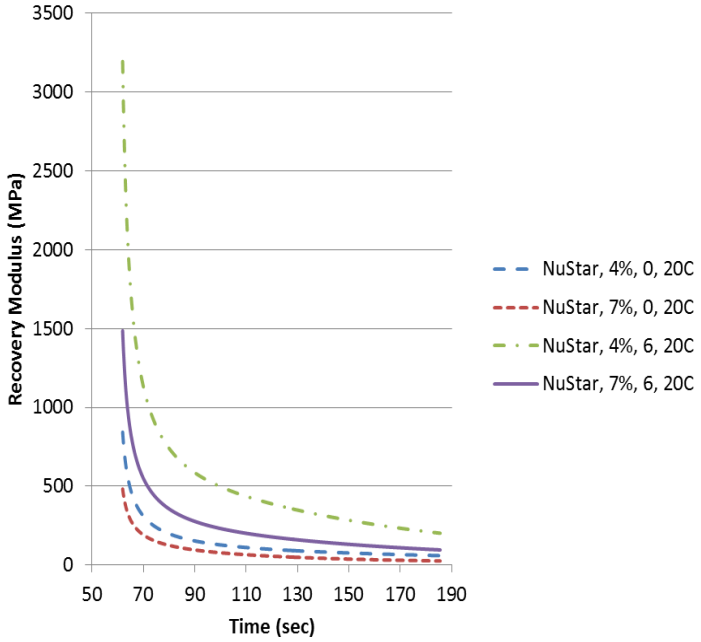

Figure 7.19 Recvoery Modulus of Asphalt Mixutres with Different Air Void Contents

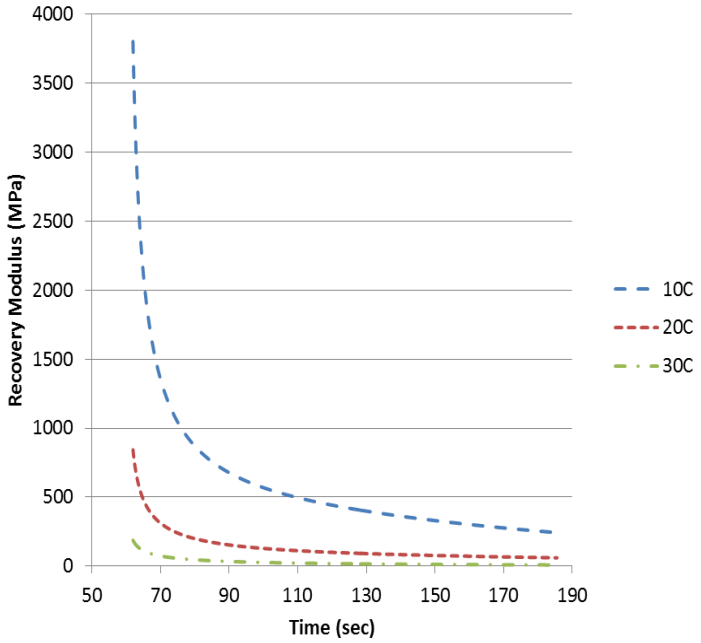

Figure 7.20 Recovery Modulus at Different Temperatures (NuStar, 4%, 0)

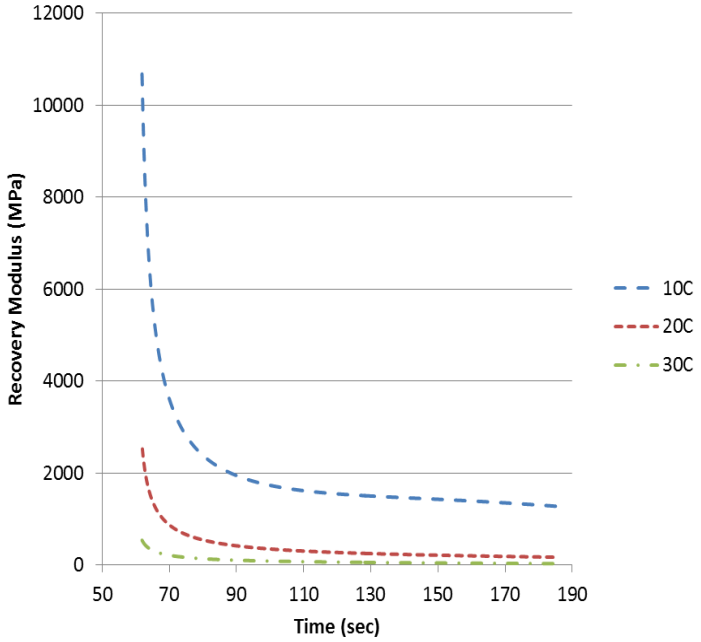

Figure 7.21 Recovery Modulus at Different Temperatures (Valero, 7%, 6)

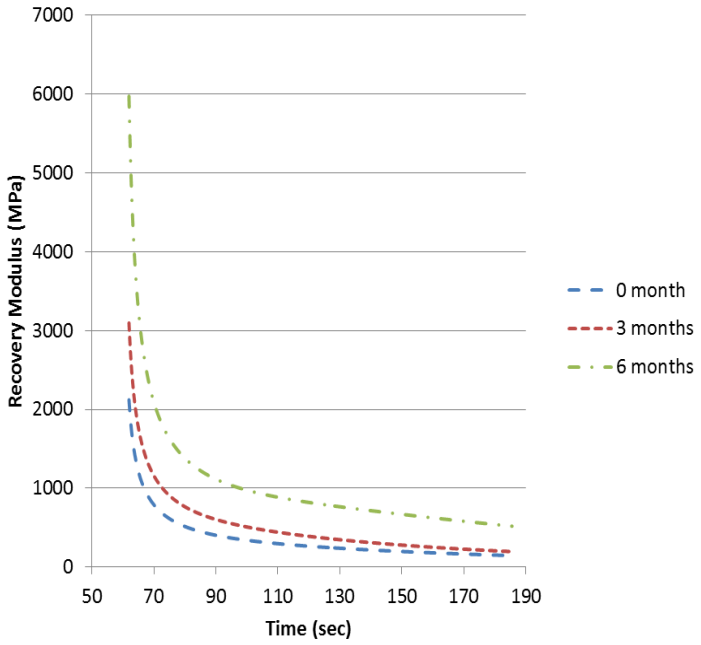

Figure 7.22 Recovery Modulus at Different Aging Periods (NuStar, 7%, 10C)

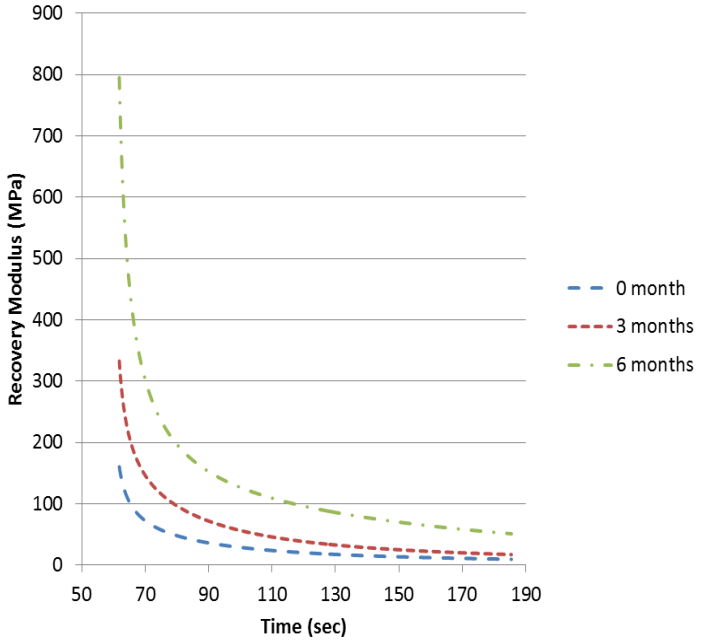

Figure 7.23 Recovery Modulus at Different Aging Periods (Valero, 4%, 30C)

7.6 Healing Ability of Different Asphalt Mixtures

In Section 6, the healing process in an asphalt mixture specimen is described by the decrease of the damage density with time during the recovery phase. The measured damage density in the healing process is used to produce the healing curve, and then the short-term healing rate, long-term healing rate, and the healing rate scale can be determined based on the determined healing curve. The healing curves of for AAD mixtures, AAM mixtures, NuStar mixtures, and Valero mixtures are presented in Figures 7.24 to 29, respectively. The healing rates obtained from the healing curves are used as indices to evaluate the healing ability of different asphalt mixtures, including different asphalt binders, air void contents and aging periods, and examine the effect of temperature on the healing ability of the asphalt mixture.

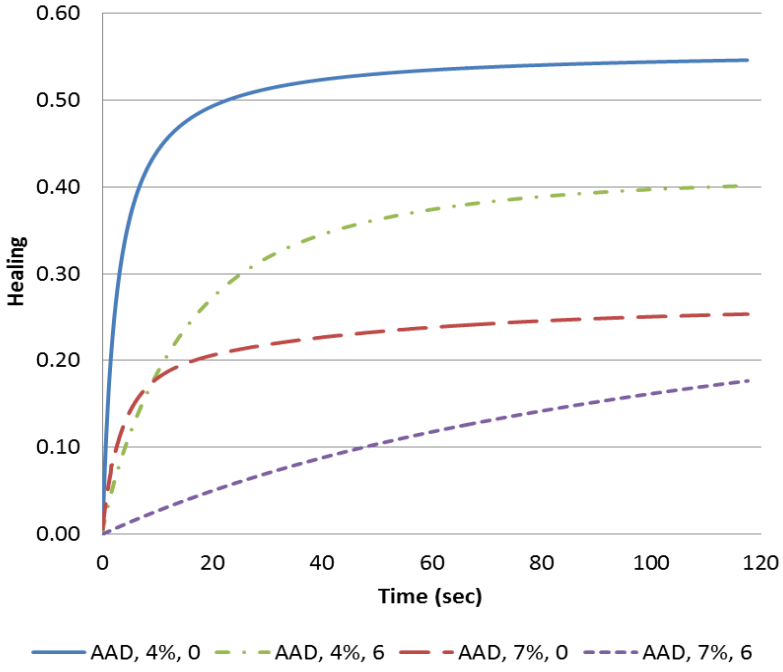

Figure 7.24 Healing Curves of AAD Asphalt Mixtures

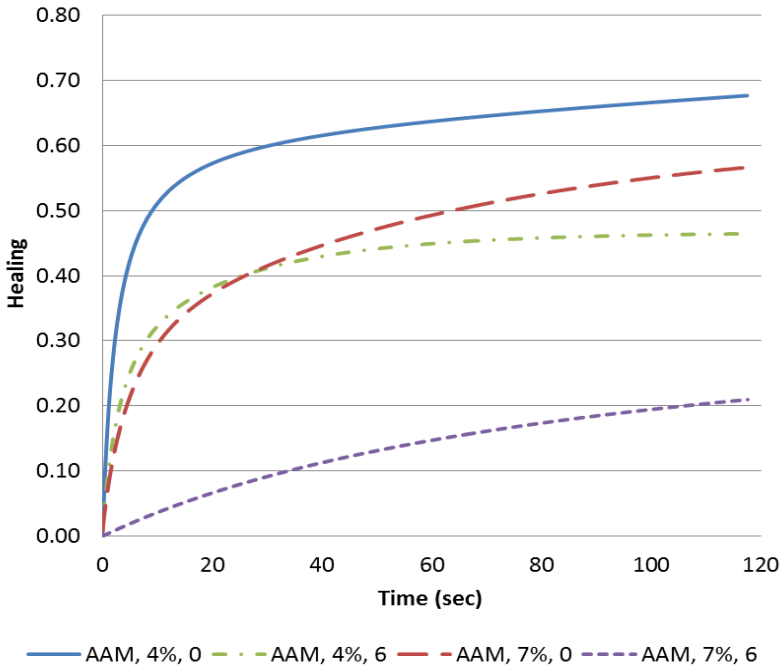

Figure 7.25 Healing Curves of AAM Asphalt Mixtures

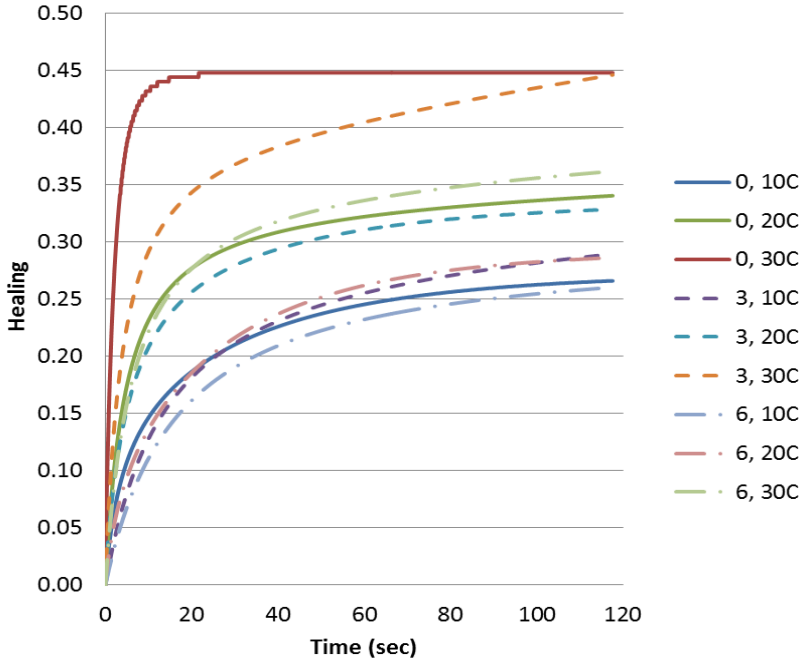

Figure 7.26 Healing Curves of NuStar Asphalt Mixtures with 4% Air Void Content

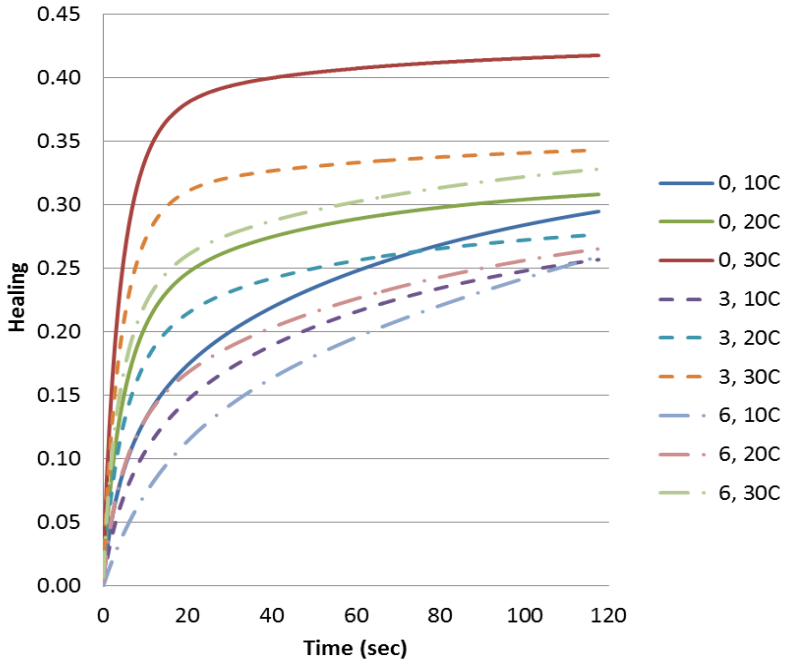

Figure 7.27 Healing Curves of NuStar Asphalt Mixture with 7% Air Void Content

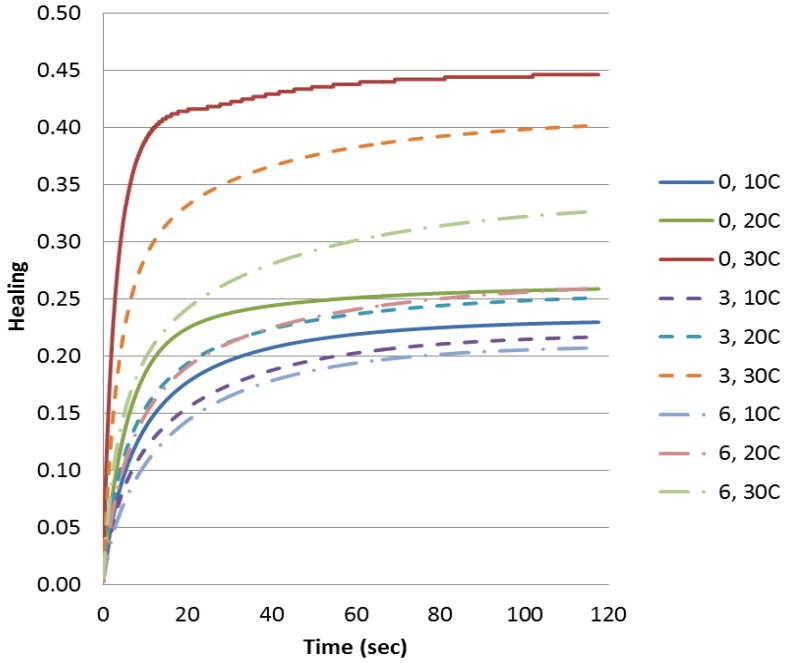

Figure 7.28 Healing Curves of Valero Asphalt Mixtures with 4% Air Void Content

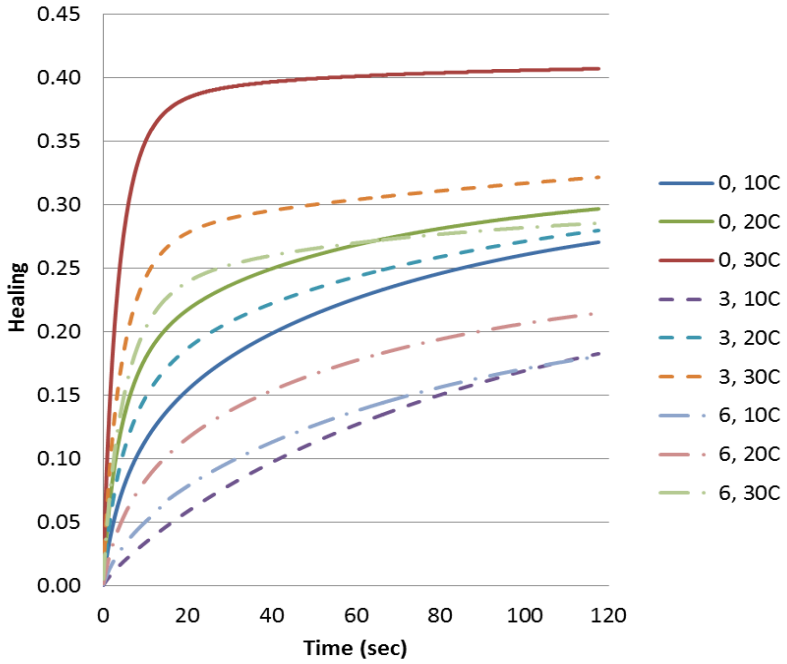

Figure 7.29 Healing Curves of Valero Asphalt Mixtures with 7% Air Void Content

7.6.1 Effect of Asphalt Binder on Healing Ability

Variation of the healing ability that is caused by different types of asphalt binder is studied and the results are given in Figures 7.30 to 7.33, which use the short-term healing rate and healing rate scale to evaluate the healing ability. Comparing AAD and AAM mixtures, which have the same aggregate, both the short-term healing rate and the healing rate scale of AAM mixtures are larger than those of AAD mixtures. Therefore, it concludes that the AAM mixtures have better healing ability than AAD mixtures. Comparing Nustar and Valero mixtures, which have the same aggregate, the NuStar mixtures have better healing ability than Valero mixtures.

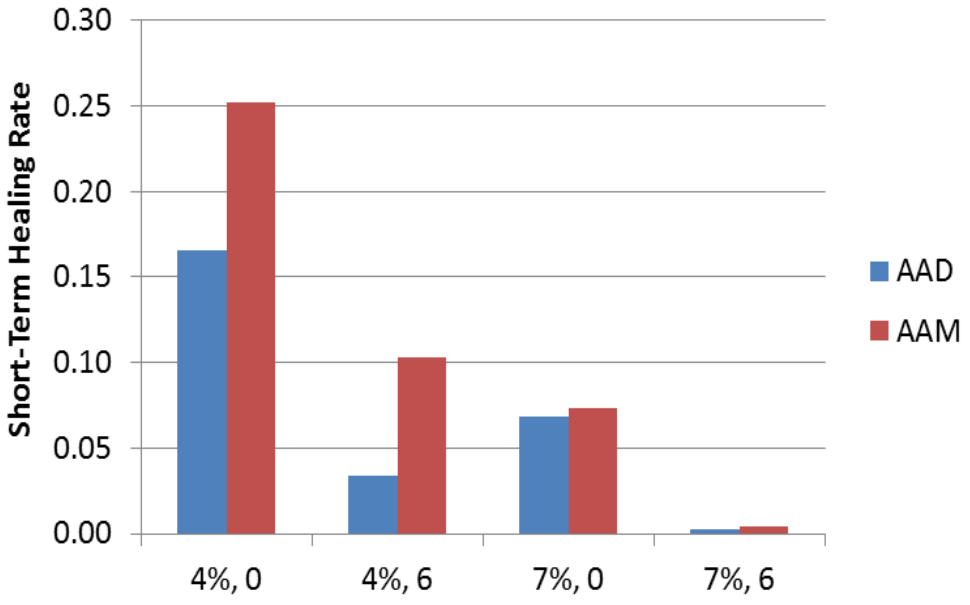

Figure 7.30 Short-Term Healing Rate of AAD and AAM Mixtures

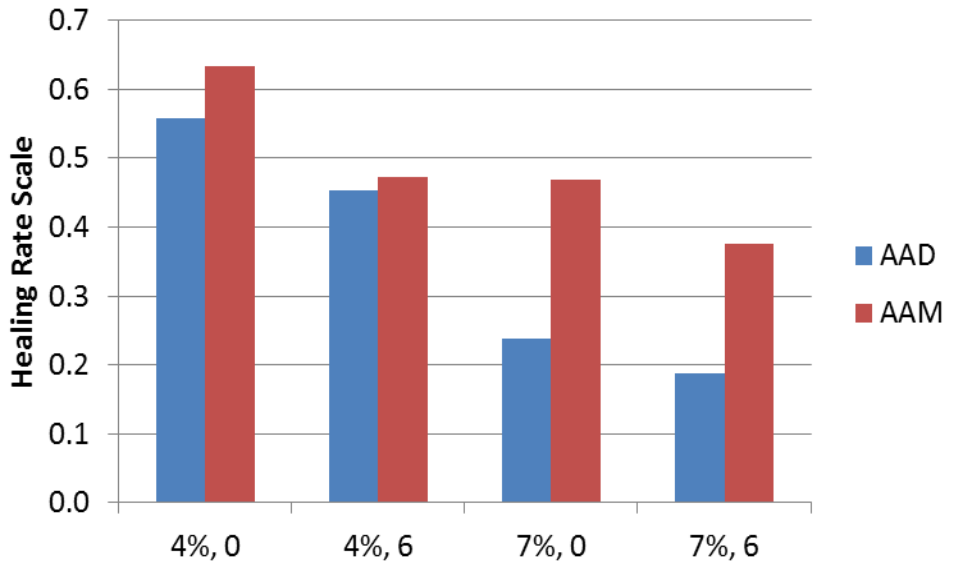

Figure 7.31 Healing Rate Scale of AAD and AAM Mixtures

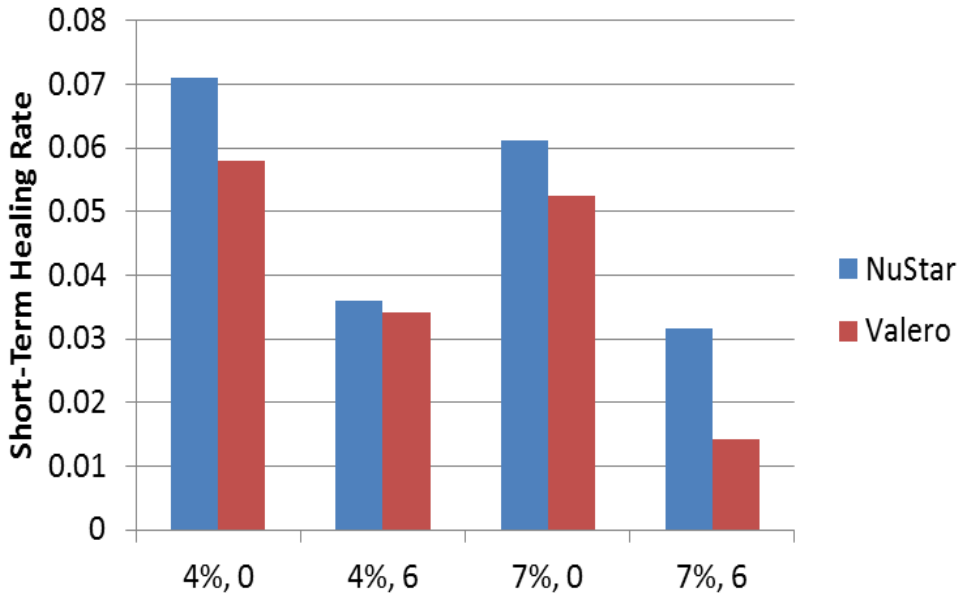

Figure 7.32 Short-Term Healing Rate of NuStar and Valero Mixtures

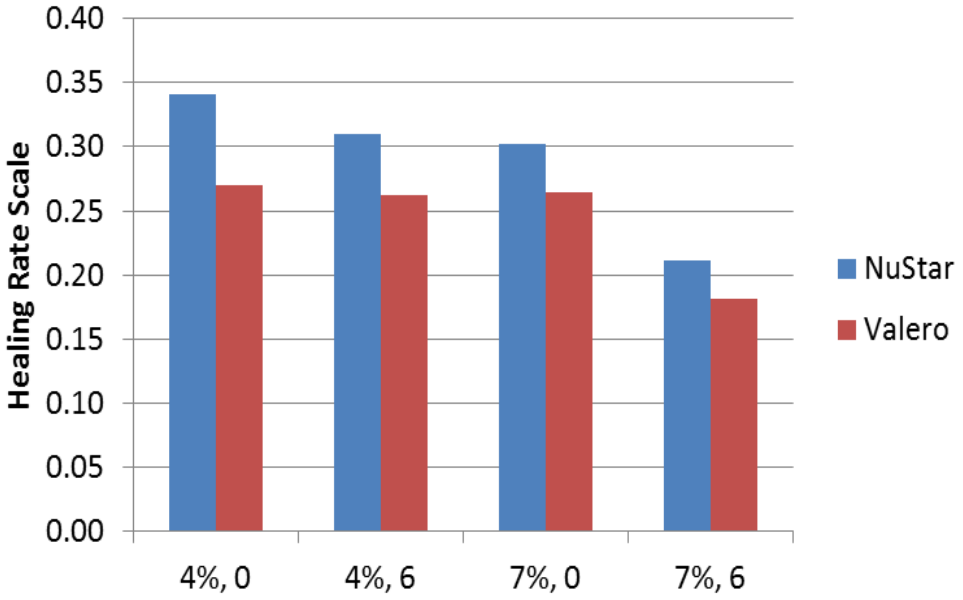

Figure 7.33 Healing Rate Scale of NuStar and Valero Mixtures

7.6.2 Effect of Air Void Content on Healing Ability

The effect of the air void content on healing ability of asphalt mixtures is examined by comparing the short-term healing rate and healing rate scale of asphalt mixtures with 4% air void content to those of asphalt mixtures with 7% air void content. Figures 7.34 and 7.35 shows the result of this comparison based on the short-term healing rate and healing rate scale, respectively. These two figures suggest that the asphalt mixtures with 4% air void content always have better healing ability than those with 7% air void content, regardless the type of asphalt binder, aging, and temperature.

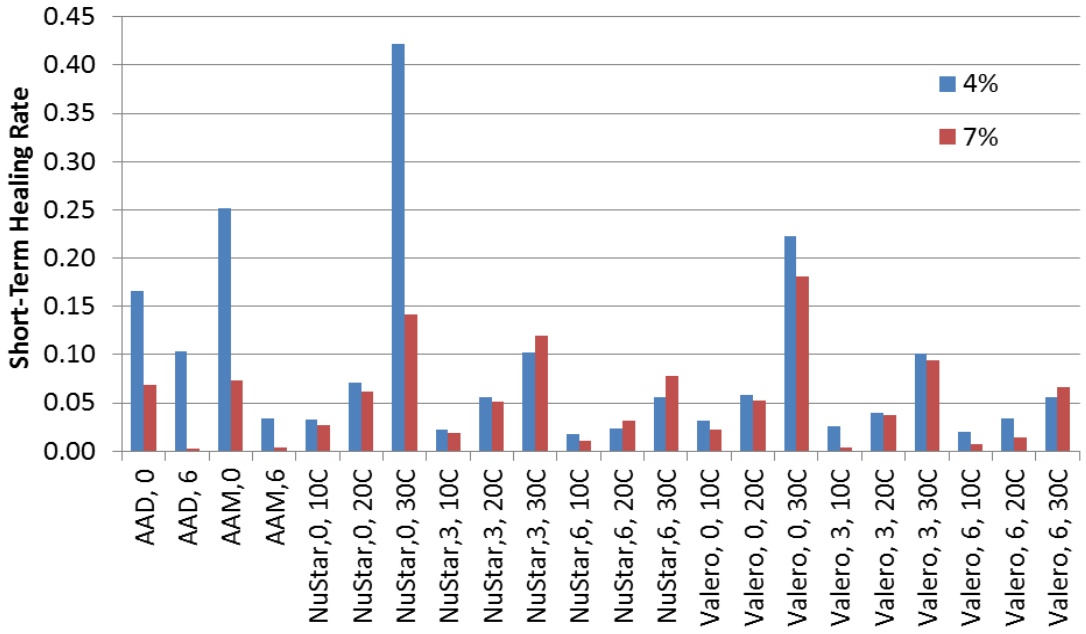

Figure 7.34 Comparison of Healing Ability due to Air Void Content by Short-Term Healing Rate

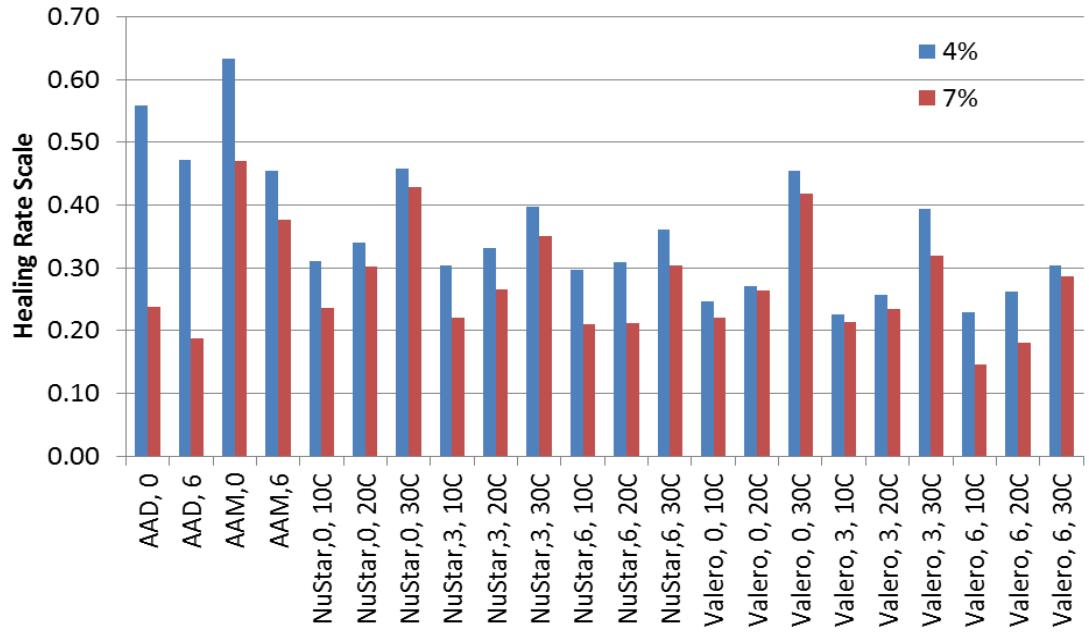

Figure 7.35 Comparison of Healing Ability due to Air Void Content by Healing Rate Scale

7.6.3 Effect of Temperature on Healing Ability

The change of the healing ability due to the change of temperature is investigated by comparing the short-term healing rate and healing rate scale at 10, 20, and 30°C. The results shown in Figures 3.36 and 3.37 indicate that the temperature has significant influence on the healing ability of the asphalt mixtures: the healing ability is the highest at 30°C and it decreases rapidly when the temperature decreases; the healing of asphalt mixtures at 10°C is much slower and the extent is smaller. This fact can also be observed from Figures 24 to 27, in which the shape of the healing curve changes significantly from 30°C to 20°C and then to 10°C.

7.6.4 Effect of Aging on Healing Ability

Aging also plays an important role in evaluating the healing ability of asphalt mixtures, as shown in Figures 7.38 to 7.41. Both the short-term healing and healing rate scale decreases as the aging period increases. Especially, there is a considerable reduction of the short-term healing rate from unaged asphalt mixtures to those aged for 6 months. This fact suggests that the healing speed becomes smaller and smaller as the aging time increases.

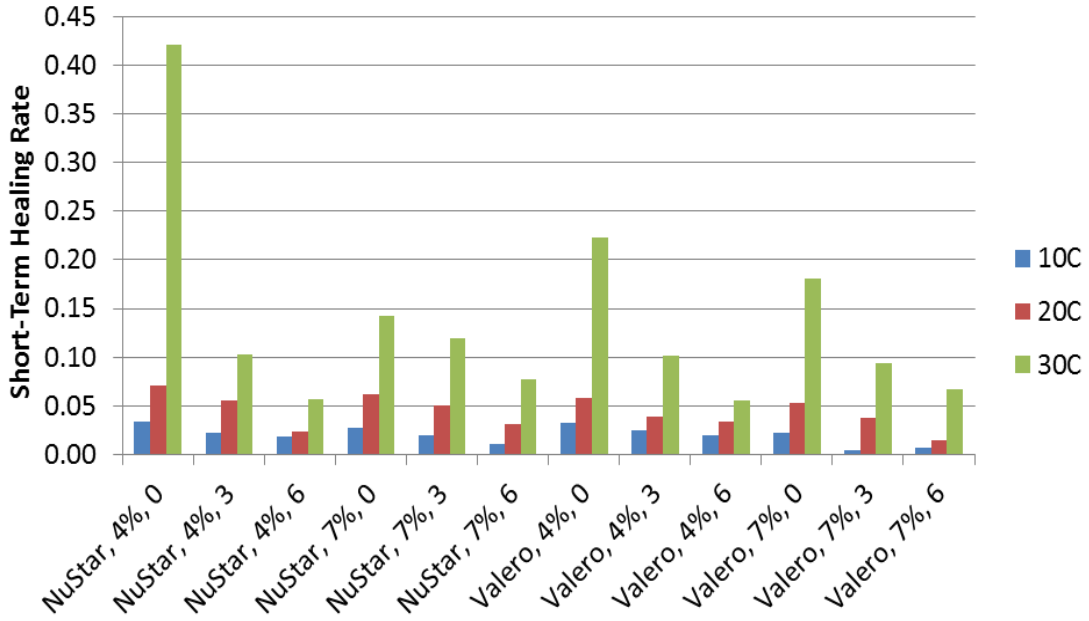

Figure 7.36 Comparison of Healing Ability due to Temperature by Short-Term Healing Rate

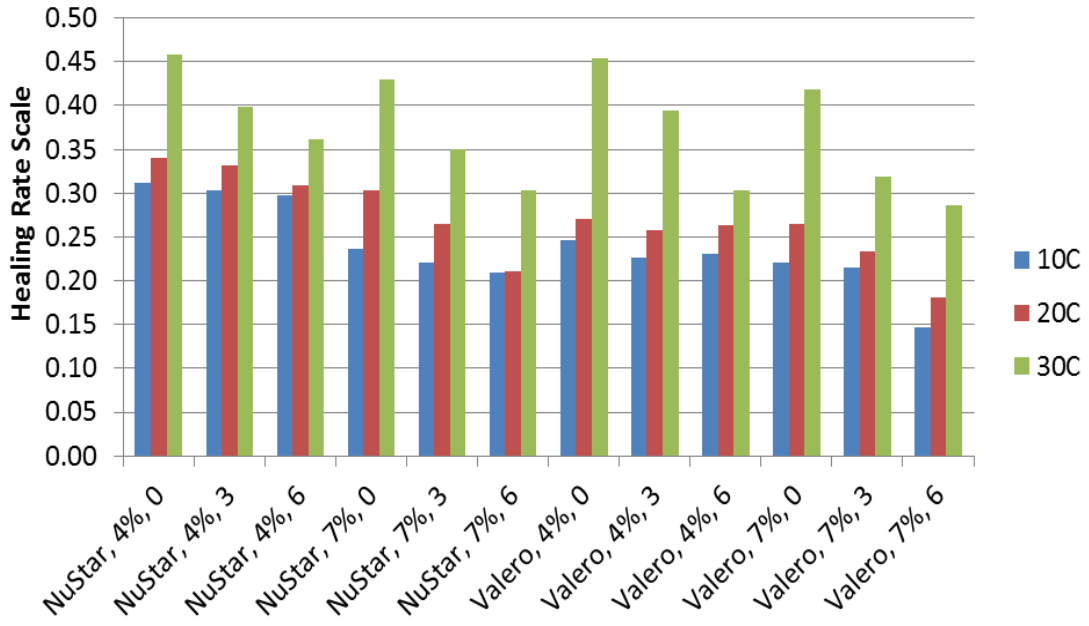

Figure 7.37 Comparison of Healing Ability due to Temperature by Healing Rate Scale

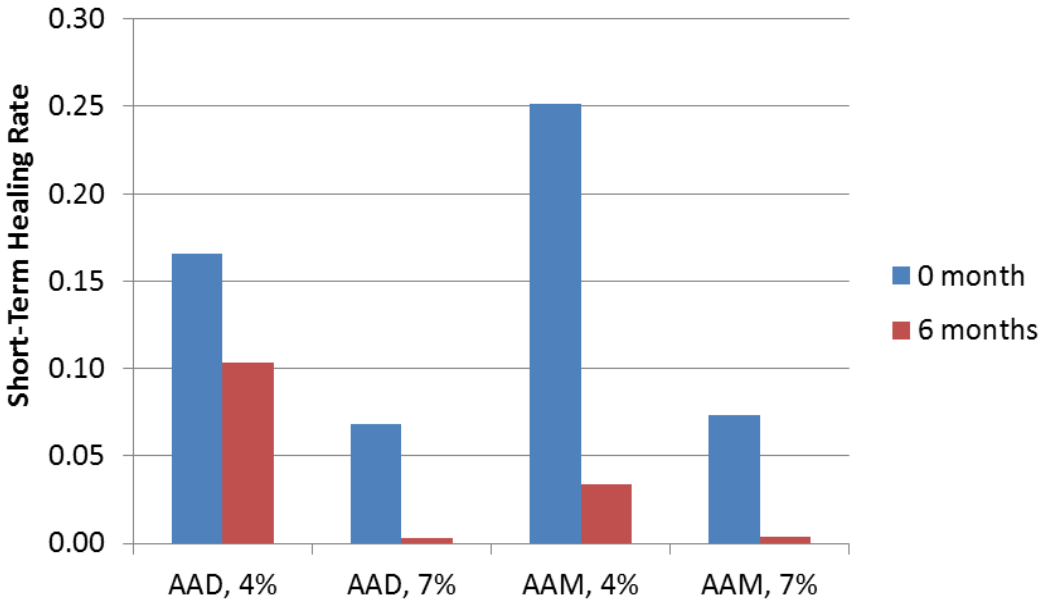

Figure 7.38 Comparison of Healing Ability due to Aging for AAD and AAM Mixtures by Short-Term Healing Rate

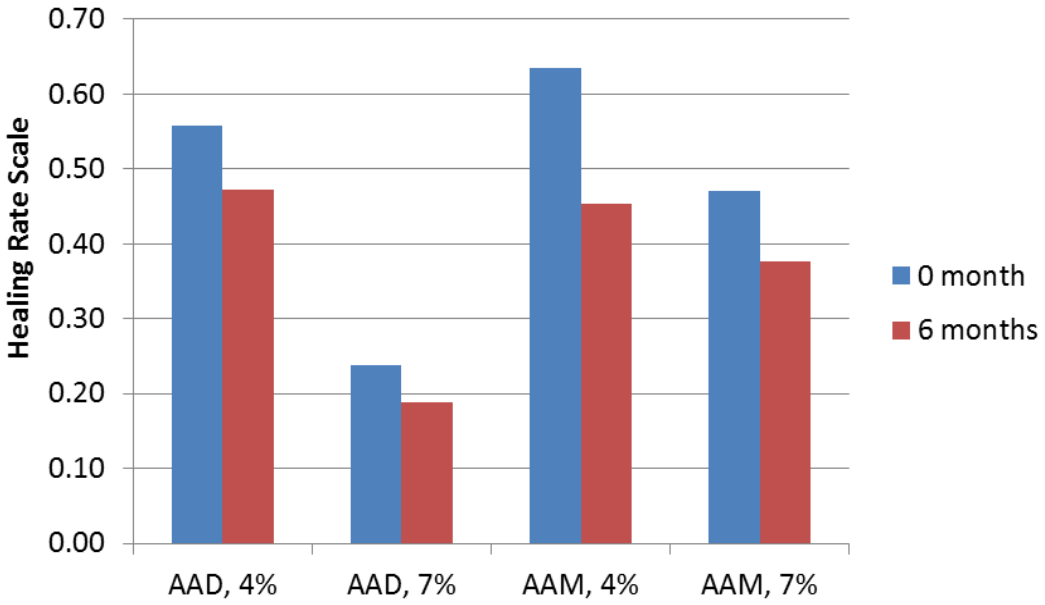

Figure 7.39 Comparison of Healing Ability due to Aging for AAD and AAM Mixtures by Healing Rate Scale

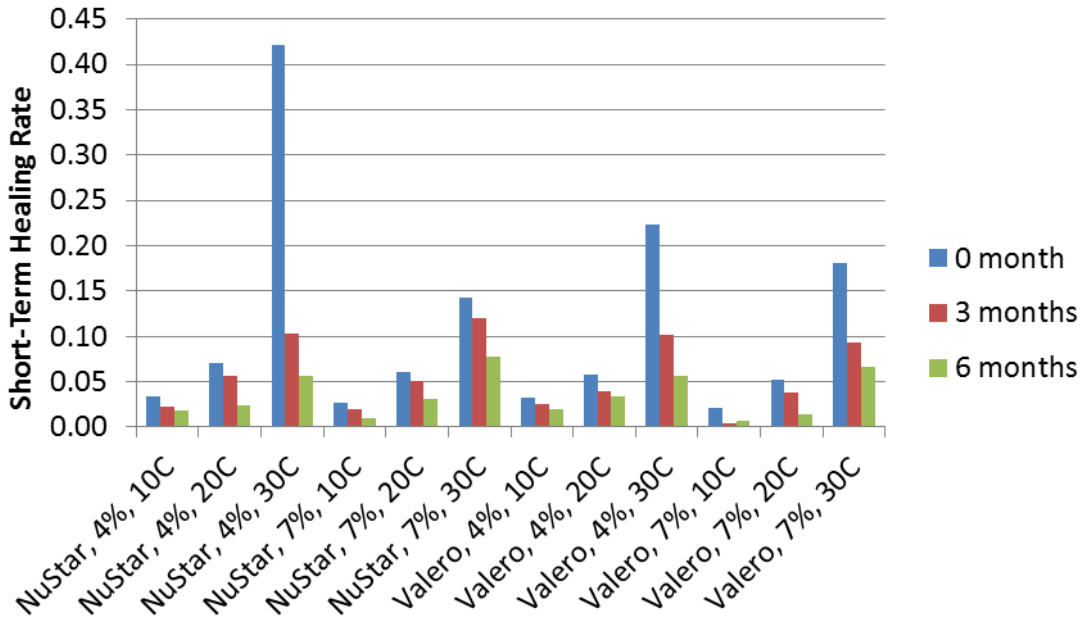

Figure 7.40 Comparison of Healing Ability due to Aging for NuStar and Valero Mixtures by Short-Term Healing Rate

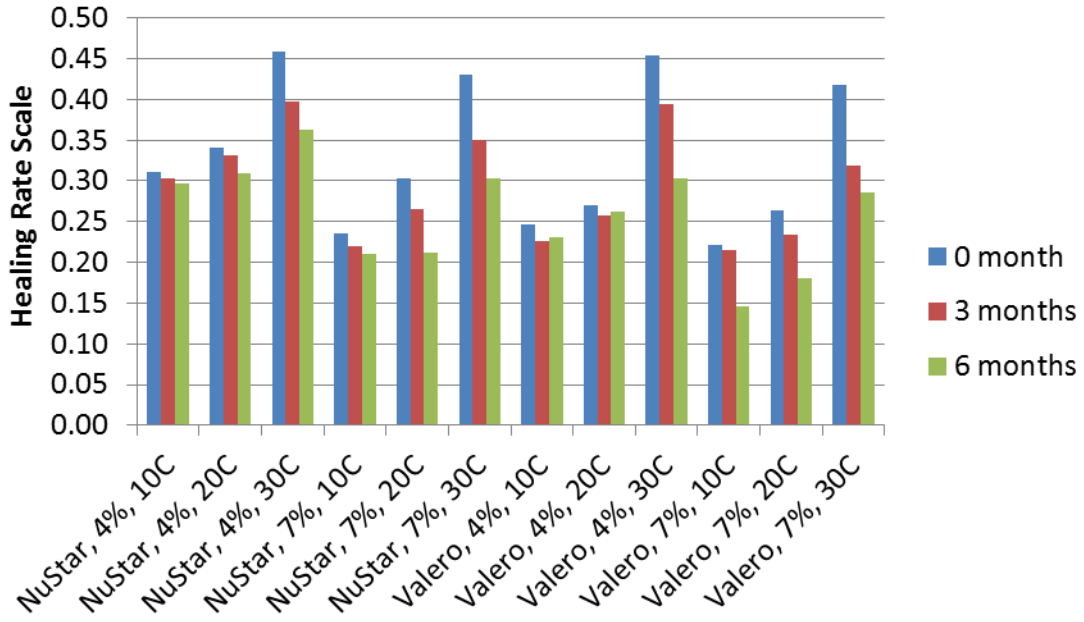

Figure 7.41 Comparison of Healing Ability due to Aging for NuStar and Valero Mixtures by Healing Rate Scale

7.7 Predict Healing Rates Using Fundamental Material Properties

In order to predict the healing rates ($\dot{h}_1$, $\dot{h}_2$, and h_β) based on fundamental material properties, they are formulated using the following equations:

$$\dot{h}_1 = a_1 \left(\frac{1}{\Delta G^{LW} E_1} \right)^{b_1 \kappa} \tag{7.1}$$

$$-\log\left(\dot{h}_2\right) = a_2 \left[-\log\left(\frac{\Delta G^{AB}}{E_1} \right) \right]^{b_2 \kappa} \tag{7.2}$$

$$h_\beta = a_\beta \left(\frac{\Delta G^{AB}}{\Delta G^{LW} E_1^{\,2}} \right)^{(1-h_0) b_\beta \kappa} \tag{7.3}$$

where ΔG^{LW} is non-polar surface bond energy; ΔG^{AB} is polar surface bond energy; E_1 and κ are fitting parameters for the relaxation modulus of undamaged asphalt mixtures; h_0 is the initial damage density; a_1 and b_1 are fitting parameters for $\dot{h}_1$; a_2 and b_2 are fitting parameters for $\dot{h}_2$; a_β and b_β are fitting parameters for h_β. Figures 7.42 to 7.44 show an example of fitting by Equation 7.1, 7.2, and 7.3, respecitvely. Take Figure 7.42 for example. The data of a_1 versus $b_1\kappa$ of unaged asphalt mixtures (0 month) is fitted using a linear regression function; the data of a_1 versus $b_1\kappa$ of aged asphalt mixtures for 3 months and 6 months is fitted by other two linear regression functions, respectively. The R-squared statistics shows the goodness of fitting by the linear regression function.

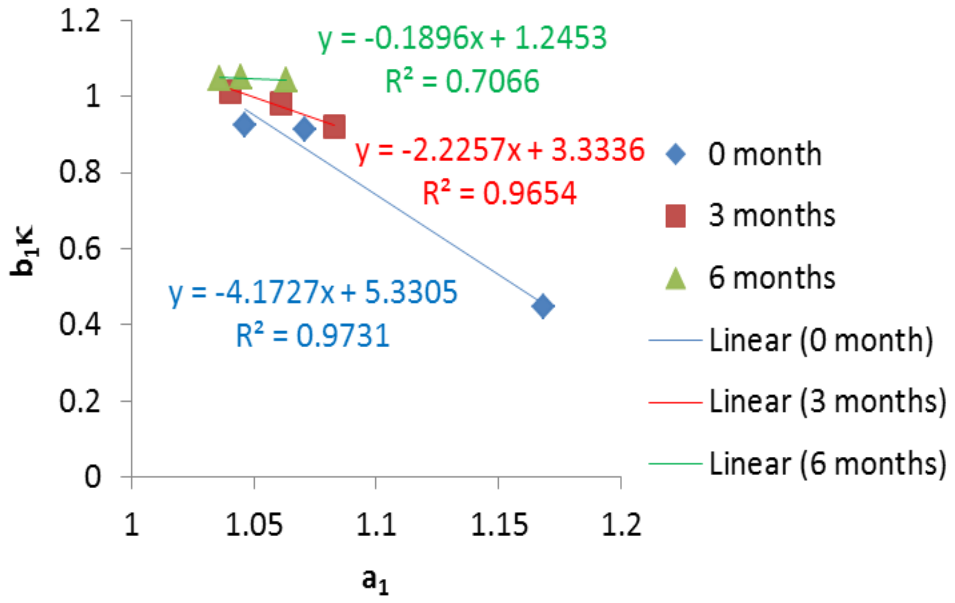

Figure 7.42 Relationship between a_1 and b_1 at Different Aging Periods

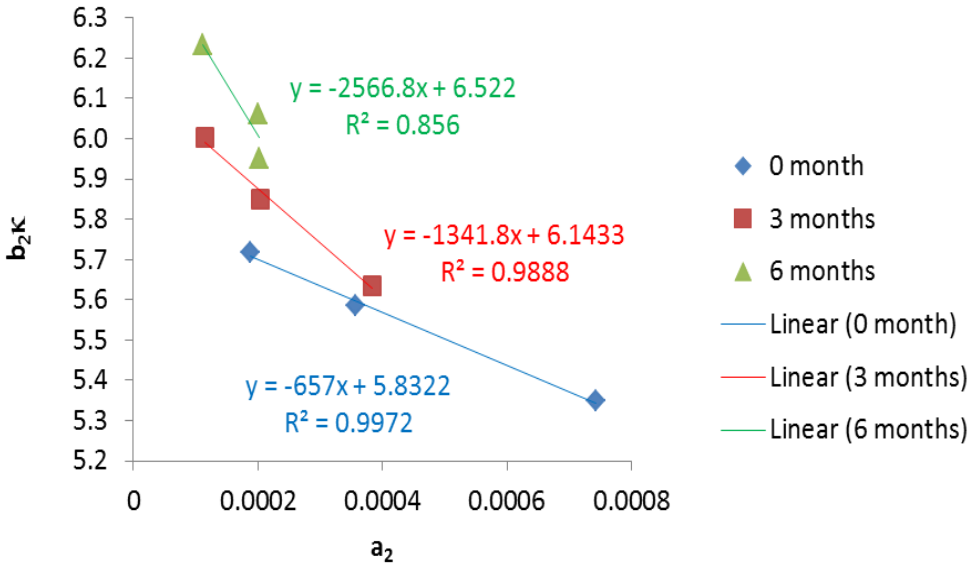

Figure 7.43 Relationship between a_2 and b_2 at Different Aging Periods

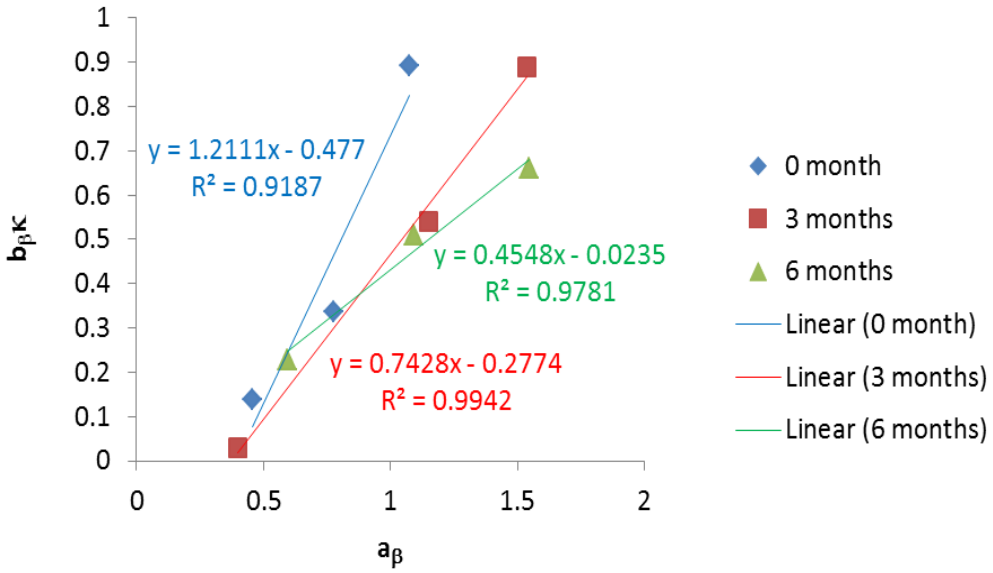

Figure 7.44 Relationship between a_β and $b\beta$ at Different Aging Periods

8. CONCLUSIONS AND RECOMMENDATIONS

8.1 Conclusions

The first issue that is addressed in this work is to develop an appropriate testing and analysis method to characterize fatigue cracking in asphalt mixtures. A controlled-strain RDT test is used to characterize the tensile properties and fatigue damage of asphalt mixtures. In such a test, the stress is composed of a tensile stress portion and a compressive stress portion in a single loading cycle. The material properties in the tensile stress portion (the tensile properties) are found to be different from the material properties in the compressive stress portion (the quasi-compressive properties). This is because of the crack opening and closure in asphalt mixtures which is discovered to exist under both nondestructive and destructive cyclic loading conditions. Consequently, the asphalt mixture should be characterized for the tensile stress portion and the compressive stress portion separately.

The asphalt mixture behaves stronger with a larger magnitude and a smaller phase angle of the complex modulus in the tensile stress portion than in the compressive stress portion due to the opening and closure of cracks or air voids and the associated delayed deformation in the vicinity of the air voids or cracks. The asphalt mixture exhibits an undamaged behavior in the nondestructive RDT test since both the tensile properties and quasi-compressive properties do not change with the increase of the number of loading cycles, and it exhibits a damaged behavior in the destructive RDT test

since both the tensile properties and quasi-compressive properties change as the number of loading cycles increases. All of these findings are verified using statistical tests.

The DSE and RSE of a loading cycle are calculated by integrating the stress and strain functions for the tensile stress portion and the compressive stress portion separately. The assumption that the tensile properties are the same as the quasi-compressive properties yields a smaller value of the DSE that underestimates the damage generated in the asphalt mixture under destructive loading. The traditional integrating range used to calculate the RSE (one quarter of the period of a loading cycle) does not yield an accurate value for the RSE. A new approach is proposed to determine the integration range from the stress-strain hysteresis loop as the phase during which the actual recovery of energy occurs.

In order to quantify the damage that develops in the asphalt mixture under destructive loading, the DSE should be further separated into the energy used to overcome the viscous resistance of the material and the energy used to drive damage. Then the flow of the energy used to drive damage can be investigated among different parts of the asphalt mixture so as to gain a better understanding of the damage process (especially the crack growth process). This is the second issue that is addressed in this work. Firstly, the separation of the DSE is conducted using the pseudo strain to eliminate the viscoelastic effect. To eliminate all the linear and nonlinear viscoelastic effects, the material properties of a typical asphalt mixture under different stress levels are firstly investigated to differentiate the linear viscoelastic, nonlinear viscoelastic and damaged regions on the stress-strain curve of the asphalt mixture. Then the controlled-strain RDT

tests are performed on asphalt mixture specimens to determine their nondestructive properties, critical nonlinear viscoelastic properties and destructive properties. The amount of energy dissipated for the fatigue damage, or the DPSE, is calculated based on the critical nonlinear viscoelastic properties in order to eliminate both linear and nonlinear viscoelastic effects. The critical nonlinear viscoelastic state is the threshold between the undamaged state and the damaged state of the asphalt mixtures.

Secondly, the energy distribution in the asphalt mixture under destructive loading is investigated at the microscopic level. At this level, the asphalt mixture specimen is further divided into the intact material and cracks. The stress, strain and energy in the intact material are what actually occur inside the specimen, whereas the stress, strain and energy measured from the test are apparent representations of the bulk material. Balance between the true and the apparent measurement is established on the basis of energy equivalence between the intact material and the bulk specimen. Four energy balance equations are established, including the DSE balance equation, RSE balance equation, DPSE balance equation and RPSE balance equation. These balance equations are utilized to completely formulate the DPSE for cracking and DPSE for permanent deformation, respectively. Therefore, the DPSE for cracking is separated from the DPSE for permanent deformation.

The formulations for the two types of DPSE and the RDT test data is then used calculate the amount of each type of DPSE. The DPSE for cracking is used to predict the crack growth in terms of damage density, average crack size and number of cracks in the asphalt mixture under repeated destructive loading, which is the third topic of this work.

The model of fatigue crack growth of an asphalt mixture is based on an energy-based mechanistic approach. The core of this approach is the energy balance equations established between the apparent energy of the bulk asphalt mixture specimen and the true energy of the intact material.

The true stress/true strain/true pseudo strain are firstly simulated to calculate the true strain energy/true pseudo strain energy. The true stress in the nondestructive test is solved from the force equilibrium equation; the true stress in the destructive test is solved from the DPSE balance equation. By studying the true stress in a damaged asphalt mixture specimen, it is found that the true stress is the driven force for the crack growth, and the crack growth in turn aggravates the stress and strain localization in the intact material. After obtaining the true stress, the true material properties are determined to obtain the true strain/true pseudo strain. The true material properties include nondestructive and destructive true material properties, which are obtained from the nondestructive and destructive tests, respectively. They are calculated using the DSE and RSE balance equations.

The ratio of the true stress to the apparent stress in a damaged asphalt mixture is used to calculate the damage density for every loading cycle of the destructive RDT test. The evolution of the damage density demonstrates the development of fatigue cracking in the asphalt mixture specimen. The curve of the damage density versus the number of loading cycles can be simulated by a power function.

The damage density of an asphalt mixture is used to modify the Paris' Law to consider the condition of numerous cracks growing under repeated loading. The fracture

coefficients in the modified Paris' Law are back-calculated using the determined damage density. These coefficients represent the fatigue resistance of an asphalt mixture.

The average crack size is further determined using the RPSE balance equation, which serves as an essential parameter to model crack size distribution for asphalt mixtures. Then the number of cracks is calculated using the determined average crack size and the damage density. The result indicates that the crack growth in an asphalt mixture specimen follows this pattern: more and more hair-like cracks are generated in the early stage of loading; then the hair-like cracks start to coalesce when the size increases to a certain value and the number of cracks reaches a peak value; after that the crack size keeps increasing while the number of cracks continues to decrease.

The calculated average crack size/number of cracks are compared to those measured by the X-ray CT system. The result suggests two advantages of the proposed method in this study: 1) more accurate values of air void size/number of air voids; 2) the ability to obtain the change of the average crack size/number of cracks in a damaged asphalt mixture.

Following the topic of crack growth of asphalt mixtures in this work, healing of asphalt mixtures is studied as a counter process to cracking, which alleviates cracking damage and significantly extends the fatigue life of the asphalt mixture. The healing process occurs with the recovery of the asphalt mixtures, so the recovery characteristics of an asphalt mixture are first investigated.

In order to characterize the recovery of an asphalt mixture, the internal stress must be determined first since it is the driving force for the recovery of the asphalt

mixture. The measurement of the internal stress is realized by adding step-loads in the recovery phase of a creep recovery test. One step-load measures the internal stress at one point. The criterion of the added load equal to the internal stress is that the resulting strain rate is zero. Such creep recovery test incorporated with several step-loads in the recovery phase is termed creep and step-loading recovery (CSR) test.

The CSR test is intended to measure the internal stress at different points in the recovery phase to characterize the recovery properties of the asphalt mixture specimen. Design of a CSR test needs to satisfy the following considerations: 1) the type of the test (nondestructive or destructive); 2) adequate data points that are representative of the characteristic of the internal stress; 3) less disturbance of the added step-loads to the recovery of the specimen; and 4) the ability to search for the zero strain rate through the added step-loads.

After designing both nondestructive and destructive CSR tests, the test results are verified to assess the validity of such tests. The first aspect that is examined is the effect of disturbance by adding step-loads to the recovery of the asphalt mixture specimen. The axial strain from the nondestructive CSR test is compared to that from a creep recovery test at the same loading level. The two axial strains match well with each other so the disturbance by the step-loads is acceptable. The other aspect that is evaluated is the accuracy of the measured internal stress. The internal stresses measured from the nondestructive CSR tests are compared to those calculated by the theory of viscoelasticity. The results show that the two kinds of stresses are very close for two types of asphalt mixtures at three different loading levels.

Since the validity of the CSR test is proved, the internal stress measured by this test is then used to determine the recovery properties of asphalt mixtures. Firstly, the measured internal stress is simulated by an appropriate mathematical model, which makes a series of discrete points of measured internal stress become a continuous curve of the internal stress versus time. The best model to simulate the internal stress within and beyond the measure range is an exponential function. Then the ratio of the simulated internal stress to the strain in the recovery phase of the CSR test is used to define a new type of modulus: recovery modulus. The characteristic of the recovery modulus is studied at three different nondestructive loading levels and one destructive loading level. It is found that the recovery modulus of the undamaged asphalt mixtures does not change with the increase of the loading level. However, the recovery modulus of the undamaged asphalt mixtures is different from that of the damaged asphalt mixtures. This difference is caused by the healing of the damaged asphalt mixtures in the recovery phase. In addition, the shape of the recovery modulus curve may be related to the healing ability of the asphalt mixture.

Since the recovery properties of a damaged asphalt mixture have a close relationship with healing, the healing process could be described through the recovery of this asphalt mixture. Characterization of the healing of damaged asphalt mixtures using recovery properties is continuing to be investigated.

Healing of asphalt mixtures is characterized using the CSR test and the energy-based mechanistic approach. The crack growth in the creep phase of the CSR test is modeled using the evolution of the damage density based on the DPSE balance equation.

The damage density at the end of the creep phase is also the initial damage density at the beginning of the healing process. The change from the initial damage density to the damage density at any time during the healing process thus represents the extent of healing that occurs during that period. The damage density at any time during the healing process is determined using the RPSE balance equation. The result shows the decrease of the damage density with time.

The initial damage density at the beginning of the healing process and the damage density at any time during the healing are used to quantify the extent of healing in the asphalt mixture. In this way, healing is described in a fundamental way using its directly measured effect. The calculated healing is used to produce the healing curve, which has three parameters: short-term healing rate, long-term healing rate, and healing rate scale. These three parameters represent the healing ability of the asphalt mixture, and can be used as indices to evaluate the healing ability of different materials.

Finally, the testing and analysis methods that are mentioned above are applied to twenty types of asphalt mixtures to evaluate their application. The effect of the asphalt binder, air void content, and aging on the fatigue resistance of asphalt mixtures are examined. In addition, the effect of the asphalt binder, air void content, temperature, and aging on the healing ability of asphalt mixtures are assessed. The results demonstrate that the controlled-strain RDT and the CSR tests are efficient and repeatable for characterizing fatigue and healing properties of asphalt mixtures. The energy-based mechanistic approach developed in this work characterizes fatigue cracking and healing in a fundamental manner.

8.2 Recommendations for Future Research

An energy-based mechanistic approach with two testing protocols has been developed in this work to characterize the fatigue damage and healing abilities of asphalt mixtures. Extensive data has demonstrated that the fatigue resistance of asphalt mixtures can be accurately evaluated using the fracture coefficients derived from the damage density. Additionally, the healing rates of different types of asphalt mixtures can be efficiently determined using the decrease of the damage density. To make this research work more complete and practical, more research directions are proposed as follows:

- The surface energy is an essential parameter to predict the crack growth and healing in asphalt mixtures. The surface energy used in this work is the cohesive bond energy of the asphalt mastic in an asphalt mixture. In the future research, the surface energy can be extended to include the adhesive bond energy between the asphalt mastic and the aggregate. It can be easily achieved by reformulating the energy balance equations using the modulus of the aggregate and the modulus of the asphalt mastic to replace the modulus of the asphalt mastic.
- The energy-based mechanistic approach can be incorporated into the computational simulation. The modeling of crack growth in the energy-based mechanistic approach can be used as the damage evolution law, and the modeling of healing can be used as the damage recovery law. The advantage of this incorporation is to provide the numerical simulation, such as the finite element method (FEM), a more solid mechanical basis.

- Another direction that this research work can be expanded is to model the development of tensile permanent deformation. The energy consumed for the tensile permanent deformation has been separated from the cracking damage. Therefore, this part of energy can be used to predict the growth of tensile permanent deformation in an asphalt mixture. Using the separated tensile permanent deformation obeys the fact that these two types of damage mechanisms (cracking and permanent deformation) always occur together.

REFERENCES

Ahlquist, C. N. and Nix, W. D. (1971). "The Measurement of Internal Stresses During Creep of Al and Al-Mg Alloys." *Acta Metallurgica*, Vol. 19, pp. 373-385.

Altus, E. (1991). "Fatigue, Fractals, and a Modified Miner's Rule." *Journal of Applied Mechanics*, Vol. 58, 99. 37-42.

American Society for Testing and Materials (2003). *Standard Test Method for Dynamic Modulus of Asphalt Mixtures*, *ASTM D 3497*, ASTM International, West Conshohocken, Philadelphia.

American Society for Testing and Materials (2010). *Standard Test Method for Determining Fatigue Failure of Compacted Asphalt Concrete Subjected to Repeated Flexural Bending*, *ASTM D 7460*, ASTM International, West Conshohocken, Philadelphia.

Anderson, D. A., Christensen, D. W., Bahia, H. U., Dongre, R., Sharma, M. G., Antle, C. E., and Button, J. (1994). "Binder Characterization and Evaluation, Volume 3: Physical Characterization." *Strategic Highway Research Program No. SHRP-A-369*, National Research Council, Washington, D.C.

Anand, J. N. and Karam, H. J. (1969). "Interfacial Contact and Bonding in Autohesion I-Contact Theory." *The Journal of Adhesion*, Vol. 1, pp. 16-23.

Anand, J. N. and Balwinski, R. Z. (1969). "Interfacial Contact and Bonding in Autohesion II-Intermolecular Forces." *The Journal of Adhesion*, Vol. 1, pp. 24-30.

Anand, J. N. (1969). "Interfacial Contact and Bonding in Autohesion III-Parallel Plate Attraction." *The Journal of Adhesion,* Vol. 1, pp. 31-37.

Anand, J. N. and Dipzinski, L. (1970). "Interfacial Contact and Bonding in Autohesion IV-Experimental Verification of Theory." *The Journal of Adhesion*, Vol. 2, pp. 16-22.

Anand, J. N. (1970). "Interfacial Contact and Bonding in Autohesion V-Bonding of Flat Surfaces." *The Journal of Adhesion*, Vol. 2. pp. 23-28.

Arambula, E, Masad, E., and Epps Martin, A. (2007). "Moisture Susceptibility of Asphalt Mixtures with Known Field Performance-Evaluated with Dynamic Analysis and Crack Growth Model." *Transportation Research Record: Journal of the Transportation Research Board*, No. 2001, pp. 20-28.

Bahia, H., Zhai, H., Bonnetti, K., and Kose, S. (1999). "Nonlinear Viscoelastic and Fatigue Properties of Asphalt Binders." *Journal of Association of Asphalt Paving Technologists*, Vol. 68, pp. 1-34.

Baney, J. M. and Hui, C.-Y. (1999). "Viscoelastic Crack Healing and Adhesion." *Journal of Applied Physics*, Vol. 86, No. 8, pp.4232-4241.

Barksdale, R. D. (1972). "Laboratory Evaluation of Rutting in Base Course Materials." processing, 3rd International Conference on Structure Design of Asphalt Pavements, University of Michigan, Michigan. pp. 161-174.

Bartlett, J. E., II, Kotrlik, J. W., and Higgins, C. (2001). "Organizational Research: Determining Appropriate Sample Size for Survey Research." *Information Technology, Learning, and Performance Journal*, Vol. 19, No. 1, pp. 43-50.

Bhasin, A., Little, D. N., Bommavaram, R. and Vasconcelos, K. L. (2008). "A Framework to Quantify the Effect of Healing in Bituminous Materials Using Materials Properties." *International Journal of Road Materials and Pavement Design*, EATA 08: pp. 219-242.

Bolzan, P.E. and Huber, G. (1993). "Direct Tension Test Experiments." *SHRP-A-641, Strategic Highway Research Program*, National Research Council. Washington, D.C

Carpenter, S. H., Ghuzlan, K. A., and Shen S. (2003). "A Fatigue Endurance Limit for Highway and Airport Pavements." Paper No. 03-3428, presented at the Annual Meeting of the Transportation Research Board, January.

Carpenter, S. H. and Shen, S. (2006). "Dissipated Energy Approach to Study Hot-Mix Asphalt Healing in Fatigue." *Transportation Research Record: Journal of the Transportation Research Board*. Transportation Research Board of the National Academies, Washington, D.C., No. 1970, pp. 84-91.

Elber, W. (1971). *Damage Tolerance in Aircraft Structure*, *STP 486*, American Society for Testing and Materials, Philadelphia, pp. 230-242.

Erkens, S. M. J. G., Molenaar, A. A. A., and Scarpas, A. (2003). "A Better Understanding of Asphalt Concrete Response." *Proceedings of 16th ASCE Engineering Mechanics Conference*, University of Washington, Seattle, July 16-18.

Findley, W. N., Lai, J. S. and Onaran, K. (1989). *Creep and Relaxation of Nonlinear Viscoelastic Materials: with an Introduction to Linear Viscoelasticity*. Dover Publications, New York.

Fotheringham, D. G. and Cherry, B. W. (1978). "The Role of Recovery Forces in the Deformation of Linear Polyethylene." *Journal of Material Science*, Vo. 13, pp. 951-964.

Ghuzlan, K.A., and Carpenter, S.H. (2000). "Energy-Derived, Damage-Based Failure Criterion for Fatigue Testing." *Transportation Research Record 1723, Transportation Research Board*, National Research Council, Washington, D.C. pp. 141–149.

Ghuzlan, K. A. and Carpenter, S. H. (2006). "Fatigue Damage Analysis in Asphalt Concrete Mixtures Using the Dissipated Energy Approach." *Canadian Journal of Civil Engineering*, Vol. 33, No. 7, pp. 890-901.

Gibson, N. H., Schwartz, C. W., Schapery, R. A., and Witczak, M. W. (2003). "Viscoelastic, Viscoplastic, and Damage Modeling of Asphalt Concrete in Unconfined Compression." *Transportation Research Record: Journal of the Transportation Research Board*, Vol. 1860, pp. 3-15.

Hashin, Z. and Rotem, A. (1978). "A Cumulative Damage Theory of Fatigue Failure." *Material Science of Engineering*, Vol. 34, pp. 147-160.

Hashin, Z. and Laird, C. (1980). "Cumulative Damage under Two Level Cyclic Loading: Some Theoretical Predictions and Test Data." *Fatigue of Engineering Materials and Structures*, Vol. 2, 99. 345-350.

Inglis, C. E. (1913). "Stresses in a Plate Due to the Presence of Cracks and Sharp Corners." *Transactions of the Institute of Naval Architects*, Vol. 55, pp. 219-241.

Jacobs, M.M.J. (1995). "Crack Growth in Asphaltic Mixes." Ph.D. dissertation, Delft University of Technology, Delft, The Netherlands.

Jones, D. R. (1993). "SHRP Materials Reference Library: Asphalt Cements: A Concise Data Compilation." *Strategic Highway Research Program Rep. No.SHRP-A-645*, National Research Council, Washington, D.C.

Jud, K., Kausch, H. H., Williams, J. G. (1981). "Fracture Mechanics Studies of Crack Healing and Welding of Polymers." *Journal of Materials Science*, Vol. 16, pp. 204-210.

Kachanov, L. M. (1958). *Introduction to Continuum Damage Mechanics*. Kluwer Academic Publishers, Dordrecht, The Netherlands.

Kausch, H. H., Petrovska, D., Landel, R. F., and Monnerie, L. (1987). "Intermolecular Interaction in Polymer Alloys as Studied by Crack Healing." *Polymer Engineering and Science*, Vol. 27, No. 2, pp. 149-154.

Kenis, W. J. (1977). "Predictive Design Procedures, VESYS Users Manual." *Report. No. FHWA-RD-77-154*, Federal Highway Administration, McLean, Virginia.

Khanal, P. P. and Mamlouk, M. S. (1995). "Tensile versus Compressive Moduli of Asphalt Concrete." *Transportation Research Record: Journal of the Transportation Research Board*, No. 1492, pp. 144-150.

Kim, Y. R., Little, D. N., and Lytton, R. L. (2001). "Evaluation of Microdamage, Healing, and Heat Dissipation of Asphalt Mixtures, Using a Dynamic Mechanical Analyzer." *Transportation Research Record: Journal of the Transportation Research Board*, Vol. 1767, pp. 60-66.

Kim, Y.R., J.S. Daniel, and H. Wen. (2002). "Fatigue Performance Evaluation of WesTrack Asphalt Mixtures using Viscoelatic Continuum Damage Approach." *Report No. FHWA/NC/2002-004,* Final Report to North Carolina Department of Transportation.

Kim, Y. R., Little, D. N., and Lytton, R. L. (2003). "Fatigue and Healing Characterization of Asphalt Mixtures." *Journal of Materials in Civil Engineering*, Vol. 15, pp.75-83.

Kim, Y.R. (2008). *Modeling of Asphalt Concrete.* ASCE Press & McGraw-Hill Professional, Reston, VA.

Kim, B and Roque, R. (2006). "Evaluation of Healing Properties of Asphalt Mixtures." *Transportation Research Record: Journal of the Transportation Research Board. No. 1970*, Transportation Research Board of the National Academies, Washington, D.C., pp. 84-91.

Kose, S., Guler, M., Bahia, H., and Masad, E. (2000) "Distribution of Strains within Hot-Mix Asphalt Binders Applying Imaging and Finite-Element Techniques." In *Transportation Research Record: Journal of the Transportation Research Board. No. 1728*, TRB, National Research Council, Washington, D.C., p. 21-27.

Krajcinovic, D. (1996). *Damage Mechanics*, Elsevier, Amsterdam, The Netherlands.

Kubat, J., Petermann, J. and Rigdahl, M. (1975). "Internal Stresses in Polyethylene as Related to Its Structure." *Material Science and Engineering*, Vol. 19, No. 2, pp. 185-191.

Lakes, R. S. (1999). *Viscoelastic Solids*. CRC Press LLC, Boca Raton, FL.

Lemaitre, J. (1992). *A Course on Damage Mechanics*, Springer-Verlag, Berlin, Germany.

Little, D. N., Lytton, R. L., Williams, D., and Kim, Y. R. (1997). "Propagation and Healing of Microcracks in Asphalt Concrete the Their Contributions to Fatigue." *Asphalt Science and Technology*, pp. 149-195.

Little, D.N., R.L. Lytton, D. Williams, and J.W. Chen. (1998). *Fundamental Properties of Asphalts and Modified Asphalts.* Final Research Report. Texas Transportation Institute, Texas A&M University, College Station, Texas, Vol. 1.

Little, D.N., Lytton, R.L., Williams, D., and Chen, C.W. (2001). "Fundamental Properties of Asphalts and Modified Asphalts – Volume 1: Microdamage and Microdamage Healing." Federal Highway Administration Final Report, No. FHWA-RD-98-141, Washington D.C.

Little, D. and Bhasin, A. (2008). "Exploring Mechanism of Healing in Asphalt Mixtures and Quantifying its Impact." *Self Healing Material*, Springer Series in Materials Science, Vol. 100, pp. 205-218.

Li, Y. and Metcalf, J. B. (2004). "Fatigue Characteristics of Asphalt Concrete from Asphalt Slab Tests." *Journal of Materials in Civil Engineering*, Vol. 16, No. 4, pp. 306-314.

Luo, R., and Lytton, R. L. (2011). "Determination of Crack Size Distribution in Asphalt Mixtures." *Transportation Research Record: Journal of the Transportation Research Board*, in print.

Lytton, R.L. (2000). "Characterizing Asphalt Pavement for Performance." *Transportation Research Record 1723*, Transportation Research Board, National Research Council, Washington, D.C., pp. 5-16.

Lytton, R. L. (2004). "Adhesive Fracture in Asphalt Concrete Mixtures." Course Notes.

Maillard, S., de La Roche, C., Hammoum, F., Gaillet, L., and Such, C. (2004). "Experimental Investigation of Fracture and Healing at Pseudo-contact of Two Aggregates." *3rd Euroasphalt and Eurobitume Congress*, Vienna

Manuel, N. G. (2010). *Rheology and engineering parameters of bitumen modified with polyolefins, elastomers and reactive polymers*, Univ.-Verl. der TU Berlin, Berlin.

Masad, E., Castelo Branco, V., Little, D., and Lytton, R. L. (2007). "A Unified Method for the Analysis of Controlled-Strain and Controlled-Stress Fatigue Testing," *International Journal of Pavement Engineering*, Vol.00, No. 0, pp.1-14.

Masad, E., Muhunhtan, B., Shashidhar, N., and Harman, T. (1999). "Internal Structure Characterization of Asphalt Concrete Using Image Analysis." *Journal of Computing in Civil Engineering*, Vol. 13, No. 2, pp. 88-95.

Masad, E., and Somadevan, N. (2002) "Microstructural Finite-Element Analysis of Influence of Localized Strain Distribution of Asphalt Mix Properties." *Journal of Engineering Mechanics*, pp. 1105-1114.

Mezger, T. G. (2006). *The Rheology Handbook*, 2nd ed., Vincentz Network, Hannover.

Mindel, M. J. and Brown, N. (1973). "Creep and Recovery of Polycarbonate." *Journal of Materials Science*, Vol. 8, pp. 863-870.

Mindel, M. J. and Brown, N. (1974). "The Relationship of Creep, Recovery and Fatigue in Polycarbonate." *Journal of Materials Science*, Vol. 9, pp. 1661-1669.

Monismith, C. L., Epps, J. A., Kasianchuk, D. A., and McLean, D. B. (1971). *Asphalt Mixture Behavior in Repeated Flexure*. Report TE 70-5, University of California, Berkeley.

Monismith, C. L., Ogawa, N., and Freeme, C. R. (1975). "Permanent Deformation Characterization of Subgrade Soils due to Repeated Loading." *Transportation Research Record. 537*, Transportation Research Board, Washington, D.C., pp. 1-17.

NCHRP 1-37A (2002). *2002 Design Guide, Design of New and Rehabilitated Pavement Structure*, Draft Final Report prepared for National Cooperative Highway Research Program, Transportation Research Board.

Nishizawa, T., Shimeno, S., and Sekiguchi, M. (1997). "Fatigue Analysis of Asphalt Pavements with Thick Asphalt Mixture Layer." *8th International conference on Asphalt Pavements*, Seattle, Washington, pp. 969-976.

Ostergren, W. J. and Krempl, E. (1979). "A Uniaxial Damage Accumulation Law for Time-Varying Loading Including Creep-Fatigue Interaction." *Journal of Pressure Vessel Technology*, Vol. 101, 99. 118-124.

Ott, R. L. and Longnecker, M. (2001). *An Introduction to Statistical Methods and Data Analysis*, 5th ed. Pacific Grove: Duxbury.

Pahutova, M., Cadek, J., and Rys, P. (1979). "Some Stress Change Experiments on Creep in á Zirconium," *Material Science and Engineering*, Vol. 39, pp.169–74..

Paris, P. C. and Erdogan, F. (1963). "A Critical Analysis of Crack Propagation Laws." *Journal of Basic Engineering*, Vol. 85, pp. 528-534.

Paris, P. C. and Sih, G. C. (1965). "Stress Analysis of Cracks." *Fracture Toughness Testing and Its Applications: A Symposium Presented at the Sixty-Seventh Annual Meeting,* American Society for Testing and Materials, Chicago, III., June 21-26.

Pellinen, T. K. (2009). "Complex Modulus Characterization of Asphalt Concrete." *Modeling of Asphalt Concrete*, Chapter 4, ASCE Press, McGraw-Hill Construction, pp. 89-119.

Raghavan, J. and Meshii, M. (1994). "Activation Theory for Creep of Matrix Resin and Carbon Fibre-reinforced Polymer Composite." *Journal of Materials Science*, Vol. 29, 5078-5084.

Rambery, W. and Osgood, W. R. (1943). "Description of Stress-Strain Curves by Three Parameters." *Technical Note No. 902,* National Advisory Committee for Aeronautics, Washington D. C.

Roberts, F. L., Kandhal, P. S., Brown, E. R., Lee, D. -Y. and Kennedy, T. W. (1996). *Hot Mix Asphalt Materials, Mixture Design, and Construction*. 2nd ed. NAPA Education Foundation, Lanham, Maryland.

Roque, R. W.G. Buttlar, B.E. Ruth, M. Tia, S.W. Dickison, and B. Reid. (1997). "Evaluation of SHRP Indirect Tension Tester to Mitigate Cracking in Asphalt Pavements and Overlays." Final Report to the Florida Department of Transportation.

Roylance, D. (2001). *Introduction to Fracture Mechanics.* Department of Materiarls Science and Engineering, Massachusetts Institute of Technology, Cambridage, MA.

Schapery, R. A. (1969). "Characterization of Nonlinear Viscoelastic Materials." *Polymer Engineering and Science*, Vol. 9, No. 9, pp. 295-310.

Schapery, R.A. (1975). "A Theory of Crack Initiation and Growth in Visco-Elastic Media; I: Theoretical Development, II: Approximate Methods of Analysis, III: Analysis of Continuous Growth." *International Journal of Fracture,* Vol. 11, No. 1, pp. 141-159, Vol. 11 No. 3, pp. 369-388, and Vol.11, No. 4, pp. 549-562.

Schapery, R.A. (1978). "A Method for Predicting Crack Growth in Non-homogeneous Visco-Elastic Media." *International Journal of Fracture*, Vol. 14, No. 3, pp. 293-309.

Schapery, R. A. (1984). "Correspondence Principles and a Generalized J-integral for Large Deformation and Fracture Analysis of Viscoelastic Media." *International Journal of Fracture*, Vol. 25, pp.195-223.

Schapery, R. A. (1989). "On the Mechanics of Crack Closing and Bonding in Linear Viscoelastic Media." *International Journal of Fracture*, Vol. 39, pp. 163-189.

Shenoy, A. (2007). "A Dynamic Oscillatory Test that Fulfills the Objective of the Elastic Recovery Test for Asphalt Binders." *Materials and Structures*, Vol. 41, No. 6, pp. 1039-1049.

Si, Z., Little, D. N., and Lytton, R. L. (2002). "Characterization of Microdamage and Healing of Asphalt Concrete Mixtures." *Journal of Materials in Civil Engineering,* Vol. 14, No. 6, pp. 461-470.

Sousa, J. B., Deacon, J. A., Weissman, S. L., Leahy, R. B., Harvey, J. T. Paulsen, G., Coplantz, J. S., and Monismith, C. L. (1994). "Permanent Deformation Response of Asphalt Aggregate Mixes." *Report SHRP-A-415*, *Strategic Highway Research Program*, National Research Council, Washington D. C..

Stephens, R. I., Fatemi, A., Stephens, R. R., and Fuchs, H. O. (2001). *Metal Fatigue in Engineering*. John Wiley & Sons, Inc., New York.

Suresh, S. and Ritchie, R. O. (1984). "Propagation of Short Fatigue Cracks." *International Metallurgical Reviews*, Vol.29, pp. 445-476.

Suresh, S. (1991). *Fatigue of Materials*, Cambridge University Press, Cambridge, UK.

Superpave Models Team, (1999). *Task F – Advanced Mixture Characterization, Team Report SLS -3*. SUPERPAVE Support and Performance models Management, NCHRP 9-19, Department of Civil and Environmental Engineering, Arizona State University, Tempe, AZ.

Tayebali, A. A. (1994). "Fatigue Response of Asphalt-Aggregate Mixtures." *Report A404. SHRP A003A*, National Research Council, Washington, D.C.

Tayebali, A. A., Rowe, G. M., and Sousa, J. B. (1992). "Fatigue Response of Asphalt–Aggregate Mixtures." *Journal of the Association of Asphalt Paving Technologists*, Vol. 61, pp. 333–360.

Teoh, S. H., Chuan, C. L., and Poo, A. N. (1987). "Application of a Modified Strain Transient Dip Test in the Determination of the Internal Stresses of PVC under Tension." *Journal of Material Science*, Vol. 22, pp. 1397-1404.

Texas Department of Transportation (2004). *Standard Specifications for Construction and Maintenance of Highways, Streets, and Bridges*. Available at ftp://ftp.dot.state.tx.us/pub/txdot-info/des/specs/specbook.pdf.

Texas Department of Transportation (2005). *Design of Bituminous Mixtures.* Available athttp://www.txdot.gov/business/contractors_consultants/test_procedures/tms_forms_and_archives.htm?tms=Tex-204-F&qtype=archive.

The Asphalt Institute. (1981). *Thickness Design Manual Series No. 1 (MS-1)*. Ninth Edition, College Park, Maryland.

Turner, S., (1973). "Creep in Glassy Polymers." In *The Physics of Glassy polymers*, ed. R. H. Howard, J. Wiley, NY.

Van Dijk, W. (1975). "Practical Fatigue Characterization of Bituminous Mixes". *Journal of the Association of Asphalt Paving Technologists*, Vol. 44, pp.38–74.

Voyiadjis, G. Z., and Kattan, P. I. (1999). *Advances in Damage Mechanics: Metals and Metals Matrix Composites*. Elsevier, Oxford.

Walubita, L. F., Epps Martin, A., Glover, C. J., A, and Lytton, R. L. (2006). "Computation of Pseudo Strain Energy and Paris Law Fracture Coefficients from Surface Energy and Uniaxial Strain-Controlled Tension Test Data." *International Journal of Pavement Engineering*, Vol. 7, No. 3, pp. 167-178.

Wang, L, Wang, Y., Li, Q., and Flintsch, G. (2007). "Stress Concentration Factor as a Performance Indicator for Asphalt Mixes." *Proceedings of the Symposium on the Mechanics of Flexible Pavements,* ASCE, June 25-30, Boulder, Colorado.

Williams, A. D., Little, D. N., Lytton, R. L., Kim, Y. R., and Kim, Y. (2001). *Microdamage Healing in Asphalt and Asphalt Concrete, Vol II: Laboratory and Field Testing to Assess and Evaluate Micordamage and Microdamage Healing*. FHWA-RD-98-142, Texas Transportation Institution, College Station, Texas.

Wineman, A. S. and Rajagopal, K. R. (2000). *Mechanical Response of Polymers: Introduction*. Cambridge University Press, Cambridge.

Wolf, P. R. and Ghilani, C. D. (2005). *Elementary Surveying: An Introduction to Geomatics.* 11th ed., Prentice Hall, New Jersey.

Wool, R. P. and O'Connor, K. M. (1981). "A Theory of Crack Healing in Polymers." *Journal of Applied Physics*, Vol. 52, No. 10, pp.5953-5963.

APPENDIX A

1. Result of independent t-test for Hypothesis I

Independent Samples Test

		Levene's Test for Equality of Variances		t-test for Equality of Means				
		F	Sig.	t	df	Sig. (2-tailed)	Mean Difference	Std. Error Difference
Modulus	Equal variances assumed	7.339	.007	40.046	158	.000	287.26600	7.17337
	Equal variances not assumed			40.046	138.807	.000	287.26600	7.17337

2. Result of independent t-test for Hypothesis II

Independent Samples Test

		Levene's Test for Equality of Variances		t-test for Equality of Means				
		F	Sig.	t	df	Sig. (2-tailed)	Mean Difference	Std. Error Difference
Phase angle	Equal variances assumed	.268	.606	-23.098	158	.000	-2.72062	.11778
	Equal variances not assumed			-23.098	155.840	.000	-2.72062	.11778

3. Result of Wilcoxon Rank Sum test for Hypothesis III.

Test Statistics[a]

	Modulus
Mann-Whitney U	3270.000
Wilcoxon W	9375.000
Z	-5.889
Asymp. Sig. (2-tailed)	.000

4. Result of Wilcoxon Rank Sum test for Hypothesis IV.

Test Statistics[a]

	Phase angle
Mann-Whitney U	248.000
Wilcoxon W	6353.000
Z	-12.311
Asymp. Sig. (2-tailed)	.000

5. Result of One way ANOVA for Hypothesis V.

ANOVA

S1

	Sum of Squares	df	Mean Square	F	Sig.
Between Groups	13503.449	7	1929.064	1.567	.159
Within Groups	88636.612	72	1231.064		
Total	102140.061	79			

6. Result of One way ANOVA for Hypothesis VI.

ANOVA

S2

	Sum of Squares	df	Mean Square	F	Sig.
Between Groups	4.260	7	.609	1.273	.276
Within Groups	34.418	72	.478		
Total	38.678	79			

7. Result of One way ANOVA for Hypothesis VII.

ANOVA

S3

	Sum of Squares	df	Mean Square	F	Sig.
Between Groups	34310.092	7	4901.442	1.870	.087
Within Groups	188759.890	72	2621.665		
Total	223069.982	79			

8. Result of One way ANOVA for Hypothesis VIII.

ANOVA

S4

	Sum of Squares	df	Mean Square	F	Sig.
Between Groups	5.272	7	.753	1.767	.107
Within Groups	30.681	72	.426		
Total	35.953	79			

9. Result of Kruskal-Wallis test for Hypothesis IX.

Test Statistics[a,b]

	S5
Chi-Square	107.959
df	10
Asymp. Sig.	.000

10. Result of Kruskal-Wallis test for Hypothesis X.

Test Statistics[a,b]

	S6
Chi-Square	107.377
df	10
Asymp. Sig.	.000

11. Result of Kruskal-Wallis test for Hypothesis XI.

Test Statistics[a,b]

	S7
Chi-Square	107.827
df	10
Asymp. Sig.	.000

12. Result of Kruskal-Wallis test for Hypothesis XII.

Test Statistics[a,b]

	S8
Chi-Square	104.127
df	10
Asymp. Sig.	.000

VITA

Name:	Xue Luo
Address:	3135 TAMU, CE/TTI Bldg., College Station, TX 77843-3135
Email Address:	xueluo@tamu.edu
Education:	B.E., Civil Engineering, Zhejiang University, China, 2006 M.E., Civil Engineering, Texas A&M University, 2009